

Water flow paths in soils of an undisturbed and landslide affected mature montane rainforest in South Ecuador

Dissertation

to obtain the academic degree of Doctor of Natural Science (Dr. rer. nat.) of the Faculty of
Biology, Chemistry and Geosciences of the University of Bayreuth

presented by
Folkert Christian Bauer
Dipl.-Geol.
born in Hofgeismar, Germany

Bayreuth, July 2010

This doctoral thesis was prepared at the Department of Soil Physics, University of Bayreuth, from July 2005 until July 2010, supervised by Prof. Dr. Bernd Huwe.

This is a full reprint of the dissertation submitted to attain the academic degree of Doctor of Natural Sciences (Dr. rer. nat.) and approved by the Faculty of Biology, Chemistry and Geosciences of the University of Bayreuth.

Acting dean:	Prof. Dr. Stephan Clemens
Date of submission:	July 29, 2010
Date of defence (disputation):	Dezember 13, 2010

Doctoral Committee:	
Prof. Dr. Bernd Huwe	1 st reviewer
Prof. Dr. Hans-Georg Frede	2 nd reviewer
Prof. Dr. Klaus Bitzer	Chairman
Prof. Dr. Stefan Peiffer	
Prof. Dr. John Tenhunen	

Summary

The number of previous hydrological studies concerning water flow paths in tropical montane rainforest is small. However, due to the increasing pressure of deforestation and land use change comprehensive knowledge of these natural ecosystems is needed if sustainable land use strategies should keep negative effects of human impacts on water flow paths as low as possible. In this context, present work addresses the identification, characterisation, and modelling of water flow paths in soils of an undisturbed and landslide affected natural Andean forest ecosystem in the south of Ecuador whose deforestation rate is one of the highest in South America. In an investigation area situated in the Andes of South Ecuador, in gentler slopes and altitudes above 2100 m ASL mainly Stagnosols and Histosols with stagnic colour pattern and low to negligible rock fragment content prevail. With increasing altitude the abundance of these soils increase, while the presence of Cambisols and Regosols is most pronounced below 2100 m ASL and clearly correlated with the slope angle. Therefore, these soils were mainly encountered in steeper, particularly landslide affected sites often resembling a melange of fine soil and high contents of rock fragments. Aside the investigation of the influence of the rock fragment content on soil hydrological- and physical parameters such as the relationship between rock fragment content and saturated hydraulic conductivity of the soil, present study aims particularly to investigate flow paths of water in soils of landslide affected and unaffected hillslopes. Therefore, we employed conventional field- and laboratory methods, dye tracer experiments including an appropriate image processing technique, as well as statistical models. Results show that both rock fragment content and bulk density control significantly, but not largely the saturated hydraulic conductivity of the mineral soils. Dye tracer experiments and soil parameters document a deeper percolation in the landslide affected hillslopes than in the landslide unaffected hillslopes, where we found preferential flow in root channels with low soil matrix interaction as dominant flow mechanism. A surface near quasi impervious layer along the interface between topsoil and subsoil limits percolation of the water giving the prerequisites of a lateral shallow subsurface flow along the interface between topsoil and organic layer. This is in line with previous studies performed in the same investigation area which already proved indirectly the existence of this flow. However, in none of these studies the shallow subsurface flow was assigned to certain slope inclinations or altitudes. Due to a recently published digital soil map and the results we obtained from the landslide unaffected sites, we know that particularly in hillslopes of less than 30 ° above 2100 m ASL prerequisites are given for spatially extended shallow subsurface flow. However, even

if these prerequisites are not evident for the landslide affected hillslopes, we cannot exclude the possibility of shallow subsurface flow occurrence here since soil cover of the steep terrain is relatively shallow while rainfall is high throughout the year. Therefore, and given that key parameters such as permeability of subsoil and bedrock, interception and evaporation remain unclear or were investigated exclusively such as the spatial variability of the saturated hydraulic conductivity, we conducted a series of virtual experiments in order to assess the potential occurrence of shallow subsurface flow in Cambisols below 2100 m ASL. In these experiments we also included the organic layer being highly abundant in the investigation area, whose hydraulic parameters were estimated by means of inverse numerical modelling. The virtual experiments were based on a two dimensional finite element model representing a steep forested hillslope transect of ~54 m length. Aside soil properties, evapotranspiration and interception, the model included the spatial variability of the saturated hydraulic conductivity, the pressure head and their spatial trends. The results of virtual experiment series show that a sound evidence of the key parameters aforementioned is obligate if process conceptualisation regarding shallow subsurface flow generation, but also landslide initiation, solute and matter transport is in the spotlight.

Zusammenfassung

Die Anzahl bisheriger hydrologischer Untersuchungen von Wasserfließpfaden in Böden tropischer Bergregenwälder ist gering. Doch erfordern zunehmende Entwaldung und Landnutzungsänderung ein umfassendes Wissen über die Funktionsweise dieser natürlichen Ökosysteme, wenn negative Auswirkungen anthropogener Einflüsse auf Wasserfließpfade im Rahmen nachhaltiger Landnutzungsstrategien möglichst gering sein sollen. Vor diesem Hintergrund befasst sich vorliegende Arbeit mit der Identifizierung, Charakterisierung und Modellierung von Wasserfließpfaden in Böden eines ungestörten und rutschungsbeeinflussten natürlichen andinen Waldökosystems im Süden des Landes Ecuador, dessen Entwaldungsrate zu den höchsten Südamerikas zählt. In einem Forschungsgebiet in den südlichen Anden Ecuadors herrschen in flacheren Hängen unterhalb von 2100 m ü. NN vor allem Stagnosole und Histosole mit Stauwassermerkmalen und mit geringen bis vernachlässigbaren Steingehalten vor. Das Auftreten dieser Böden nimmt mit steigender Höhe ü. NN zu, während Cambisole und Regosole vor allem unterhalb 2100 m ü. NN und in Abhängigkeit von der Hangsteilheit auftreten. Daher sind diese Bodentypen häufig in rutschungsbeeinflussten Hangbereichen anzutreffen und entsprechen oft einer Melange aus Feinboden und hohem Steingehalten. Neben der Untersuchung des Einflusses der Gesteinsgehalte auf bodenhydrologische und -physikalische Parameter wie beispielsweise die Beziehung zwischen Steingehalt und gesättigter hydraulischer Leitfähigkeit des Mineralbodens zielt vorliegende Arbeit vor allem darauf ab, Wasserfließpfade in Böden hangrutschungsbeeinflusster und -unbeeinflusster Bereiche zu untersuchen. Dazu wendeten wir neben klassischen Feld- und Labormethoden Farbmarkierungs- und Bildverarbeitungsmethoden sowie statistische Modelle an. Die Ergebnisse zeigen einen zwar schwachen, aber signifikanten Einfluss sowohl des Steingehaltes als auch der Lagerungsdichte auf die gesättigte Leitfähigkeit. Die Farbmarkierungsversuche und Bodenparameter belegen für die Böden in den rutschungsbeeinflussten Hängen eine tieferreichende vertikale Perkolation als in den nicht rutschungsbeeinflussten Hängen, wo die Wasserbewegung hauptsächlich entlang von Wurzelröhren in geringem Austausch mit der Bodenmatrix stattfindet. Zudem ist die vertikale Perkolation hier durch eine oberflächennahe nahezu wasserundurchlässige Schicht entlang der Grenze zwischen Ober- und Unterboden begrenzt, wodurch die Voraussetzung für einen lateralen Zwischenabfluss zwischen Oberboden und organischer Auflage gegeben ist. Dieser Befund koinzidiert mit früheren Arbeiten im selben Untersuchungsgebiet, die zwar die Existenz dieses Zwischenabflusses bereits indirekt nachwiesen, ohne diesen jedoch bestimmten Hangneigungen oder Höhestufen

zuzuordnen. Aufgrund einer jüngst publizierten digitalen Bodenkarte und den in den von Rutschungen unbeeinflussten Bereichen gewonnenen Ergebnissen wissen wir, dass vor allem in Hängen mit weniger als 30° Einfallen oberhalb 2100 m ü. NN die Voraussetzung zu großflächigem Auftreten oberflächennahen Zwischenabflusses gegeben ist. In den rutschungsbeeinflussten Hängen wurden diese Voraussetzungen zwar nicht nachgewiesen, dennoch kann die Möglichkeit eines oberflächennahen Zwischenabflusses wegen relativ geringmächtiger Böden, hoher Niederschlagsmengen und des steilen Geländes nicht ausgeschlossen werden. Aus diesem Grunde, und da zudem Schlüsselparameter wie die Leitfähigkeit des Unterbodens und Grundgebirges, Interzeption und Verdunstung unklar sind oder ausschließlich wie die räumliche Variabilität der gesättigten hydraulischen Leitfähigkeit im Mineralboden untersucht wurden, führten wir eine Serie virtueller Experimente zum Nachweis eines potentiellen oberflächennahen Zwischenabflusses in Cambisolen unterhalb 2100 ü. NN durch. Dabei berücksichtigten wir auch wegen ihrer starken Präsenz im Untersuchungsgebiet die organische Auflage, deren hydraulische Parametrisierung wir mittels inverser numerischer Modellierung vornahmen. Die virtuellen Experimentserien basierten auf einem zweidimensionalen finite Elemente Modell, das einen ca. 54 m langen Transekt unter Waldvegetation simulierte. Neben Bodenparametern, Evapotranspiration und Interzeption umfasste das Modell die räumliche Variabilität der gesättigten hydraulischen Leitfähigkeit, des Matrixpotentials und ihrer räumlichen Trends. Die Ergebnisse der virtuellen Experimente verdeutlichen, dass im Hinblick auf Prozessmodellierung von oberflächennahem Zwischenabfluss und Stofftransport, aber auch Auslösung von Hangrutschungen im Untersuchungsgebiet durch physikalisch basierte Modellansätze eine genaue Kenntnis der Schlüsselparameter Klima, hydraulische Leitfähigkeiten und deren räumliche Verteilung sowie Permeabilität des Unterbodens und Grundgebirges erforderlich ist.

Resumen

El número de los estudios previos relacionado a las trayectorias de flujo de agua en los bosques tropicales de montaña es bajo. Sin embargo, a causa de la presión creciente por la deforestación y el cambio del uso de la tierra, un conocimiento amplio sobre estos ecosistemas naturales es necesario para que en el marco de las estrategias del manejo sostenible los efectos negativos de los impactos humanos en las trayectorias de flujo de agua sean lo más bajo posible. En este contexto, el presente estudio se ocupa de la identificación, caracterización y modelaje de las trayectorias de flujo de agua en suelos de un ecosistema forestal natural no perturbado y perturbado por derrumbes en el sur del Ecuador, cuya proporción de la deforestación es una de las mayores en Sudamérica. En un área de investigación que esta ubicada en los Andes del Sur del Ecuador, en zonas de pendientes poco pronunciadas por encima de 2100 m SNM, éstas se caracterizan por la presencia de suelos tipo Histosol y Stagnosol mostrando patrones de estancamientos de agua y fragmentos de roca en cantidades bajas hasta despreciables. La presencia de dichos suelos incrementa con la altitud, mientras los suelos del tipo Cambisol y Regosol aparecen particularmente por debajo de 2100 m SNM, y están claramente relacionados con el ángulo de la pendiente. Por consiguiente, estos tipos de suelos se presentan frecuentemente en pendientes afectadas por derrumbes y equivalen a un conglomerado hecho de suelo fino y contenido alto de fragmentos de rocas. A par de la investigación de la influencia del contenido de roca sobre parámetros hidrológicos y físicos de suelos como por ejemplo la relación entre el contenido de fragmentos de rocas y la conductividad hidráulica saturada del suelo mineral, el presente estudio se enfoca particularmente en investigar las trayectorias de flujo de agua en suelos de pendientes afectadas y no afectadas por derrumbes. Para esto, empleamos métodos convencionales de trabajo de campo y laboratorio, marcador trazador y técnicas de procesamiento de imágenes, tal como modelos estadísticos. Los resultados demuestran que el contenido de fragmentos de roca y la densidad del suelo, mantienen una influencia leve pero significativa sobre la conductividad hidráulica saturada del suelo mineral. Los experimentos de trazador y los parámetros de suelo documentaron una percolación vertical más profundo en las pendientes afectadas por derrumbes que en los suelos de pendientes no afectadas por derrumbes donde los flujos preferenciales se realizan en los macroporos con baja interacción con la matriz del suelo. Cerca de la superficie se encuentra una capa casi impermeable a lo largo del interfaz entre subsuelo y suelo superior que limita la percolación revelando prerequisites para flujos laterales a lo largo de la interfaz entre suelo mineral y capa organica. Estudios previos llevados a cabo en la misma área de investigación demuestran

indirectamente la existencia de dicho flujo lateral. Sin embargo, en ninguno de estos estudios se relacionó este flujo subsuperficial con ángulos particulares de la pendiente o altitudes. A causa de una carta digital de suelos recientemente publicada y en base a los resultados obtenidos de las pendientes no afectas por derrumbes, sabemos que particularmente en pendientes inclinadas menores de 30° que están por encima de 2100 m SNM, los prerequisites están dados para un flujo subsuperficial extendido. En cambio, en las pendientes afectadas por derrumbes estos prerequisites no están aún evidentes. De todas formas no podemos excluir la posibilidad de la presencia de un flujo subsuperficial en los suelos relativamente poco profundos en un terreno empinado con cantidades altas de lluvia durante todo el año. Por eso, y dado que los parámetros claves como permeabilidad del subsuelo, material parental, interceptación y evaporación están poco claros o se han investigado exclusivamente variables como la variabilidad espacial de la conductividad hidráulica, condujimos una serie de experimentos virtuales para evaluar la presencia potencial de un flujo subsuperficial en Cambisoles debajo de 2100 m SNM. En estos experimentos incluimos también la capa orgánica por su abundancia alta en el área de investigación, de la cual se estimaron parámetros hidráulicos a través de modelos numéricos inversos. Los experimentos virtuales se basaron en un modelo de elementos finitos bidimensionales que representó secuencialmente un transecto de ~54 m de largo debajo de la cobertura vegetal del bosque. A par de los parámetros de suelo, la evapotranspiración y la interceptación, este modelo englobó la variabilidad espacial de la conductividad hidráulica, el potencial de la matriz del suelo e incluso tendencias espaciales. Los resultados obtenidos de los experimentos virtuales aclaran la necesidad de tener un conocimiento profundo de dichos parámetros claves y la conceptualización de los procesos con la generación de escorrentía, tal como la activación de derrumbes, transporte de solubles y masa que están en el centro de la investigación.

Acknowledgements

Even though it is “just a doctoral thesis”, but for providing me the opportunity to enjoy the scientist’s life to the full, for his thought provoking critical comments and his support, I would like to express my sincere thanks to Prof. Dr. Bernd Huwe.

A special thank goes to Andreas Kolb for most challenging field work and his staying power, as well to Iris Schmiedinger, who patiently answered my questions regarding laboratory work. Moreover, I really appreciated the thrustworthy support of the Geogarage team, in particular for the laboratory irrigation device, which ensured to accomplish the organic layer experiments successfully.

People, who I surely will never forget and who made living at the station a little more familiar – the Feijóo family (Maria y hijos, Tati, Rocio y hijos), Abrahan Pacheco, Don Polivio, and Don Julio.

And I have to thank my colleagues Benjamin Leutner, Franz Cofrep, Lenin Salinas, Luis Balcazar, Pablo Viñan, and Peter Brandstetter, who helped me to move mountains of field-, laboratory- and computational work – thank you for supporting my plans even if kind of “wacky” sometimes!

Also, I gratefully appreciated the enlightening hours of talks and discussions concerning life – and work of course – with Alexandra Zach, Amelie Bucker, Florian Werner, Frank Haubrich, Guntars Martinsson, Kalle Dirl, Katrin Wolf, Reiner Zimmermann, and Thorsten Peters.

With time, my colleagues Christina Bogner, Mareike Liess and Marco Lara have become good friends with whom I shared good moments and fruitful discussions. I regret that the time we have spent together was too short.

Words are not sufficient to appreciate the patient company of my fiancé Daniela Ivonne Vazquez Quezada – I hope that our future life will give me the opportunity therefore!

After all, there are my parents who enabled, supported and encouraged me to walk the way I have chosen – what more can I say than thank you for this!

Table of contents

Summary	i
Zusammenfassung	iii
Resumen	v
Acknowledgements	vii
Table of contents	ix
List of figures	xiii
List of tables	xvi
List of abbreviations	xvii
List of symbols	xix
Chapter 1 General introduction	1
1.1 Hydrological studies in tropical environments, and newer concepts in vadose zone hydrology.....	2
1.2 Subsurface flow in mountainous environments.....	3
1.2.1 Subsurface flow driven by matrix flow	3
1.2.2 Subsurface flow driven by preferential flow	4
1.3 Objectives of this thesis	5
1.4 Study area.....	6
1.5 Synopsis	8
1.5.1 Flow paths in soils landslide affected and unaffected areas (Chapter 2, 3)	8
1.5.2 Hydrological parameterisation of the organic layer (Chapter 4).....	10
1.5.3 Assessing the occurrence of potential shallow subsurface flow in steep hillslopes below 2100 m ASL by virtual experiments (Chapter 5).....	11
1.5.4 Concluding remarks.....	13
1.6 Summary of the authors' contributions	15
1.7 References.....	17

Chapter 2	Flow paths in soils of landslide affected and unaffected hillslopes in a montane rain forest of South Ecuador, part A.....	25
	Abstract.....	26
	2.1 Introduction	27
	2.2 Materials and methods.....	28
	2.2.1 Study area	28
	2.2.2 Study sites.....	31
	2.2.3 Dye tracer experiment design.....	32
	2.2.4 Field sampling and laboratory analysis.....	32
	2.2.5 Image processing of dye stain patterns	33
	2.2.6 Analysis of binary images.....	34
	2.3 Results and discussion	35
	2.3.1 Young (YL) and old landslide (OL)	35
	2.3.2 Plateau area (PA).....	46
	2.4 Conclusions	47
	2.5 Acknowledgements.....	48
	2.6 References.....	48
Chapter 3	Flow paths in soils of landslide affected and unaffected hillslopes in a montane rain forest of South Ecuador, part B.....	55
	Abstract.....	56
	3.1 Introduction	56
	3.2 Materials and methods.....	58
	3.2.1 Study area	58
	3.2.2 Data basis	60
	3.2.3 Image processing and analysis of dye stain patterns	61
	3.2.4 Extreme value statistics.....	61
	3.2.5 Multivariate statistical analysis	63
	3.3 Results and discussion	65
	3.3.1 Extreme value statistics.....	65
	3.3.2 Multivariate statistical analysis	71

3.4 Conclusions	73
3.5 Acknowledgements	74
3.6 References.....	74
Chapter 4 Water flow in the organic layer of a tropical montane rainforest in southern Ecuador – an inverse modelling study	79
Abstract.....	80
4.1 Introduction	80
4.2 Materials and methods.....	83
4.2.1 Study area	83
4.2.2 Field sampling	84
4.2.3 Experimental design	85
4.2.4 Inverse modelling	87
4.2.4.1 Model approaches	87
4.2.4.2 Model design.....	90
4.2.5 Sensitivity analysis	90
4.3 Results and discussion	91
4.3.1 Sensitivity analysis	92
4.3.2 Inverse modelling: parameter estimation.....	94
4.3.3 Direct modelling.....	97
4.4 Conclusions	99
4.5 Acknowledgements	100
4.6 References.....	100
Chapter 5 A virtual experiment approach for assessing the spatiotemporal occurrence of lateral shallow subsurface flow in a steep forested hillslope transect in the Andes of South Ecuador	105
Abstract.....	106
5.1 Introduction	107
5.2 Materials and methods.....	110
5.2.1 Study area	110
5.2.2 Study site and acquisition of field data	111

5.2.2.1 Soil parameter and pressure heads	112
5.2.2.2 Climate data.....	113
5.2.3 Virtual experiment model design	113
5.2.4 Model input parameters: climate.....	115
5.2.5 Model input parameters: soil and organic layer	119
5.2.6 Spatial variability of the saturated hydraulic conductivity $K(h)$ and pressure head h	121
5.2.7 Acquisition of modelled data.....	126
5.3 Results	127
5.4 Discussion.....	137
5.5 Outlook and conclusions	139
5.6 Acknowledgements	140
5.7 References.....	140
Appendices	147
Appendix A List of other publications.....	147
Appendix B Content of data DVD.....	147
Declaration of authenticity.....	150
Erklärung.....	150

List of figures

Figure 1.1 The core area of the RBSF investigation area. Microcatchments are denoted by MC 1, MC 2 and MC 3. Altitudes are in m ASL. Coordinate system is UTM WGS84 17S.....	7
Figure 2.1 Map of the core RBSF investigation area. The closed triangles denote the locations of experimental plots. Microcatchments are denoted by MC 1, MC 2 and MC 3. Altitudes are in m ASL. Coordinate system is UTM WGS84 17S.....	30
Figure 2.2 (a) binary image of a dye tracer pattern. (b) Exemplary detail of an array output given by the Image Processing Toolbox (MathWorks, 2008a).	34
Figure 2.3 Percentages of fine soil fractions of sand, silt, and clay of the old landslide (a), young landslide (b), and plateau area (c)	40
Figure 2.4 Boxplots of Ksat, pF- and hydraulic capacity curves of the old landslide (a), young landslide (b), and plateau area (c)	41
Figure 2.5 Exemplary binary images, dye coverages and associated probability density functions (pdf) of the old landslide (OL), the young landslide (YL) and the plateau area (PA)	42
Figure 3.1 Core area of the RBSF investigation area. Except for PA 3, ... PA 6, the experimental plots described in section 3.2.1 were adopted from Bauer et al. (in review). Altitudes are in m ASL. Coordinate system is UTM WGS84 17S.....	59
Figure 3.2 Boxplots of the MC 2 data set comprising 22 measurements of the A-, 18 measurements for the B-, and 19 measurements of the C horizon distributed over 22 pits. (a) log of Ksat; (b) fine soil fractions; (c) fine soil bulk density; (d) rock fragment content; (e) altitude ASL	61
Figure 3.3 Boxplots of the mean maximum dye stain width (a), rock fragment content (b), counts of roots per dm ² (c), and fine soil bulk density (d).....	64
Figure 3.4 Exemplary binary images of the dye tracer distributions (black stains) and the corresponding dye coverage functions (open grey circles) derived from the experimental plots within the old landslide (OL), young landslide (YL), and plateau area (PA). The black lines designate the 1- <i>H</i> distributions fitted to the dye coverage functions.....	68
Figure 3.5 Exemplary probability density functions (= pdfs) corresponding to the binary images shown in figure 3.4, where 3.5a relates to 3.4i, 3.5b to 3.4j, and so on. We calculated the pdfs as seen in Bauer et al. (in review)	71

Figure 3.6 (a) Quantile-Quantile plot to test visually for normal distribution of the residuals; (b) residuals versus fitted logarithmic Ksat values [log(mm/h)]; (c) measured versus fitted logarithmic Ksat values [log(mm/h)]	73
Figure 4.1 Map of the core part of the RBSF investigation area. The sampling site is situated at the western part of MC 3 above 2120m ASL. Coordinate system is UTM WGS84 17S.....	82
Figure 4.2 Experimental set-up of the irrigator apparatus following Kosugi et al. (2001).....	85
Figure 4.3 Topography of the objective function along the parameter planes $\alpha - K_s$ (a), $\alpha - n$ (b), $n - K_s$ (c), $\theta_s - \alpha$ (d), and $\theta_s - n$ (e)	93
Figure 4.4 Results of the sensitivity analysis of the initial (INIT.) parameters against optimised (OPT.) parameters of the MvG approach.....	94
Figure 4.5 Exemplary drainage hydrographs obtained from the experiments P4 (a) and P8 (b) for discrete descending irrigation rates.....	95
Figure 4.6 Water retention functions (WRF, θ) and relative hydraulic conductivity functions (RHC, K_r) derived from the optimised and averaged parameter sets of the MvG (a) and DPD (b) approach.	97
Figure 4.7 Exemplary observed drainage hydrograph and irrigation levels of the validation from experiment P8 (a). Curves show model prediction of the MvG- and DPD approach, each with the final (a) and the averaged (b, parameters from P1, ... , P10) parameter set).....	98
Figure 5.1 Overview of the core area of the RBSF investigation site in South Ecuador. The black point north of MC 2 denotes the climate station. Altitudes are above sea level. Coordinate system is UTM WGS84 17S.....	111
Figure 5.2 Digital elevation map of microcatchment 2 with delineated positions of the plots as mentioned in the text. Altitudes are above sea level. Coordinate system is UTM WGS84 17S.	112
Figure 5.3 (a) 3D FE model of the slope at the western ridge of MC 2 between 2000 m and 2050 m ASL with viewing direction to SE; (b) 2D FE model derived from the 3D FE model as indicated in (a); (c) detail in the top left-hand corner shows positions of the soil horizons and the mesh structure.....	114
Figure 5.4 Diurnal variation of the canopy conductance (g_c) depending on the vapor pressure deficit (D) and the photosynthetic active radiation (PAR)	116

Figure 5.5 Hourly values of N_{field} recorded by the climate station delineated in figure 5.1. The grey lines below the precipitations denote the 95 % confidence intervals around the mean pressure head (black line)	118
Figure 5.6 Scaling factors [-] for $K^*(h^*)$ generated by RandomFields and transferred to the 3D FE mesh. The distribution is shown for the top layer of the organic layer (a), for the basal layers of the A horizon (b), B horizon (c), and C horizon (d).....	125
Figure 5.7 2D FE slope showing 14 observation nodes (white points). The observation nodes are situated 20 cm below the mineral soil surface. The detail in the top left-hand corner shows the soil horizons O, A, B, and C and positions of the depth ranges of the classes 1-3.....	126
Figure 5.8 Hourly mean values of the modelled pressure heads (black line) 15 cm below the mineral soil surface taken from the lower part of the modelled slope. The grey line delineates the alternating width of the 95 % confidence intervals of the daily pressure heads measured at the tensiometer plot (fig. 5.2). (a) modelled pressure heads from experiment I_a; (b) modelled pressure heads from experiment I_b.....	128
Figure 5.9 Summary of the saturation events in the 3 depth classes (defined in section 5.2.7) recorded over the ~16 month time series for the lower and the upper part of the model slope given for each model set-up.....	129
Figure 5.10 Summary of the spatiotemporal occurrence of saturation events given for the lower part of the modelled slope of the 6 model set-ups	133
Figure 5.11 Exemplary model runs of model set-ups I_b, I_c, II, and III_b. In the uppermost modelled slope of each column, scaling factors for the reference Ksat value are given. Below, a time series over half a day is shown for the pressure heads.....	135

List of tables

Table 2.1 Data from soil profile descriptions and laboratory analysis.....	36
Table 3.1 Results of the extreme value analysis	67
Table 3.2 Averaged fine soil fractions and bulk densities (= av. bd) of experimental plots within the plateau area.....	70
Table 3.3 Pearson’s correlation coefficients among soil parameters shown in figure 3.3.	72
Table 3.4 Summary of the multivariate linear regression of equation 3.....	72
Table 4.1 Summary of the 18 laboratory multi rate irrigation experiments including repetitions (= P*) and validation experiments (= Pv)	87
Table 4.2 Initial parameters provided for the MvG and DPD approach.....	90
Table 4.3 Mean and median of the optimised parameters θ_s [-], n [-], K_s [cm s-1], w_2 [-], α_2 [cm-1] and n_2 [-] of the MvG and DPD model approach as well as standard deviation, variation coefficient, minimum, maximum, and 95 % confidence intervals (CI). The repetitions P1*, P2* and P3* are not included.....	96
Table 5.1 Summary of the proportions of transpiration and evaporation from incident precipitation as found by Motzer (2003), Fleischbein et al. (2006), and Ösker (2008).....	109
Table 5.2 Summary of the reproduced percentages to N_{field} and absolute amounts of ET_{act} , E_{act} , and T_{act} of the corresponding researchers. The values refer to the time span between 09.01.2005 and 12.26.2006 provided in the virtual experiments.....	118
Table 5.3 van Genuchten-Mualem Parameters computed by Rosetta.....	120
Table 5.4 Overview of parameters used in RandomFields to produce isotropic Gaussian random fields of scaling factors for Ksat (= α_K).	122
Table 5.5 Summary of the virtual experiment model set-ups.	123

List of abbreviations

<i>abbreviation</i>	<i>meaning</i>
ACC	accumulation zone
AG	Arbeitsgruppe
ASL	above sea level
av. bd	averaged bulk density
bd	bulk density
DEM	digital elevation model
DEPL	depletion zone
DPD	double porosity model approach of Durner et al. (1999)
FE	finite element
HSI	Hue, Saturation, Intensity: parameters of a colour model
HOF	Hortonian overland flow
INIT.	initial parameter
Ksat	saturated hydraulic conductivity
max.	maximum
MC	microcatchment
min.	minimum
MvG	Mualem - van Genuchten model approach of Mualem (1976) and van Genuchten (1980).
O	organic layer
O/T	interface between organic layer and mineral topsoil
OL	old landslide
OL_ACC	accumulation zone old landslide
OL_DEPL	depletion zone old landslide
OPT.	optimised parameter
P	experiment for parameter optimisation
P*	repeated laboratory multi rate irrigation experiment
PA	plateau area
pdf	probability density function
pF	decadal logarithm of the absolute value of the soil matric potential
pHOF	pseudo Hortonian overland flow
Pv	validation experiments
P _w	weathered parent material

RBSF	Reserva Biológica San Francisco
RF	Gaussian random field
RGB	Red, Green, Blue: colours of an additive colour model
sd	standard deviation
SNM	sobre el nivel del mar
sSF	shallow subsurface flow
S/P	interface between mineral subsoil and weathered parent material
T	mineral topsoil
T/S	interface between mineral topsoil and mineral subsoil
ü. NN	über Normalnull
UTM	Universal Transverse Mercator
WGS84	World Geodetic System 1984
WRB	World Reference Base
YL	young landslide
YL_ACC	accumulation zone young landslide
YL_DEPL	depletion zone young landslide
2D	two dimensional
3D	three dimensional

List of symbols

L: length unit

M: mass unit

T: time unit

<i>symbol</i>	<i>definition</i>	<i>unit</i>
C_{Int}	canopy interception storage	[L]
$C_{Int(max)}$	maximum canopy interception storage	[L]
c_p	specific heat capacity at constant pressure	[J M ⁻¹ K ⁻¹]
D	saturated vapor pressure deficit	[hPa; L]
d_0	zero plane displacement height	[L]
d	depth	[L]
E_{act}	actual Evaporation	[L T ⁻¹]
E_{pot}	potential Evaporation	[L T ⁻¹]
ET_{pot}	potential evapotranspiration	[L T ⁻¹]
g_a	aerodynamic conductance	[L T ⁻¹]
g_c	the canopy conductance	[L T ⁻¹]
$gRad$	global radiation	[W L ⁻²]
h	pressure head [synon. matric potential]	[hPa; L]
h^*	reference pressure head	[hPa; L]
$K^*(h^*)$	reference hydraulic conductivity	[L T ⁻¹]
$K(h)$	hydraulic conductivity	[L T ⁻¹]
K_s	saturated hydraulic conductivity	[L T ⁻¹]
K_{sat}	saturated hydraulic conductivity	[L T ⁻¹]
l	tortuosity parameter	[-]
$L(\mu, \sigma)$	likelihood of a normal distribution	[-]
LAI	Leaf Area Index	[-]
ln, log	natural logarithm	[-]
log ₁₀	decadal logarithm	[-]
m, m_1, m_2	form parameter	[-]
n, n_1, n_2	form parameter	[-]
N_{field}	incident precipitation	[L T ⁻¹]
N_{net}	throughfall	[L T ⁻¹]

p	number of parameters	[-]
\bar{P}	mean percentage of stained pixels which are used to fit the 1- H distribution	[%]
PAR	photosynthetic active radiation	[$\mu\text{mol L}^{-2} \text{T}^{-1}$]
$P(d)$	percentage of stained pixels	[%]
$\hat{P}(d)$	estimated percentage of stained pixels in depth d	[%]
$p(d)$	number of stained pixels at depth d	[-]
p_{max}	maximum number of stained pixels at a certain depth d	[-]
$Q_{rad.net}$	radiation balance	[W L^{-2}]
Q_{soil}	soil heat flux	[W L^{-2}]
R^2	Coefficient of determination	[-]
r	Pearson's correlation coefficient	[-]
rH	relative humidity	[%]
RLD	root length densities	[L L^{-3}]
rRLD	relative root length densities	[-]
s	scale parameter	[-]
T	temperature	[K]
T_{act}	actual Transpiration	[L T^{-1}]
T_{pot}	potential Transpiration	[L T^{-1}]
V_w	wind velocity	[L T^{-1}]
w_2	weighting factor	[-]
x, y	Cartesian coordinates	[L]
Z_{rH}	measuring height of rH	[L]
Z_r	roughness parameter	[L]
Z_w	measuring height of V_w	[L]
$\alpha, \alpha_1, \alpha_2$	form parameter	[L^{-1}]
α_h	lognormal distributed scaling factor for the reference pressure head	[-]
$\alpha_{h_j TREND}$	lognormal distributed scaling factor for the reference pressure head with trend	[-]
α_K	normal distributed scaling factor for the reference Ksat	[-]
α_K^{TR}	lognormal distributed scaling factor for the reference Ksat	[-]
$\alpha_{K TREND}^{TR}$	lognormal distributed scaling factor for the reference Ksat	

	with trend	[-]
β_0	intercept	[-]
β_1, \dots, β_n	regression coefficients, where n is the number of predictors	[-]
Δ	slope of the vapor pressure deficit	[hPa K ⁻¹]
γ	psychrometer constant	[hPa K ⁻¹]
κ	Kármán constant	[-]
λ	latent heat of vaporisation	[J M ⁻¹]
μ	mean value	[L T ⁻¹]
θ_r	residual water content	[-]
θ_s	saturated water content	[-]
ρ_a	density of dry air	[M L ⁻³]
σ	standard deviation	[L T ⁻¹]
ξ_r	risk index according to Schlather and Huwe (2008)	[-]
ξ_T	transmissibility index	[-]

Chapter 1 General introduction

The current debate on the impact of global change on the biosphere is due to the novel, potentially devastating nature of “anthropogenic” climate change in many ecosystems. Human society associates high values with the biosphere, since it is the primary source of food, fiber, and clean water beside spiritual and other values which can be summarised as “ecosystem services” (Cramer, 2008). The loss of these important services will be disproportionately felt by the poor being most vulnerable to such environmental problems (World Resources Institute, 2005). Scholes and van Breemen (1997) state that global change consists primarily of three causally-linked aspects: land use change, atmospheric composition change and climate change. Demographic and economic factors will control the rate of these changes, whereas soil-, climate- and political factors will co-determine their location.

In the tropics, land use change will be the dominant driver of environmental change for the next several decades. It may comprise both fundamental change of vegetation cover including land degradation and deforestation (Cramer, 2008), or intensification of existing land use without substantial change in cover type. These factors can affect the functioning of tropical ecosystems, particularly processes related to carbon and nutrient assimilation and their interactions. Moreover, structure and productivity of especially subhumid- and dry tropic ecosystems are said to be very sensitive to changes in water balance, which could be caused by a combination of changes in precipitation and temperature (Scholes and van Breemen, 1997).

Given these widespread disturbances in the humid tropics, there is a demand to understand the intrinsic processes such as rainfall-runoff responses, flowpaths, and matter fluxes of relatively undisturbed ecosystems if land management strategies for this sensitive zone shall be sustainable (Bonell and Balek, 1993). Also, this would at least conserve ecosystem services such as water availability for human needs or hydropower (Célleri and Feyen, 2009), or fixing atmospheric carbon to biomass and soil (Letts, 2003). This applies particularly to tropical montane ecosystems, which are among the most sensitive environments to changes in climatic conditions as emphasized by Francou et al. (2000) for tropical glaciers, Ruiz et al. (2008) for high mountain ecosystems in Colombia, Soulsby et al. (1997) for a highly biodiverse montane rainforest catchment in Queensland, Australia, and Bruijnzeel (2004) for tropical montane cloud forests. The latter seems to be most vulnerable to global warming as these forests often occur on exposed ridges and mountain tops with shallow soils of limited storage capacity (Stadtmüller, 1987; Werner, 1988).

1.1 Hydrological studies in tropical environments, and newer concepts in vadose zone hydrology

Despite the topicality of the issue aforementioned, few studies were conducted within tropical environments concerning hydrological processes while most of them in tropical lowlands (e.g. Bonell and Gilmour, 1978; Bonell, 2004; Chappell and Sherlock, 2005; Elsenbeer et al., 1994; Noguchi et al., 1997a; Noguchi et al., 1997b; Dyke and Thornes, 2000). While for tropical montane environments the number of soil hydrological- and water cycle studies (e.g. Bogner et al., 2008a; Bruijnzeel, 2004; Caballero et al., 2002; Licata et al., 2008; Vanclay, 2009) remains scarce, first attempts of generalisations about magnitude and direction of water flow within specific soil groups in the lowland humid tropics were already made (e.g. Elsenbeer et al., 2001).

However, as tracer experiments found increasingly their way in soil hydrology, these generalisations became difficult to maintain as suggested by Chappell and Sherlock (2005). Their study revealed the lack of correspondence between observed tracer signals and conventional methods such as hydrometric predictions. For this reason, they emphasized the need for a much greater set of hillslope experiments, which must contain synchronous tracer studies in order to identify hillslope flow pathways and their physical controls in rain forests. In this respect, the advantages of dye tracer experiments have been emphasised in numerous soil hydrological studies, particularly in the past decade (e.g. Bogner 2009; Droogers et al., 1998; Flury et al., 1994; Germán-Heins and Flury, 2000; Kulli et al., 2003; Morris and Mooney, 2004; Noguchi et al., 1999; Weiler and Flühler, 2004; Li et al., 2009). Dye tracer experiments provide high resolution images of a relatively high spatial informative value (Öhrström et al., 2004). In combination with appropriate digital image processing methods as employed by Bogner (2009), Forrer et al. (2000), Schwartz et al. (1999), Weiler and Naef (2003), and Weiler and Flühler (2004) a relatively fast visualisation and identification of different forms of water flow regimes within the vadose soil zone. This qualitative information can be used to derive quantitative measures such as the dye coverage function (Flury et al., 1994) or dye stain widths (Weiler, 2001). More recent studies proposed to fit the the two parametric generalised Pareto distribution to the dye coverage function in order to assess the vulnerability of groundwater by pollutants (Schlather and Huwe, 2005), or to estimate a propagation index concerning solute transport in the soil (Bogner et al., 2008b).

Nevertheless, since the end of the International Hydrological Decade (= IHD, 1965-1974) the plenitude of hydrological field studies on hillslope processes in general have produced

barely generalisable results or definitions of suitable state variables in different environments (Weiler and McDonnell, 2004). The resulting lack of common conceptualisation in hillslope hydrology is reflected by the minimal transfer value among neighbouring hillslopes due to changing soil properties, slope- and bedrock topography for example. Based on this dilemma, Weiler and McDonnell (2004) promoted the idea of virtual experiments as a more appropriate tool that is considered as numerical experiments driven by collective field intelligence. Therefore, calibrating a model to field data and observations is not at first rank than usually applied in hillslope hydrology. The aim of virtual experiments is to clarify or at least to locate weak points within an existing perceptual- or numerical model by exploring the effect of individual parameters such as duration and frequencies of rainfall, canopy interception, soil properties, bedrock permeability and -topography, slope angle, and hillslope geometry (Hopp and McDonnell, 2009; Keim et al., 2006; Weiler and McDonnell, 2004, Weiler and McDonnell, 2006). Also, generalisations for the purpose of model simplification can be proven promptly (Weiler and McDonnell, 2004).

However, the relatively new concepts of virtual experiments and dye tracer studies have not yet been adopted or were sparsely adopted, respectively, to tropical montane ecosystems. In case of the tropical montane forest in the Reserva Biológica San Francisco (= RBSF) in South Ecuador (fig. 1.1), application of these methods and modelling concepts is therefore a challenging task, all the more due to the extraordinary high biodiversity, abiotic heterogeneities and their potential interactions (Beck et al., 2008).

1.2 Subsurface flow in mountainous environments

Shallow subsurface flow (= sSF) or subsurface stormflow is a frequent phenomenon in steep forested hillslopes (e.g. Bonell et al., 1998; Mulholland et al., 1990) and is seen as the main mechanism of runoff generation in many catchments worldwide (Weiler et al., 2005). It can also contribute to positive pore pressure development in steep hillslopes and thus to landslide initiation. It is furthermore seen as an important driver for flushing of labile nutrients, changes in water quality, and hydrograph response in streams.

1.2.1 Subsurface flow driven by matrix flow

Lateral matrix flow can occur as sSF, when areas close to saturation form a connected transient ground water body along the hillslope (Chappell et al., 1990; Jenkins et al., 1994). The occurrence of sSF is often linked to the decline of the hydraulic conductivity with

increasing soil depth. If amount and intensity of rainfall are sufficiently high to develop and rise a transient water table up to the higher permeable topsoil, sSF develops (DeWalle and Pionke, 1994). Weiler and McDonnell (2004) attributed this process, named transmissivity feedback by Rodhe (1987), particularly to glaciated till-mantled terrain, and more temperate as well subtropical areas with saprolite underlying the mineral soil cover.

Shallow subsurface flow that is caused by saturation excess does not depend primarily on precipitation intensity but on precipitation volume compared to Hortonian overland flow (= HOF) which is caused by infiltration excess (Scherrer et al., 2007). For the same reason, sSF can also occur along the interface between organic layer and unsaturated mineral soil due to highly contrasting saturated hydraulic conductivities. McDonnell et al. (1991) described this flow as pseudo Hortonian overland flow (= pHOF).

1.2.2 Subsurface flow driven by preferential flow

As observed by Beven and Germann (1982), and Mosley (1979, 1982) macropores play an constitutive role in draining hillslopes as corroborated by tracer experiments (Ghodrati and Jury, 1990; Flury et al., 1994; Weiler and Naef, 2003). Macropores augment the infiltration- and percolation rate as infiltrating water bypasses the soil matrix (Bronstert, 1999; Jones and Connelly, 2002).

In forested hillslopes preferential flow often prevails due to plant roots, root channels, and soil fauna providing macropores, in which water flows only under gravity. Macropores that extend more or less laterally along the hillslope may substantially contribute to runoff (Beven and Germann, 1982; Scherrer et al., 2007), which can be mitigated or negated if a permeable bedrock is present. According to Weiler et al. (2005), areas of higher permeability due to a coarse soil texture and larger pore space than the surrounding soil matrix are considered as well as preferential flow paths. This heterogeneous matrix flow is often attributed to high permeability layers in landslide debris, talus slopes, periglacial solifluction deposits, or unconsolidated moraine material.

The combination of vertical preferential flow paths and declining drainable porosity facilitates the rapid formation of subsurface flow (Weiler et al., 2005). If macropores are less in number and restricted to the topsoil, HOF can occur if water uptake by the soil matrix either at the soil surface or from the macropores is low (Scherrer et al., 2007). The reasons for a reduced interaction between soil matrix and macropore can be a high actual soil water content or a material related low hydraulic capacity of the soil. Conversely, the formation of

HOF or subsurface flow is delayed if interaction between macropores and soil matrix is high (Weiler et al., 2005).

1.3 Objectives of this thesis

Previous soil hydrological studies using different methods in landslide affected sites revealed mutually inconsistent results, while flow paths in soils of landslide unaffected hillslopes have not yet been investigated in detail. Therefore, in chapter 2 and 3 we combined conventional field- and laboratory methods with dye tracer experiments and statistical models to assess the flow regime in mineral soils of landslide affected and unaffected sites.

Particularly in the forested parts of the RBSF investigation area, mineral soils are almost entirely overlain by a thick organic layer that is assumed to have a moderating effect on lateral subsurface flow. To our knowledge, tropical montane organic layers have not yet been parameterised for hydrological modelling purposes. Therefore, in chapter 4 we employed a series of laboratory multi rate irrigation experiments in order to estimate the soil hydraulic parameters provided in the widely used model approach of van Genuchten (1980), and in the multi porosity model approach of Durner et al. (1999).

Basing on a recently published digital soil map and the results of chapter 2 and 3, it is suggested that particularly in landslide unaffected hillslopes of less than 30 ° above 2100 m above sea level (= ASL) prerequisites are given for shallow subsurface flow. However, even if these prerequisites are not evident for steeper hillslopes with different soil cover below 2100 m ASL, we cannot exclude the possibility of shallow subsurface flow occurrence here since soil cover of the steep terrain is relatively shallow while rainfall is high throughout the year. Therefore, in chapter 5 we performed a series of virtual experiments in order to assess the potential occurrence of shallow subsurface flow under varying hydrological key parameters in a steep hillslope below 2100 m ASL.

In general, present thesis aims to raise new aspects which may be considered in future conceptual and numerical models regarding the RBSF investigation area and similar tropical montane environments

1.4 Study area

All field work of this thesis was performed in the RBSF investigation area located between the province capitals Loja and Zamora in the Andes of South Ecuador (fig. 1.1). The RBSF area is situated within the deeply incised valley of the San Francisco river, which belongs to the eastern escarpment of the Cordillera Real forming a weather divide between the humid Amazon and the dry Inter-Andean region.

Within the RBSF study area, the southern valley side of San Francisco river is covered by mostly undisturbed mature forest, while at the northern side most of the forest had been converted to pastures by slash and burn (Beck et al., 2008). The mature forest on the southern valley side can be termed as evergreen montane rain forest (Balslev and Øllgaard, 2002) showing a fuzzy altitudinal zonation of evergreen lower (< 2150 m ASL) and upper broad-leaved montane rain forest, which gradually turns into sub-páramo shrubland between 2700 m and 3000 m ASL (Beck et al., 2008). Compared to lowland tropical rain forests, the canopy height of the RBSF investigation area usually do not exceed 20 m, whereas most of the rare bigger trees can be found in ravines (Müller-Hohenstein et al., 2004). Most important tree families are Clusiaceae, Chloranthaceae, Melastomataceae, Lauraceae and Arecaceae (Homeier et al., 2002) frequently bearing vascular epiphytes (Werner et al., 2005). The ground vegetation layer is dominated by ferns and large herbs (Homeier et al., 2002; Homeier, 2004; Paulsch, 2002).

The climate at the RBSF study area is determined by strong easterlies all over the year. Betimes, westerlies occur particularly during the austral summer (Beck et al., 2008). At the RBSF study area, the wetter months are between April and August, while rainfall is high throughout the year (Bendix et al., 2008). Average annual precipitation amounts 2050 mm at 1960 m ASL and 4400 mm at 3160 m ASL (Rollenbeck, 2006) while the mean annual air temperature ranges between 19.4 °C at the valley bottom and 9.4 °C at the highest elevations (Fries et al., 2009).

The geomorphological features of the RBSF investigation area originate from Pleistocene glacial processes, but are particularly linked to geological structures. Here, the bedrock belongs to the Chiguinda unit, a thick sequence of Paleozoic semipelites consisting of interbedded phyllites, metasandstones, and quartzites (Hungerbühler, 1997). As suggested by Sauer (1971), narrow ridges striking S-N and SSE-NNW originate from quartzite dikes, while the deeply incised V-shaped valleys from schist and phyllites. As a result of the predominance of steep slopes and the perhumid climate, the natural cover has been locally removed by shallow landslides which occur frequently within the RBSF study area.

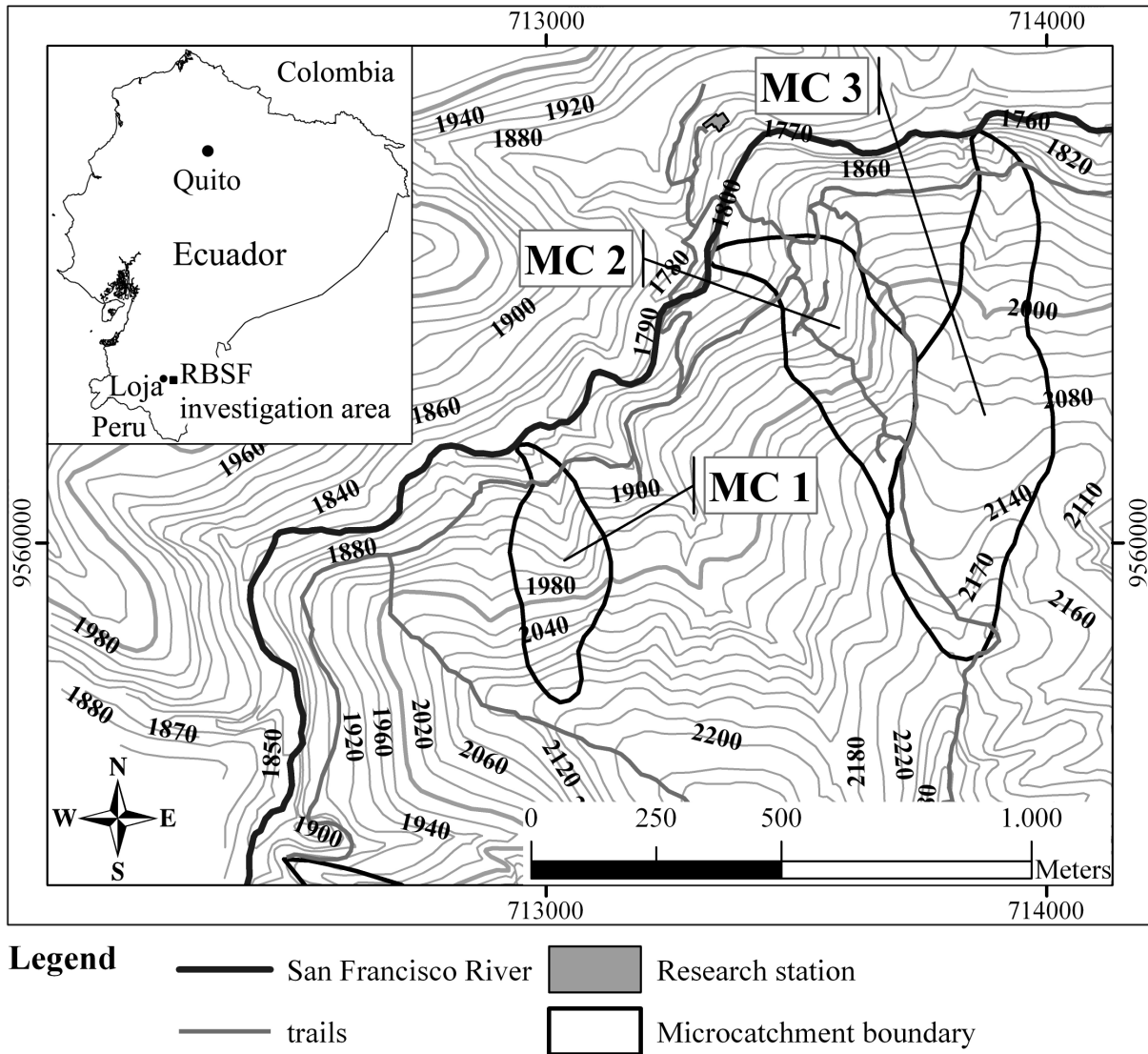


Figure 1.1 The core area of the RBSF investigation area. Microcatchments are denoted by MC 1, MC 2 and MC 3. Altitudes are in m ASL. Coordinate system is UTM WGS84 17S.

An analysis of aerial photographs taken in 1998 revealed that 3.7 % of the RBSF investigation area was covered by visible shallow landslides (Wilcke et al., 2003). Frequently, the landslide deposits resemble a melange of fine soil and variably high contents of rock fragments (up to 80 vol.-%) often bearing Cambisols and Regosols (IUSS, 2007) according to Schruppf et al. (2001), Wilcke et al. (2003), and Liess et al. (2009). More general, Liess et al. (2009) found that Histosols (IUSS, 2007) form the majority of soils under mature forest and natural vegetation, many of them with a stagnic colour pattern. In particular, below 2100 m ASL Cambisols and Regosols are relatively more represented than Stagnosols (IUSS, 2007). However, the coverage of the latter becomes more important within increasing altitude and decreasing slope angle (Liess et al., 2009). Therefore, the Stagnosols appear frequently at landslide unaffected sites usually showing rock fragment contents below 10 vol.-% (Beck et

al., 2008). In the following, we term the soils according to the World Reference Base for Soil Resources (IUSS, 2007).

As already indicated by the predominance of the Histosols, forest soils are generally overlain in sharp contrast by an organic layer. Its average thickness amounts 15 cm at 1900 m, 16 cm at 2400 m and 31 cm at 3000 m ASL (Soethe et al., 2006). Retarded microbial activity due to frequent saturation of the topsoil and a barely present soil fauna facilitates its accumulation up to 50 cm (Beck et al., 2008; Maraun et al., 2008; Schrumpf et al., 2001; Wilcke et al., 2002).

1.5 Synopsis

1.5.1 Flow paths in soils landslide affected and unaffected areas (Chapter 2, 3)

Previous numerical modelling studies of a stony Cambisol conducted by Bogner et al. (2008a) in the RBSF study area illustrated that rock fragments funnel the percolating water into preferential flow paths, whereas near the stones and especially in the gaps between them high flow velocities occur. Studies in other environments reported an increasing effect of the rock fragment content on the soil saturated hydraulic conductivity (= K_{sat}) due to additional lacunar pore space (Ravina and Magier, 1984; Sauer and Logsdon, 2002; Verbist et al., 2009) or decreased fine soil bulk density (e.g. van Wesemael et al., 2001).

Also, dye tracer studies of Bogner et al. (2008a) on a young and an old landslide with advanced vegetation succession revealed that pedogenetic processes and plant activity increase the occurrence of preferential flow paths. The implied difference in K_{sat} among the differently aged landslides could not be reproduced by Zimmermann and Elsenbeer (2008), whose conclusion bases on *in situ* K_{sat} measurements only. However, for interpreting purposes comparison of the results of both studies is ambitious, since both studies employed different methods. Moreover, Bogner et al. (2008a) did not designate the locations of the dye tracer experiments within the investigated landslides, while Zimmermann et al. (2008) conducted their measurements mainly directly below the landslide scar.

Regarding the inconsistency between both studies, we combined dye tracer experiments at pedon scale with soil profile descriptions and conventional laboratory- and field methods such as *in situ* K_{sat} measurements in order to visualise and quantify the flow regime in the depletion- and accumulation zone of two typical shallow landslides differing in age and

vegetation succession. We also apply these methods to landslide unaffected hillslopes of low inclination under mature forest, since flow paths there have not yet been studied in detail.

According to the image processing technique of Bogner (2009), we deskewed and converted the photographed dye stain patterns into binary images, which depict the dye tracer distribution by black pixels while all other colour information is replaced by white pixels. From the binary images we derived quantitative measures such as the dye coverage function (Flury et al., 1994) and dye stain widths (Weiler, 2001). We visualised the distribution of the dye stain widths with depth by probability density functions. More recent studies proposed to fit the two parametric generalised Pareto distribution to the dye coverage function in order to assess the vulnerability of groundwater by pollutants (Schlather and Huwe, 2005), or to estimate a propagation index concerning solute transport in the soil (Bogner et al., 2008b). For our purpose, we interpreted the two parameters of the generalised Pareto distribution as estimates, whether an impeding layer can be seen as impervious, or permits negligible or at least small amounts of water to percolate into deeper depths. We used these parameters and the probability density functions of the dye stain widths in combination with soil profile descriptions and measured soil properties in order to assess the water flow regime in soils of landslide affected and unaffected sites. Furthermore, with respect to the stony soils usually occurring in landslide affected sites we tested the hypothesis that rock fragment content and bulk density controls K_{sat} by applying multivariate linear regressions.

The results of the multivariate statistical analysis show that rock fragment content and bulk density controls significantly, although not largely the saturated hydraulic conductivity of the mineral soils. However, basing on measured soil parameters and the analysis of the binary images, we assume that at a distinct threshold between 50 vol.-% and 75 vol.-% the rock fragment content predominantly controls the permeability of the mineral soil cover due to an increasing amount of drainable pores, whereas the influence of the vegetation cover becomes less important. Beyond this threshold water flow appears as heterogeneous matrix flow in between the rock fragments while below in distinct flow paths such as root channels. Moreover, in the depletion zone of the young landslide, the mineral soil permeability seem to be also controlled by cracks and fissures, which we suggest to have been caused by slow movement of the mineral soil layer situated upon an impervious weathered bedrock. In the accumulation zone, percolation was predominantly impeded within the subsoil due to the sparse abundance of roots and root channels of the young vegetation cover, whereas the investigated mineral soils within the depletion and accumulation zone of the old landslide were throughout permeable with a permeable mineral soil/weathered bedrock interface.

In the landslide unaffected hillslopes above 2100 m ASL, water flow occurs mainly in macropores with low soil matrix interaction, while deeper percolation is restricted by a surface near impervious layer along the topsoil/subsoil interface. Therefore, in combination with a recently published digital soil map (Liess et al., 2009) we conclude that prerequisites are given at larger scales for lateral shallow subsurface flow along the interface between organic layer and mineral topsoil, which we denote as pseudo Hortonian overland flow following McDonnell (1991). This shallow subsurface flow was already suggested by Fleischbein et al. (2006) and Huwe et al. (2008), who reported considerably contrasting Ksat values between organic layer and mineral soil. Also, based on isotope signals and element concentration studies in receiving streams, Wilcke et al. (2008) corroborated the existence of this subsurface flow. Goller et al. (2005) attributed a moderating function to the organic layer to slow down the lateral shallow subsurface flow and to prevent flash floods.

1.5.2 Hydrological parameterisation of the organic layer (Chapter 4)

Despite of its importance, the organic layer have received little attention in hydrological research compared to numerous investigations concerning rainfall interception by the living vegetation (Walsh and Voigt, 1977).

In contrast to forests from lower tropical regions, densely rooted and thick organic layers are common in tropical montane forests (Grieve et al., 1990; Hafkenschied, 2000; Tanner et al., 1998). Also in the RBSF study area forest mineral soils are widely overlain in sharp contact by a well developed organic layer featuring high densities of living roots (Hertel et al., 2003). Retarded microbial activity due to frequent saturation of the topsoil and a barely present soil fauna facilitates its accumulation up to 50 cm (Beck et al., 2008; Maraun et al., 2008; Schrupf et al., 2001; Wilcke et al., 2002).

To our knowledge, tropical montane organic layers have not yet been parameterised for hydrological modelling purposes. Regarding this, even though the organic layer as found in the RBSF area certainly is a porous medium, it is not quite sure whether its hydraulic behaviour can be at least sufficiently described by the widely used Mualem-van Genuchten approach (van Genuchten, 1980).

Direct and indirect methods allow to estimate material functions of the organic layer, whereas direct methods are often time consuming and boundary conditions are difficult to control in the field. Since it is technically ambitious to measure the matric potential of highly porous forest floors, Kosugi et al. (2001) conducted laboratory experiments using a rainfall simulator to derive the corresponding water retention and hydraulic conductivity functions via

inverse modelling. This method allows a flexible design of the boundary conditions (Hopmans et al., 2002) which can be easily controlled in laboratory experiments (e.g. amount and duration of irrigation) under otherwise constant ambient conditions (e.g. temperature, negligible evaporation, no transpiration) for a series of experiments.

Therefore, we took undisturbed samples of organic layer of a mature forest for laboratory column experiments. We applied defined irrigation rates and fitted the observed drainage data by inverse numerical modelling in order to estimate the hydraulic parameters of the organic layer using the model approaches of van Genuchten (1980) and Durner et al. (1999). Additional validation experiments resulted in a high predictive power of the optimised parameter sets in terms of simulating water flow. Thus, both model approaches used are principally capable to describe water flow in the ecologically vital organic layer of the RBSF investigation area. Nevertheless, response-surface analyses and a sensitivity study identified the problem of having a non unique parameter set, which does not allow a physical interpretation of the optimised parameter sets. Furthermore, due to its high organic content we assume the organic layer to be hydrophobic, which is ambitious to assess by column experiments. Favoured by dry spells, the water repellency may produce different parameters than achieved in this study. However, for wetter periods in the RBSF study area we proposed the averaged parameter set of the Mualem-van Genuchten model, since it features an acceptable predictive power while low parameterisation is required.

1.5.3 Assessing the occurrence of potential shallow subsurface flow in steep hillslopes below 2100 m ASL by virtual experiments (Chapter 5)

As aforementioned, several authors having worked in the RBSF study area (Fleischbein et al., 2006; Goller et al., 2005; Huwe et al., 2008; Wilcke et al., 2008) indirectly provided evidence for sSF along the interface between organic layer and mineral topsoil. In none of these studies the sSF was assigned to a particular slope angle or altitude. In combination with the recently published digital soil map of Liess et al. (2009) the results of the dye tracer experiments described in chapter 2 and 3 revealed that sSF occurs particularly in gentle landslide unaffected areas above 2100 m ASL. However, even if these prerequisites are not evident for the Cambisols and Regosols often situated in landslide affected steeper slopes below 2100 ASL (e.g. Schrupf et al., 2001), we cannot exclude the possibility of shallow subsurface flow occurrence here due to the relatively shallow mineral soil cover and the incident rainfall being high throughout the year (Bendix et al., 2008). Consequently, and given that hydrological key parameters such as permeability of subsoil and bedrock, canopy interception

and evaporation remain unclear or were investigated exclusively such as the spatial variability of the saturated hydraulic conductivity (Zimmermann and Elsenbeer, 2008), we conducted a series of virtual experiments in order to assess the potential occurrence of sSF in Cambisols below 2100 m ASL considering varying hydrological key parameters.

For the virtual experiment series we present in chapter 5, we applied a two dimensional finite element model representing a steep hillslope transect of ~54 m length under mature forest. As a new approach regarding hydrological modelling in the RBSF study area, we parameterised the model with data obtained by collective field intelligence such as the horizon wise spatial variability of measured Ksat values including their spatial trends, soil properties, and the organic layer which we parameterised in chapter 3. We also included ecoclimate- and ecophysiological parameters by computing the diurnal variation of evapotranspiration using the Penman-Monteith approach (Monteith, 1965) and the canopy conductance measured by Motzer et al. (2005). Furthermore, in microcatchment 2 (= MC 2, fig. 1.1) within the past decade three researchers estimated highly differing amounts of water intercepted by and evaporated from the canopy. Moreover, contrary to the common assumption in hydrological science, decrease of the saturated hydraulic conductivity with depth was not significant as found by Zimmermann and Elsenbeer (2008) in MC 2 (fig. 1.1) and other sites in the RBSF study area.

In order to consider these key parameters simultaneously and investigate their influence on the spatiotemporal dynamic of the presumed sSF, we defined 6 different virtual experiment model set-ups, each with a defined set of key parameters. Each of 5 model set-ups comprised 15 model runs numbered from 1 to 15. Here, model runs with the same number had the same individual randomly assembled set of horizon wise spatial variabilities of Ksat and the pressure head (= h) in order to investigate their influence on the potential occurrence of sSF. For the same reason, we examined the effect of the stepwise reduction of the model by the spatial trends, and subsequently by the spatial variabilities of Ksat and h for which we used the 6th model set-up.

We tested the plausibility of the model by comparing the modelled tensiometric responses with measured values along a time series of ~16 months. It turned out that particularly during wetter periods the modelled soil pressure heads reproduced satisfactorily the measured values. Spatially extended subsurface flow within the mineral topsoil occurred due to saturation excess attributed to transmissivity feedback (Rodhe, 1987). Consequently, laterally routed soil water from the upper part of the modelled hillslope was required, which necessitated an

impervious bedrock. Spatially extended subsurface flow along the base of the organic layer due to infiltration excess of the mineral topsoil was not evident.

Contrary to the model set-up without spatial variabilities of K_{sat} , frequency and spatial extent of shallow subsurface flow was largely controlled by the spatial pattern of K_{sat} . The importance of the K_{sat} spatial variability was highlighted by the virtual experiment design, since within a model set-up fields of K_{sat} spatial variabilities were randomly combined horizon wise while all other key parameter were kept constant. Also, the frequency of the shallow subsurface flow was notably lowered if the spatial trend of K_{sat} was omitted, and many times over if the proportion of canopy evaporation was doubled.

In line with other virtual experiment studies (e.g. Hopp and McDonnell, 2009; Keim et al., 2006; Weiler et al., 2006) the results of this study highlight the crucial importance of the subsoil- and bedrock permeability, canopy interception and evaporation, and particularly the spatial variability of K_{sat} if process conceptualisation regarding storm runoff generation, landslide initiation, solute and matter transport at the hillslope scale is in the spotlight.

1.5.4 Concluding remarks

Investigating flow paths in an tropical montane ecosystem that is known as one of the hottest biodiversity hotspot worldwide is accordingly an ambitious challenge.

In the landslide unaffected sites, for example, within the same soil profile a matrix driven flow regime can exist aside a preferential driven flow regime depending on the status of vegetation succession, rock fragment content, cracks and fissures in the mineral soil cover caused by slow movement of the soil layer, and further parameters which are yet unknown. It becomes clear that these observations arise new questions resulting in high scientific efforts, which one discipline alone cannot afford. At least, an integrated interdisciplinary approach is necessary in order to highlight at least some crucial interactions between the variety of biotic and abiotic factors in this biodiversity hotspot, and which must be also frank to attend to new methods. Although not in highly diverse ecosystems, this approach has been already realised in hydrology resulting in the growing interest in ecohydrology as prognosticated by Nuttle (2002), and Porporato and Rodriguez-Iturbe (2002). Additionally, since the plenitude of experimental field studies on hydrological hillslope processes have produced sparse generalisable results or definition of suitable state variables in different environments, Weiler and McDonnell (2004) proposed the idea of virtual experiments to respond to this issue. More recent studies combined virtual experiments with ecohydrology such as Keim et al. (2006) who showed a smoothening effect of vegetation cover on the hydrological response to

General introduction – Synopsis

precipitation at hillslope scale, or Barnard et al. (2010) who attributed the transpiration on hillslopes to be important in diel variation in subsurface discharge in a mountainous area. All the more, it is reasonable to resort to virtual experiments in order to assess properly the intrinsic processes of an ecosystem instead of reproducing exactly what have been observed – particularly when hydrological key parameters such as the bedrock permeability or evapotranspiration are not thoroughly known as in the RBSF investigation area.

1.6 Summary of the authors' contributions

Present thesis comprises four articles. In the following, all authors having participated in the corresponding article are listed with their contribution in percent.

Manuscript 1

Authors	Folkert Bauer, Pablo Viñan, Luis Balcázar, Christina Bogner, Bernd Huwe		
Title	Flow paths in soils of landslide affected and unaffected hillslopes in a montane rain forest of South Ecuador, part A		
Status	in review		
Journal	Journal of Hydrology		
Contributions	Bauer	65 %	idea, methods, data collection, data analysis, figures, manuscript writing, manuscript editing, corresponding author
	Viñan	15 %	data collection, data processing
	Balcázar	05 %	data collection, data processing
	Bogner	05 %	data processing
	Huwe	10 %	idea, discussion, manuscript editing

Manuscript 2

Authors	Folkert Bauer, Luis Balcázar, Pablo Viñan, Christina Bogner, Jörg Zeilinger, Bernd Huwe		
Title	Flow paths in soils of landslide affected and unaffected hillslopes in a montane rain forest of South Ecuador, part B		
Status	in review		
Journal	Journal of Hydrology		
Contributions	Bauer	55 %	idea, methods, data collection, data analysis, figures, manuscript writing, manuscript editing, corresponding author
	Balcázar	15 %	data collection, data processing
	Viñan	05 %	data collection, data processing
	Bogner	05 %	data processing
	Zeilinger	10 %	data collection, data processing
	Huwe	10 %	idea, discussion, manuscript editing

Manuscript 3

Authors	Benjamin Leutner, Folkert Bauer, Bernd Huwe		
Title	Water flow in the organic layer of a tropical montane rainforest in southern Ecuador – an inverse modelling study.		
Status	in review		
Journal	Hydrological Processes		
Contributions	Bauer	45 %	idea, methods, data analysis, figures, manuscript writing, manuscript editing, corresponding author
	Leutner	45 %	data collection, data analysis, figures, manuscript writing
	Huwe	10 %	idea, discussion, manuscript editing

Manuscript 4

Authors	Folkert Bauer, Stefan Engelhardt, Jörg Zeilinger, Bernd Huwe		
Title	A virtual experiment approach for assessing the spatiotemporal occurrence of shallow subsurface flow in a steep forested hillslope transect in the Andes of South Ecuador.		
Status	in review		
Journal	Ecological Modelling		
Contributions	Bauer	75 %	idea, data analysis, model calculations, figures, manuscript writing, corresponding author
	Engelhardt	10 %	data collection
	Zeilinger	05 %	data collection
	Huwe	10 %	idea, discussion, manuscript editing

1.7 References

- Balslev, H., Øllgaard, B., 2002. Mapa de vegetación del sur de Ecuador, in: Aguirre, M.Z., Madsen, J.E., Cotton, E., Balslev, H. (Eds.), *Botanica Austroecuatorialiana. Estudios sobre los Recursos Vegetales en las Provincias de El Oro, Loja y Zamora-Chinchipe*, Quito, pp. 51-64.
- Barnard, H.R., Graham, C.B., Van Verseveld, W.J., Brooks, J.R., Bond, B.J., McDonnell, J.J., 2010. Mechanistic assessment of hillslope transpiration controls of diel subsurface flow: a steady-state irrigation approach. *Ecohydrol.* 3,133-142.
- Beck, E., Makeschin, F., Haubrich, F., Richter, M., Bendix, J., Valerezo, C., 2008. The Ecosystem (Reserva Biológica San Francisco), in: Beck, E., Bendix, J., Kottke, I., Makeschin, F., Mosandl, R. (Eds.), *Gradients in a Tropical Mountain Ecosystem of Ecuador*, Springer Verlag, Berlin, Heidelberg, pp. 1-14.
- Bendix, J., Rollenbeck, R., Richter, M., Fabian, P., Emck, P., 2008. Climate, in: Beck, E., Bendix, J., Kottke, I., Makeschin, F., Mosandl, R. (Eds.), *Gradients in a Tropical Mountain Ecosystem of Ecuador*, Springer Verlag, Berlin, Heidelberg, pp. 63-73.
- Beven, K. J., Germann, P., 1982. Macropores and water flow in soils, *Water Resour. Res.* 18, 1311-1325.
- Bogner, C., Engelhardt, S., Zeilinger, J., Huwe, B., 2008a. Visualisation and analysis of flow patterns and water flow simulations in disturbed and undisturbed tropical soils, in: Beck, E., Bendix, J., Kottke, I., Makeschin, F., Mosandl, R. (Eds.), *Gradients in a Tropical Mountain Ecosystem of Ecuador. Ecological Studies*, Springer, Berlin, pp 387-397.
- Bogner, C., Wolf, B., Schlather, M., Huwe, B., 2008b. Analysing flow patterns from dye tracer experiments in a forest soil using extreme value statistics. *Eur. J. Soil Sci.* 59(1), 103-113.
- Bogner, C., 2009. Analysis of flow patterns and flow mechanisms in soils. PhD thesis. URL <http://opus.ub.uni-bayreuth.de/volltexte/2009/607/> (accessed on July 2010), University of Bayreuth, Bayreuth.
- Bonell, M., Gilmour, D.A., 1978. The development of overland flow in a tropical rainforest catchment. *J. Hydrol.* 39, 365-382.
- Bonell, M., Balek, J., 1993. Recent scientific developments and research needs in hydrological processes of the humid tropics, in: *Hydrology and Water Management in the Humid Tropics*, Bonell, M., Hufschmidt, M.M., Gladwell, J.S. (Eds.), Cambridge University Press, Cambridge, pp. 167-260.
- Bonell, M., Barnes, C.J., Grant, C.R., Howard, A., Burns, J., 1998. High rainfall, response-dominated catchments: A comparative study of experiments in tropical northeast Queensland

- with temperate New Zealand, in: McDonnell J.J., Kendall C. (Eds.), *Isotope Tracers in Catchment Hydrology*. Elsevier Science Publishers, Amsterdam, pp 347-390.
- Bonell, M., 2004. Runoff generation processes in tropical forests in: Bonell, M., Bruijnzeel, L.A. (Eds.), *Forests, Water and People in the Humid Tropics*. Cambridge University Press, Cambridge, pp 314-406.
- Bronstert, A., 1999. Capabilities and limitations of detailed hillslope hydrologic modelling, *Hydrol. Process.* 13, 21-48.
- Bruijnzeel, L.A., 2004. Hydrological functions of tropical forests: not seeing the soil for the trees? *Agr. Ecosyst. Environ.* 104, 185-228.
- Caballero, Y., Jomelli, V., Chevallier, P., Ribstein, P., 2002. Hydrological characteristics of slip deposits in high tropical mountains (Cordillera Real, Bolivia). *Catena* 47, 101-116.
- Chappell, N.A., Ternan, J.L., Williams, A.G., Reynolds, B. 1990. Preliminary analysis of water and solute movement beneath a coniferous hillslope in mid-Wales, U.K. *J. Hydrol.* 116, 201-215.
- Chappell, N.A., Sherlock, M.D., 2005. Contrasting flow pathways within tropical forest slopes of Ultisol soils. *Earth Surf. Process. Landforms* 30, 735-753.
- Céleri, R., Feyen, J., 2009. The Hydrology of Tropical Andean Ecosystems: Importance, Knowledge Status, and Perspectives. *Mt. Res. Dev.* 29, 350-355.
- Cramer, W., 2008. Global change impacts on the biosphere, in: Jørgensen, S.E., and Fath, B.D. (Eds), *Global Ecology*. Elsevier, Oxford, pp. 1736-1741.
- DeWalle, D.R., Pionke, H.B., 1994. Stream low generation on a small agricultural catchment during autumn recharge; II. Stormflow periods. *J. Hydrol.* 163, 23-42.
- Droogers, P. Stein, A., Bouma, J., de Boer G., 1998. Parameters for describing soil macroporosity derived from staining patterns. *Geoderma* 83, 293-308.
- Durner, W., Priessack, E., Vogel, H.J., Zurmühl, T., 1999. Determination of Parameters for Flexible Hydraulic Functions by Inverse Modelling, in: van Genuchten, M.T., Leij, F.J., Wu, L. (Eds.), *Proceedings of the International Workshop on Characterization and Measurement of the Hydraulic Properties of Unsaturated Porous Media*. University of California, Riverside, USA, pp. 817-829.
- Dykes, A.P., Thornes, J.B., 2000. Hillslope hydrology in tropical rainforest steeplands in Brunei. *Hydrol. Process.* 14, 215-235.
- Elsenbeer, H., West, A., Bonell, M., 1994. Hydrological pathways and stormflow hydrochemistry at South Creek, N.E. Queensland. *J. Hydrol.* 162, 1-21.

- Elsenbeer, H. 2001., Hydrologic flowpaths in tropical rainforest soils - a Review. *Hydrol. Process.* 15, 1751-1759.
- Fleischbein, K., Wilcke, W., Valarezo, C., Zech, W., Knoblich, K., 2006. Water budgets of three small catchments under montane Forest in Ecuador: experimental and modelling approach. *Hydrol. Process.* 20, 2491-2507.
- Flury, M., Flühler, H., Jury, W.A., Leuenberger, J., 1994. Susceptibility of soils to preferential flow of water: a field study. *Water Resour. Res.* 30(7), 1945-1954.
- Forrer, I., Papritz, A., Kasteel, R., Flühler, H., Luca, D., 2000. Quantifying dye tracers in soil profiles by image processing. *Eur. J. Soil. Sci.* 51(2), 313-322.
- Francou, B., Ramirez, E., Cáceres, B., Mendoza, J., 2000. Glacier Evolution in the Tropical Andes during the Last Decades of the 20th Century: Chacaltaya, Bolivia, and Antizana, Ecuador. *Ambio* 29(7), 416-422.
- Fries, A., Rollenbeck, R., Göttlicher, D., Nauss, T., Homeier, J., Peters, T., Bendix, J., 2009. Thermal structure of a megadiverse Andean mountain ecosystem in southern Ecuador, and its regionalization. *Erdkunde* 63, 321-335.
- Germán-Heins, J., Flury, M., 2000. Sorption of brilliant blue FCF in soils affected by pH and ionic strength. *Geoderma* 97, 87-101.
- Ghodrati, M., Jury, W.A., 1990. A field study using dyes to characterize preferential flow of water. *J. Amer. Soc. Soil Sci.* 54, 1558-1563.
- Goller, R., Wilcke, W., Leng, M.J., Tobschall, H.J., Wagner, K., Valarezo, C., Zech, W., 2005. Tracing water paths through small catchments under a tropical montane rain forest in South Ecuador by an oxygen isotope approach. *J. Hydrol.* 308, 67-80.
- Grieve, I.C., Proctor, J., Cousins, S.A., 1990. Soil variation with altitude on Volcán Barva, Costa Rica. *Catena* 17, 525-534.
- Hafkenschied, R., 2000. Hydrology and biogeochemistry of tropical montane rain forests of contrasting stature in the Blue Mountains, Jamaica. PhD thesis, Free University of Amsterdam, Amsterdam.
- Hertel, D., Leuschner, C., Holscher, D., 2003. Size and structure of fine root systems in old growth and secondary tropical montane forests (Costa Rica). *Biotropica* 35, 143-153.
- Homeier, J., Dalitz, H., Breckle, S.W., 2002. Waldstruktur und Baumartendiversität im montanen Regenwald der Estación Científica San Francisco in Südecuador. *Berichte der Reinhold Tüxen Gesellschaft* 14(1), 109-118.
- Homeier, J., 2004. Baumdiversität, Waldstruktur und Wachstumsdynamik zweier tropischer Bergregenwälder in Ecuador und Costa Rica. *Dissertationes Botanicae*, Berlin.

- Hopmans, J.W., Šimůnek, J., Romano, N., Durner, W., 2002. Inverse Methods, in: Dane, J.H., Topp, G.C. (Eds.), *Methods of Soil Analysis, Part 4 - Physical Methods*. SSSA, Madison, pp. 879-898.
- Hopp, L., McDonnell, J.J., 2009. Connectivity at the hillslope scale: Identifying interactions between storm size, bedrock permeability, slope angle and soil depth. *J. Hydrol.* 376, 378-391.
- Hungerbühler, D., 1997. Neogene basins in the Andes of southern Ecuador: evolution, deformation and regional tectonic implications. PhD thesis. URL <http://e-collection.ethbib.ethz.ch/view/eth:40985> (accessed on July 2010), ETH Zürich, Zürich.
- Huwe, B., Zimmermann, B., Zeilinger, J., Quizhpe, M., Elsenbeer, H., 2008. Gradients and patterns of soil physical parameters at local, field and catchment scales, in: Beck, E., Bendix J., Kottke, I., Makeshin, F., Mosandl, R., (Eds.), *Gradients in a Tropical Mountain Ecosystem of Ecuador*. Ecological Studies, Springer, Berlin, Heidelberg, 198, 375-387.
- IUSS Working Group WRB., 2007. World Reference Base for Soil Resources 2006, first update 2007. World Soil Resources Reports No. 103. FAO, Rome.
- Jenkins, A., Ferrier, R.C., Harriman, R., Ogunkoya, Y.O., 1994. A case study in catchment hydrochemistry: Conflicting interpretations from hydrological and chemical observations. *Hydrol. Processes* 8, 335-349.
- Jones, J.A.A., Connelly, L.J., 2002. A semi distributed simulation model for natural pipe flow. *J. Hydrol.* 262, 28-49.
- Keim, R.F., Meerveld, H., McDonnell, J.J., 2006. A virtual experiment on the effects of Evaporation and intensity smoothing by canopy interception on subsurface stormflow Generation. *J. Hydrol.* 327, 352-364.
- Kosugi, K., Mori, K., Yasuda, H., 2001. An inverse modelling approach for the characterization of unsaturated water flow in an organic forest floor. *J. Hydrol.* 246(1-4), 96-108.
- Kulli, B., Gysi, M., Flühler, H., 2003. Visualizing soil compaction based on flow pattern analysis. *Soil Till. Res.* 70(1), 29-40.
- Letts, M.G., 2003. Carbon Assimilation and Productivity in a North-west Andean Tropical Montane Cloud Forest. PhD thesis. URL <http://people.uleth.ca/~matthew.letts/letts%20thesis%202003.pdf> (accessed on July 2010), Kings College London, London.
- Li, X.Y., Yang, Z.P., Li Y.T., Lin, H., 2009. Connecting ecohydrology and hydrogeology in desert shrubs: stemflow as a source of preferential flow in soils. *Hydrol. Earth Syst. Sci.* 13, 1133-1144.

- Licata, J.A., Gyenge, J.E., Fernandez M.E., Schlichter, T.M., Bond, B.J., 2008. Increased water use by ponderosa pine plantations in northwestern Patagonia, Argentina, compared with native forest vegetation. *For. Ecol. Manage.* 255(3), 753-764.
- Liess, M., Glaser, B., Huwe, B., 2009. Digital Soil Mapping In Southern Ecuador. *Erdkunde* 63(4), 309-319.
- Maraun, M., Illig, J.D., Sandman, D., Krashevskaya, V., Norton, R.A., Scheu, S., 2008. Soil Fauna, in: Beck, E., Bendix, J., Kottke, I., Makeschin, F., Mosandl, R. (Eds.), *Gradients in a Tropical Mountain Ecosystem of Ecuador*, Springer Verlag, Berlin, Heidelberg, pp. 181-192.
- McDonnell, J.J., Owens, I.F., Stewart, M.K., 1991. A case study of shallow flow paths in a steep zero-order basin. *Water Resour. Bul.* 27, 679-685.
- Morris, C., Mooney, S.J., 2004. A high-resolution system for the quantification of preferential flow in undisturbed soil using observations of tracers. *Geoderma* 118, 113-143.
- Mosley, P.M., 1979. Stream low generation in a forested watershed, New Zealand. *Water Resour. Res.* 15, 795-806.
- Mosley, P.M., 1982. Subsurface flow velocities through selected forest soils, South Island, New Zealand. *J. Hydrol.* 52, 321-335.
- Motzer, T., Munz, N., Küppers, M., Schmitt, D., Anhof, D., 2005. Stomatal conductance, transpiration and sap flow of tropical montane rain forest trees in the southern Ecuadorian Andes. *Tree Physiol.* 25, 1283-1293.
- Mulholland, P.J., Wilson, G.V., Jardine, P.M., 1990. Hydrogeochemical response of a forested watershed to storms: effects of preferential flow along shallow and deep pathways. *Wat. Resour. Res.* 26, 3021-3036.
- Müller-Hohenstein, K., Paulsch, A., Paulsch, D., Schneider, R., 2004. Vegetations- und Agrarlandschaftsstrukturen in den Bergwäldern Südecuadors. *Geogr. Rund.* 56, 48-55.
- Noguchi, S., Nik, A.R., Kasran, B., Tani, M., Sammori, Z., Morisada, K., 1997a. Soil physical properties and preferential flowpaths in tropical rainforest, Bukit Tarek, Peninsular Malaysia. *J. Forest Res.* 2, 115-120.
- Noguchi, S., Nik, AR., Yusop, Z., Tani, M., Sammori, Z., 1997b. Rainfall-runoff responses and roles of soil moisture variations in tropical rainforest, Bukit Tarek, Peninsular Malaysia. *J. Forest. Res.*
- Noguchi, S., Tsuboyama, Y., Sidle, R.C., Hosoda, I., 1999. Morphological Characteristics of Macropores and the Distribution of Preferential Flow Pathways in a Forested Slope Segment. *Soil Sci. Soc. Am. J.* 63, 1413-1423.
- Nuttle, W.K., 2002. *Eco-hydrology's Past and Future in Focus*. American Geophysical Union

Eos 83:205, 211, and 212.

Öhrström, P., Hamed, Y., Persson, M., Berndtsson, R., 2004. Characterizing unsaturated solute transport by simultaneous use of dye and bromide. *J. Hydrol.* 289, 23-35.

Paulsch, A. 2002. Development and application of a classification system for undisturbed and disturbed tropical montane forests based on vegetation structure. PhD thesis. URL <http://opus.ub.uni-bayreuth.de/volltexte/2002/1/> (accessed on July 2010), University of Bayreuth, Bayreuth.

Porporato, A., Rodriguez-Iturbe, I., 2002. Ecohydrology – a challenging multidisciplinary research perspective. *Hydrological Sciences – Journal – des Sciences Hydrologiques* 47(5).

Ravina, I. and Magier, J., 1984. Hydraulic conductivity and water retention of clay soils containing coarse fragments. *Soil Sci. Soc. Am. J.* 48: 736-740.

Rodhe A., 1987. The Origin of Streamwater Traced by Oxygen-18. PhD thesis, Uppsala University, Uppsala.

Rollenbeck R., 2006. Variability of precipitation in the Reserva Biológica San Francisco / Southern Ecuador. *Lyonia* 9(1), 43-51.

Ruiz, D., Moreno, A.H., Gutiérrez, M.E., Zapata, P.A., 2008. Changing climate and endangered high mountain ecosystems in Colombia. *Sci. Total Environ.* 398(1), 122-132.

Sauer, W., 1971. Geologie von Ecuador. Beiträge zur regionalen Geologie der Erde, vol. 11. Bornträger, Berlin.

Sauer, T.J., Logsdon, S.D., 2002. Hydraulic and Physical Properties of Stony Soils in a Small Watershed. *Soil Sci. Soc. Am. J.* 66:1947-1956.

Scherrer, S., Naef, F., Faeh, A.O., Cordery, I., 2007. Formation of runoff at the hillslope scale during intense precipitation. *Hydrol. Earth Syst. Sci.* 11, 907-922.

Schlather, M., Huwe, B., 2005. A risk index for characterising flow pattern in soils using dye tracer distributions. *J Contam Hydrol* 79, 25-44.

Scholes, R.J., van Breemen, N., 1997. The effects of global change on tropical ecosystems. *Geoderma* 79, 9-24.

Schrumpf, M., Guggenberger, G., Schubert, C., Valarezo, C., Zech, W., 2001. Tropical montane rain forest soils: development and nutrients status along an altitudinal gradient in the south Ecuadorian Andes. *Die Erde* 132, 43-59.

Schwartz, R.C., McInnes, K.J., Juo, A.S.R., Reddell, D.L., Wilding, L.P., 1999. Boundary effects on solute transport in finite soil columns. *Water Resour. Res.* 35, 671-681.

Soethe, N., Lehmann, J., Engels, C., 2006. The vertical pattern of rooting and nutrient uptake at different altitudes of a south Ecuadorian montane forest. *Plant and Soil* 286(1-2), 287-299.

- Soulsby, C., Pomeroy, A., Gibbins, C., 1997. Hydrology and hydrochemistry of a montane rainforest catchment in Queensland, Australia, in: Peters, N.E. and Coudrain-Ribstein, A. (Eds), Hydrochemistry Symposium, Int. Assoc. Hydrol. Sci., Rabat, Morocco.
- Stadtmüller, T., 1987. Cloud Forests in the Humid Tropics. A Bibliographic Review. United Nations University, Tokyo, and CATIE, Turrialba, Costa Rica
- Tanner, E.V.J., Vitousek, P.M., Cuevas, E., 1998. Experimental investigation of nutrient limitations of forest growth on wet tropical mountains. *Ecology* 79, 10-22.
- van Genuchten, M.Th., 1980. A closed-form equation for predicting the hydraulic conductivity of unsaturated soils. *Soil Sci. Soc. Am. J.* 44, 892–898.
- van Wesemael, B., Mulligan, M., Poesen, J., 2001. Spatial Patterns in Water Use Efficiency Created by Intensive Cultivation on Semi-arid Hillslopes, in: Stott, D.E., Mohtar, R.H., Steinhardt, G.C. (Eds.), Selected papers from the 10th International Soil Conservation Organization Meeting, May 24-29, 1999, West Lafayette, IN. International Soil Conservation Organization in cooperation with the USDA and Purdue University, West Lafayette, IN. URL <http://topsoil.nserl.purdue.edu/nserlweb-old/isco99/pdf/ISCOdisc/SustainingTheGlobalFarm/P056-Wesemael.pdf> (accessed July 2010).
- Vanclay, J.K., 2009. Managing water use from forest plantations. *For. Ecol. Manage.* 257(2), 385-389.
- Verbist, K., Baetens, J., Cornelis, W.M., Gabriels, D., Torres, C., Soto, G., 2009. Hydraulic Conductivity as Influenced by Stoniness in Degraded Drylands of Chile. *Soil. Sci. Soc. Am. J.* 73, 471-484.
- Walsh, R.P.D., Voigt, P.J., 1977. Vegetation Litter - Underestimated Variable in Hydrology and Geomorphology. *J. Biogeogr.* 4(3), 253-274.
- Weiler, M., 2001. Mechanism controlling macropore flow during infiltration - dye tracer experiments and simulation. PhD thesis. URL <http://e-collection.ethbib.ethz.ch/eserv/eth:24150/eth-24150-02.pdf> (accessed on June 2010), ETH Zürich, Zürich.
- Weiler, M., Naef, F., 2003. An experimental tracer study of the role of macropores in infiltration in grassland soils. *Hydrol. Process.* 17(2), 477-493.
- Weiler, M., Flühler, H., 2004. Inferring flow types from dye patterns in macroporous soils. *Geoderma*, 120(1-2), 137-153.
- Weiler, M., McDonnell, J.J., 2004. Virtual experiments: a new approach for improving process conceptualization in hillslope hydrology. *J. Hydrol.* 285, 3-18.

General introduction – References

- Weiler, M., McDonnell, J.J., Tromp-van Meerveld, I., Uchida, T., 2005. Subsurface Stormflow, in: Anderson, M.G, McDonnell, J.J. (Eds.), *Encyclopedia of Hydrological Sciences*, John Wiley & Sons 3, 1719-1732.
- Weiler, M., McDonnell, J.J., 2006. Testing nutrient flushing hypotheses at the hillslope scale: A virtual experiment approach. *J. Hydrol.* 319, 339-356.
- Werner F.A., Homeier, J., Gradstein, S.R., 2005. Diversity of vascular epiphytes on isolated remnant trees in the montane forest belt of southern Ecuador. *Ecotropica* 11, 21-40.
- Werner, W.L., 1988. Canopy dieback in the Upper Montane rain forests of Sri Lanka. *GeoJournal* 17, 245–248.
- Wilcke, W., Yasin, S., Abramoski, U., Valarezo, C., Zech, W., 2002. Nutrient storage and turnover in organic layers under tropical montane rainforest in Ecuador. *Eur. J. Soil. Sci.* 5(1), 15-27.
- Wilcke, W., Valladarez, H., Stoyan, R., Yasin, S., Valarezo, C., Zech, W., 2003. Soil properties on a chronosequence of landslides in montane rain forest, Ecuador. *Catena* 53, 79-95.
- Wilcke, W., Yasin, S., Fleischbein, K., Goller, R., Boy, J., Knuth, J., Valarezo, C., Zech, W., 2008. Water Relations, in: Beck, E., Bendix, J., Kottke, I., Makeschin, F., Mosandl, R. (Eds.), *Gradients in a Tropical Mountain Ecosystem of Ecuador*. Ecological Studies, Springer, Berlin, pp. 193-201.
- World Resources Institute, 2005. *Millennium ecosystem assessment - ecosystems and human well-being: biodiversity synthesis*. IslandPress, Washington D.C.
- Zimmermann, B., Elsenbeer, H., 2008. Spatial and temporal variability of soil saturated hydraulic conductivity in gradients of disturbance. *J. Hydrol.* 361, 78-95.

Chapter 2 Flow paths in soils of landslide affected and unaffected hillslopes in a montane rain forest of South Ecuador, part A

Folkert Bauer ^{1,*}, Pablo Viñan ², Luis Balcázar ², Christina Bogner ³, and Bernd Huwe ¹

¹ Department of Soil Physics, University of Bayreuth
Universitätsstraße 30
95440 Bayreuth, Germany

² Universidad Nacional de Loja,
Loja, Ecuador

³ Ecological Modelling
Dr. Hans-Frisch-Straße 1-3
95448 Bayreuth, Germany

* corresponding author

Email: folkert.bauer@googlemail.com

phone: +49 921 55 2193; fax: +49 921 55 2246

in review at *Journal of Hydrology*

Abstract

Experimental studies identifying hydrological flow paths in soils of tropical montane forests are scarce. Increasing pressure of deforestation by land use change, however, demands further knowledge to contribute to the understanding of forest disturbance effects on rainfall-runoff response, flow paths, and matter fluxes. Also in the Andes of South Ecuador, deforestation has become an increasing problem. Here, in the investigation area of the Reserva Biológica San Francisco between 1800 m and 2100 m above sea level (= ASL) soils of steep slopes often developed from landslide deposits resembling a melange of fine soil and high rock fragment content. Above 2100 m ASL, gentle hillslopes are widely covered by soils with stagnant moisture features and low to negligible rock fragment contents. To date, flow paths in these soils have not yet been investigated in detail while results of previous soil hydrological studies in landslide affected sites are not mutually consistent. In order to elucidate this discrepancy and to elaborate eventual differences between landslide affected and unaffected sites, we combined dye tracer experiments with conventional field- and laboratory methods. From digitised dye tracer patterns we derived quantitative measures such as dye coverage functions and probability density functions of dye stain widths with depth, which we related to physical and hydrological soil properties and profile descriptions. Results show that in the investigated landslide unaffected sites prerequisites are clearly given for rapid shallow subsurface flow since percolation is mainly controlled by root channels with low soil matrix interaction and restricted to the shallow mineral topsoil. Concerning the landslide affected sites, we assume that at a distinct threshold between 50 vol.-% and 75 vol.-% of rock fragment content the permeability of the mineral soil cover increases due to an increasing amount of drainable pores, whereas the influence of the vegetation cover becomes less important. Below this threshold, water flow occurs along distinct structures such as root channels. Moreover, this study opens new starting points for further investigations in terms of bedrock permeability, and parameters controlling the occurrence of cracks and fissures in soils within landslide affected sites.

Keywords: tropical montane forest, hillslope hydrology, landslides, flow path, dye tracer

2.1 Introduction

In the tropics, land use change will be the dominant driver of environmental change for the next several decades. It may comprise both fundamental change of vegetation cover including land degradation and deforestation (Cramer, 2008). It is therefore necessary to understand the intrinsic processes of undisturbed ecosystems if the perturbing effects of future land management strategies on rainfall-runoff responses, flowpaths, and matter fluxes should be minimal as possible (e.g. Bonell and Balek, 1993).

This applies particularly to tropical montane ecosystems, which are among the most sensitive environments to changes in climatic conditions as shown by Francou et al. (2000), Ruiz et al. (2008), Soulsby et al. (1997), and Bruijnzeel (2004). Nevertheless, the number of studies (e.g. Bruijnzeel, 2004; Licata et al., 2008; Vanclay, 2009) having reported on the hydrology and water cycle in Andean montane forests is small, while first attempts of generalisations about magnitude and direction of water flow within specific soil groups in the lowland humid tropics were already made (e.g. Elsenbeer et al., 2001).

With the increasing application of tracer experiments in soil hydrology these generalisations became difficult to maintain as suggested by Chappell and Sherlock (2005). They emphasise the need for a much greater set of hillslope experiments, which must contain synchronous tracer studies in order to identify hillslope flow pathways and their physical controls. For the same reasons numerous studies (e.g. Bogner 2009; Bouma and Dekker, 1978; Droogers et al., 1998; Flury et al., 1994a; Kulli et al., 2003; Kung, 1990; Morris and Mooney, 2004; Noguchi et al., 1999; Weiler, 2001; Weiler and Flühler, 2004) recognised dye tracer experiments as an adequate tool to investigate hydrological processes in the vadose zone. While small scale heterogeneities and their spatial extent are difficult to detect using conventional methods such as soil core samples, dye tracer experiments provide additional information in form of high resolution images of dye stain patterns in a comparatively larger soil volume (Öhrström et al., 2004).

In the Reserva Biológica San Francisco (= RBSF) located in the Andes of South Ecuador, Bogner et al. (2008) conducted dye tracer experiments on a young landslide and an old landslide with advanced vegetation succession. They could show that pedogenetic processes and plant activity increase the occurrence of preferential flow paths. However, the implied difference in the soil saturated hydraulic conductivity (= K_{sat}) among the differently aged landslides could not be reproduced by Zimmermann and Elsenbeer (2008), whose conclusion were based on *in situ* K_{sat} measurements only which they have mainly conducted directly at the landslide scars. Moreover, numerical simulation studies of a stony Cambisol conducted by

Bogner et al. (2008) revealed that a high rock fragment content funnel the percolating water into preferential flow paths with high flow velocities near the stones and especially in the gaps between them. Other studies in different environments have reported an increasing effect of the rock fragment content on the soil hydraulic conductivity due to additional lacunar pore space (Ravina and Magier, 1984; Sauer and Logsdon, 2002; Verbist et al., 2009) or decreased fine soil bulk density (Poesen and Lavee, 1994; Torri et al., 1994; van Wesemael et al., 2001). In this context, in the RBSF investigation area landslides are a common phenomenon mainly initiated by the combination of steep relief and long lasting rainfalls (Ohl and Bussmann, 2004; Stoyan, 2002; Wilcke et al., 2003). Stoyan (2002) and Wilcke et al. (2003) classify these landslides as an intermediate stage between translational debris slides and rapid earth flows. They are typically shallow and can be divided into an upper mass depletion zone and a lower accumulation zone. The landslide deposits resemble frequently a melange of fine earth soil and high alternating contents of phyllites, metasiltstones, and sandstones differing in size and shape. Thus, compared to mineral soil without or low rock fragment contents, in the landslide deposits higher permeability due to a lower bulk density of the fine soil may be expected.

In order to solve the discrepancy between the findings of Bogner et al. (2008) and Zimmermann and Elsenbeer (2008), a direct comparison between the study results may be meaningful but is not possible since both studies employed different methods, which were applied a different sites within the investigated landslides.

For this reason, we combine dye tracer experiments at pedon scale with profile descriptions and conventional field- and laboratory methods in order to visualise and describe the flow regime in the depletion and accumulation zone of two typical shallow landslides differing in age and vegetation succession. We also apply these methods to a landslide unaffected hillslope of low inclination under mature forest with a relative high abundance of Stagnosols (IUSS, 2007), since flow paths in these soils have not yet been investigated in detail.

2.2 Materials and methods

2.2.1 Study area

The RBSF study area (fig. 2.1) is located at the eastern slope of the „Cordillera Real“, a weather divide between the humid Amazon and the dry Inter-Andean region, in the Andes of South Ecuador between the province capitals Loja and Zamora. The RBSF area extends over

11.2 km² and an altitudinal gradient from 1800 m to 3160 m ASL and is characterised by steep slopes (30 ° - 50 °). The area is divided by the deeply incised SW-NE striking San Francisco river valley. Its southern side is covered by mostly undisturbed mature forest, while at the northern side the forest had been converted to pastures by slash and burn (Beck et al., 2008).

The RBSF mature forest cover can be termed as evergreen montane rain forest (Balslev and Øllgaard, 2002) featuring a fuzzy altitudinal zonation of evergreen lower (< 2150 m ASL) and upper broad-leaved montane rain forest, which gradually turns into sub-páramo shrubland between 2700 m and 3000 m ASL (Beck et al., 2008). Most important tree families are Clusiaceae, Chloranthaceae, Melastomataceae, Lauraceae and Arecaceae (Homeier et al., 2002) frequently bearing vascular epiphytes (Werner et al., 2005). The ground vegetation layer is dominated by ferns and large herbs (Homeier et al., 2002; Paulsch, 2002; Homeier, 2004).

For the most time of the year, the climate at the RBSF study area is determined by strong easterlies (Beck et al., 2008). The wetter months are between April and August, while rainfall is high throughout the year (Bendix et al., 2008). Average annual precipitation amounts 2050 mm at 1960 m ASL and 4400 mm at 3160 m ASL (Rollenbeck, 2006), while the mean annual air temperature ranges between 19.4 °C at the valley bottom and 9.4 °C at the highest elevations (Fries et al., 2009).

The bedrock of the RBSF study area belongs to the Chiguinda unit, a thick sequence of Paleozoic semipelites consisting of interbedded phyllites, metasandstones, and quartzites (Hungerbühler, 1997). As suggested by Sauer (1971), narrow ridges striking S-N and SSE-NNW originate from quartzite dikes, while the deeply incised V-shaped valleys from schist and phyllites. Due to the predominance of steep slopes and the perhumid climate the natural cover has been locally removed by shallow landslides. The landslide deposits often feature a melange of fine soil and variably high contents of rock fragments (up to 80 vol.-%) and often resemble Cambisols and Regosols (Schrumpf et al., 2001; Wilcke et al., 2003).

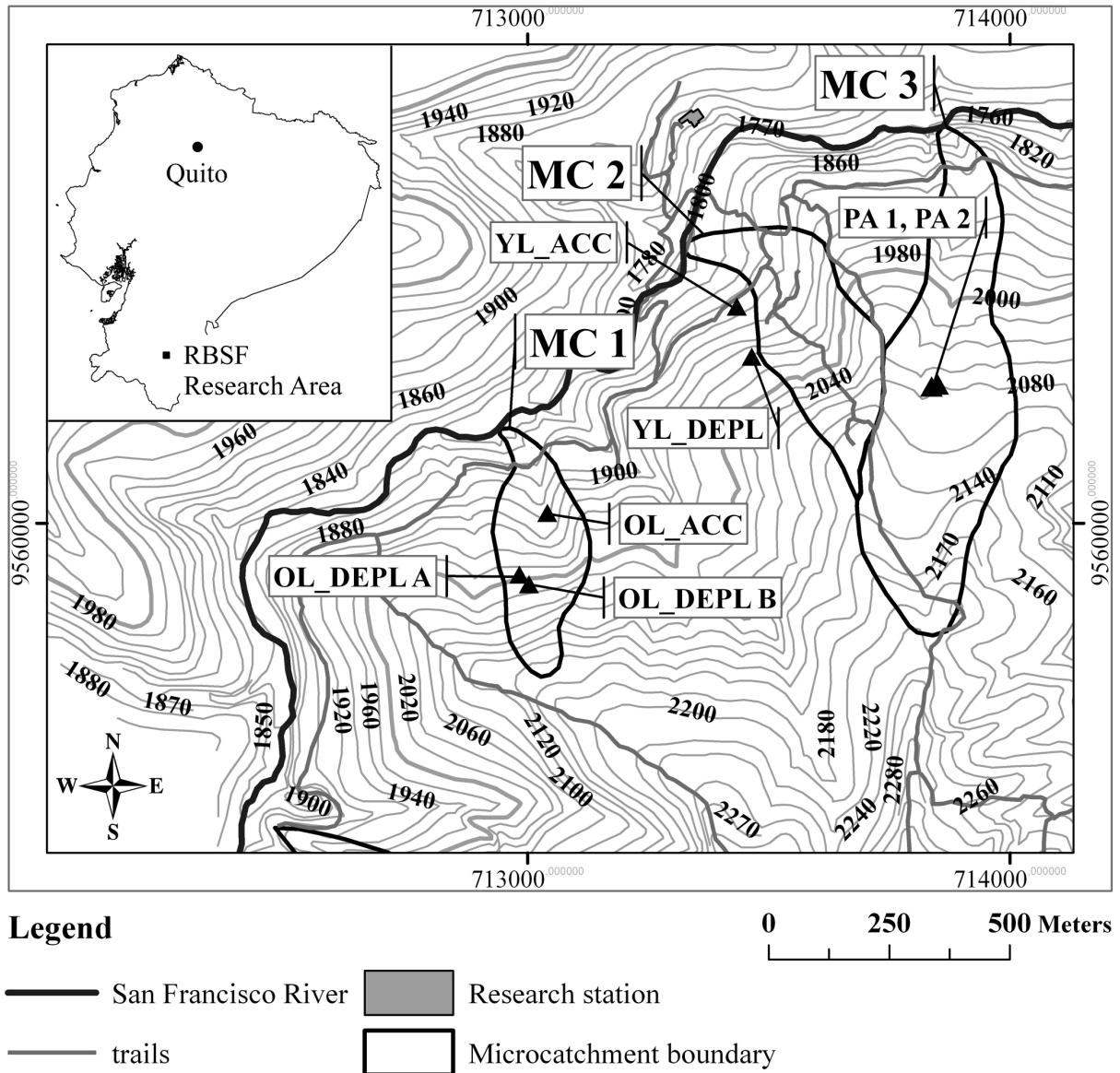


Figure 2.1 Map of the core RBSF investigation area. The closed triangles denote the locations of experimental plots. Microcatchments (= MC) are denoted by MC 1, MC 2 and MC 3. Altitudes are in m ASL. Coordinate system is UTM WGS84 17S.

Throughout the RBSF study area, Liess et al. (2009) found Histosols (IUSS, 2007) being most abundant under mature forest and natural vegetation, many of them with a stagnic colour pattern. More particular, below 2100 m ASL the abundance of the Cambisols and especially Regosols exceeds the presence of Stagnosols. With increasing altitude the presence of the Cambisols and Regosols (IUSS, 2007) decreases for the benefit of Stagnosols. Often, Stagnosols occur at landslide unaffected sites and feature usually rock fragment contents below 10 vol.-% (Beck et al., 2008). In the following, we term the soils according to the World Reference Base for Soil Resources (IUSS, 2007).

2.2.2 Study sites

The experimental plots within we conducted the pedon scale dye tracer experiments, soil sampling, and Ksat measurements were situated on the southern side of the San Francisco valley between 1900 m and 2100 m ASL (fig. 2.1). Below 2050 m ASL, we selected two shallow landsides as they typically occur within the RBSF investigation area. Two dye tracer experiments were conducted on a young landslide (= YL) formed in 1998, where the first experiment was situated within the accumulation (= YL_ACC, fig. 2.1) and the second in the depletion zone (= YL_DEPL, fig. 2.1). This configuration was adopted to an old landslide (= OL) situated within microcatchment 1 (= MC 1), where the accumulation zone is denoted as OL_ACC and the depletion zone as OL_DEPL (fig. 2.1). Within the latter, we conducted two dye tracer experiments denoted as OL_DEPL A and OL_DEPL B (fig. 2.1), which were ~20 m far from each other. This was necessary, since the considerably high rock fragment content at OL_DEPL and the thin mineral soil layer at OL_DEPL A complicated realisation of the dye tracer experiments. For the same reason, it was not possible for us to take undisturbed soil core samples from both OL_DEPL A and OL_DEPL B in order to estimate the soil moisture characteristics. Therefore, we resorted to soil moisture characteristics and fine earth soil fractions sampled and determined by Markwardt (2005) from a closely situated soil profile within OL_DEPL. Aerial photos revealed that the old landslide must have been formed before 1962. Soil profile surveys featured at least two verifiable slide events.

The vegetation cover at YL_ACC consisted of herbage, fern and bushes accompanied by a patchy abundance of an organic layer of less than 10 cm. With the onset of YL_DEPL the vegetation cover thins out leaving space for a patchy light grass cover and bare soil incrustated by lichens and mosses. An organic layer was not developed. At OL_ACC, secondary forest with closed canopy prevailed aging between 20 and 25 years. The mineral soil was entirely covered by at least a 10 cm thick organic layer. At OL_DEPL bushes, grasses, and particularly fern predominated aside few single young trees. An organic layer was throughout present with thicknesses between a few cm under grass and up to 50 cm under fern cover.

As landslide unaffected we considered the upper part of MC 3 between 2050 m and 2100 m ASL with slope angles ranging between 5 ° and 15 ° (fig. 2.1). For the following, we call this part plateau area (PA), where we performed two dye tracer experiments named PA 1 and PA 2 (fig. 2.1) in a mature forest. The canopy was relatively open while the shrub layer considerably dense consisting mainly of Bromeliaceae and Orchidaceae. The organic layer averaged a thickness of 33 cm.

2.2.3 Dye tracer experiment design

For the purpose to visualise potential lateral flow paths such as macropore networks or less permeable or impervious layers in this steep environment, for each experiment we applied a total amount of 200 l of a Brilliant Blue FCF solution ($c = 10 \text{ g/l}$) in 1.5 hours using a fixed line source sprinkler. A similar sprinkler design was used by Noguchi et al. (1999) in order to investigate lateral flow paths at pedon scale. The sprinkler we used consisted of a water conducting tube with diameter and length of 2.54 cm and 1.5 m, respectively. Without moving or turning the tube, the dye tracer solution was applied on the ground surface by six fan nozzles installed equidistantly from each other along the tube. The range between the nozzles and the ground surface averaged 30 cm to achieve a nearly homogeneous wetting of the irrigated area comprising $\sim 20 \text{ cm} \cdot \sim 170 \text{ cm}$. During irrigation we kept the pumping rate constant. The mean of the matric potential decadal logarithm (= pF) of the soils before irrigation were between $\text{pF} = 2$ and $\text{pF} = 2.5$ at OL_ACC, OL_DEPL A and OL_DEPL B, $\text{pF} = 1.42$ at YL_ACC, $\text{pF} = 1.21$ at YL_DEPL, $\text{pF} = 0.71$ at PA 1, and $\text{pF} = 1.34$ at PA 2.

We used Brilliant Blue FCF as dye tracer due to its low toxicity and good visibility against the background colour of most soils (Flury and Flühler, 1994b; Germán-Heins and Flury, 2000). After irrigation, each plot was covered immediately by a 3 m x 3 m plastic tarp to prevent infiltration of subsequent rainfall. On the following day we started to open the pit with the first soil profile 200 cm downslope and parallel the line source sprinkler. The 2th, 3rd and subsequent profiles followed in steps of 20 cm towards the sprinkler. In some cases we had to excavate in somewhat larger steps if big rock fragments occurred.

Each soil profile was marked with an equilibrated 1 m^2 square frame and photographed with a Nikon Coolpix 4500 digital camera having applied a resolution of $2272 \cdot 1704$ pixel. The frame was placed in such a manner that visually most of the stained part of the soil profile was encompassed by the frame.

2.2.4 Field sampling and laboratory analysis

From the middle soil profile of each pit, i.e. $\sim 1 \text{ m}$ downslope from the irrigator soil samples were taken, if possible horizon wise. Except from PA 1 and PA 2, rock fragment content was generally high. Consequently, we could take soil core samples of 100 cm^3 only at spots where no rock fragments occurred, and where the soil macro structure enabled sampling of undisturbed cores.

For the water content at pressure head $\text{pF} = 4.2$ (applying overpressure in a pressure pot, threefold repetition) and texture analysis we took disturbed samples at the same spots and

around, respectively. The water contents of the undisturbed samples were evaluated at pressure heads $pF = 0, 0.5, 1, 1.5$ and 2 applying the hanging water column method. For each horizon or depth range, we estimated the soil water retention curve (= pF curve) by fitting the measured retention data using the model approach of van Genuchten (1980) implemented in RETC, ver. 6.0 (van Genuchten et al., 1998), a software to analyse the soil water retention and hydraulic conductivity functions of unsaturated soils. After 48 h of drying at $105\text{ }^{\circ}\text{C}$, bulk densities were determined from the undisturbed soil samples. We obtained the grain size distribution by wet sieving of the sand fraction and by the sedimentation/aliquot-weighting method after Köhn (1928) for the silt- and clay fraction. We classified the fine soil fractions between 2 mm and 0.063 mm for Sand, between 0.063 mm and 0.002 mm for silt, and smaller than 0.002 mm for clay.

From the first, middle and last soil profile of each pit we performed a soil description after AG Boden (2005). Since there were no obvious differences between the profiles within a pit, we merged the data for reasons of clarity. K_{sat} was measured *in situ* within a radius of $\sim 5\text{ m}$ around the pedon scale experiments using an Amoozometer for practical reasons (Amoozegar, 1989a; Amoozegar, 1993). By means of Glover's equation (Amoozegar, 1989b) we computed the final K_{sat} values.

2.2.5 Image processing of dye stain patterns

Before converting the profile colour photographs to binary images, we corrected the lens- and perspective distortion using the software PTLense (Niemann, 2008) and HALCON (MVTec Software GmbH, 2005), respectively. As applied by Bogner (2009) we classified the Brilliant Blue distribution in stained and non stained areas by transforming the profile photos from RGB to HSI (Hue, Saturation, Intensity: parameters of a colour model) colour space. The latter allows segmentation of the desired colour range by applying a lower and an upper threshold. Between, the colour values representing stained pixels are decoded as black pixels and the unstained as white (fig. 2.2a, b). Misclassification due to shadows or rock fragments were corrected manually. For better orientation and to avoid misinterpretation, we levelled unevenness of the mineral soil surface by cutting and set the cutting edge as reference depth with 0 cm .

2.2.6 Analysis of binary images

From the binary images (fig. 2.2a) we used for qualitative description of the dye patterns, we derived the dye coverage function (Flury et al., 1994a) using the Image Processing Toolbox (The MathWorks, 2008a) provided in the Matlab software (The MathWorks, 2008b). As we have decoded a black pixel as “1” and a white as “0” (fig. 2.2b), for each row we simply computed the sum of “1”. Its portion on the number of all pixels within the row is expressed as percentage as exemplarily illustrated at the right margin of figure 2.2b. By multiplying each row with the virtual height of a pixel and adding up the rows from the upper to the lower edge of the binary image we assigned the stained pixel percentage of each row to its corresponding real depth in cm related to the 1 m² square frame. The virtual height of a pixel was computed by dividing the height of the frame (in our case 100 cm) by the number of all pixel within a column, i.e. along the vertical axis.

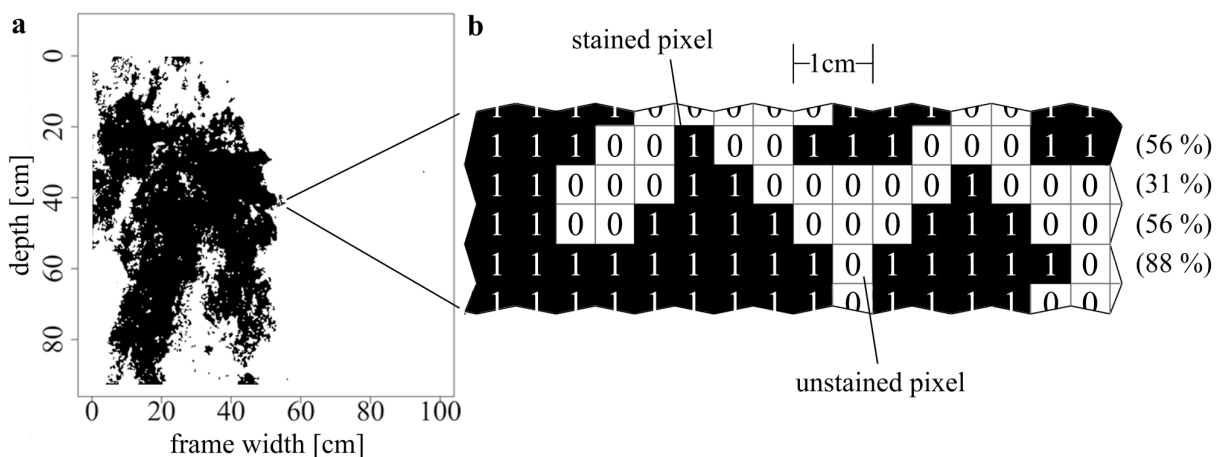


Figure 2.2 (a) Binary image of a dye tracer pattern. (b) Exemplary detail of an array output given by the Image Processing Toolbox (MathWorks, 2008a). Black pixels are decoded as “1”, white as “0”. Left: percentages of black pixels within each row. For reasons of simplicity, in this example 1 cm equals two pixels. Thus, the first row contain each two times the “1 cm” and the “2 cm” width class, the second row three times the “1 cm” width class, and so on.

We furthermore quantified the horizontal stain widths depicted on a binary image (fig. 2.2a) by probability density functions (= pdf) in depth increments of 2 cm. In each pixel row a sequence of „1“, delimited by „0“, is interpreted as a stain width as exemplarily shown in figure 2.2b. Via Matlab, for each row we computed the length of each sequence by simply summarising the „1“. By multiplying each sum with the virtual width of a pixel (computed by dividing the width of the frame, i.e. 100 cm, by the maximum number of pixel along the horizontal axis) we converted the widths to centimetre relative to the 1 m² frame. Now, each row can be seen as a vector containing the magnitudes of the stain widths. Consequently, each

row exhibits a distribution of stain widths, which we classified in increments of 1 cm thus achieving width classes of $0 \text{ cm} \leq 1 \text{ cm}$, $1 \text{ cm} \leq 2 \text{ cm}$, ..., $99 \text{ cm} \leq 100 \text{ cm}$. For the purpose of clarity, we computed the arithmetic mean of the countings of each width class over increments of 2 cm along the vertical axis resulting in depth steps of $0 \text{ cm} \leq 2 \text{ cm}$, $2 \text{ cm} \leq 4 \text{ cm}$, ..., $98 \text{ cm} \leq 100 \text{ cm}$. Consequently, the sum of all countings of any depth increment equals 1, we calculated (1):

$$\frac{1}{n} \sum_{i=1}^k n_i = 1, \quad 1$$

where k is the maximum number of width classes, n the sum of countings of width classes within a depth increment, and n_i the countings of the i^{th} width class.

2.3 Results and discussion

According to AG Boden (2005) the soil texture of the investigated soil profiles within the landslides OL and YL can be classified as silt loam and in the plateau area PA as sandy loam. In all soil profiles we did not encounter animal burrows nor a notable soil fauna, e.g. earth worms, ants or termites. Except for PA 1 and PA 2 within the plateau area, all investigated soil profiles generally featured rock fragment contents of more than 30 vol.-% comprising a mixture of angular, weakly metamorphic siltstones and phyllites mainly sizing between 2 mm and 63 mm in diameter up to individual rock fragments of maximum 40 cm. The landslides presented in this paper were not triggered by human impact.

2.3.1 Young (YL) and old landslide (OL)

The topsoil- and subsoil Ksat values we measured in OL_ACC and OL_DEPL (fig. 2.4a) are considerably higher than those of YL_ACC and YL_DEPL (fig. 2.4b), from where we obtained less steep pF curves and higher bulk densities (tab. 2.1) implying rather impeding subsoils. Most of the dye coverages from YL_ACC (fig. 2.5d) show a strong decrease of the stained pixel percentage from the soil surface below 20 cm depth accompanied by a decrease of the root density (tab. 2.1) and dye stain widths (fig. 2.5d). Thus, the rather matrix driven flow regime at the topsoil converts to a bypass dominated flow regime in the subsoil. However, in some profiles in YL_ACC between 20 cm and 50 cm depth this bypass flow was interrupted by remnants of a buried A horizon mixed with an organic layer (tab. 2.1) being almost throughout stained (fig. 2.5e).

Table 2.1 Data from soil profile descriptions and laboratory analysis.

^a horizon	^b depth [cm]	^c colour	^d rock fragment content [vol.-%]	^d counts of roots per dm ²	bulk density ±stand. dev. [g/cm ³]	ⁱ n
OL_ACC; Cambisol (skeletic, siltic) ^a						
Ah	40-50	10YR 4/3	50	6-10	1.20 ±0.16	11
Bw	75-90	2.5 Y 5/4	65	3-5	1.45 ±0.15	9
C	>120	10 YR 5/4	80	1-2 (until 90 cm depth)	1.54 ±0.10	15
slope: ~35 °; aspect: NW						
OL_DEPL A; Regosol (skeletic, siltic) ^a						
C	5-20	10 YR 3/3	50	6-10	0.92 ±0.11 ^h	3
2C	>80	2.5 Y 6/4	res. rock structure	1-2 (until 30 cm depth)	1.27 ±0.02 ^h	2
slope: ~30 °; aspect: NE						
OL_DEPL B; Cambisol (skeletic, siltic, novic) ^a						
Ah	10-25	10 YR 3/3	30	6-10	0.93 ±0.09 ^h	5
Ahb	20-50	10 YR 2/2	75	6-10	n.d. ^g	
Bwb	35-65	10 YR 4/3	75	3-5	1.28 ±0.07 ^h	2
Bwb-C	65-75	10 YR 4/6	80	3-5	1.19 ±0.19 ^h	3
C	>80	n.d. ^g	residual rock structure	1-2 ^e (until 80 cm depth)	n.d. ^g	
slope: ~30 °; aspect: N						
YL_ACC; Haplic Regosol (skeletic, siltic) ^a						
A ^e	1-10	10 YR 4/4	30	6-10	0.85 ±0.12	5
Ob+Ahb ^e	20-50	7.5 YR 3/3	n.d.	50+6-10	0.68 ±0.25	4
C	>80	2.5 Y 6/3	50	3-5 (until 30 cm depth) 1-2 ^e (until 50 cm depth)	1.59 ±0.07	5
slope: ~25 °; aspect: NE						
YL_DEPL; Haplic Regosol (skeletic, siltic) ^a						
C	0-25 25-60	10 YR 5/4	50	3-5 ^e 1-2 ^e	1.46 ±0.14	5
2C	>60	2.5 Y 6/3	residual rock structure	0	1.73 ±0.09	5
slope: ~35 °; aspect: N						
PA 1; Histic Stagnosol (albic, endosiltic) ^a						
E	0-10 10-20	7.5 YR 3/1 7.5 YR 5/1	<5	3-5 1-2	0.96 ±0.10 1.74 ±0.10	5 5
Bg	20-35 35-60	7.5 YR 7/1 5 YR 6/8	<5	0	1.22 ±0.07 1.03 ±0.04	5 7
C	> 80	n.d. ^g	residual rock structure	0	n.d. ^g	
slope: ~5 °; aspect: N						
PA 2; Histic Stagnosol (albic, endosiltic) ^a						
E	0-10 10-25	10 YR 3/1 7.5 YR 4/1	<5	3-5 1-2	1.25 ±0.17 1.71 ±0.04	5 4
Bg	25-40	10 YR 8/8	<5	0	1.64 ±0.15	5
C	> 80	n.d. ^g	residual rock structure	0	n.d. ^g	5
slope: ~5 °; aspect: NNE						

^a after IUSS (2007) // ^b soil depth indicates depth range of lower horizon boundary // ^c wet, after Munsell soil colour chart (1994) // ^d after AG-Boden (2005), approximated lower limiting values // ^e patchy occurrence // ^g n.d. = no data // ^h some samples contained small rock fragments // ⁱ number of bulk density samples

We attribute these remnants to a former soil surface, which was covered by a subsequent landslide event. Furthermore, in YL_ACC we found in two successive profiles ~ 180 cm far from the line source irrigator a vertical crack several cm thick reaching at least until 100 cm depth, which was traced by the dye as shown in figure 2.5f. Also at YL_DEPL we encountered dye tracer patterns that reproduced a preferential flow path network as shown by the binary images of figure 2.5k and 2.5l. Since the vegetation cover in YL_DEPL consisted only of some patches of light grass, but mainly lichens and mosses we exclude the possibility that these preferential flow paths were mainly formed by plant roots. Between 40 cm and 50 cm depth the flow path network abruptly declines figure (2.5k, l) due to an impervious weathered bedrock underlying the shallow mineral soil layer. We attribute this preferential flow path network to fissures, which we suggest to have been caused by a slow movement of the shallow mineral soil layer due to the high slope inclination of ~35 ° at YL_DEPL and the impervious weathered bedrock below enabling the formation of a perched water table. We also attribute the vertical cracks in YA_ACC to slow movement of the mineral soil layer. In the plots of the old landslide, we did not encounter such distinct structures.

Assessing the role of vegetation succession

The difference in the vegetation succession levels between YL_ACC and YL_DEPL are reflected by the lower topsoil bulk densities (tab. 2.1) and higher topsoil hydraulic capacities (fig. 2.4b) in YL_ACC that revealed a more advanced vegetation succession than YL_DEPL. Moreover, we can exclude textural differences of the fine earth fractions due to the high coincidence between accumulation and depletion zone (fig. 2.3b). However, the effect of the vegetation succession in the topsoil properties is not reflected by the topsoil Ksat values being higher at YL_DEPL than at YL_ACC (fig. 2.4b). We suggest this discrepancy to be caused by the fissure network at YL_ACC being visualised by the dye stain patterns in figure 2.5k and 2.5l. This network provides preferential flow paths enhancing the permeability of the mineral soil layer, while in YL_ACC bypass flow derived mostly from plant activity.

Also in OL, Ksat is higher in OL_DEPL than in OL_ACC (fig. 2.4a) even if vegetation succession is more advanced within the latter. Textural differences between OL_DEPL and OL_ACC consist in ~5 % regarding the clay and sand fraction (fig. 2.3a), which we do not consider to cause the large spread of Ksat between OL_DEPL and OL_ACC (fig. 2.4a). In OL the relative influence of the vegetation on the soil permeability is clearly documented by the decrease of Ksat (fig. 2.4a) from the topsoil to the subsoil accompanied by declining root densities (tab 2.1). Such a relative decrease of Ksat is not evident at YL_DEPL and YL_ACC

(fig. 2.3b) both featuring an earlier degree of vegetation succession than the corresponding zones in OL. We can also exclude differences in soil texture, since we measured a slightly higher sand fraction in YL (fig. 2.3b) than in OL, which reveals a slightly higher clay fraction (fig. 2.3a). Consequently, by comparing YL and OL the influence of the vegetation succession on Ksat is evident, but appears subordinated if we distinguish between OL_DEPL and OL_ACC.

Assessing the role of rock fragment content

As aforementioned, at OL_DEPL an earlier succession stadium (bushes and trees sheltered by ferns) prevailed, while the overall saturated hydraulic conductivity was invariably higher than in OL_ACC (fig. 2.4a) being covered by a secondary forest with closed canopy. Moreover, the pF curves of OL_DEPL (fig. 2.4a) reveal a fast draining mineral soil layer featuring the highest rock fragment contents (tab. 2.1) with a subsoil bulk density that is lower than in OL_ACC. In this context, Poesen and Lavee (1994) and Torri et al. (1994) argued that rock fragments increase the porosity attributed to the fine soil bulk density which they conceptually explained by loosely packed spheres of different size and shape. As aforementioned, we mainly found angular rock fragments between 2 mm and 63 mm in diameter, but particularly in OL_DEPL a higher portion of larger rock fragments. In combination with the high rock fragment content (tab. 2.1), there may be insufficient fine earth to fill the voids in between the rock fragments (Poesen and Lavee, 1994), or the smaller particles cannot pack as closely to the larger particles as they can with each other (Stewart et al., 1970).

Regarding this, we may conclude that the rock fragment content in OL_DEPL controls the fine soil bulk density and thus the soil permeability more than the vegetation cover does. In this context, we may also expect larger dye stain widths due to an increased transversal mechanical dispersion caused by the rock fragments and the increased porosity of the soil matrix between. Such an increase of the stain widths with increasing rock fragment content is illustrated in figure 2.5i, j of OL_DEPL B. During irrigation, part of the dye tracer flew laterally ~2.5 m along the organic layer/mineral topsoil interface while infiltrating the mineral topsoil. Here, until ~25 cm depth we encountered a lower rock fragment content (tab. 2.1) than in the subsoil and small distinct dye stains indicating bypass flow in macropores as documented in figures 2.5i and 2.5j. With transition to the soil below ~25 cm depth, the dye tracer was released in broad fingers in the material with its higher rock fragment content (tab. 2.1) resulting in larger dye stain widths (fig. 2.5i, j). Similar is illustrated in the study of Bogner et al. (2008) for a skeletal Cambisol in MC 2 under mature forest. Furthermore, the

lateral flow of the dye tracer along the organic layer/mineral topsoil interface implies a lower permeability of the mineral topsoil in OL_DEPL B compared to OL_ACC, where such a subsurface flow did not occur and where we encountered a higher rock fragment content in the topsoil (tab. 2.1). At OL_ACC, the soil profile directly below the irrigator was almost completely stained, whereas ~20 cm far from this profile larger dye stains appeared mostly at ~50 cm depth (fig. 2.5a). The larger dye stains may be attributed to the increasing rock fragment content between 40 cm and 50 cm depth (tab. 2.1) leading to a higher dispersion of the vertically percolating dye below the irrigator which therefore expands laterally to the profile shown figure 2.5a. However, the increase of the rock fragment content and dye stain widths is accompanied by notably higher bulk densities (tab. 2.1) and lower Ksat values (fig. 2.4a). Conversely, there is no evidence given for lower Ksat values in the topsoil in OL_DEPL B (fig. 2.4a), where we encountered relatively low rock fragment contents (tab. 2.1) and notably smaller dye stains widths (fig. 2.5i, j). However, in this case we can explain this discrepancy by a subsequent landslide event, since we could visually identify a buried A horizon (denoted as Ahb in table 2.1) below the mineral topsoil in OL_DEPL B. At OL_DEPL A, however, no evidence was given for such a subsequent landslide event. Thus, the subsequent landslide occurred as local event and is therefore not sufficiently considered by the Ksat measurements, since we merged the Ksat values measured in OL_DEPL B and in OL_DEPL A.

Nevertheless, the observations we made in OL_ACC, and also in YL_DEPL where we mainly found distinct flow paths (fig. 2.5k, l) in a mineral soil cover with a relatively high rock fragment content of 50 vol.-% (tab. 2.1) does not corroborate the assumption that the rock fragment content decreases the fine soil bulk density in benefit of a higher amount of drainable pores according to the conceptual approach of Torri et al. (1994) and Poesen and Lavee (1994). On the other hand, at OL_DEPL B the rock fragment contents are contrasting markedly between the topsoil (~30 vol.-%) and subsoil (~75 vol.-%). Following van Wesemael et al. (1995), we may assume a threshold between ~50 vol.-% and ~75 vol.-% at which the rock fragment content largely determine the permeability of the mineral soil layer while the influence of the vegetation cover becomes less important. However, due to the few observations and lack of clarity, further studies using a more comprehensive data set are recommended to verify at least the assumption, that rock fragment content and fine soil bulk density controls Ksat in stony soils of the RBSF study area.

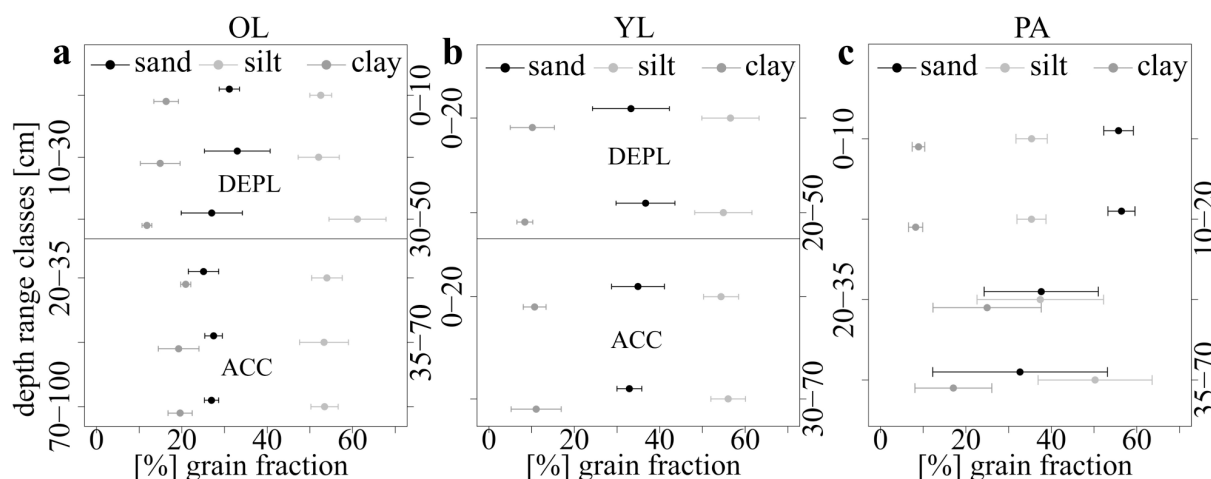


Figure 2.3 Percentages of fine soil fractions of sand, silt, and clay of the old landslide (a), young landslide (b), and plateau area (c). Fine soil fractions of OL_DEPL were estimated by Markwardt (2005).

Assessing the role of weathered bedrock

The sharp boundary between mineral soil and parent material we encountered at YL_DEPL (fig. 2.5k, l) implies that during the sliding process the latter was abraded until more resistant, less weathered and impervious parent material. The dye tracer having infiltrated the weathered parent material at OL_DEPL A (fig. 2.5g, h) suggests that the well defined mineral soil layer/weathered parent material interface at YL_DEPL becomes gradual due to progressing alteration. This would also mean a shift of potential shallow subsurface flow into the deteriorating parent material. This is also illustrated by the binary images we obtained from OL_ACC (fig. 2.5a, b), where between 80 cm and 100 cm below the mineral soil surface weathered parent material set gradually in. Here, a part of dye tracer was retained and flew laterally some 90 cm downslopes while infiltrating the weathered bedrock resulting in the dye pattern of figure 2.5c. However, since we did not trace the deeper percolation of the dye tracer we cannot estimate the parent material permeability for greater depths. Moreover, based on these few observations we cannot conclude that within the RBSF study area the permeability of the parent material increases by the grade of its alteration. To our knowledge, nothing is known about the bedrock permeability in the RBSF investigation area, which is seen as an important hydrological key parameter. Montgomery et al. (1997), for example, observed at a steep zero order catchment the importance of lateral flow through weathered and fractured bedrock on pore pressure development in shallow colluvial soils. Less permeable localities within the weathered bedrock forces the water upwards into the colluvial soil which provides a significant control on pore pressure development in the overlying colluvium and therefore on landslide initiation. With respect to our findings, we may draw the same conclusions, but

within the framework of the present study this conception cannot be proven. Consequently, further studies are needed to elucidate this important issue.

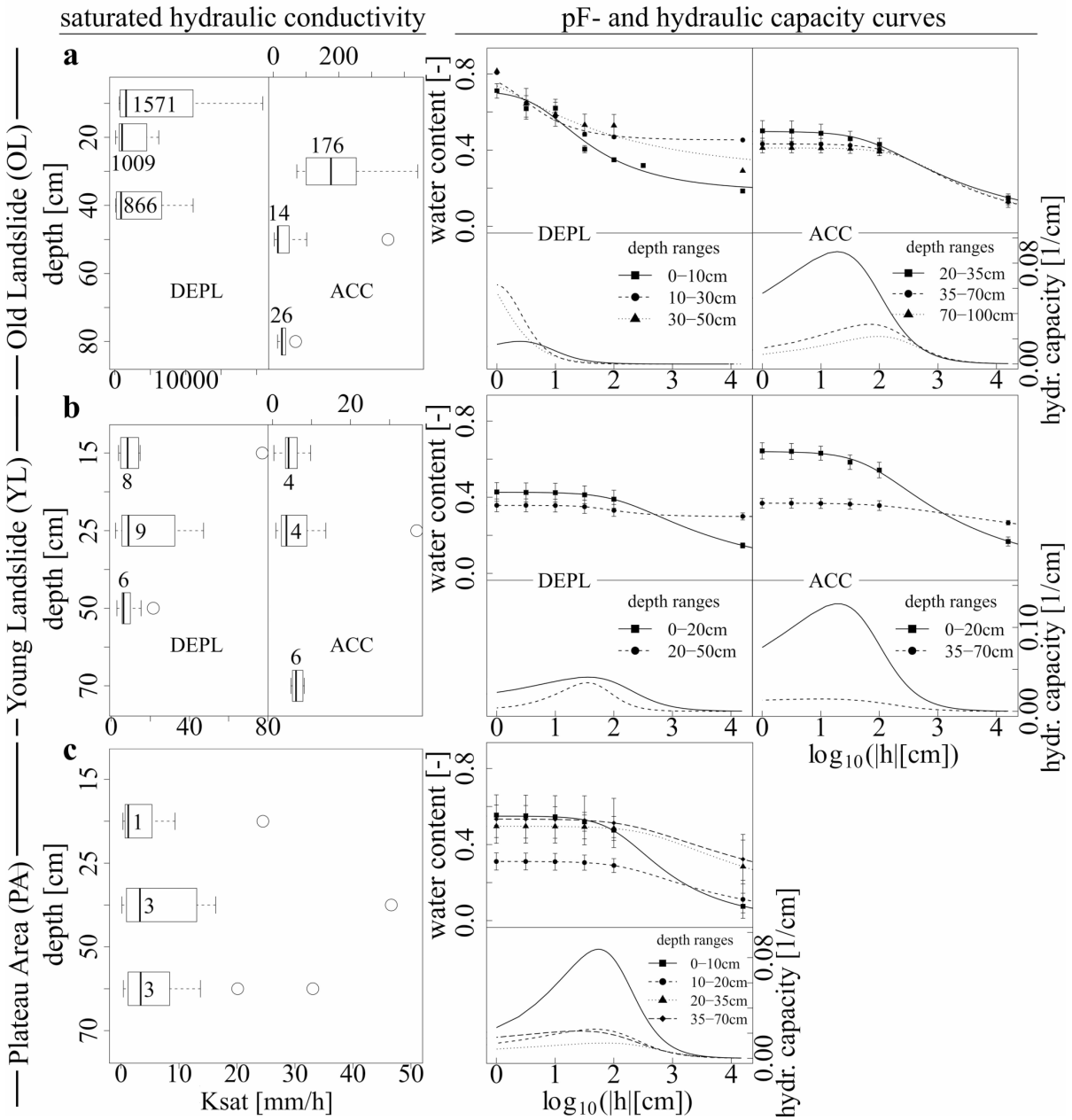


Figure 2.4 Boxplots of Ksat, pF- and hydraulic capacity curves of the old landslide (a), young landslide (b), and plateau area (c). The value at the crossbar within a box designate the median. The length of a box equals the interquartile range, the whiskers indicate the range for data not being counted among outliers. These are denoted by the open circles which are at least 1.5 times the interquartile range away from the lower and upper quartile. The modelled pF curves and corresponding hydraulic capacities (line symbols) were obtained by fitting measured retention data (closed symbols) via RETC (van Genuchten et al., 1998). Error bars denote standard deviation of the fine earth fractions and measured retention data. Due to high coincidence, we merged the data of PA 1 and PA 2. For the landslides, “DEPL” denotes depletion zone, and “ACC” accumulation zone. The measured retention curves of OL_DEPL were estimated by Markwardt (2005).

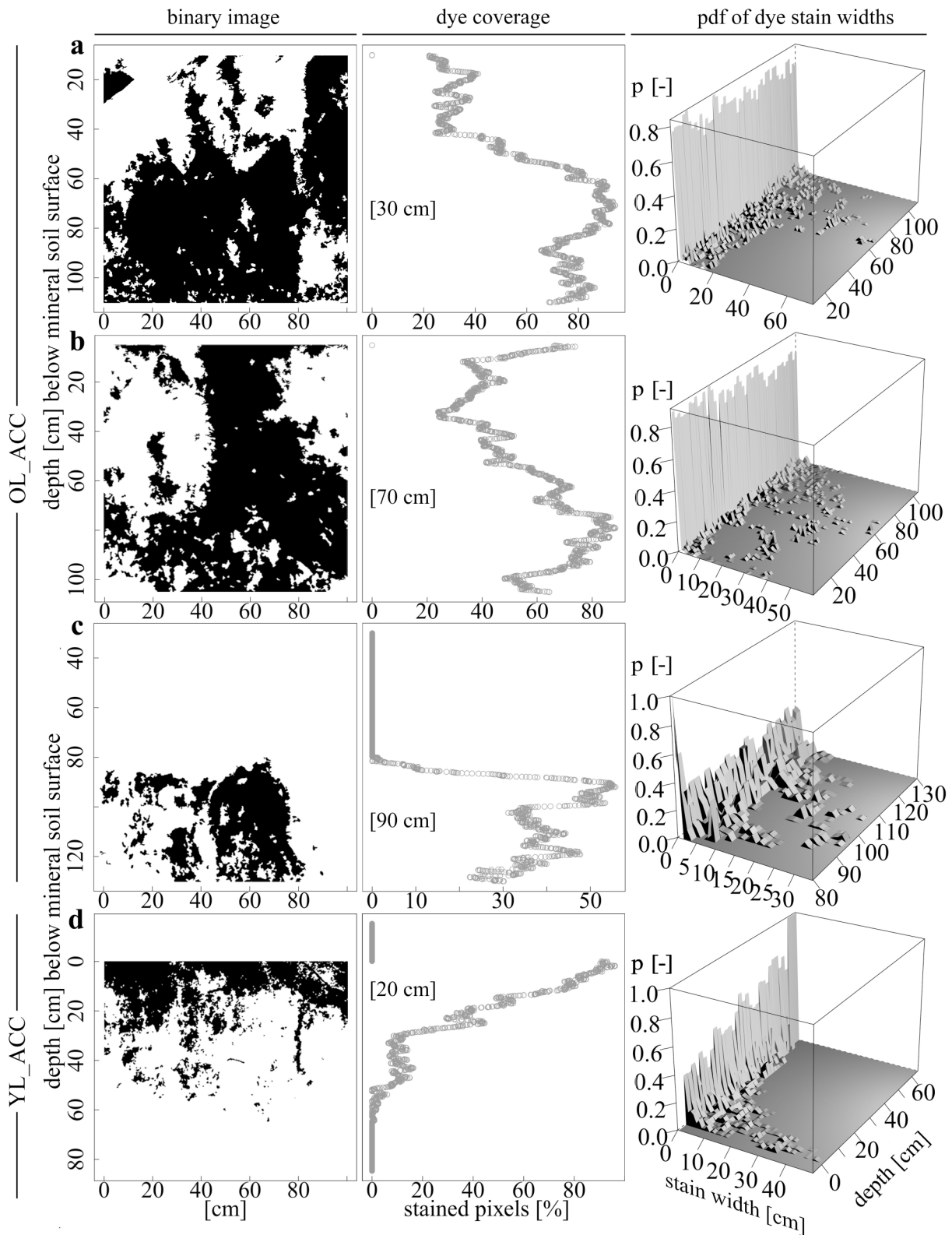


Figure 2.5 Exemplary binary images, dye coverages and associated probability density functions (pdf) of the old landslide (OL), the young landslide (YL) and the plateau area (PA). Note that each pdf within a 3D graph denotes the arithmetic mean of dye stain widths over a depth increment of 2 cm. The values in [] in the dye coverage graphs indicate the distance to the line source sprinkler in cm. At OL_ACC, the profile directly underneath the line source sprinkler (not shown here) was almost completely stained. The vertical stains ranging from the upper margin of the binary images in 2.5a and 2.5b resulted from distinct lateral flow paths at the mineral soil surface during tracer application.

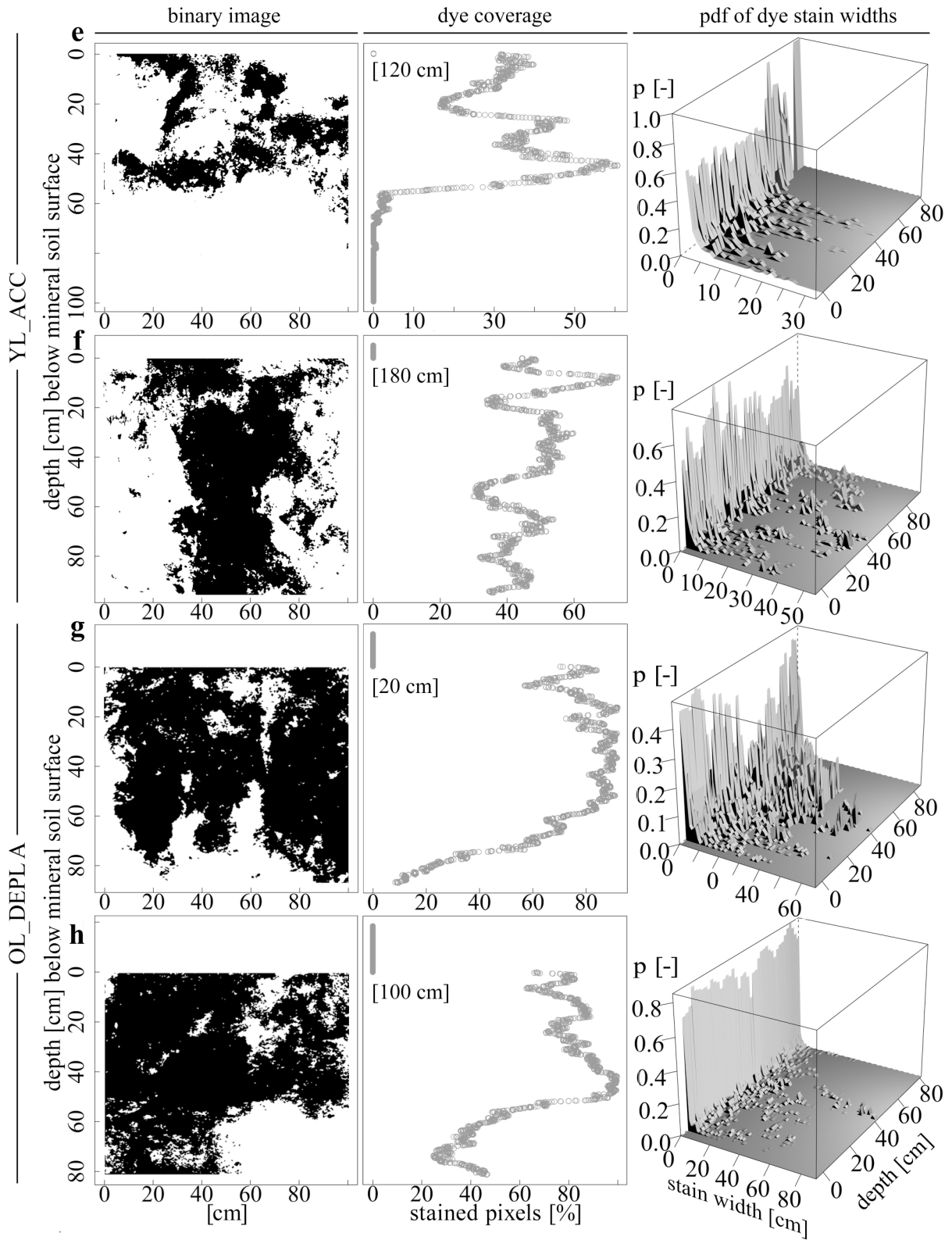


Figure 2.5 (continued from previous page)

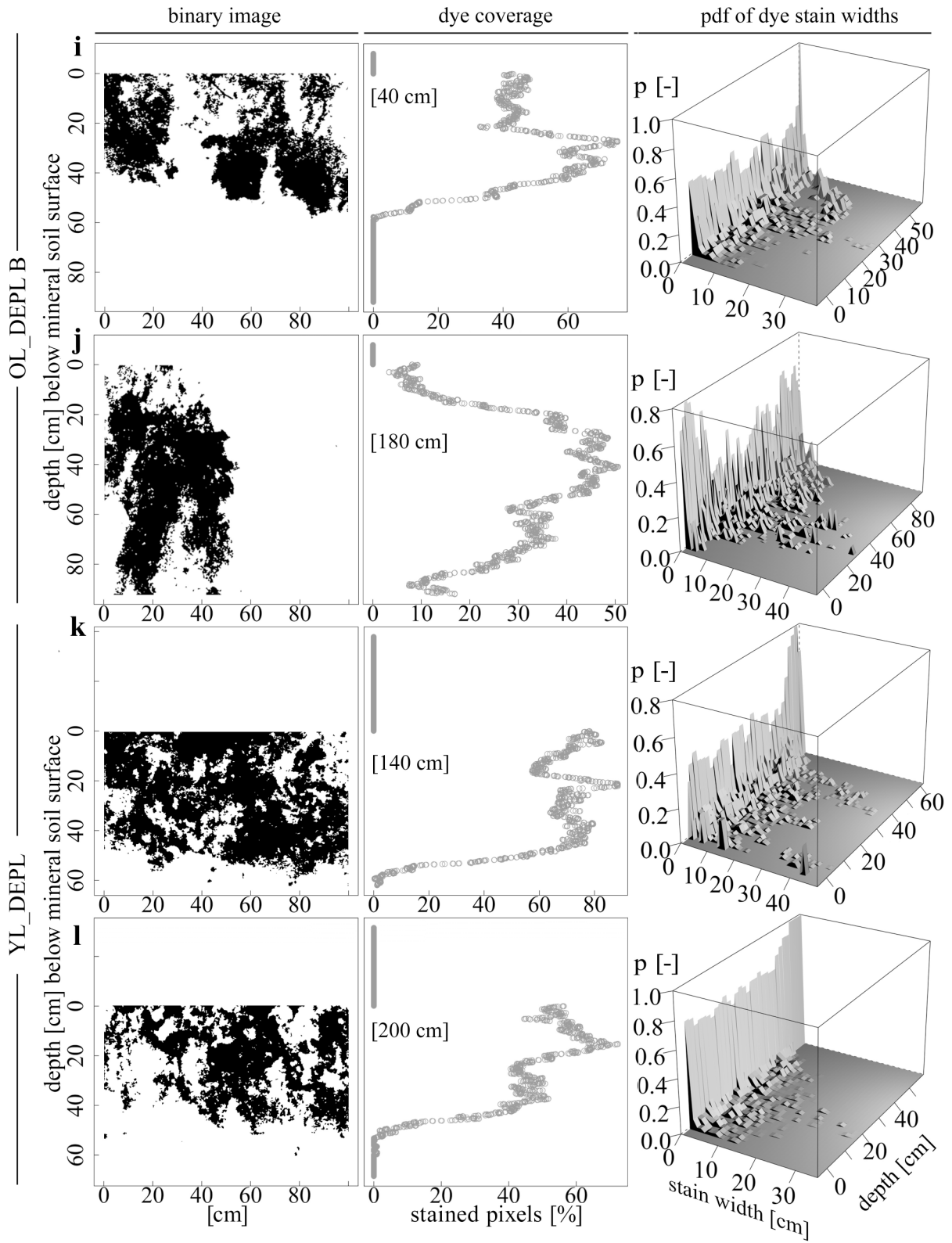


Figure 2.5 (continued from previous page)

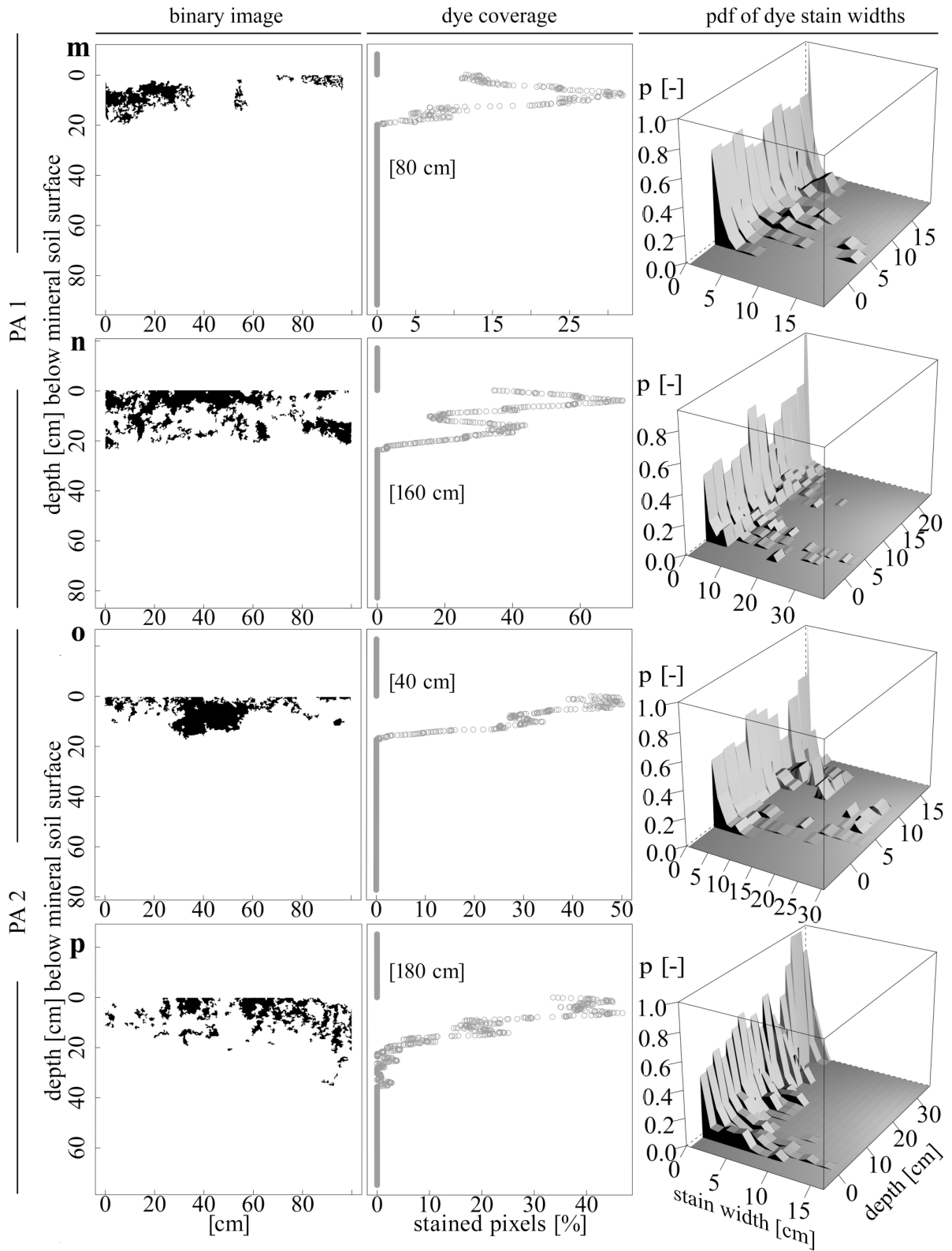


Figure 2.5 (continued from previous page)

2.3.2 Plateau area (PA)

In comparison to the landslide affected sites, in both experimental plots PA 1 and PA 2 within the plateau area (fig. 2.1) we found lowest root densities, negligible rock fragment contents and a throughout coherent soil macro structure. While excavating we frequently found stained roots giving evidence that the dye stains mostly derived from root channels. The binary images (fig. 2.5m-p) indicate that the percolation of the dye tracer reached its maximum depth at ~20 cm depth. Small amounts of dye tracer that have been detected below were due to local pocket-shaped bulges of the E- into the Bg horizon as indicated at the right side of the binary image in figure 2.5p. Within the mineral topsoil, the relatively largest dye stain widths (fig. 2.5m-p) occurred with relatively high root densities (tab. 2.1) until 10 cm depth, while further below widths of less than 5 cm and low root densities prevail. Also, the steeper slope of the pF curve obtained from the uppermost 10 cm of the topsoil (fig. 2.4c) reveal a higher amount of drainable pores and a larger total pore volume than in deeper depths. Here, particularly between 10 cm and 20 cm depth bulk density is highest (tab. 2.1) and the total porosity lowest regarding the pF curve in figure 2.4c. Moreover, we measured the lowest Ksat values at 20 cm depth (fig. 2.4c). In combination with the dye stain widths being considerably smaller compared to those of the landslide affected sites, we conclude predomination of preferential flow in the root channels with low soil matrix interaction, particularly in the lower part of the mineral topsoil. Since we found the relative lowest root densities here (tab. 2.1), we suggest a limited connectivity between the macropores. Therefore, infiltrating water may back up in the latter up to the organic layer/mineral topsoil interface leading to rapid lateral flow as supposed by Fleischbein et al. (2006), Goller et al. (2005) and Wilcke et al. (2001, 2008).

Below the topsoil/subsoil interface at ~20 cm, the clay fraction increases notably within 15 cm depth and decreases somewhat further below (fig. 2.3c) implying a vertical relocation of clay particles from the topsoil to the upper subsoil. We suggest that due to long lasting unhindered soil forming processes, i.e. disaggregation and relocation of soil particles, eluviation of mineral components, and subsequent subsidence permeability was reduced. Consequently, as shown by the binary images and dye stain widths, soil physical and hydrological parameters we encountered the part along the interface between mineral topsoil and subsoil as quasi impermeable.

2.4 Conclusions

In the Andes of southern Ecuador on landslide affected and unaffected hillslopes, we conducted pedon scale dye tracer experiments and assessed soil physical- and hydraulic parameters. With respect to the investigated soils and flow paths, we can principally distinguish between landslide affected and unaffected sites.

In the gentle sloping plateau area that is unaffected by landslides, we found the percolation being mainly controlled by root channels with low soil matrix interaction and restricted to the shallow mineral topsoil. Since we assume limited lateral connectivity of the macropores, infiltrating water may back up in the latter up to the organic layer/mineral topsoil resulting in a rapid shallow subsurface flow. As the Stagnosols are not only well represented in the plateau area (Liess et al., 2009), we may upscale our findings to a larger area, but we recommend further investigations to corroborate this suggestion.

With respect to the landslide affected sites, we assume that at a distinct threshold between 50 vol.-% and 75 vol.-% the rock fragment content predominantly controls the permeability of the mineral soil cover due to an increasing amount of drainable pores, whereas the influence of the vegetation cover on flow path formation becomes less important. Beyond this threshold water flow may appear as heterogeneous matrix in between the rock fragments while below in distinct flow paths such as root channels.

Also, within the young landslide we found cracks and fissures to control the mineral soil permeability. We suggest these structures to have been caused by slow movement of the mineral soil layer due to the general steepness in the investigated landslides. This effect can be amplified if the permeability of the underlying weathered bedrock allows formation of a perched water table resulting in a lateral shallow subsurface flow. In this context, the permeability of the weathered bedrock is unclear within the RBSF investigation area. Such a knowledge, however, is necessary in terms of subsurface flow formation as highlighted by the virtual experiment series of Hopp and McDonnell (2009), catchment hydrological behaviour concerning land use change by Bruijnzeel (2004), or landslide occurrence as found by Montgomery et al. (1997). Therefore, suitable information of the bedrock permeability is needed for future hydrological modelling studies in the RBSF study area.

With this study, our observations concur with the study of Bogner et al. (2008) regarding vegetation succession and rock fragment content on flow paths in landslide affected sites. However, the insights we made in this study do not concur with the generalisations of Zimmermann and Elsenbeer (2008), who found undistinguishable K_{sat} among two different aged landslides and a natural forest. They rather assume that landslides in the RBSF study

area affect mainly organic horizons but not the mineral soil. That conflicts our profile descriptions revealing considerably thinner soil material covers in the depletion zones than in the accumulation zones and soil profiles with buried topsoil horizons.

2.5 Acknowledgements

We would like to thank Iris Schmiedinger and Andreas Kolb as well as Ingrid Hausinger, Lisa Höhn, Stefanie Schier, Tobias Biermann and Daniela Vasquez for laboratory- and field assistance. This study was supported and funded by the German Research Foundation (DFG) grant nr. DFG FOR 402/1-1 Hu 636/9-3 and DFG FOR 816 - HU 636/14-1.

2.6 References

- Adams P.W., Sidle R.C., 1987. Soil conditions in three recent landslides in southeast Alaska. *For. Ecol. Manag.* 18, 93-102.
- AG Boden, 2005. *Bodenkundliche Kartieranleitung*, 5. Auflage. Bundesanstalt für Geowissenschaften und Rohstoffe und Geologische Landesämter der Bundesrepublik Deutschland, Hannover.
- Amoozegar, A., 1989a. A compact, constant-head permeameter for measuring saturated hydraulic conductivity of the vadose zone. *Soil Sci. Soc. Am. J.* 53, 1356-1361.
- Amoozegar, A., 1989b. Comparison of the Glover solution with the simultaneous equations approach for measuring hydraulic conductivity. *Soil Sci. Soc. Am. J.* 53, 1362-1367.
- Amoozegar, A., 1993. Comments on "Methods for analyzing constant-head well permeameter data". *Soil Sci. Soc. Am. J.* 57, 559-560.
- Balslev, H., Øllgaard, B., 2002. Mapa de vegetación del sur de Ecuador, in: Aguirre, M.Z., Madsen, J.E., Cotton, E., Balslev, H. (Eds.), *Botanica Austroecuatoriana. Estudios sobre los Recursos Vegetales en las Provincias de El Oro, Loja y Zamora-Chinchi*, Quito, pp 51-64.
- Beck, E., Makeschin, F., Haubrich, F., Richter, M., Bendix, J., Valerezo, C., 2008. The Ecosystem (Reserva Biológica San Francisco), in: Beck, E., Bendix, J., Kottke, I., Makeschin, F., Mosandl, R. (Eds.), *Gradients in a Tropical Mountain Ecosystem of Ecuador*, Springer Verlag, Berlin, Heidelberg, pp. 1-14.
- Bendix, J., Rollenbeck, R., Richter, M., Fabian, P., Emck, P., 2008. Climate, in: Beck, E., Bendix, J., Kottke, I., Makeschin, F., Mosandl, R. (Eds.), *Gradients in a Tropical Mountain Ecosystem of Ecuador*, Springer Verlag, Berlin, Heidelberg, pp 63-73.

Chapter 2 – References

- Bogner, C., Engelhardt, S., Zeilinger, J., Huwe, B., 2008. Visualisation and analysis of flow patterns and water flow simulations in disturbed and undisturbed tropical soils, in: Beck, E., Bendix, J., Kottke, I., Makeschin, F., Mosandl, R. (Eds.), *Gradients in a Tropical Mountain Ecosystem of Ecuador*. Ecological Studies, Springer, Berlin, pp 387-397.
- Bogner, C. 2009., Analysis of flow patterns and flow mechanisms in soils. PhD thesis. URL <http://opus.ub.uni-bayreuth.de/volltexte/2009/607/> (accessed on July 2010), University of Bayreuth, Bayreuth.
- Bonell, M., Balek, J., 1993. Recent scientific developments and research needs in hydrological processes of the humid tropics, in: *Hydrology and Water Management in the Humid Tropics*, Bonell, M., Hufschmidt, M.M., Gladwell, J.S. (Eds.), Cambridge University Press, Cambridge, pp. 167-260.
- Bouma, J., Dekker, L.W., 1978. A case study on infiltration into a dry clay soil: 1. Morphological observations. *Geoderma* 20, 27-40.
- Bruijnzeel, L.A., 2004. Hydrological functions of tropical forests: not seeing the soil for the trees? *Agr. Ecosyst. Environ.* 104, 185-228.
- Chappell, N.A., Sherlock, M.D., 2005. Contrasting flow pathways within tropical forest slopes of Ultisol soils. *Earth Surf. Process. Landforms* 30, 735-753.
- Cramer, W. 2008. Global change impacts on the biosphere, in: Jørgensen, S.E., and Fath, B.D. (Eds), *Global Ecology*. Elsevier, Oxford, pp. 1736-1741.
- Droogers, P., Stein, A., Bouma, J., de Boer, G., 1998. Parameters for describing soil macroporosity derived from staining patterns. *Geoderma* 83, 293-308.
- Elsenbeer, H., 2001. Hydrologic flowpaths in tropical rainforest soils - a Review. *Hydrol. Process.* 15, 1751-1759.
- Fleischbein, K., Wilcke, W., Valarezo, C., Zech, W., Knoblich, K., 2006. Water budgets of three small catchments under montane Forest in Ecuador: experimental and modelling approach. *Hydrol. Process.* 20, 2491-2507.
- Flury, M., Flühler, H., Jury, W.A., Leuenberger, J., 1994a. Susceptibility of soils to preferential flow of water: a field study. *Water Resour. Res.* 30(7), 1945-1954.
- Flury, M., Flühler, H., 1994b. Brilliant Blue FCF as a dye tracer for solute transport studies - a toxicological overview. *J. Environ. Qual.* 23(5), 1108-1112.
- Forrer, I., Papritz, A., Kasteel, R., Flühler, H., Luca, D., 2000. Quantifying dye tracers in soil profiles by image processing. *Eur. J. Soil. Sci.* 51(2), 313-322.

Chapter 2 – References

- Francou, B., Ramirez, E., Cáceres, B., Mendoza, J., 2000. Glacier Evolution in the Tropical Andes during the Last Decades of the 20th Century: Chacaltaya, Bolivia, and Antizana, Ecuador. *Ambio* 29(7), 416-422.
- Fries, A., Rollenbeck, R., Göttlicher, D., Nauss, T., Homeier, J., Peters, T., Bendix, J., 2009. Thermal structure of a megadiverse Andean mountain ecosystem in southern Ecuador, and its regionalization. *Erdkunde* 63, 321-335.
- Germán-Heins, J., Flury, M., 2000. Sorption of brilliant blue FCF in soils affected by pH and ionic strength. *Geoderma* 97, 87-101.
- Goller, R., Wilcke, W., Leng, M.J., Tobschall, H.J., Wagner, K., Valarezo, C., Zech, W., 2005. Tracing water paths through small catchments under a tropical montane rain forest in South Ecuador by an oxygen isotope approach. *J. Hydrol.* 308, 67-80.
- Guariguata, M.R., 1990. Landslide disturbance and forest regeneration in the upper Luquillo mountains of Puerto Rico. *J. Ecol.* 78, 814-832.
- Homeier, J., Dalitz, H., Breckle, S.W., 2002. Waldstruktur und Baumartendiversität im montanen Regenwald der Estación Científica San Francisco in Südecuador. *Berichte der Reinhold-Tüxen-Gesellschaft* 14, 109-118.
- Homeier, J., 2004. Baumdiversität, Waldstruktur und Wachstumsdynamik zweier tropischer Bergregenwälder in Ecuador und Costa Rica. *Dissertationes Botanicae*, Berlin.
- Hopp, L., McDonnell, J.J., 2009. Connectivity at the hillslope scale: Identifying interactions between storm size, bedrock permeability, slope angle and soil depth. *J. Hydrol.* 376, 378-391.
- Hungerbühler, D., 1997. Neogene basins in the Andes of southern Ecuador: evolution, deformation and regional tectonic implications. PhD thesis. URL <http://e-collection.ethbib.ethz.ch/view/eth:40985> (accessed on January 2010), ETH Zürich, Zürich.
- IUSS Working Group WRB, 2007. World Reference Base for Soil Resources 2006, first update 2007. World Soil Resources Reports No. 103. FAO, Rome.
- Köhn, M., 1928. 3. Bemerkungen zur mechanischen Bodenanalyse. III. Ein neuer Pipetteapparat. *Zeitschrift für Pflanzenernährung, Düngung und Bodenkunde A. Wissenschaftlicher Teil*, XI, 50-54.
- Kulli, B., Gysi, M., Flühler, H., 2003. Visualizing soil compaction based on flow pattern analysis. *Soil Util. Res.* 70(1), 29-40.
- Kung, K.-J.S., 1990. Preferential flow in a sandy vadose zone: 1. Field observation. *Geoderma* 46, 51-58.
- Licata, J.A., Gyenge, J.E., Fernandez M.E., Schlichter, T.M., Bond, B.J., 2008. Increased

Chapter 2 – References

- water use by ponderosa pine plantations in northwestern Patagonia, Argentina, compared with native forest vegetation. *For. Ecol. Manage.* 255(3), 753-764.
- Liess, M., Glaser, B., Huwe, B., 2009. Digital Soil Mapping In Southern Ecuador. *Erdkunde* 63 (4), 309-319.
- Markwardt, S., 2005. Validity of two pedotransfer functions in two microcatchments of a tropical mountain rainforest in Southern Ecuador. Unpubl. diploma thesis, University of Bayreuth, Bayreuth.
- Montgomery, D.R., Dietrich, W.E., Torres, R., Anderson, S.P., Heffner, J.T., Loague, K., 1997. Hydrologic response of a steep, unchanneled valley to natural and applied rainfall. *Water Resour. Res.*, 33(1), 91-109.
- Morris, C., Mooney, S.J., 2004. A high-resolution system for the quantification of preferential flow in undisturbed soil using observations of tracers. *Geoderma* 118, 113-143.
- Munsell Colours, 1994. Munsell Soil Colour Charts, Revised Edition. Macbeth Division of Kollmorgen Instruments. New Windsor, New York.
- MVTec Software GmbH, 2005. Halcon, ver 7.1. URL <http://www.mvtec.com/halcon/> (accessed on January 2010).
- Niemann, T., 2008. PT Lens Software to correct lens pincushion/barrel distortion, vignetting, chromatic aberration and perspective, ver 6.4. Oregon, Portland. URL <http://epaperpress.com/ptlens/index.html> (Accessed January 2010).
- Noguchi, S., Tsuboyama, Y., Sidle, R.C., Hosoda, I., 1999. Morphological Characteristics of Macropores and the Distribution of Preferential Flow Pathways in a Forested Slope Segment. *Soil Sci. Soc. Am. J.* 63, 1413-1423.
- Ohl, C., Bussmann, R., 2004. Recolonisation of natural landslides in tropical mountain forests of Southern Ecuador. *Feddes Repertorium* 115 (3-4), 248-264.
- Öhrström, P., Hamed, Y., Persson, M., Berndtsson, R., 2004. Characterizing unsaturated solute transport by simultaneous use of dye and bromide. *J. Hydrol.* 289, 23-35.
- Paulsch, A., 2002. Development and application of a classification system for undisturbed and disturbed tropical montane forests based on vegetation structure. PhD thesis. URL <http://opus.ub.uni-bayreuth.de/volltexte/2002/1/> (accessed on January 2010), University of Bayreuth, Bayreuth.
- Poesen, J., Lavee, H., 1994. Rock fragments in topsoils: Significance and processes. *Catena*, 23, 1-28.
- Ravina, I. and Magier, J., 1984. Hydraulic conductivity and water retention of clay soils containing coarse fragments. *Soil Sci. Soc. Am. J.* 48: 736-740.

Chapter 2 – References

- Rollenbeck, R., 2006. Variability of precipitation in the Reserva Biológica San Francisco / Southern Ecuador. *Lyonia* 9 (1), 43-51.
- Ruiz, D., Moreno A.H., Gutiérrez, M.E., Zapata, P.A., 2008. Changing climate and endangered high mountain ecosystems in Colombia. *Sci. Total Environ.* 398(1), 122-132.
- Sauer, W., 1971. *Geologie von Ecuador. Beiträge zur regionalen Geologie der Erde*, vol. 11. Bornträger, Berlin.
- Sauer, T.J., Logsdon, S.D., 2002. Hydraulic and Physical Properties of Stony Soils in a Small Watershed. *Soil Sci. Soc. Am. J.* 66:1947-1956.
- Schrumpf, M., Guggenberger, G., Schubert, C., Valarezo, C., Zech, W., 2001. Tropical montane rain forest soils: development and nutrients status along an altitudinal gradient in the south Ecuadorian Andes. *Die Erde* 132, 43-59.
- Soulsby, C., Pomeroy, A., Gibbins, C., 1997. Hydrology and hydrochemistry of a montane rainforest catchment in Queensland, Australia, in: Peters, N.E. and Coudrain-Ribstein, A. (Eds.), *Hydrochemistry Symposium*, International Association of Hydrological Sciences, Rabat, Morocco.
- Stewart, V.I., Adams, W.A., Abdullah, H.H., 1970. Quantitative pedological studies on soils derived from Silurian mudstones II. The relationship between stone content and the apparent density of the fine earth. *J. Soil Sci.* 21: 248-255.
- Stoyan, R., 2002. *Aktivität, Ursachen und Klassifikation der Rutschungen in San Francisco / Südecuador*. Unpubl. diploma thesis, University of Erlangen-Nuremberg, Erlangen.
- The MathWorks, Inc., 2008a. *Image Processing Toolbox*, ver 6.2. URL <http://www.mathworks.com/products/image/> (accessed on July 2010).
- The MathWorks, Inc., 2008b. *Matlab*, ver 7.7. URL <http://www.mathworks.com> (accessed on July 2010).
- Torri, T., Poesen, J., Monaci, F., Busoni, E., 1994. Rock fragment content and fine soil bulk density. *Catena* 23, 65-71.
- van Genuchten, M.Th., 1980. A closed-form equation for predicting the hydraulic conductivity of unsaturated soils. *Soil Sci. Soc. Am. J.* 44, 892-898.
- van Genuchten, M.Th., Simunek, J., Leij, F.J., Sejna, M., 1998. *The RETC code for Quantifying the Hydraulic Functions of Unsaturated Soils*, ver 6.0. US Salinity Laboratory, USDA, Riverside, Colorado. URL <http://www.pc-progress.com/en/Default.aspx?retc> (accessed on January 2010).
- van Wesemael, B., Poesen J., de Figueiredo, T., 1995. Effects of rock fragments on physical degradation of cultivated soils by rainfall. *Soil & Tillage Res.* 33, 229-250.

Chapter 2 – References

- van Wesemael, B., Mulligan, M., Poesen, J., 2001. Spatial Patterns in Water Use Efficiency Created by Intensive Cultivation on Semi-arid Hillslopes, in: Stott, D.E., Mohtar, R.H., Steinhardt, G.C. (Eds.), Selected papers from the 10th International Soil Conservation Organization Meeting, May 24-29, 1999, West Lafayette, IN. International Soil Conservation Organization in cooperation with the USDA and Purdue University, West Lafayette, IN. URL <http://topsoil.nserl.purdue.edu/nserlweb-old/isco99/pdf/ISCOdisc/SustainingTheGlobalFarm/P056-Wesemael.pdf> (accessed July 2010).
- Vanclay, J.K., 2009. Managing water use from forest plantations. *For. Ecol. Manage.* 257(2), 385-389. Vanclay, J.K., 2009. Managing water use from forest plantations. *For. Ecol. Manage.* 257(2), 385-389.
- Verbist, K., Baetens, J., Cornelis, W.M., Gabriels, D., Torres, C., Soto, G., 2009. Hydraulic Conductivity as Influenced by Stoniness in Degraded Drylands of Chile. *Soil. Sci. Soc. Am. J.* 73, 471-484.
- Weiler, M., 2001. Mechanism controlling macropore flow during infiltration - dye tracer experiments and simulation. PhD thesis. URL <http://e-collection.ethbib.ethz.ch/eserv/eth:24150/eth-24150-02.pdf> (accessed on July 2010), ETH Zürich, Zürich.
- Weiler, M., Flühler, H., 2004. Inferring flow types from dye patterns in macroporous soils. *Geoderma* 120(1-2), 137-153.
- Werner F.A., Homeier, J., Gradstein, S.R., 2005. Diversity of vascular epiphytes on isolated remnant trees in the montane forest belt of southern Ecuador. *Ecotropica* 11, 21-40.
- Wilcke, W., Yasin, S., Valarezo, C., Zech, W., 2001. Change in water quality during the passage through a tropical montane forest in Ecuador. *Biogeochemistry* 55, 45-72.
- Wilcke, W., Valladarez, H., Stoyan, R., Yasin, S., Valarezo, C., Zech, W., 2003. Soil properties on a chronosequence of landslides in montane rain forest, Ecuador. *Catena* 53, 79-95.
- Wilcke, W., Yasin, S., Fleischbein, K., Goller, R., Boy, J., Knuth, J., Valarezo, C., Zech, W., 2008. Water Relation, in: Beck, E., Bendix, J., Kottke, I., Makeschin, F., Mosandl, R. (Eds.), *Gradients in a Tropical Mountain Ecosystem of Ecuador*. Ecological Studies, Springer, Berlin, pp 193-201.
- Zimmermann, B., Elsenbeer, H., 2008. Spatial and temporal variability of soil saturated hydraulic conductivity in gradients of disturbance. *J. Hydrol.* 361, 78-95.

**Chapter 3 Flow paths in soils of landslide affected and
unaffected hillslopes in a montane rain forest of
South Ecuador, part B**

Folkert Bauer ^{1,*}, Luis Balcázar ³, Pablo Viñan ³, Christina Bogner ², Jörg Zeilinger ¹, and
Bernd Huwe ¹

¹ Department of Soil Physics, University of Bayreuth
Universitätsstraße 30
95440 Bayreuth, Germany

² Ecological Modelling
Dr. Hans-Frisch-Straße 1-3
95448 Bayreuth, Germany

³ Universidad Nacional de Loja,
Loja, Ecuador

* corresponding author

Email: folkert.bauer@googlemail.com

phone: +49 921 55 2193; fax: +49 921 55 2246

in review at *Journal of Hydrology*

Abstract

Tropical montane forests are known to be the most sensitive environments to changes in climatic conditions and the increasing pressure of deforestation by land use change. However, the number of studies having reported on the hydrology of Andean montane forests remains scarce, whereas such knowledge essentially contributes to the understanding why forest disturbance affects rainfall-discharge response, matter fluxes, and water flow paths. In the Andes of South Ecuador, previous studies postulated the existence of rapid shallow subsurface flow along the interface between organic layer and mineral soil under mature forest. Dye tracer experiments provided evidence that this subsurface may occur in soils of landslide unaffected sites, while rock fragment content and bulk density are suggested to control the mineral soil permeability in landslide affected sites. In order to substantiate the existence of shallow subsurface flow in landslide unaffected hillslopes, we performed further dye tracer experiments. In combination with digitised dye tracer patterns we evaluated the transmissibility of impeding soil layers for water percolation by the two parametric generalised Pareto distribution. Via multivariate linear regressions we proved the hypothesis that rock fragment content and bulk density controls the saturated hydraulic conductivity of the mineral soils in landslide affected sites. The results corroborate the findings of a previous study that prerequisites are given for lateral subsurface interflow in soils within a large landslide unaffected area above 2100 m ASL. Below, for soils within landslide affected sites we can show by multivariate linear regression that both rock fragment content and bulk density significantly, although not largely controls the saturated hydraulic conductivity of the mineral soil. Moreover, due to lacking information of the bedrock permeability it remains unclear, whether lateral shallow subsurface flow, or vertical percolation and lateral flow along the interface between mineral soil and parent material prevails.

Key words: tropical montane forest, shallow landslide, flow paths, dye tracer, extreme value analysis, multivariate linear regression

3.1 Introduction

More recent studies (e.g. Francou et al., 2000; Ruiz et al., 2008; Soulsby et al., 1997; Bruijnzeel, 2004) emphasised that aside the humid tropics particularly tropical mountain ecosystems are among the most sensitive environments to changes in climatic conditions and the increasing pressure of deforestation. In this regard and against the background of the scarce number of hydrological investigations in tropical montane environments, Céleri and

Feyen (2009) proposed an integrated approach that aims at the understanding of intrinsic processes of undisturbed ecosystems in order to estimate the perturbing effects of land management strategies on rainfall-runoff responses, flowpaths, and matter fluxes which should be minimal as possible (Bonell and Balek, 1993). In order to identify hillslope flow pathways and their physical controls, Chappell and Sherlock (2005) emphasised the advantages of tracer in hydrological studies in the humid tropics, which have been applied scarcely in tropical montane ecosystems (e.g. Bauer et al., in review; Bogner et al., 2008a; Caballero et al., 2001).

In addition to classical field methods, dye tracer experiments provide qualitative informations of flow regimes in soils, for example by visualising small scale heterogeneities and their spatial extent in form of high resolution images in a comparatively larger soil volume (Öhrström et al., 2004). Weiler (2001) and Flury et al. (1994) used dye tracer experiments to derive quantitative information such as dye stain widths and dye coverage, respectively. More recent studies proposed to fit the dye coverage function by the two parametric generalised Pareto distribution in order to assess the vulnerability of groundwater by pollutants (Schlather and Huwe, 2005), or to estimate a propagation index concerning solute transport in the soil (Bogner et al., 2008b).

In the Andes of South Ecuador, in landslide affected sites and steep hillslopes Bauer et al. (in review) and Bogner et al. (2008a) documented via pedon scale dye tracer experiments and numerical modelling studies that rock fragments, pedogenetic processes and plant activity increase the occurrence of preferential flow paths. Bauer et al. (in review) assumed that at a distinct threshold the rock fragment content leads to an increase of the saturated hydraulic conductivity (= K_{sat}) due to a decreasing fine soil bulk density between the rock fragments. They derived their assumption from measured soil properties, a small number of dye tracer experiments, and the conceptual approach of loosely packed spheres of different size and shape according to Torri et al. (1994) and Poesen and Lavee (1994), who argued that rock fragments increase the porosity attributed to the fine soil bulk density.

Moreover, aside the landside affected sites, Bauer et al. (in review) conducted also dye tracer experiments on two adjacent plots for a detailed study of flow paths in Stagnosols (IUSS, 2007) on a gentler hillslope under mature forest. Their study revealed that percolation is mainly controlled by root channels with low soil matrix interaction and restricted to the shallow mineral topsoil leading to a rapid subsurface flow along the interface between organic layer and mineral topsoil. As the Stagnosols are well represented in the plateau area above 2100 m above sea level (= ASL) (Liess et al., 2009), the finding of Bauer et al. (in review)

may be upscaled, whereas they recommend further investigations to corroborate this suggestion.

In this study, we continue the dye tracer studies of Bauer et al. (in review) within an landslide unaffected plateau area in order to substantiate their findings. By applying the two parametric generalised Pareto distribution following Schlather and Huwe (2005) and Bogner et al. (2008b), we seek to evaluate the transmissibility of impeding layers and horizons for percolating water within the plateau area and the landslide affected sites investigated by Bauer et al. (in review).

Moreover, following the suggestions of Bauer et al. (in review) we test the hypothesis that rock fragment content and fine soil bulk density controls K_{sat} .

3.2 Materials and methods

3.2.1 Study area

The experimental plots we consider in this study were located in the Reserva Biológica San Francisco (= RBSF) study area in southern Ecuador (Fig. 3.1) between the province capitals Loja and Zamora. This area is part of the eastern slope of the „Cordillera Real“ at ~2000 m ASL, characterised by steep slopes (30 ° - 50 °) and a natural vegetation cover of evergreen montane forest (Balslev and Øllgaard, 2002). Bruijnzeel and Hamilton (2000) classify the area as Lower Montane Rain Forest gradually changing to Lower Montane Cloud Forest. In the RBSF area, the wetter months are between April and August, while rainfall is high throughout the year (Bendix et al., 2008). Average annual precipitation amounts 2050 mm at 1960 m ASL and 4400 mm at 3160 m ASL (Rollenbeck, 2006), while the mean annual air temperature ranges between 19.4 °C at the valley bottom and 9.4 °C at the highest elevations (Fries et al., 2009). The bedrock of the San Francisco study area belongs to the Chiguinda unit (within the Zamora series) consisting of interbedded paleozoic phyllites, metasandstones, and quartzites (Hungerbühler, 1997).

Within the RBSF study area under mature forest and natural vegetation, Liess et al. (2009) found Histosols (IUSS, 2007) as predominating soil type, many of them showing a stagnic colour pattern. In particular, below 2100 m ASL and in hillslopes dipping more than 31 ° the relative presence of Cambisols and Regosols (IUSS, 2007) is most pronounced while with increasing altitude, and declining slope inclinations Stagnosols and Histosols prevail (Liess et al., 2009). In the following, we term the soils according to the World Reference Base for Soil

Resources (IUSS, 2007). More detailed information of the RBSF investigation area is given by Bauer et al. (in review), who conducted pedon scale dye tracer experiments within a young (YL) and an old (OL) shallow landslide typically occurring in the RBSF investigation area. On the young landslide (< 15 years), they performed a pedon scale dye tracer experiment within the depletion (= YL_DEPL) and the accumulation (= YL_ACC) zone. This has been adopted to an old landslide (> 48 a), where the accumulation zone is denoted as OL_ACC and the depletion zone as OL_DEPL (fig. 3.1). Within the latter, two dye tracer experiments were conducted denoted as OL_DEPL A and OL_DEPL B (fig. 3.1) due to the considerably high rock fragment content at OL_DEPL and the thin mineral soil layer at OL_DEPL A.

As not affected by landslides Bauer et al. (in review) considered the upper part of MC 3 between 2050 m and 2200 m ASL with slope angles ranging between 5 ° and 15 ° (fig. 3.1).

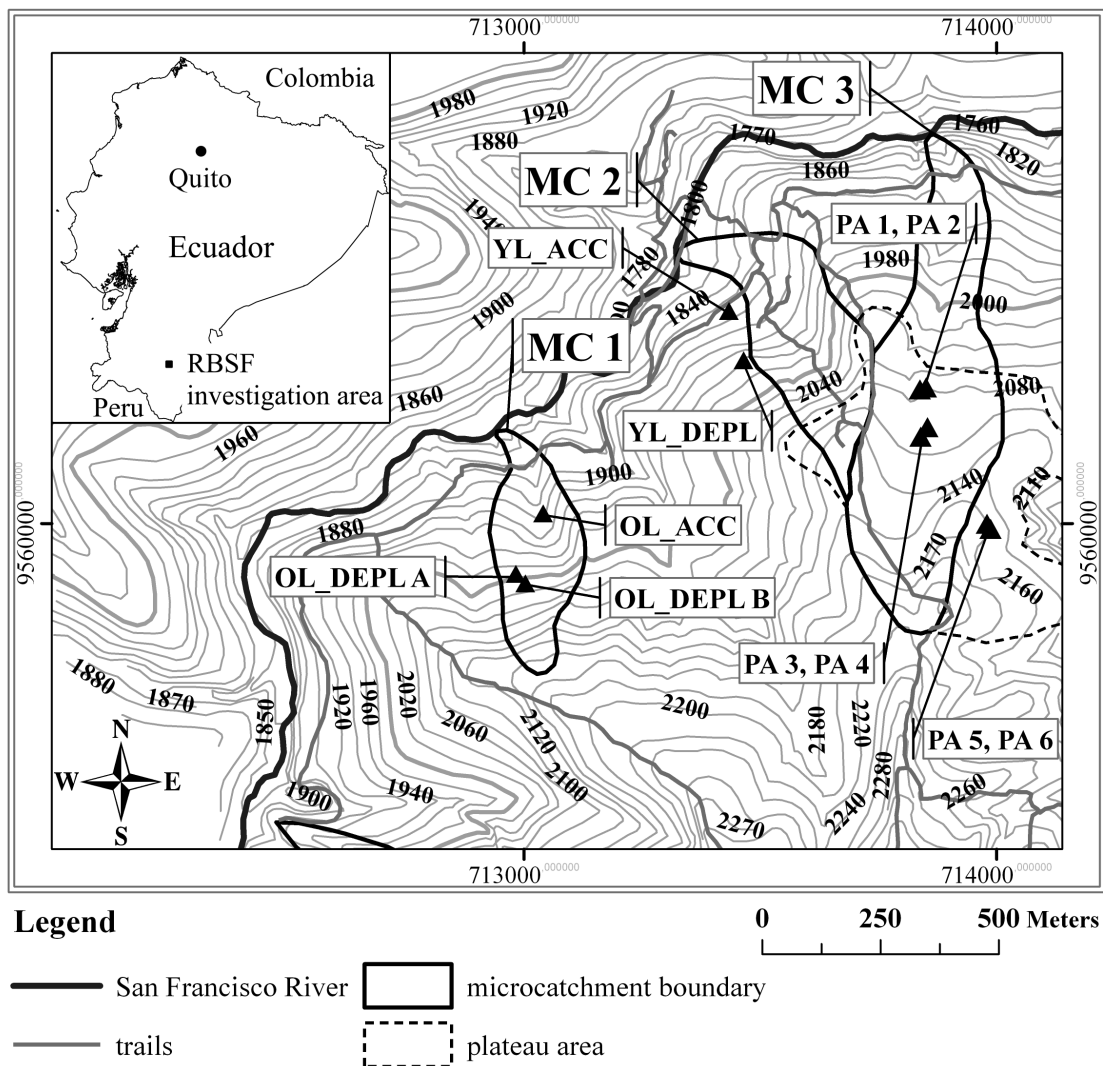


Figure 3.1 Core area of the RBSF investigation area. Except for PA 3, ... PA 6, the experimental plots described in section 3.2.1 were adopted from Bauer et al. (in review). Altitudes are in m ASL. Coordinate system is UTM WGS84 17S.

Here, they performed two dye tracer experiments (PA 1, PA 2) in a mature ridge forest (fig. 3.1). Detailed descriptions of the plots mentioned in section are given in Bauer et al. (in review).

3.2.2 Data basis

To the pedon scale dye tracer experiments and analysis performed by Bauer et al. (in review) which we use in this study, we conducted further experiments on the plateau area named PA 3, PA 4, PA 5, and PA 6 (fig. 3.1). The mean of the matric potential decadal logarithm (= pF) of the soils before the dye tracer application were pF = 1.43 at PA 3, pF = 0.71 at PA 4, pF = 1.64 at PA 5, pF = 1.63 at PA 6. The dye tracer experiments, excavation of the plots, soil sampling, determination of the fine soil fractions and bulk densities were performed as seen in Bauer et al. (in review).

In order to assess the control of rock fragment content and bulk density on the mineral soils Ksat, we resort to data collected in microcatchment 2 (= MC 2, fig. 3.1), named MC 2 data set in the following. The MC 2 data set (fig. 3.2) comprised 22 pits excavated in Cambisols, which were situated between 1850 m and 2100 m ASL and consistently covered by primary forest. Above 2100 m ASL within gentler hillslopes, soils resembled Stagnosols with negligible rock fragment contents (Kreutzer and Martini, 2002). We did not consider these soils in the MC 2 data set. From the soil horizons A, B and C of each pit, the data set contained of the fine soil fractions (= *sand*, *silt*, *clay*), fine soil bulk density (= *bd*), rock fragment content (= *stones*), altitude ASL (= *alt*) of the sampling points, and Ksat (= *Ksat*). Soil texture, bulk density, and rock fragment content were determined according to Bauer et al. (in review). Ksat was measured with a constant-head well permeameter (Elrick and Reynolds, 1992). An elaborate description of the soils within MC 2 is given in Kreutzer and Martini (2002).

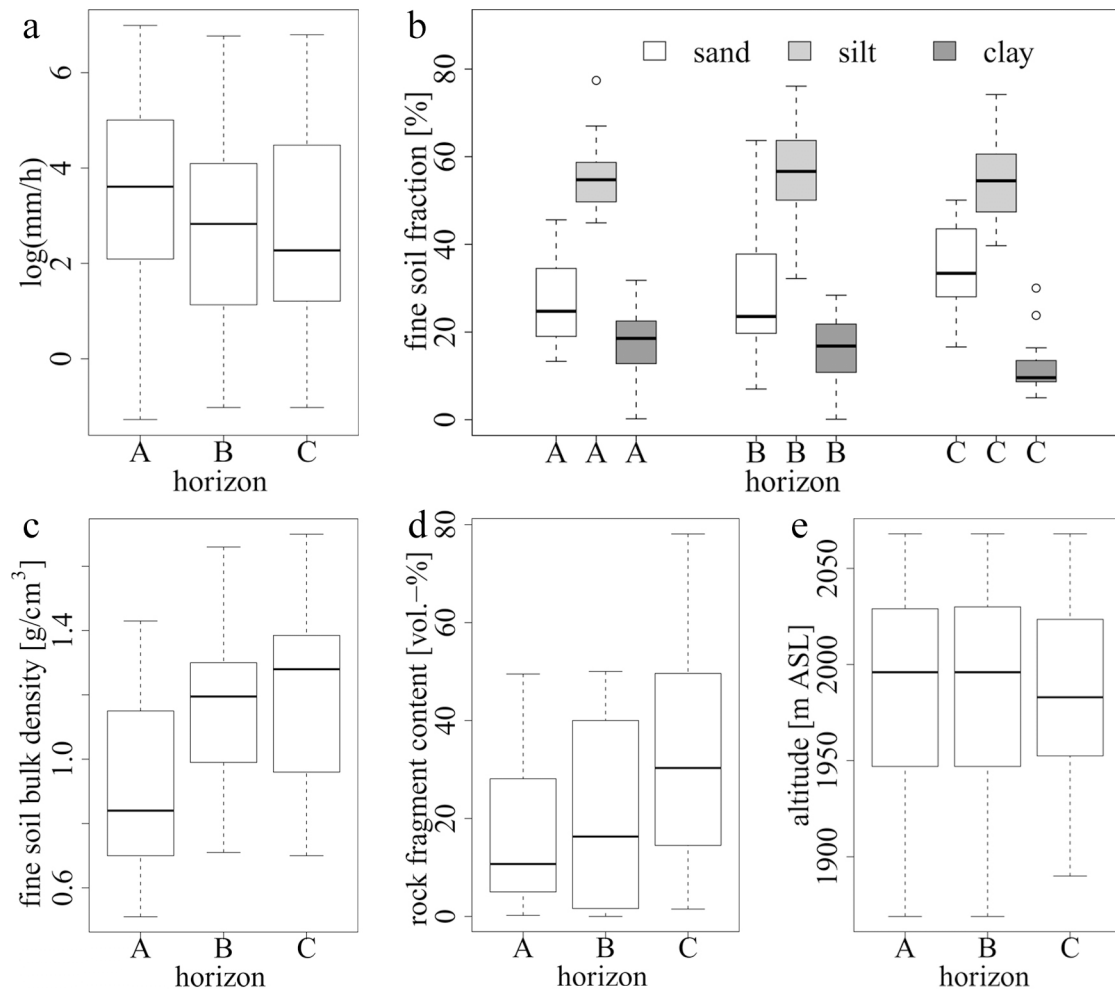


Figure 3.2 Boxplots of the MC 2 data set comprising 22 measurements of the A-, 18 measurements for the B-, and 19 measurements of the C horizon distributed over 22 pits. (a) log of Ksat; (b) fine soil fractions; (c) fine soil bulk density; (d) rock fragment content; (e) altitude ASL. The crossbar within a box designate the median. The length of a box equals the interquartile range, the whiskers indicate the range for data not being counted among outliers. These are denoted by the open circles which are at least 1.5 times the interquartile range away from the lower and upper quartile.

3.2.3 Image processing and analysis of dye stain patterns

In order to obtain binary images and dye coverage functions (Flury et al., 1994) of the dye stain patterns observed in the soil profiles, and to visualise the distribution of the dye stain widths by probability density functions (= pdf) we digitised and processed the dye stain patterns obtained from PA 3, ..., PA 6 as seen in Bauer et al. (in review).

3.2.4 Extreme value statistics

In order to evaluate the transmissibility of less permeable layers or soil horizons for percolating water, we resort to a measure introduced by Schlather and Huwe (2005) for the

purpose to assess, for example, the vulnerability of groundwater by pollutants. In their study, Schlather and Huwe (2005) called this measure risk index ξ_r , which is defined as the form parameter ξ of the generalised Pareto distribution (1). The basic idea is to describe the excess of small dye tracer quantities below larger quantities, i.e. below a predefined appropriate threshold via the generalised Pareto distribution H (Embrechts et al. 1997):

$$H(z) = H(z; \xi, s) = 1 - \left(1 + \frac{\xi \cdot z}{s}\right)^{\frac{-1}{\xi}}, \quad (1)$$

where $s > 0$, ξ and z must take values so that $1 + \xi z / s > 0$. If $\xi = 0$, $H(z)$ is understood as the limit of $H(z; \xi, s)$ as $\xi \rightarrow 0$. The second parameter s is called scale parameter (Schlather and Huwe, 2005). A higher value of s contributes to a higher risk if all other conditions such as soil properties are the same. In their study, Schlather and Huwe (2005) categorise ξ_r as follows:

- (i) if ξ_r takes negative values, the dye tracer does not exceed a certain depth. The higher the absolute value of ξ_r , the sharper the boundary between the stained upper and the unstained lower part of the observed profile
- (ii) for $\xi_r = 0$, the amount of a dye tracer excess below the major stained area can be neglected
- (iii) for positive values of ξ_r , an excess of small dye tracer quantities below the mayor stained part exist. The larger the value of ξ_r , the higher the probability that an entered flow path is run through into great depth.

The approach of Schlather and Huwe (2005) does not only refer to preferential flow, since matrix flow replacing paths by micropaths and drops by packages of infinitesimal volume can be considered as well. Thus, the risk index ξ_r is determined by the predominating flow system. For stratified soils, estimation of ξ_r can be problematic if a distinct secondary maximum intercepts the decline of the dye coverage function with depth. This discontinuity can be caused, for example by a less permeable subsoil as shown in Bauer et al. (in review). According to Bogner et al. (2008b), by ignoring the first maximum above (generally situated at the ground surface), ξ_r can be estimated regarding the secondary maximum. Since we will apply equation 1 to dye coverage functions derived from stratified soils according to Bauer et al. (in review), we interpret the form parameter ξ as an index of transmissibility ($= \xi_T$) for water within less permeable soil horizons or layers.

For the purpose to determine ξ_T , an automatic procedure is proposed in *SoPhy* ver. 1.0.39 by Schlather et al. (2009), a package for the statistical software *R* (R Development Core Team

2010). Here, the fraction of the stained soil profile at depth d is represented by the number of stained pixels $p(d)$. By dividing $p(d)$ with p_{max} , which is the maximum of stained pixels at a certain depth d , an estimate for the probability that a path is stained at least up to depth d is obtained. In order to fit the distribution $1-H(1)$ an appropriate decline of $p(d_i)/p_{max}$ with depth is required, with $i = 1, \dots, k$, where k is the number of rows of the binary image. By default of the software, this decline should be located between 50 % and 80 % of the considered stained pixel maximum. A detailed description of the fitting procedure can be found in Schlather and Huwe (2005). However, in the automatic fitting procedure of *SoPhy* determination of the scale parameter s was not included. As successfully applied by Bogner et al. (2008b), we estimated the scale parameter s in a second step by fitting $1-H$ to $p(d_i)/p_{max}$ via non linear least squares while the previous estimated transmissibility index ξ_T was kept constant.

In order to obtain an appropriate goodness of fit, we computed the coefficient of determination R^2 following to Kvålseth (1985) and Bogner et al. (2008b) as (2):

$$R^2 = 1 - \frac{\sum \{P(d) - \hat{P}(d)\}^2}{\sum \{P(d) - \bar{P}\}^2}, \quad (2)$$

where $P(d)$ is the percentage of stained pixels in the depth d to which $1-H$ was fitted, $\hat{P}(d)$ is the estimated percentage of stained pixels in depth d , and \bar{P} the mean percentage of stained pixels within the part of the profile which was used to fit the $1-H$ distribution.

3.2.5 Multivariate statistical analysis

More recent studies have reported an increasing effect of the rock fragment content on the soil hydraulic conductivity due to an increased macroporosity (Ravina and Magier, 1984; Sauer and Logsdon, 2002; van Wesemael et al., 1995; Verbist et al., 2009), which Torri et al. (1994) and Poesen and Lavee (1994) conceptually explained by loosely packed spheres of different size and shape. In this regard, Bauer et al. (in review) suggested that the rock fragment content controls K_{sat} by lowering the fine soil bulk density, which may also lead to larger dye stain widths due to an increased transversal mechanical dispersion provided by the rock fragments and the increased porosity of the soil matrix in between.

Taking these considerations into account, we hypothesise that the higher the rock fragment content, the greater the dye stain widths due to increasing transversal dispersion caused by the rock fragment and a less dense fine soil matrix in between (*i*), and therefore a higher K_{sat} (*ii*). In order to prove the hypothesis from (*i*), we related the dye stain widths to

soil parameters determined by Bauer et al. (in review) from soils within the young (YL) and old landslide (OL). From their probability density functions of dye stain widths we computed the mean of the maximum dye stain widths for each soil horizon (fig. 3.3a), from which Bauer et al. (in review) obtained the corresponding soil parameters (figure 3.3b-d).

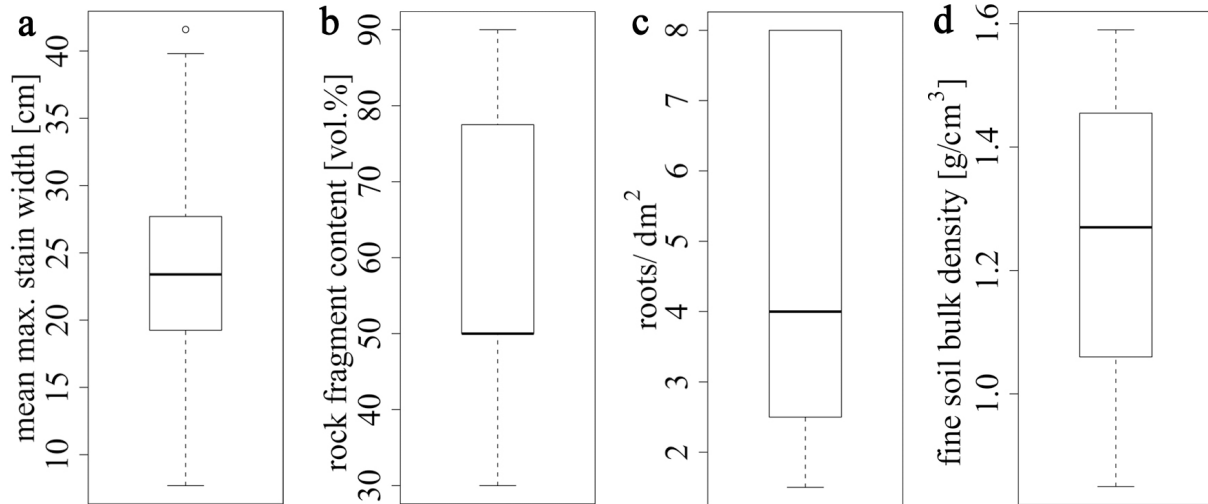


Figure 3.3 Boxplots of the mean maximum dye stain width (a), rock fragment content (b), counts of roots per dm^2 (c), and fine soil bulk density (d). The data of (a), (b), and (c) was borrowed from table 2.1 in Bauer et al. (in review). The crossbar within a box designate the median. The length of a box equals the interquartile range, the whiskers indicate the range for data not being counted among outliers. These are denoted by the open circles which are at least 1.5 times the interquartile range away from the lower and upper quartile. The data shown in (a), (b), and (c) was borrowed from table 2.1 in the study of Bauer et al. (in review).

Regarding (ii), we provided the MC 2 data set (see section 3.2.2). Exploration of the data showed some minor outliers for sand and silt (fig. 3.2b), but clear negative correlations between sand and silt ($r = -0.76$), and sand and clay ($r = -0.62$), which necessitated to drop the sand as predictor. Due to the wide of span $\sim 10^4$ mm/h, we applied a log-transformation on the K_{sat} which we considered as response variable. In undocumented preliminary studies we verified that subdividing the MC 2 data set into three topographical groups of pits along *becks*, *ridges*, and within *midslopes* neither revealed significant different relationships, i.e. a random effect between K_{sat} and the predictors given in figure 3.2b-e nor significant heteroscedasticity of the residuals among the groups. Also, we did not find significant random effects among the horizons A, B, and C of the MC 2 data set. Moreover, we observed a collinearity between the *alt* predictor and the model intercept, which we resolved by mean centring of the former. Therefore, we provide a multivariate linear regression model (3):

$$\log(Ksat_i) = \beta_0 + \beta_1 \cdot (stones)_i + \beta_2 \cdot (bd)_i + \beta_3 \cdot (silt)_i + \beta_4 \cdot (clay)_i + \beta_5 \cdot (alt)_i + \varepsilon_i, \quad (3)$$

with $i = 1, \dots, n$, and $\varepsilon_i \sim N(0, \sigma^2)$

where $Ksat_i$ is the response variable, β_0 the intercept, β_1, \dots, β_5 the regression coefficients, ε_i the error term, and n the number of measurements ($n = 59$). We consider the null hypothesis as $H_0: \beta_1 = \beta_2 = 0$ and the alternative hypothesis as $H_1: \beta_1 + \beta_2 \neq 0$, with β_1 and β_2 as regression coefficients of the *stones*- and the *bd* predictor, respectively. We started the model procedure with all corresponding predictors as mentioned above. In order to seek for the best model result, we omitted each predictor variable one time from the full model and compared the model results via the Akaike's Information Criterion (AIC) (Akaike, 1974), a measure of goodness of fit (4):

$$AIC = -2 \log(L) + 2(p + 1), \text{ with} \quad (4)$$

$$L(\mu, \sigma) = \frac{1}{(\sigma\sqrt{2\pi})^n} \exp\left[-\frac{1}{2\sigma^2} \sum_{i=1}^n (Ksat_i - \mu)^2\right], \text{ which is maximised if} \quad (5)$$

$$\sigma^2 = \frac{\sum (Ksat_i - \mu)^2}{n - 1}, \text{ with} \quad (6)$$

$$\mu = \frac{\sum Ksat_i}{n}, \quad (7)$$

where p is the number of parameters in the model, $L(\mu, \sigma)$ is the likelihood of a normal distribution, μ the mean and σ the standard deviation, and n the number of values of the response variable $Ksat_i$, where $i = 1, \dots, n$. Subsequently, the model with the lowest AIC is chosen. From this model, again each of the remaining predictor variables is omitted one time, and again that model is chosen which reveals the lowest AIC. This procedure is repeated until a decrease of the AIC cannot be achieved.

3.3 Results and discussion

3.3.1 Extreme value statistics

For the soil profiles Bauer et al. (in review) investigated in YL_DEPL we estimated mostly negative ξ_T values (tab. 3.1). Here, the distribution 1- H was fitted to the pronounced decline of the dye coverage at the interface between mineral soil layer and weathered parent material

(fig. 3.4c). The negative ξ_T values clearly reveal that the weathered parent material at YL_DEPL can be seen as quasi impervious. Also the very small and negative ξ_T values we estimated for YL_ACC document a restricted deeper percolation at the pedon scale. However, compared to YL_DEPL the notably higher mean scale parameters (tab. 3.1) indicate a rather gradual decline of the dye coverage with depth. This decline occurs within the mineral soil layer, since the maximum of the dye coverage function which permits to fit $1-H$ occurs either in the mineral subsoil (fig. 3.4a) or -topsoil (fig. 3.4b). The maxima which occurred within the subsoil were due to almost throughout stained remnants of a buried Ah horizon and organic layer between 20 cm and 50cm depth as reported by Bauer et al. (in review). Also, in the middle of a profile in YL_ACC a vertical crack ranging from the soil surface deeper than the soil profile, which was throughout stained by the tracer. In this, we could not fit the $1-H$ distribution to the dye coverage function.

For OL_ACC, OL_DEPL A and O_DEPL B we could fit $1-H$ only to those sections of the dye coverages which declines at the interface between mineral subsoil and weathered parent material (fig. 3.4d, g, h), or within the weathered parent material (fig 3.4e, f). This issue, and the relative large positive ξ_T values and scale parameters (tab. 3.1) reveal a rather unhindered percolation through the mineral soil layer into the weathered parent material. Note that in table 3.1 no results are given for OL_ACC, since we excluded fits of $1-H$ whose coefficients of determination R^2 (2) did not exceed 0.5. The reason therefore is exemplarily illustrated in figure 3.4d, where the dye coverage do not clearly tends to smaller values at deeper depths due to a permeable mineral soil/weathered parent material interface.

With respect to our findings, we observed that in case of negative ξ_T values, and positive ξ_T values smaller than 1 the value of the scale parameter describes the vertical extent of the transition between the stained and unstained area below. Similar was observed by Bogner et al. (2008b) by comparing the propagation of two different solutes within the same soil. In our case, this can be readily seen by comparing the fitted $1-H$ distributions and scale parameters in figure 3.4g (OL_DEPL B) and figure 3.4i (PA 1) for negative ξ_T values, and in figure 3.4b (YL_ACC) and 3.4k (PA 3) for small positive ξ_T values. The scale parameters and vertical extents of the transitions between the stained and the unstained part below are larger in figures 3.4b and 3.4g than in figures 3.4i and 3.4k. Practically, this means that the scale parameter can be seen as a measure of the bulk percolation depth, but under given boundary conditions such as irrigation intensity, type of dye tracer, and soil moisture before irrigation according to Bogner et al. (2008b). Regarding this, the values we estimated for ξ_T and s seem to be plausible by relating them to the soil parameters measured by Bauer et al. (in review).

Moreover, the interpretation of the scale parameter is limited to horizontal layers as it is overestimated if the number of stained pixels declines along an inclined interface between two soil horizons as exemplarily shown in figures 3.4c and 3.4f.

Table 3.1 Results of the extreme value analysis. Here, only those fittings are considered whose R^2 (2) was higher than 0.5. Since the sites of each pair PA 1/PA 2, PA 3/PA 4, and PA5/PA 6 revealed similar soil types and due to its close vicinity to each other, results of each pair were merged. sd = standard deviation; min. = minimum; max. = maximum.

plot	soil type ^a	n ^b	inter- face ^c	transmissibility index ξ_T			scale parameter s		
				mean \pm sd.	min.	max.	mean \pm sd.	min.	max.
PA 1, PA 2	Stagnosols	6	O/T	0.12 \pm 0.29	-0.28	0.60	43.81 \pm 17.66	24.60	70.50
		10	T/S	-0.17 \pm 0.36	-0.65	<0.01	41.36 \pm 24.64	12.03	91.50
PA 3, PA 4	Podzols	12	O/T	-0.06 \pm 0.10	-0.31	0.02	41.86 \pm 14.07	21.31	68.17
		5	T/S	-0.29 \pm 0.30	-0.62	0.17	23.66 \pm 13.01	4.10	38.22
PA 5, PA 6	Stagnosols	5	O/T	0.08 \pm 0.28	-0.19	0.40	53.13 \pm 15.03	35.44	69.58
		12	T/S	0.33 \pm 0.28	-0.11	0.94	38.81 \pm 21.44	11.35	78.53
YL_DEPL	Regosols	5	S/P _w	-0.11 \pm 0.13	-0.31	<0.01	58.03 \pm 19.05	27.60	77.03
YL_ACC		3	T ^d	0.06 \pm 0.10	<0.01	0.17	148.06 \pm 88.59	52.95	228.22
		6	S ^d	-0.05 \pm 0.28	-0.36	0.40	106.15 \pm 101.68	14.3	298.10
OL_DEPL A	Cambisols	3	P _w ^d	1.85 \pm 2.79	-0.75	4.81	60.65 \pm 40.75	17.91	99.07
OL_DEPL B		4	S/P _w	0.46 \pm 0.81	-0.42	1.34	111.41 \pm 110.85	32.80	269.80

^a according to IUSS (2007) // ^b number // ^c maximum of stained pixel percentage at the interface of two layers or horizons, below which the distribution 1- H was fitted; O/T = organic layer/topsoil; T/S = topsoil/subsoil; S/P_w = subsoil/weathered parent material // ^d horizon, in which the maximum of the pixel percentage was considered by 1- H .

Contrary to the results we obtained from the landslides, in the plateau area the deepest dye tracer infiltration occurred until ~40 cm depth below the mineral soil surface in some profiles of PA 1 (fig. 3.4i), and most profiles of PA 5 (fig. 3.4m) and PA 6 (fig. 3.4n). Here, the lower boundary of the mineral topsoil layer showed locally pocket- or tongue shaped bulges extending into the subsoil. Visual inspections revealed that these bulges were produced by former roots which have left macropores enabling the percolation of the dye tracer into the subsoil. In these cases, we fitted 1- H to the decline of the secondary maximum at the topsoil/subsoil interface resulting in negative and positive ξ_T values smaller than 1 and scale parameter smaller than those we obtained from the landslide affected sites (tab. 3.1). For the Podzols at PA 3 and PA 4 (fig. 3.4k, l) we estimated mostly negative ξ_T values by fitting 1- H to the stained pixel first maximum at the organic layer/mineral soil interface, while just for 5 profiles respectively dye cover functions we could fit 1- H to the stained pixel secondary maximum at the topsoil/subsoil interface (tab. 3.1).

Thus, in most cases within the plateau area transmissibility of the mineral topsoil for water percolation is given until the topsoil/subsoil interface. In combination with the small scale parameters we obtained by fitting $1-H$ to the secondary maximum of the dye coverage at the topsoil/subsoil interface (tab. 3.1), the small positive and negative ξ_T values document an abrupt change of the flow regime at the topsoil/subsoil interface, below which no evidence of deeper percolation was found.

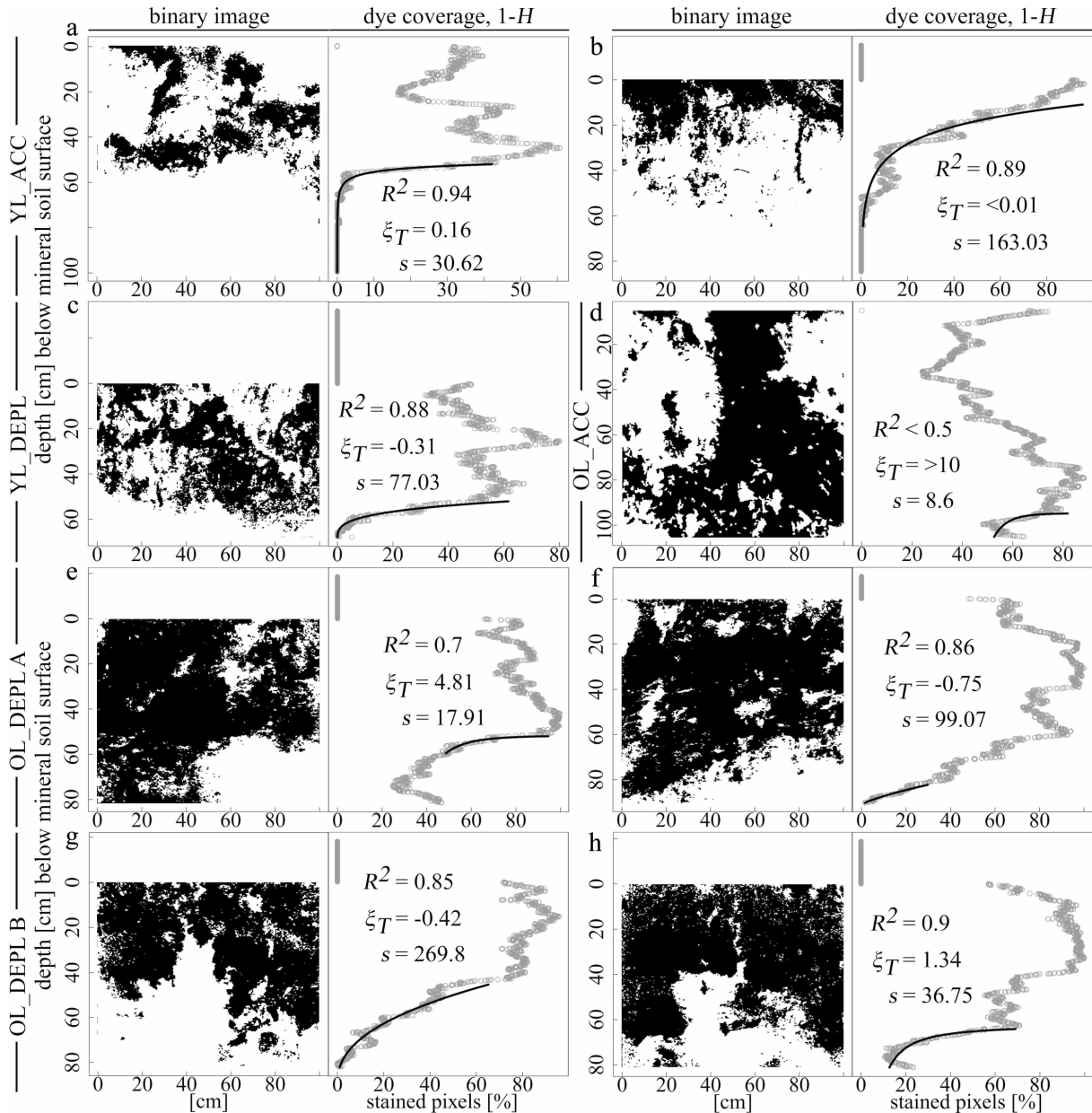


Figure 3.4 Exemplary binary images of the dye tracer distributions (black stains) and the corresponding dye coverage functions (open grey circles) derived from the experimental plots within the old landslide (OL), young landslide (YL), and plateau area (PA). The black lines designate the $1-H$ distributions fitted to the dye coverage functions, where ξ_T denotes the transmissibility index, s the scale parameter, and R^2 the goodness of fit computed by equation 2.

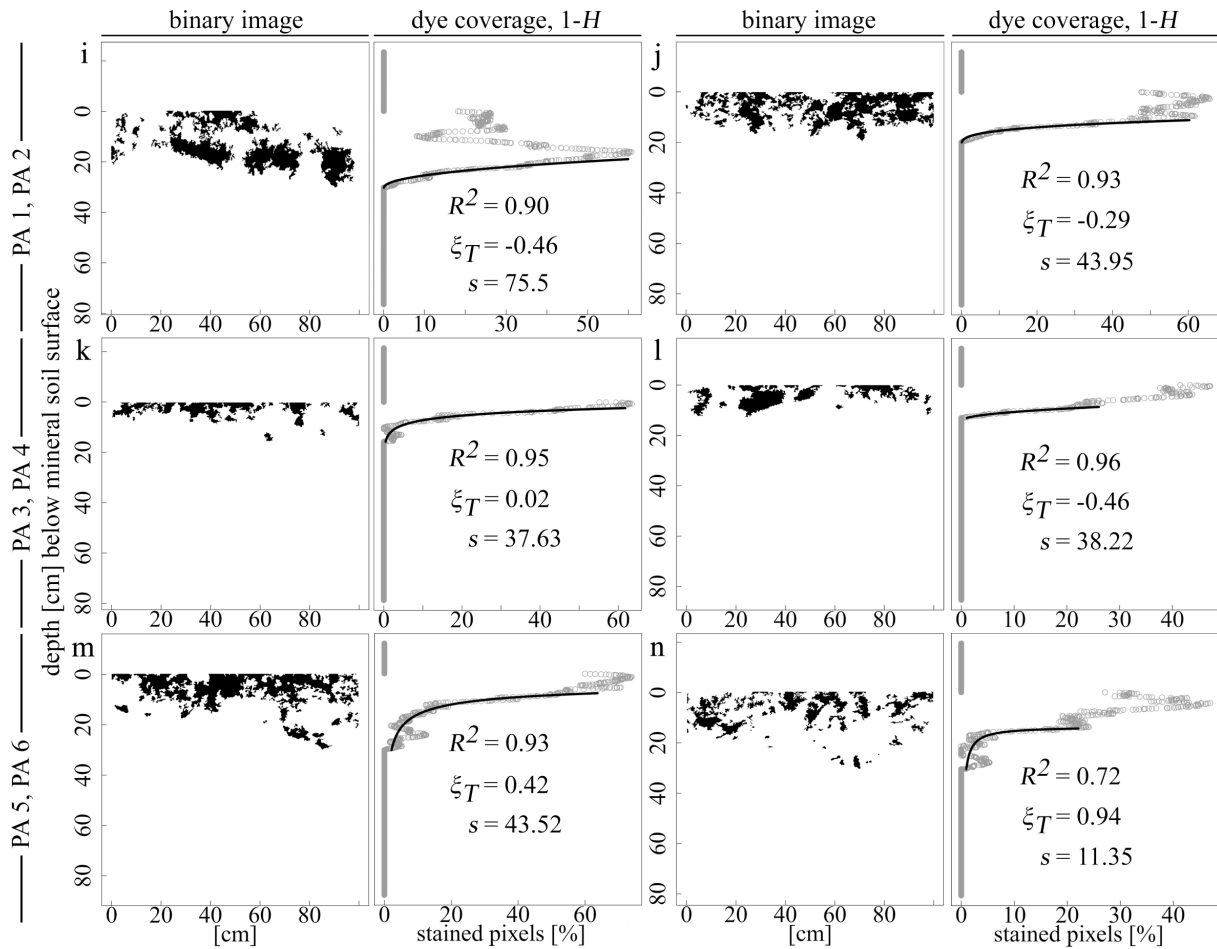


Figure 3.4 (continued from previous page)

Probability density functions of the dye stain widths and soil properties

The probability density functions of the dye stain widths (fig. 3.5c-f) we computed for PA 3, ..., PA 6 resemble well those of PA 1 and PA 2 (fig. 3.5a, b) computed by Bauer et al. (in review). Also, we found similar fine soil textures, topsoil- and subsoil bulk densities (tab. 3.2) as well as negligible rock fragment contents as in PA 1 and PA 2. Therefore, we follow Bauer et al. (in review) who concluded a low interaction between macropores and soil matrix at PA 1 and 2. On the one hand, the relatively high water contents of the soil matrix in PA 3, ... PA 6 before the dye tracer application (see section 3.2.2 for details) have certainly led to a reduced water interchange between soil matrix and macropore. On the other hand, the flat soil moisture characteristics estimated by Bauer et al. (in review) from PA 1 and PA 2, the high soil bulk densities which were measured for all investigated sites in the plateau area, and the prevailing humid climate in the RBSF study area indicate that the soil matrix provides a rather

small portion of drainable pores which may be rapidly filled up to saturation even by small rainfall events. Thus, water flow is mostly driven by gravity bypassing much of the soil matrix and rapid percolation within the mineral topsoil. The presence of an impervious soil layer along the topsoil/subsoil interface impedes an efficient vertical drainage of the macropores. Consequently, within the hillslope a rapid shallow subsurface flow would be provoked, if the macropores form a well interconnected and thus effectively draining network. However, if such a network is not given, the infiltrated water backs up in the macropores until the organic layer/mineral soil interface, where it contributes to the formation of a rapid lateral subsurface flow. This mechanism of shallow subsurface flow formation resembles the observations of Scherrer et al. (2007), who attributed Hortonian overland flow (Horton, 1933) to rapid initial infiltration via macropores but little uptake by the soil matrix either at the surface or from macropores. This seems to be most probable for the plateau area, since the first maximum of most of the dye coverage functions derived from the plateau area was situated at the organic layer/mineral soil interface including the profiles 200 cm downslope from the line source sprinkler. Otherwise, with increasing distance to the sprinkler we would have observed a shift of the first maximum from the organic layer/mineral soil interface to the topsoil/subsoil interface indicating a well interconnected lateral macropore flow network within the mineral topsoil. Since the mineral soils in the plateau area are overlain by a thick organic layer, the expression pseudo Hortonian overland flow according to McDonnell et al. (1991) is more suitable.

Table 3.2 Averaged fine soil fractions and bulk densities (= av. bd) of experimental plots within the plateau area. The standard deviation is denoted by sd.

plot	soil type ^a	soil layer ^c	<i>n</i> ^b	averaged fine soil fractions [%]			<i>n</i> ^b	av. bd ±sd. [g/cm ³]
				sand ±sd.	silt ±sd.	clay ±sd.		
PA 3	Albic Endoleptic	topsoil	7	53.5 ±1.7	30.4 ±4.6	5.9 ±6.1	9	1.22 ±0.50
		subsoil	11	52.0 ±2.9	34.2 ±3.9	5.8 ±2.5	12	1.58 ±0.16
PA 4	Histic Podzols (Densic)	topsoil	9	55.0 ±3.0	40.1 ±3.4	3.0 ±2.4	9	1.39 ±0.55
		subsoil	8	52.8 ±8.5	39.5 ±7.9	2.6 ±1.7	8	1.68 ±0.04
PA 5	Histic Stagnosols	topsoil	7	49.5 ±1.2	38.5 ±1.8	8.1 ±2.8	9	1.19 ±0.30
		subsoil	10	49.3 ±6.9	40.2 ±3.5	6.3 ±4.3	12	1.39 ±0.15
PA 6 (Albic)		topsoil	6	40.3 ±2.6	40.8 ±3.1	14.7 ±3.6	7	1.36 ±0.52
		subsoil	7	31.9 ±8.6	49.1 ±15.4	15.4 ±7.7	8	1.59 ±0.28

^a according to IUSS (2007) // ^b number // ^c in this study, we consider the uppermost 20 cm of the mineral soil layer as topsoil

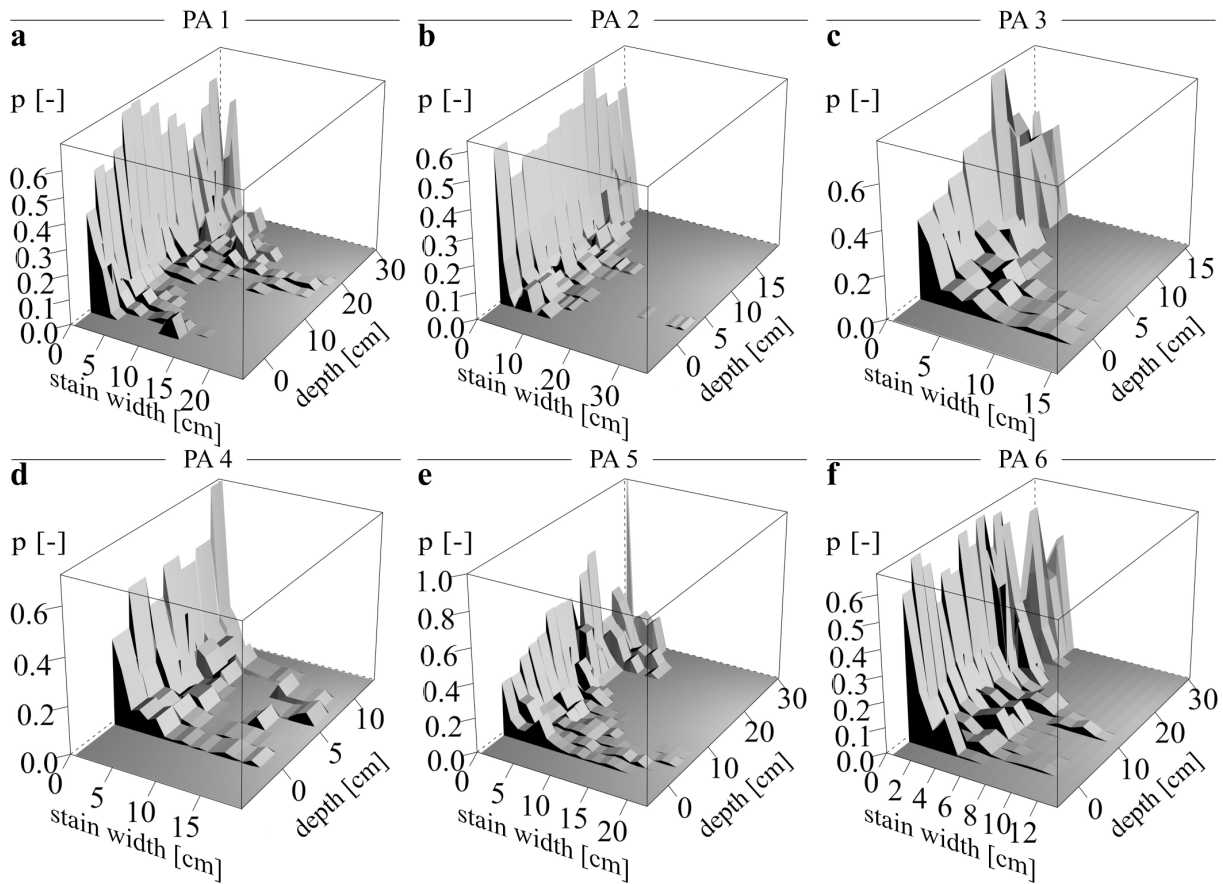


Figure 3.5 Exemplary probability density functions (= pdfs) corresponding to the binary images shown in figure 3.4, where 3.5a relates to 3.4i, 3.5b to 3.4j, and so on. We calculated the pdfs as seen in Bauer et al. (in review). Note that each single pdf within a graph denotes the arithmetic mean of dye stain widths over depth increments of 2 cm.

3.3.2 Multivariate statistical analysis

From the parameters given in figure 3.3 we computed the Pearson's correlation coefficients show in table 3.3. Here, among the parameters there is a strong negative correlation between bulk density and roots per dm^2 . The correlation between rock fragment content and bulk density is rather weak. Also, we determined a low Pearson's correlation coefficient of $r = 0.14$ between the *stones*- and *bd* predictor of the MC 2 data set. Moreover, none of the soil parameters given in table 3.3 correlate clearly with the mean maximum dye stain width. This and the low correlation between bulk density and rock fragment content show that we have to reject the hypothesis that the higher the rock fragment content, the greater the dye stain widths due to increasing transversal dispersion caused by the rock fragments and a less dense fine soil matrix in between as proposed in (i) of subsection 3.2.5.

Table 3.3 Pearson's correlation coefficients among soil parameters shown in figure 3.3.

	mean max. stain width	rock fragment content	counts of roots per dm ²	bulk density
mean max. stain width	1			
rock fragment content	0.39	1		
counts of roots per dm ²	-0.02	-0.73	1	
bulk density	-0.11	0.51	-0.84	1

Concerning (ii), the final result of the multivariate linear regression (3) reveals the remaining predictors *stones* and *bd* (tab. 3.4) as clearly significant ($p < 0.05$) allowing us to reject $H_0: \beta_1 = \beta_2 = 0$. Figure 3.6 shows normally distributed residuals (a) without recognisable heteroscedasticity or other patterns (b). However, the goodness of fit with an adjusted $R^2 = 0.37$ (tab. 3.4) indicates that *Ksat* is not largely controlled by both the rock fragment content and the bulk density (fig. 3.6c). Consequently, there must be further predictors which we did not include in the multivariate model (3). Such a parameter, for example, could be the presence of fissures and cracks in the mineral soil layer as encountered by Bauer et al. (in review) in the young landslide (YL). Furthermore, Bauer et al. (in review) assumed that at a distinct threshold between 50 vol.-% and 75 vol.-% the rock fragment content predominantly controls the permeability of the mineral soil cover, whereas the influence of the vegetation cover becomes less important. Below this threshold, rock fragment contents may play a rather subordinate role. At least, this assumption may provide an explanation why the influence of the rock fragment content on *Ksat* is low (tab. 3.4). In order to analyse this issue thoroughly, more data records with higher rock fragment contents would be needed than actually provided in the MC 2 data set (fig. 3.2d).

Table 3.4 Summary of the multivariate linear regression of equation 3.

predictors	estimates of coefficients	standard error	<i>t</i> value	<i>p</i> value	R^2	Model	
						$R^2_{adj.}$	<i>p</i> value
<i>intercept</i>	4.18	0.86	4.86	9.79e-06	0.39	0.37	8.99e-07
<i>stones</i> (β_1)	0.04	0.01	3.44	0.001			
<i>bd</i> (β_2)	-4.04	0.75	-5.36	1.65e-06			

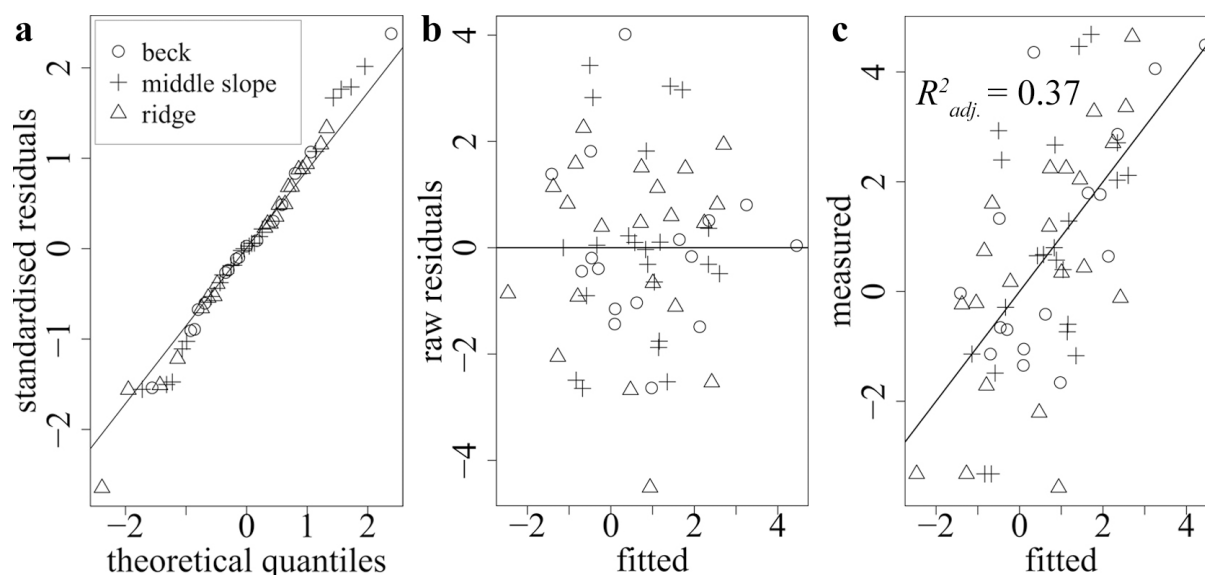


Figure 3.6 (a) Quantile-Quantile plot to test visually for normal distribution of the residuals; (b) residuals versus fitted logarithmic Ksat values [$\log(\text{mm/h})$]; (c) measured versus fitted logarithmic Ksat values [$\log(\text{mm/h})$]. Note that in all three graphs data points are grouped (legend for all three graphs in (a)) according to the undocumented mixed effect models as described in subsection 3.2.5.

3.4 Conclusions

From pedon scale dye tracer experiments conducted in soils within landslide affected and unaffected hillslopes in the Andes of southern Ecuador we computed a transmissibility index ξ_T and scale parameter s , both belonging to the two parametric generalised Pareto distribution, in order to evaluate the transmissibility of impeding soil horizons or layers for percolating water. In this regard, we found that in combination with the scale parameter, negative and small positive ξ_T values provide useful information which allows to assess the percolation depth under given boundary conditions such as type of dye tracer, irrigation intensity, and soil moisture before irrigation. Moreover, the interpretation of s is limited to horizontal layers as it is overestimated if the number of stained pixel declines along an inclined interface between two soil horizons or -layers.

In accordance with the study of Bauer et al. (in review), the analysis of the dye tracer binary images we obtained from the plateau area (fig. 3.1) reveal that prerequisites are given for lateral shallow subsurface flow along the organic layer/mineral topsoil interface, which we denote as pseudo Hortonian overland flow following McDonnell (1991). Though already postulated, this subsurface flow was not allocated to a distinct area within the microcatchments MC 2 and MC 3 (fig. 3.1) investigated by Fleischbein et al. (2006), Goller et al. (2005) and Wilcke et al. (2008). Considering the findings of this study and the digital soil

map of Liess et al. (2009), the area providing this shallow subsurface flow can now be localised within MC 2 and MC 3, since both overlap with the plateau area above 2060 m ASL (fig. 3.1). Deforestation by slash and burn as commonly applied in the Andes of South Ecuador (Beck et al., 2008) would instantly disable the intercepting and moderating effect of the canopy and the abundant organic layer for rainfall. The pseudo Hortonian overland flow would be instantly converted to Hortonian overland flow with all its consequences concerning soil erosion and -degradation.

In contrast to the plateau area, particularly in the old landslide the analysis of the dye tracer experiment revealed unhindered percolation through the mineral soil layer into the parent material, while only in the young landslide percolation was impeded due to a weathered bedrock in the depletion zone and an impervious subsoil in the accumulation zone. We assume that in the latter percolation depth will be enhanced by progressive vegetation succession on the young landslide. Moreover, via multivariate linear regression we could show that at least for the stony Cambisols in MC 2 (fig. 3.1) both rock fragment content and particularly bulk density significantly, but not largely control Ksat of the mineral soil. Bauer et al. (in review) assumed that at a distinct threshold between 50 vol.-% and 75 vol.-% the rock fragment content mainly controls Ksat. Since our MC 2 data set did not provide sufficient data records with larger fragments contents, we recommend further studies to verify this issue.

3.5 Acknowledgements

We would like to thank Jörn Martini, Detlef Kreutzer, Katrin Drastig and Wolfgang Wilcke for parts of soil data provided in the MC 2 data set. This study was supported and funded by the German Research Foundation (DFG) grant nr. DFG FOR 402/1-1 Hu 636/9-3 and DFG FOR 816 - HU 636/14-1.

3.6 References

Akaike, H., (1974): A new look at the Statistical Model Identification. *IRRR Trans. Automat. Control* 19, 716-723.

Chapter 3 – References

- Balslev, H., Øllgaard, B., 2002. Mapa de vegetación del sur de Ecuador, in: Aguirre, M.Z., Madsen, J.E., Cotton, E., Balslev, H. (Eds), *Botnica Austroecuadoriana. Estudios sobre los Recursos Vegetales en las Provincias de El Oro, Loja y Zamora-Chinchipe*, Quito, pp. 51-64.
- Beck, E., Makeschin, F., Haubrich, F., Richter, M., Bendix, J., Valarezo, C., 2008. The Ecosystem (Reserva Biológica San Francisco), in: Beck, E., Bendix, J., Kottke, I., Makeschin, F., Mosandl, R. (Eds), *Gradients in a Tropical Mountain Ecosystem of Ecuador*. *Ecological Studies*, Springer, Berlin, pp 1-14.
- Bendix, J., Rollenbeck, R., Richter, M., Fabian, P., Emck, P., 2008. Climate, in: Beck, E., Bendix, J., Kottke, I., Makeschin, F., Mosandl, R. (Eds.), *Gradients in a Tropical Mountain Ecosystem of Ecuador*, Springer Verlag, Berlin, Heidelberg, pp 63-73.
- Bogner, C., Engelhardt, S., Zeilinger, J., Huwe, B., 2008a. Visualisation and analysis of flow patterns and water flow simulations in disturbed and undisturbed tropical soils, in: Beck, E., Bendix, J., Kottke, I., Makeschin, F., Mosandl, R. (Eds.), *Gradients in a Tropical Mountain Ecosystem of Ecuador*. *Ecological Studies*, Springer, Berlin, pp 387-397.
- Bogner, C., Wolf, B., Schlather, M., Huwe, B., 2008b. Analysing flow patterns from dye tracer experiments in a forest soil using extreme value statistics. *Eur. J. Soil Sci.* 59(1), 103-113.
- Bonell, M., Balek, J., 1993. Recent scientific developments and research needs in hydrological processes of the humid tropics, in: Bonell, M., Hufschmidt, M.M., Gladwell, J.S. (Eds.), *Hydrology and Water Management in the Humid Tropics*. Cambridge University Press, Cambridge, pp. 167–260.
- Bruijnzeel, L.A., Hamilton, L.S., 2000. Decision Time for Cloud Forest. *IHP Humid tropics Programme Series* 13(44).
- Bruijnzeel L. A., 2004. Hydrological functions of tropical forests: Not seeing the soil for the trees? *Agriculture Ecosystems & Environment* 104, 185-228.
- Caballero, Y., Jomelli, V., Chevallier, P., Ribstein, P., 2002. Hydrological characteristics of slip deposits in high tropical mountains (Cordillera Real, Bolivia). *Catena* 47, 101-116.
- Céleri, R., Feyen, J., 2009. The Hydrology of Tropical Andean Ecosystems: Importance, Knowledge Status, and Perspectives. *Mountain Research and Development* 29(4), 350-355.
- Chappell, N.A., Sherlock, M.D., 2005. Contrasting flow pathways within tropical forest slopes of Ultisol soils. *Earth Surf. Process. Landforms* 30, 735-753.
- Elrick, D.E., Reynolds, W.D., 1992. Infiltration From Constant Head Well Permeameters And Infiltrimeters, in: Topp, G.C., Reynolds, W.D., Green, R.E. (Eds.), *Advances in Measurement*

- of soil Physical Properties. Bringing Theory Into Practice. SSSA Spec. Publ. 30, Madison, WI, pp 1-24.
- Embrechts, P., Klüppelberg, C., Mikosch, T., 1997. Modelling Extremal Events. Springer, Berlin.
- Fleischbein, K., Wilcke, W., Valarezo, C., Zech, W., Knoblich, K., 2006. Water budgets of three small catchments under montane Forest in Ecuador: experimental and modelling approach. *Hydrol. Process.* 20, 2491-2507.
- Flury, M., Flühler, H., Jury, W.A., Leuemberger, J., 1994. Susceptibility of soils to preferential flow of water: a field study. *Water Resour. Res.* 30(6), 1945-1954.
- Francou, B., Ramirez, E., Cáceres, B., Mendoza, J., 2000. Glacier Evolution in the Tropical Andes during the Last Decades of the 20th Century: Chacaltaya, Bolivia, and Antizana, Ecuador. *Ambio* 29(7), 416-422.
- Fries, A., Rollenbeck, R., Göttlicher, D., Nauss, T., Homeier, J., Peters, T., Bendix, J., 2009. Thermal structure of a megadiverse Andean mountain ecosystem in southern Ecuador, and its regionalization. *Erdkunde* 63, 321-335.
- Goller, R., Wilcke, W., Leng, M.J., Tobschall, H.J., Wagner, K., Valarezo, C., Zech, W., 2005. Tracing water paths through small catchments under a tropical montane rain forest in South Ecuador by an oxygen isotope approach. *J. Hydrol.* 308, 67-80.
- Horton, R.E., 1933. The role of infiltration in the hydrological cycle. *Trans. AGU* 14, 460-466.
- Hungerbühler, D., 1997. Neogene basins in the Andes of southern Ecuador: evolution, deformation and regional tectonic implications. PhD thesis. URL <http://e-collection.ethbib.ethz.ch/view/eth:40985> (accessed on January 2010), ETH Zürich, Zürich.
- IUSS Working Group WRB, 2007. World Reference Base for Soil Resources 2006, first update 2007. World Soil Resources Reports No. 103. FAO, Rome.
- Kreutzer, D., Martini, J., 2002. Bestimmung und Regionalisierung der gesättigten hydraulischen Leitfähigkeiten in Böden unter tropischem Bergregenwald in Ecuador mit verschiedenen Methoden. Unpubl. diploma thesis, University of Giessen, Giessen.
- Kvålseth, T.O., 1985. Cautionary note about R^2 . *American Statistician* 39, 279-285.
- Liess, M., Glaser, B., Huwe, B., 2009. Digital Soil Mapping In Southern Ecuador. *Erdkunde* 63 (4), 309-319.
- McDonnell, J.J., Owens, I.F., Stewart, M.K., 1991. A case study of shallow flow paths in a steep zero-order basin. *Water Resour. Bul.* 27, 679-85.

- Öhrström, P., Hamed, Y., Persson, M., Berndtsson, R., 2004. Characterizing unsaturated solute transport by simultaneous use of dye and bromide. *J. Hydrol.* 289, 23-35.
- Poesen, J., Lavee, H., 1994., Rock fragments in topsoils: Significance and processes. *Catena*, 23, 1-28.
- R Development Core Team, 2010. R: A language and environment for statistical computing. R Foundation for Statistical Computing. URL <http://www.R-project.org> (accessed on July 2010), Vienna, Austria.
- Ravina, I., Magier, J., 1984. Hydraulic conductivity and water retention of clay soils containing coarse fragments. *Soil Sci. Soc. Am. J.* 48, 736-740.
- Rollenbeck, R., 2006. Variability of precipitation in the Reserva Biológica San Francisco / Southern Ecuador. *Lyonia* 9(1), 43-51.
- Ruiz, D., Moreno, H.A., Gutierrez, M.E., Zapata, P.A., 2008. Changing climate and endangered high mountain ecosystems in Colombia. *Science of the Total Environment* 398(1), 122-132.
- Sauer, T.J., Logsdon, S.D., 2002. Hydraulic and Physical Properties of Stony Soils in a Small Watershed. *Soil Sci. Soc. Am. J.* 66, 1947-1956.
- Scherrer, S., Naef, F., Faeh, A.O., Cordery, I., 2007. Formation of runoff at the hillslope scale during intense precipitation. *Hydrol. Earth Syst. Sci.*, 11, 907-922.
- Schlather, M., Huwe, B., 2005. A risk index for characterising flow pattern in soils using dye tracer distributions. *J. Contam. Hydrol.* 79, 25-44.
- Schlather, M., 2009. SoPhy: Soil Physics Tools. URL <http://www.cran.r-project.org> (accessed on January 2010), contributed package.
- Soulsby, C., Pomeroy, A., Gibbins, C., 1997. Hydrology and hydrochemistry of a montane rainforest catchment in Queensland, Australia, in: Peters, N.E. and Coudrain-Ribstein, A. (Eds.), *Hydrochemistry Symposium*, Int. Assoc. Hydrol. Sci., Rabat, Morocco.
- Torri, T., Poesen, J., Monaci, F., Busoni, E., 1994. Rock fragment content and bulk density. *Catena* 23, 65-71.
- van Wesemael, B., Poesen J., de Figueiredo, T., 1995. Effects of rock fragments on physical degradation of cultivated soils by rainfall. *Soil and Tillage Res.* 33, 229-250.
- Verbist, K., Baetens, J., Cornelis, W.M., Gabriels, D., Torres, C., Soto, G., 2009. Hydraulic Conductivity as Influenced by Stoniness in Degraded Drylands of Chile. *Soil. Sci. Soc. Am. J.* 73, 471-484.
- Weiler, M., 2001. Mechanism controlling macropore flow during infiltration - dye tracer experiments and simulation. PhD thesis. URL <http://e-collection.ethbib.ethz.ch/eserv/eth:>

Chapter 3 – References

24150/eth-24150-02.pdf (accessed on June 2010), ETH Zürich, Zürich.

Weiler, M., McDonnell, J.J., Tromp-van Meerveld, I., Uchida, T., 2005. Subsurface Stormflow, in: Anderson, M.G, McDonnell, J.J. (Eds.), *Encyclopedia of Hydrological Sciences*, John Wiley & Sons 3, pp. 1719-1732.

Wilcke, W., Yasin, S., Fleischbein, K., Goller, R., Boy, J., Knuth, J., Valarezo, C., Zech, W., 2008. Water Relation, in: Beck, E., Bendix, J., Kottke, I., Makeschin, F., Mosandl, R. (Eds.), *Gradients in a Tropical Mountain Ecosystem of Ecuador*. *Ecological Studies*, Springer, Berlin, pp 193-201.

**Chapter 4 Water flow in the organic layer of a tropical
montane rainforest in southern Ecuador – an
inverse modelling study**

¹ Leutner, B. F., ^{1,*} Bauer, F., and ¹ Huwe, B.

¹ Department of Soil Physics, University of Bayreuth
Universitätsstraße 30
95440 Bayreuth, Germany

* corresponding author

Email: folkert.bauer@googlemail.com

phone: +49 921 55 2193; fax: +49 921 55 2246

in review at *Journal of Hydrological Processes*

Abstract

The organic layer of tropical montane rainforests plays a crucial role concerning water balance and transport in these ecosystems. Knowledge of hydraulic conductivity- and water retention functions allows for the quantification of water movement in unsaturated and saturated porous media using Richards Equation. In this study we collected ten samples of organic layer from a mature tropical montane rainforest in southern Ecuador, which we provided for multi rate irrigation experiments. By applying inverse modelling techniques on the observed drainage data, soil hydraulic parameters were estimated using two different model approaches. Modelled discharge based on these parameter sets reproduced well the observed drainage hydrographs. Response-surface analyses as well as a sensitivity study were carried out. The optimised parameter sets were tested against validation experiments revealing a high predictive power. For the purpose of simulating water flow at this site we propose the averaged parameter set of the Mualem-van Genuchten model, since it features an acceptable predictive power while only low parameterisation is required.

Keywords: tropical montane forest, organic layer, parameterisation, inverse modelling, Hydrus 1D

4.1 Introduction

In contrast to forests from lower regions, densely rooted and thick organic layers are common in tropical montane forests (Grieve et al., 1990; Hafkenscheid, 2000; Tanner et al., 1998). Also in the “Reserva Biológica San Francisco” (= RBSF), situated in the Andes of southern Ecuador (fig. 4.1), forest mineral soils are widely overlain in sharp contrast by a well developed organic layer featuring high densities of living roots (Hertel et al., 2003). Its average thickness amounts to 15 cm at 1900 m, 16 cm at 2400 m and 31 cm at 3000 m above sea level (= ASL) (Soethe et al., 2006). In most cases the organic layer can be clearly subdivided into a sequence of Oi, Oe and Oa layers (Wilcke et al., 2008). The Oi layer consists of weakly moulded litter, the Oe of fragmented and fermented litter, and the Oa of loose organic material without macroscopically recognisable plant structures (Bahr, 2007; Wilcke et al., 2008). The Oi layer is less than 1 cm thick while the Oe and Oa range from centimetres up to a few decimetres. Extremely low microbial activity due to frequent saturation of the topsoil and a barely present soil fauna facilitates its accumulation up to 50 cm (Beck et al., 2008; Maraun et al., 2008; Schrumpf et al., 2001; Wilcke et al., 2002). In this regard, Liess et al. (2009) found Histosols (IUSS, 2007) as predominating soil type in the

RBSF area under mature forest, many of them showing a stagnic colour pattern. Histosols and Stagnosols (IUSS, 2007) are particularly well represented in slopes of less than 30 ° above 2100 m ASL (Liess et al., 2009), for which Bauer et al. (in review, a; in review, b) found prerequisites for lateral subsurface flow along the interface between organic layer and mineral soil. Their finding is corroborated by Fleischbein (2004) and Huwe et al. (2008), who reported considerably contrasting saturated hydraulic conductivities between organic layer and mineral soil. Basing on isotope signals and element concentration studies made in microcatchments 1, 2 and 3 (fig. 4.1), Wilcke et al. (2008) indirectly proved evidence of such a shallow subsurface flow. Goller et al. (2005) attribute a moderating function to the organic layer in order to slow down the lateral subsurface flow and to prevent flash floods.

Despite of its importance, dynamics of forest floor or organic layer water content have received little attention in hydrological research compared to rainfall interception by living vegetation (Walsh and Voigt, 1977). Studies in German, Romanian and Czechoslovakian forests report retained amounts of throughfall by the organic layer of up to 40 % (e.g. Brechtel, 1970; Brechtel and Krecmer, 1971). Therefore, during rainstorm events the infiltration capacity of the mineral soil may not be exceeded, since the intercepting character of the organic layer allows more time for infiltration into the mineral soil underneath (e.g. Blow, 1955; Brechtel, 1970). Some studies (e.g. Schaap et al., 1997; Tiktak and Bouten, 1992) modelling forest floor water content dynamics successfully, recognised its importance among hydrological processes. In order to describe the water budget or water flow in forest floors via physical based models considering the Richards Equation (Richards, 1931), it is necessary to know the water retention function $\theta(h)$ and the hydraulic conductivity function $K(h)$. Laboratory experiments of Kosugi et al. (2001), Pitman (1989), Putuhena and Cordery (1996), and Walsh and Voigt (1977) suggest the suitability of the Richards Equation to describe the forest floor water dynamics.

There are several direct and indirect methods to quantify these material functions. Direct methods are often time consuming and boundary conditions are difficult to control in the field. In case of the highly porous forest floor, it is technically ambitious to measure its matrix potential. Regarding this, Kosugi et al. (2001) conducted laboratory experiments using a rainfall simulator to obtain the water retention and hydraulic conductivity functions of forest floors via the inverse modelling approach. This method allows a flexible design of the boundary conditions (Hopmans et al., 2002) that can be easily controlled in laboratory experiments (e.g. amount and duration of irrigation) under otherwise constant ambient conditions (e.g. temperature, negligible evaporation, no transpiration) for a series of

experiments. According to Hopmans and Šimůnek (1999), the inverse modelling method aims to deduce the intrinsic functionality of a system by observing its response to an assigned input signal. Here, van Dam et al. (1994) and Hopmans et al. (2002) reported that the drainage hydrograph of multi rate irrigation experiments can be sufficient to obtain a unique solution of the final optimised parameter set.

Since omnipresent in the RBSF investigation area and being assumed to have a moderating effect on lateral subsurface flow, the organic layer cannot be neglected in future hydrological physical based models. To our knowledge, tropical montane organic layers have not yet been parameterised and therefore modellers cannot resort to comparable parameters from literature.

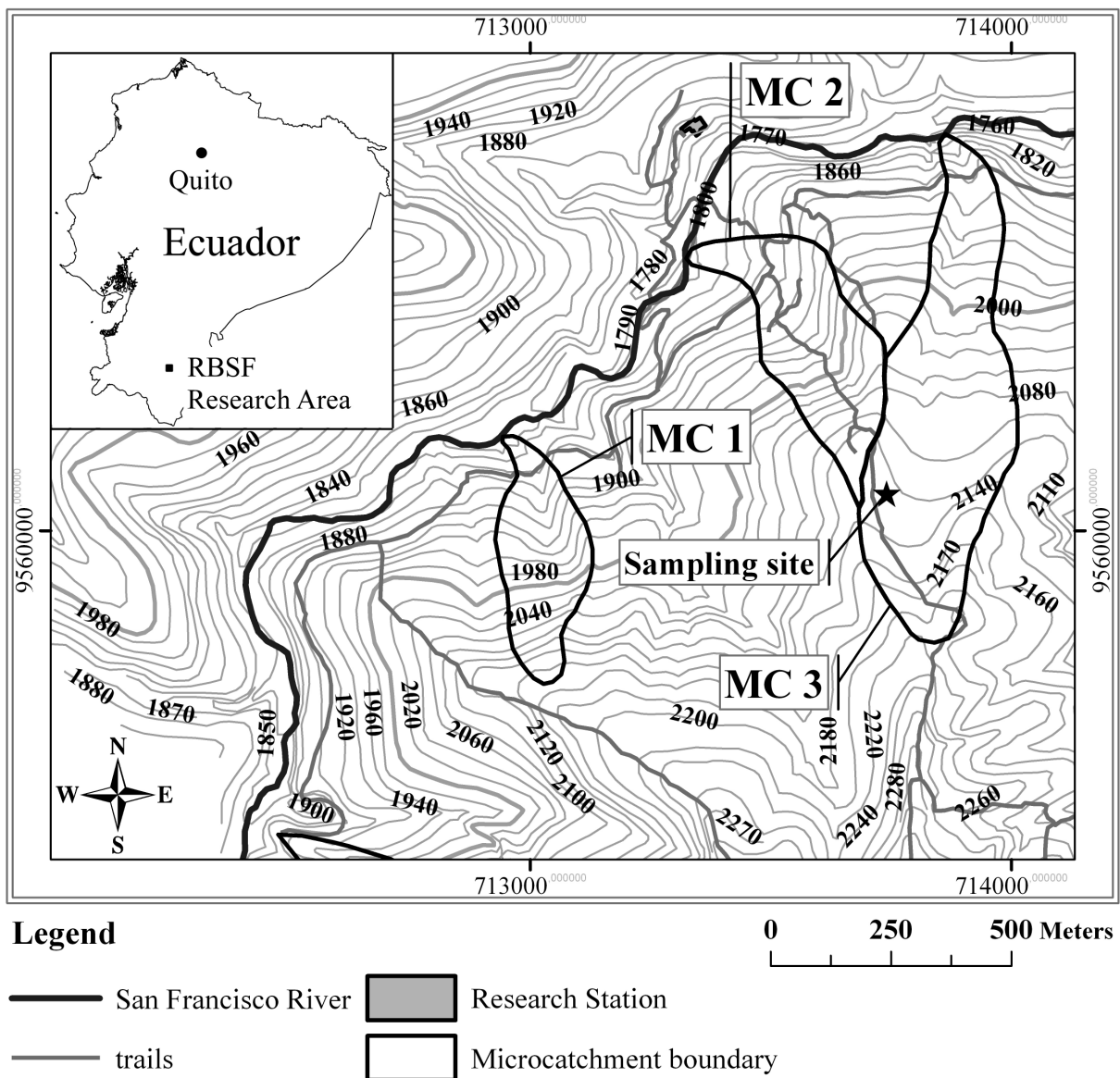


Figure 4.1 Map of the core part of the RBSF investigation area. The sampling site is situated at the western part of MC 3 above 2120 m ASL. Coordinate system is UTM WGS84 17S.

Furthermore, even though the organic layer as found in the RBSF area certainly is a porous medium, it is not quite sure whether its hydraulic behaviour can be sufficiently described by the conventional Mualem-van Genuchten approach (van Genuchten, 1980), or other approaches such as the multi porosity model of Durner et al. (1999). Finally, for modelling purposes the obtained parameters should ensure a high predictive power in future hydrological process models.

Therefore, we conducted a series of laboratory multi rate irrigation experiments with samples of organic layer taken from a mature forest in the RBSF investigation area. By means of the inverse modelling method we test the hypothesis that the hydraulic behaviour of the organic layer can be described by the conventional soil hydraulic parameters as provided in the model approaches of Durner et al. (1999) and van Genuchten (1980).

4.2 Materials and methods

4.2.1 Study area

Sampling and laboratory experiments were conducted in the RBSF study area which is situated on an eastern slope of the Andes in Southern Ecuador (fig. 4.1), halfway between the province capitals Loja and Zamora. The RBSF investigation area comprises 11.2 km² and extends from 1800 m to 3160 m ASL. It belongs to the Cordillera Real forming the weather divide between the humid Amazonian lowlands and the dryer inter-Andean highlands. The climate is perhumid with a unimodal precipitation regime. The wetter months are between April and August while rainfall is high all through the year (Bendix et al., 2008). At 1960 m ASL average annual precipitation amounts to 2050 mm increasing with altitude up to 4400 mm at 3160 m ASL (Rollenbeck, 2006). The mean annual air temperature ranges from 19.4 °C at the valley bottom to 9.4 °C at the highest elevations (Fries et al., 2009).

According to Bruijnzeel (2001) the forest can be classified as “tropical mountain cloud forest” with trees up to 30 m and closed canopy in the ravines. On ridges, trees generally reach heights of up to 15 m with a light canopy. The dominant tree families are Clusiaceae, Chloranthaceae, Melastomataceae, Lauraceae and Arecaceae (Homeier et al., 2002), whereas *Graffenrieda emarginata* (Ruiz and Pav.) Triana (Melastomataceae) is most abundant between 1800 m and 2200 m ASL. Most of the forest is mature primary forest with various vascular and cryptogamic epiphytes.

The geology of the region features interbedded palaeozoic metasiltsstones, sandstones, phyllites, and clay schist belonging to the low metamorphic Chiguinda unit of the Zamora series (Hungerbühler, 1997). Soils below 2000 m ASL are generally loamy skeletal as they mainly developed from landslide deposits and probably periglacial sediments (Schrumpf et al., 2001; Wilcke et al., 2001). Above 2100 m ASL, Stagnosols and Histosols (IUSS, 2007) prevail, particularly in slopes of less than 31 ° (Liess et al., 2009).

With increasing altitude soil nutrient content, -pH and -temperature decrease while the C/N proportion increases (Schrumpf et al., 2001). Probably due to the low soil pHs, densities of soil macrofauna and microarthropods are low (Maraun et al., 2008). Consequently, turnover times of organic matter range up to more than 15 years leading to the enormous accumulation of the organic layer of up to 50 cm thickness (Beck et al., 2008; Schrumpf et al., 2001; Wilcke et al., 2002).

4.2.2 Field sampling

The sampling area was located on a ridge at ~2150 m ASL (fig. 4.1) and extended to several tens of metres. Most abundant tree families were Clusiaceae (31 %), Arecaceae (16 %), Melastomataceae (14 %), Araliaceae (11 %) and Lauraceae (9 %) with a relatively light canopy. The herb and shrub layer was considerably dense with prevailing Bromeliaceae and Orchidaceae situated onto the organic layer. The latter averaged a thickness of 33 cm (max. 45 cm). The samples were taken from the uppermost 20 cm of the organic layer by carefully inserting sharp core samplers made of transparent acrylic glass. Each core sampler had a radius of 14.5 cm and a height of 10.5 cm. The relatively large radius should reduce possible boundary effects which may occur during irrigation. In this case, the acrylic glass material allowed us to assess these effects. After having inserted the sampler completely, roots were cut off carefully at the bottom side in order to receive undisturbed samples. The lowermost Oa horizon was incoherent as it consisted of small light organic particles, which we could therefore not include in the samples. In order to remove the uppermost Oi layer, we let it slightly overlap the upper margin of the acrylic glass cylinder and cut it off using a scissor. Finally, each core sampler contained only the coherent Oe layer, where most of the roots (almost exclusively fine roots) were situated. In total, we collected 25 samples, which we used to conduct 18 multi rate irrigation experiments including repetition- and validation experiments (tab. 4.1).

4.2.3 Experimental design

For the irrigation apparatus (fig. 4.2), the core samplers were piled up to columns of two or three samples. Over the sample column an irrigator head was placed without having contact to the sample column below. It consisted of a closed chamber made of acrylic glass with a raindrop simulator of 270 injection needles, each with an inner diameter of 0.4 mm. The rainfall intensity was controlled using a programmable peristaltic pump, which altered the rate of water entering the sprinkler (fig. 4.2). To avoid hollow spaces at the interface between upper and lower sample, we carefully removed the Oi layer until the Oe. To ensure a continuous connection along this interface, we pivoted the upper cylinder a bit in order to interlock the sample with the lower one. Piling-up was necessary in order to amplify the output signal formed by the samples. For a single sample the difference between input (irrigation) and output (drainage) signal would be very small. Small measurement errors could lead to large errors in the final results according to Kosugi et al. (2001).

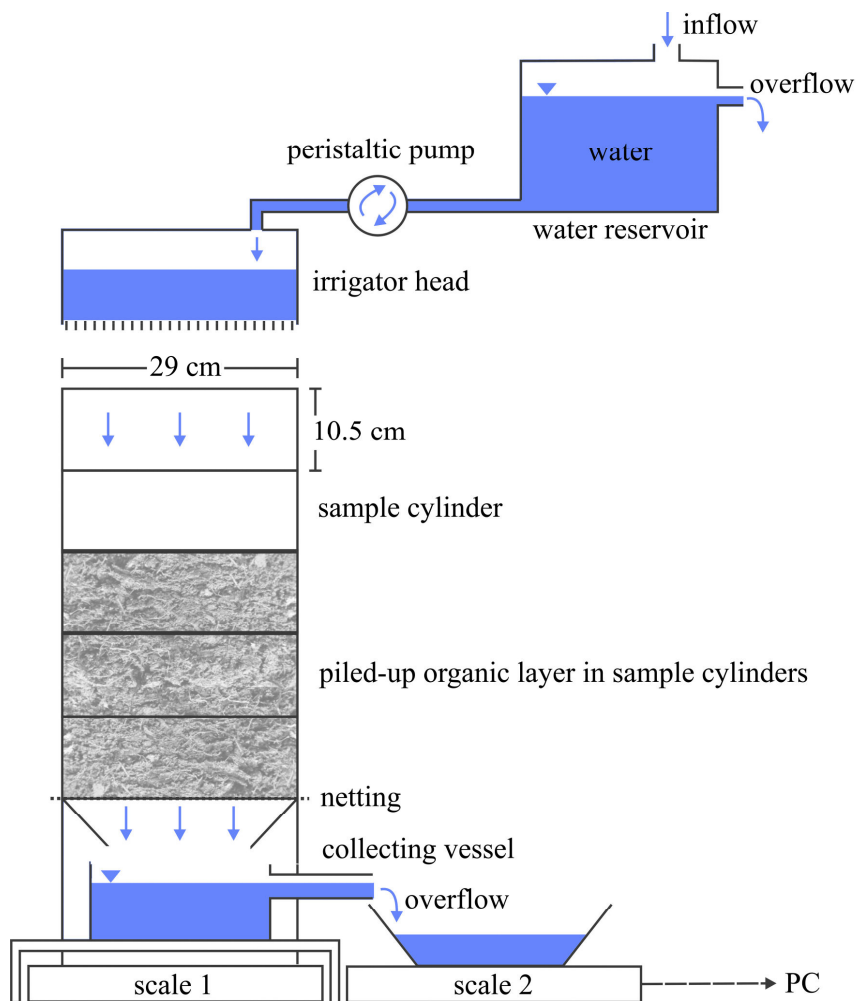


Figure 4.2 Experimental set-up of the irrigator apparatus following Kosugi et al. (2001).

Due to the assumed high porosity, we provided a coarse mesh netting underneath the bottom sample instead of a ceramic plate. By using a mesh size of 1 mm · 2 mm, the risk of loosing small sample particles clogging the hose connection between the collecting vessels at scale 1 (model: Kern STB 20K2IP) and scale 2 (model: Kern 573-56NM) (fig. 4.2) was lowest. The weight of the sample column and the discharge were recorded by scale 1 and scale 2. We connected scale 2 to a personal computer to record changes in weight in intervals of 3 seconds. The first collecting vessel, situated above scale 1, did not have any contact to the sample column nor to the scale underneath (fig. 4.2). Before we started irrigation, we manually filled the first vessel until first drops left to the second vessel situated on scale 2.

To avoid hydrophobic effects (Bouma, 1990; Kosugi et al., 2001), we irrigated the samples over several hours before beginning with the multi rate irrigation experiment. We subsequently started the latter when equilibrium between inflow and outflow rate at the maximal possible irrigation rate of 92.6 mm h⁻¹ of the peristaltic pump was achieved, i.e. we adjusted the next lower rate (77.8 mm h⁻¹), when the weight increase of the sample column on scale 1 was below 0.4 g min⁻¹ for at least 15 min which we define as equilibrium weight. This allowed us to determine the water content in the sample column giving the initial water content for the model calculations. For each model run in Hydrus 1D, ver. 4.05 (Šimůnek et al., 2008), we provided a homogeneously distributed volumetric water content that we computed from dry matter weight, sample volume, and equilibrium weight at the highest irrigation rate (92.6 mm h⁻¹) from the corresponding laboratory experiment.

During the multi rate irrigation experiments irrigation intensities were lowered in discrete descending steps of 92.6 mm h⁻¹, 77.8 mm h⁻¹, 39.7 mm h⁻¹, 24.2 mm h⁻¹, 14.4 mm h⁻¹, and 6.1 mm h⁻¹ (fig. 4.5). Due to a somewhat non linear time lag to changes of the peristaltic pump, we measured the actual irrigation rates with the complete experimental set up, but without samples. Deviations from a predefined irrigation discharge curve were compensated by subsequent adjustment of the pumping rate. This method allowed us to get the transitions between the irrigation steps very precisely.

The subsequent irrigation levels were switched to the next lower one after intervals of exactly 60 min. As pilot studies have shown, each irrigation level reached equilibrium in discharge after no more than 25 min, which legitimates the chosen 60 min intervals. Only the maximal intensity level (92.6 mm h⁻¹) was considered for just 10 min, since the system was already at equilibrium due to the irrigation until saturation. After the lowest intensity level (6.1 mm h⁻¹), irrigation was stopped and the drainage hydrograph was recorded for another 6 h.

Table 4.1 Summary of the 18 laboratory multi rate irrigation experiments including repetitions (= P*) and validation experiments (= Pv).

Multi rate irrigation experiments (= P)	Multi rate irrigation experiments that were repeated (= P*)	Measured discharge of multi rate irrigation experiments used for parameter optimisation in Hydrus 1D	Optimised parameter sets used for direct modelling, i.e. validation experiments (= Pv)
P1	●	●	
P2	●	●	
P3	●	●	
P4		●	
P5		●	●
P6		●	
P7		●	●
P8		●	●
P9		●	●
P10		●	●

For the validation experiments we applied irrigation levels differing in sequence, intensities, and duration. As shown by figure 4.7, step transitions of increasing irrigation level were provided. We reproduced the validation experiments with the same version of Hydrus 1D as we used for the inverse model calculations. In each validation experiment we entered the final optimised soil hydraulic parameter set of its corresponding inverse model (tab. 4.1). Subsequently, we repeated the procedure with the averaged final parameters per model approach.

After completion of each experiment, the samples were dried until constant weight. Drying occurred at 80 °C to prevent biases through mass loss by volatile organic substances. Subsequently, we decomposed the samples into humified particles (including twigs, dead roots), moulded leaves as well as living coarse and fine roots, which then were once again weighted.

4.2.4 Inverse modelling

4.2.4.1 Model approaches

As aforementioned, in this study we performed the inverse modelling procedure using Hydrus 1D, ver. 4.05 (Šimůnek et al., 2008). Here, instationary one-dimensional water flow is described by the Richards Equation (Richards, 1931) (1):

$$\frac{\partial \theta}{\partial t} = \frac{\partial}{\partial z} \left[K(h) \left(\frac{\partial h}{\partial z} + 1 \right) \right], \quad (1)$$

where θ is the volumetric water content [$\text{cm}^3 \text{cm}^{-3}$], t the time [s], $K(h)$ the hydraulic conductivity function [cm s^{-1}], h the pressure head [cm] and z the depth of the sample column [cm].

To solve equation (1) it is necessary to know the water retention- and the unsaturated hydraulic conductivity function, for which exist different model approaches. Van Genuchten (1980) expanded Mualem's theoretical model (Mualem, 1976) for the hydraulic conductivity function with an empirical model for the water retention curves. Both are of highly non linear nature. These closed form equations are referred to as Mualem-van Genuchten Model (= MvG) in this study. The water retention function (2) is defined as:

$$\theta(h) = \begin{cases} \theta_r + \frac{\theta_s - \theta_r}{\left[1 + |\alpha h|^n\right]^m} & h < 0 \\ \theta_s & h \geq 0 \end{cases}, \quad (2)$$

where θ_r is the volumetric residual water content [$\text{cm}^3 \text{cm}^{-3}$], θ_s the volumetric water content at saturation [$\text{cm}^3 \text{cm}^{-3}$], α [cm^{-1}], n [-], and m [-] are empirical curve fitting parameters.

The physical definition of θ_r is being debated. In practice, θ_r is either treated as a physically meaningless fitting parameter or as water content at dry soil. "Dry", however, is again differently defined. In this paper, we follow the definition of dry as "air dry state". θ_s is defined as the water content at which the matrix potential becomes zero. Parameter m is described by the relationship $m = 1 - n^{-1}$ for $n > 1$ and $0 < m < 1$ (van Genuchten, 1980). Due to the fitting of parameter n in this study, parameter m is not separately considered in the optimisation procedure. The approach of van Genuchten (1980) refers to the hydraulic conductivity function (3) defined as:

$$K(h) = K_s \cdot S_e^l \cdot \left[1 - (1 - S_e^{1/n})^m\right]^2, \text{ with } m = 1 - n^{-1}, \quad (3)$$

where K_s is the saturated hydraulic conductivity [cm s^{-1}], S_e the effective saturation [$\text{cm}^3 \text{cm}^{-3}$] and l the tortuosity and connectivity parameter [-].

The effective saturation S_e (4) describes the proportion of soil water being actually involved in water flow. It is defined as:

$$S_e = \frac{\theta - \theta_r}{\theta_s - \theta_r}, \text{ with } \theta_r < \theta < \theta_s, \quad (4)$$

A measure used to compare different $K(h)$ functions is the relative hydraulic conductivity $K_r(h)$ (5) defined as:

$$K_r(h) = \frac{K(h)}{K_s}, \text{ with } 0 < K_r < 1, \quad (5)$$

Durner et al. (1999) extended the MvG model to a bimodal or multimodal model assuming a bimodal or multimodal pore size distribution, respectively. The approach of Durner et al. (1999) (= DPD) divides the porous medium into two or more fractions. Each of them can be described by the van Genuchten functions (2) and (3). For the bimodal approach, superposition of two fractions results in the bimodal distribution (6), which we considered in this study:

$$S_e(h) = w_1 \left[1 + (\alpha_1 h)^{n_1} \right]^{-m_1} + w_2 \left[1 + (\alpha_2 h)^{n_2} \right]^{-m_2}, \quad (6)$$

where w_1 and w_2 are weighting factors with $0 < w_i < 1$ and $\sum w_i = 1$. α_i , n_i and m_i are the individual MvG parameters (as described above) of each fraction, whereas i denotes the number of the pore fraction. In combination with the pore size distribution model of Mualem (1976), the following hydraulic conductivity function (7) can be derived (Durner et al., 1999):

$$K(S_e) = K_s \frac{(w_1 S_{e_1} + w_2 S_{e_2}) \left(w_1 \alpha_1 \left[1 - (1 - S_{e_1}^{1/m_1})^{m_1} \right] + w_2 \alpha_2 \left[1 - (1 - S_{e_2}^{1/m_2})^{m_2} \right] \right)^2}{(w_1 \alpha_1 + w_2 \alpha_2)^2} \quad (7)$$

With respect to the model approaches as describes above, the following has to be considered using the inverse modelling method: (i) effects of the air phase on the water flow are negligible; (ii) there is no temperature influence on soil properties and water flow; (iii) the relation of water potential and water content are independent from the flow rate (Šimůnek and Hopmans, 2002).

In Hydrus 1D estimation of the final parameters was achieved by inversion of the Richards Equation and non linear minimisation of the sum of squares of the distances between simulated and measured drainage hydrograph using the Marquardt-Levenberg descending

algorithm (Marquardt, 1963). Here, parameters are iteratively changed until a minimum in the objective function, ideally a global minimum, is achieved (Hopmans et al., 2002). The results of the minimisation technique can respond sensitively on the choice of the initial parameter set. Therefore, Šimůnek and Hopmans (2002) suggest to test different initial parameter sets and to choose that one that minimises the objective function to a global minimum. In this study, we adopted the suggestion of Šimůnek and Hopmans (2002).

4.2.4.2 Model design

The inverse model procedure requires definition of the upper and lower boundary condition, the height of the sample column and the initial water content. In Hydrus 1D, the upper boundary condition represented the applied irrigation [cm s^{-1}] via the *atmospheric*-, and the lower the discharge [cm s^{-1}] via the *free drainage* Boundary condition. We estimated the initial water content in the modelled column from the dry matter weight, sample volume, and equilibrium weight at the highest irrigation rate (92.6 mm h^{-1}) from the corresponding laboratory experiment.

The input data irrigation- and discharge rates were calculated from the cumulative records of scale 2 (fig. 4.2) and referred to the irrigated area of 660.52 cm^2 . Then, for both the MvG and DPD approach a set of initial fit parameter was selected (tab. 4.2). For all optimised parameter sets except for those derived from repetitions (tab. 4.1) we calculated mean, median, standard deviation, coefficient of variation, minimum and maximum (tab. 4.3). Additionally, coefficients of determination R^2 between simulated and measured discharge data as well as correlation matrices (Pearson's correlation coefficient r) of the optimised final parameters were computed by Hydrus 1D.

Table 4.2 Initial parameters provided for the MvG and DPD approach. See sections 4.2.5 and 4.3.1 for the choice of parameters being fixed and left for optimisation.

	n [-]	K_s [cm s^{-1}]	θ_s [-]	θ_r [-]	α, α_l [cm^{-1}]	l [-]	w_2 [-]	α_2 [cm^{-1}]	n_2 [-]
fixed?	no	no	no	yes	yes	yes	no	no	no
MvG	1.15	0.09	0.55	0.005	0.03	0.5	--	--	--
DPD	1.15	0.09	0.55	0.005	0.03	0.5	0.5	0.0003	1.5

4.2.5 Sensitivity analysis

A sensitivity analysis was carried out for the objective function as well as for the optimised parameter sets. For the purpose to examine the uniqueness of the inverse problem, we performed a response surface analysis. Therefore, we used a modified version of the Hydrus

1D software package (Šimůnek, pers. comm.). The principle of this analysis is the reduction of the multidimensional objective function onto three dimensions, which is achieved by a cross cut along a plane spanned by the parameters. Therefore, two parameters were varied in a defined range, while the others were kept constant. We applied this analysis on the parameter combinations $\alpha - K_s$, $\alpha - n$, $n - K_s$, $\theta_s - n$, and $\theta_s - \alpha$ (fig. 4.3a-e). $K_s - \theta_s$ was not calculable due to technical problems of the modified Hydrus 1D software. Moreover, in the modified version of the Hydrus 1D software the response surface analysis was not available for the DPD approach. Furthermore, we proved the sensitivity of the initial parameters α , K_s , n , and θ_s (tab. 4.2) to its corresponding final estimated parameter (fig. 4.4a-d).

For the purpose to minimise uniqueness problems, several authors (e.g. Hopmans et al., 2002; Russo et al., 1991; Šimůnek et al., 2008) recommend to keep the number of parameters to be optimised low. In this regard, we *a priori* excluded the parameters θ_r and l from the optimisation process. According to estimates of Sharratt (1997) for organic forest floors, we assumed $\theta_r = 0.005$ [-] being reasonable in regard to the high porosity of the organic layer we have sampled. This value is also supported by other studies (e.g. Schaap et al., 1996). The parameter l was fixed at $l = 0.5$ [-] as estimated by Mualem (1976), which is widely accepted for coarse textured soils (Schuh and Cline, 1990; Wösten and van Genuchten, 1988) corresponding well to the highly porous organic layer samples.

Finally, by previous pilot studies we ensured that the relatively high irrigation intensities do not have a significant influence on the optimised parameters. Optimisations without the two highest irrigation levels (92.6 mm h^{-1} and 77.8 mm h^{-1}) led to very similar parameters. Kool et al. (1985) showed that using a wide span of water contents contributes to minimise non uniqueness. This justifies using higher irrigation intensities than normally provided by natural rainfall events in the study area.

4.3 Results and discussion

Decomposition of the organic layer samples (tab. 4.1) show that the largest part of the dry mass weight belong to humified particles with 71 %, while 11 % to fine and coarse living roots, and 7 % to moulded leaves.

The repetition experiments P1*, P2* and P3* neither revealed a substantial difference in the modelled drainage hydrographs nor in the optimised parameters to the previous experiments P1, P2 and P3 (tab. 4.1). Thus, the initial irrigation until saturation did not alter

the physical properties of the organic layer samples. This allows to assume comparability between the experiments.

4.3.1 Sensitivity analysis

Exemplarily, in figure 4.3a-e the topographies of the objective function calculated from the response surface analysis of experiment P1 are plotted. The parameter plane $\alpha - K_s$ (fig. 4.3a) shows a long narrow valley parallel to the α axis revealing the parameter α being sensitive to the chosen initial parameter value of K_s and *vice versa* (fig. 4.4e), which is well defined between 0.005 and 0.07 cm s⁻¹. Parameter plane $\alpha - n$ (fig. 4.3b) shows the same behaviour with α being unidentifiable unlike n , which is precisely defined between 1.1 and 1.15 [-]. Figure 4.3c shows a hyperbolic shaped minimum valley indicating an inverse relationship between n and K_s . Here, K_s can vary between 0.04 and 0.11 cm s⁻¹ and n between 1.10 and 1.22 [-]. Parameter plane $\alpha - \theta_s$ (fig. 4.3d) is similar to those shown in figure 4.3a and 4.3b. The parameter α is stretched along its axis, whereas θ_s has a small minimum between 0.47 and 0.48 [-]. Parameter α [cm⁻¹] even reacts sensitively to its corresponding initial parameter as documented by the sensitivity analysis (fig. 4.4a). Parameter plane $\theta_s - n$ (fig. 4.3e) shows a distinctive minimum for both with θ_s between 0.48 and 0.5 [-] and n between 1.1 and 1.16 [-].

The response surface- and sensitivity analysis clearly revealed that α of the MvG model cannot be identified. For the parameters K_s , α_1 , and α_2 of the DPD approach we observed a similar sensitivity on its initial values (not shown here). Consequently, we excluded α of the MvG approach, and α_1 of the DPD approach from the parameter optimisation procedure described in the following section. Instead, we used a mean value for α and α_1 taken from literature for similar soil types (Fleischbein, 2004; Greiffenhagen et al., 2006; Kosugi et al., 2001; Schaap et al., 1997; Wösten and van Genuchten, 1988), and set both α and $\alpha_1 = 0.03$ cm⁻¹. Since we did not find a reasonable replacement of α_2 in literature, and since K_s values obtained by the parameter estimation procedure were similar to those determined by field measurements via Guelph Permeameter (Kreutzer and Martini, 2002), we kept α_2 and K_s for optimisation. The sensitivity analysis of parameters θ_s and n provided in the MvG and DPD approach reveals these parameters as well defined (fig. 4.3b, d, e; fig. 4.4c, d).

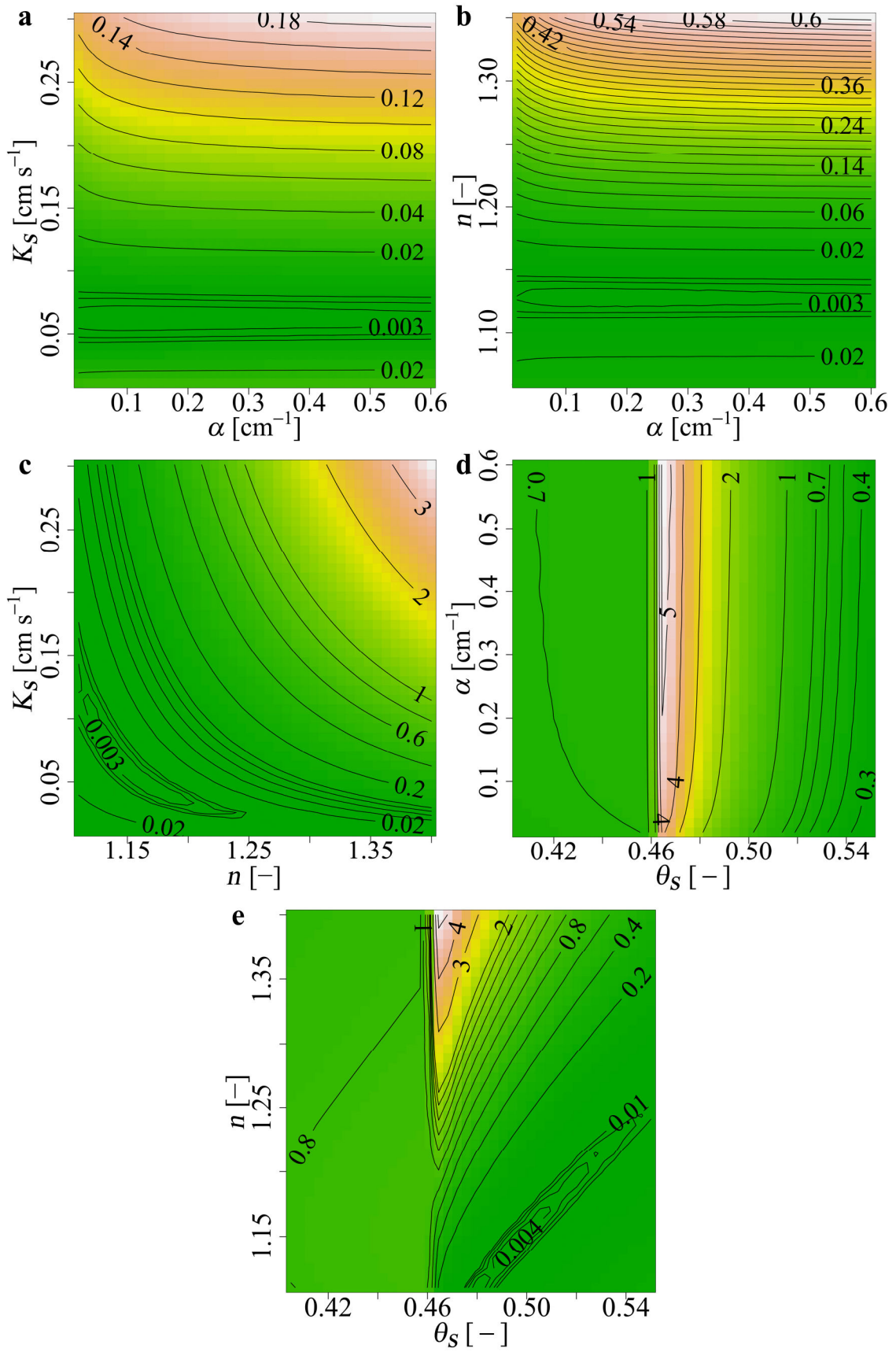


Figure 4.3 Topography of the objective function along the parameter planes $\alpha - K_s$ (a), $\alpha - n$ (b), $n - K_s$ (c), $\theta_s - \alpha$ (d), and $\theta_s - n$ (e). Density of contours increases towards the minima.

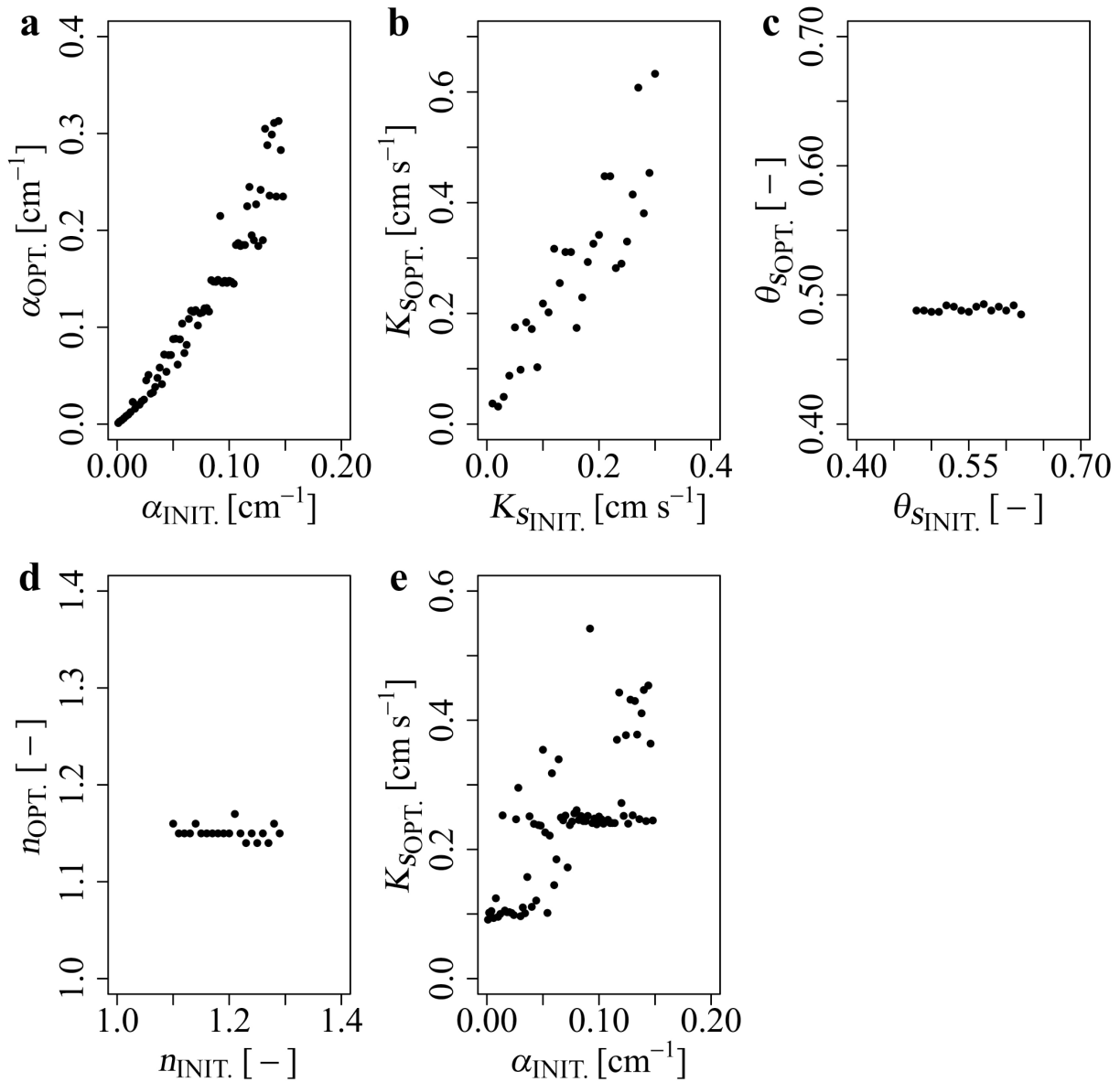


Figure 4.4 Results of the sensitivity analysis of the initial (INIT.) parameters versus optimised (OPT.) parameters of the MvG approach.

4.3.2 Inverse modelling: parameter estimation

Figure 4.5 exemplarily shows a measured drainage hydrograph of experiment P8, the applied irrigation levels as well as the optimised model responses. Generally, both model approaches fit the observed discharge consistently well. The coefficients of determination between measured discharge and model discharge are generally $R^2 \approx 1$ (min 0.996). For both, the MvG and DPD approach standard errors and thus 95 % confidence intervals were considerably small (tab. 4.3). As reported by Hopmans et al. (2002), high correlations between optimised parameters and the non linear character of the MvG- and DPD approach underestimate

standard errors and increase non uniqueness. As a consequence, the observed discharge are better reproduced resulting in high R^2 . From the three parameters we optimised using the MvG approach (tab. 4.2), in 6 from 13 experiments the parameter combination of $\theta_s - n$ showed correlation coefficients below 0.7, while correlation coefficients of $\theta_s - K_s$, and $K_s - n$ ranged from 0.2 to 0.5, and from -0.3 to -0.5, respectively. For the remaining 7 experiments, $\theta_s - n$ showed correlation coefficients between 0.7 and 0.8, while correlations among $\theta_s - K_s$, and $K_s - n$ tend to be lower than in the 6 experiments aforementioned. However, the differences of the correlation coefficients between $\theta_s - n$ do not result in obvious differences among the R^2 of the 13 experiments. Furthermore, Hopmans et al. (2002) assign the influence of correlation coefficients on standard errors at values larger than ± 0.9 . Therefore, we conclude that the correlations between the optimised parameters are too weak to contribute to non uniqueness.

Nevertheless, even if the final optimised parameters did not differ notably from those of the repetitions P1*, P2* and P3*, non uniqueness is given for the parameters obtained by the MvG approach due to the sensitivity of K_s on its initial values (fig. 4.4b) and the K_s variation coefficient (tab. 4.3) being higher than those of the insensitive parameters θ_s and n (fig. 4.4c, d).

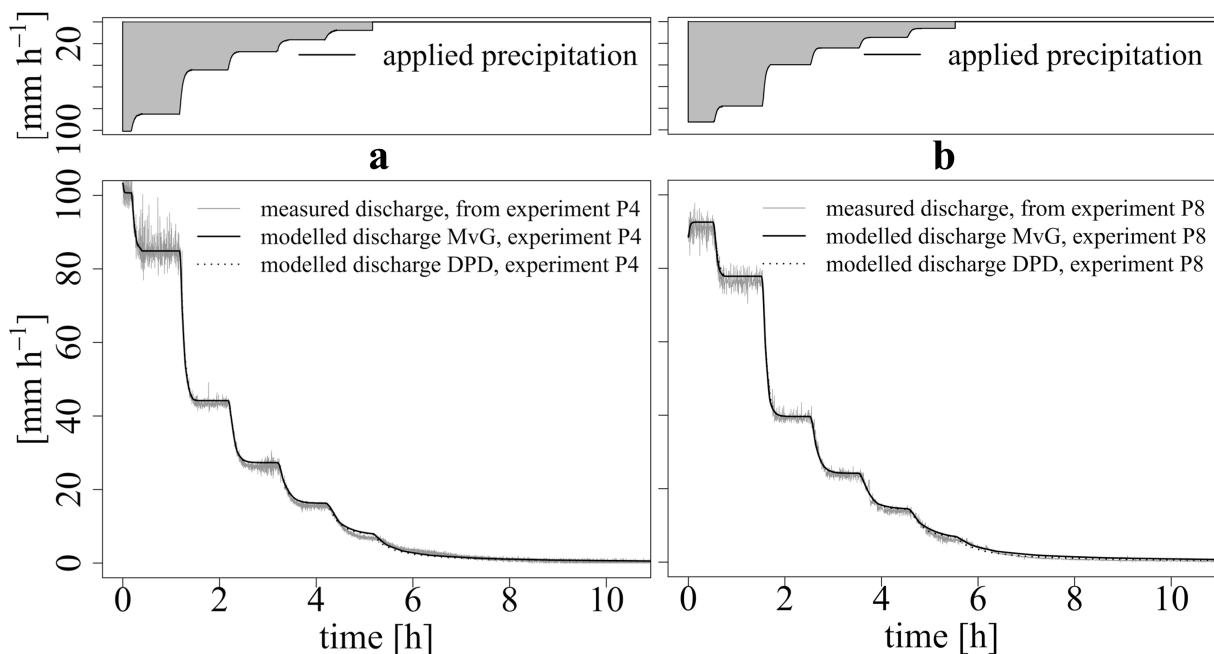


Figure 4.5 Exemplary drainage hydrographs obtained from the experiments P4 (a) and P8 (b) for discrete descending irrigation rates. Curves show the outputs of the MvG and DPD approaches with the final parameter sets. Note that units are given in [mm] and [h] instead of [cm] and [s].

Similar to the MvG approach, the majority (~90 %) of correlation coefficients between the optimised parameters was lower than ± 0.8 for the DPD approach. However, the correlation coefficients of all 14 pairs (composed of the 7 parameters to be optimised) did not show a consistent behaviour as for the MvG model. For example, between K_s and α_2 we found weak (0.68) to high (0.92) correlations in 8 of 13 experiments, and even negative correlations in 3 cases. Moreover, the parameters θ_s , n , and K_s optimised by the DPD approach scatter more than those of the MvG approach, but are in approximately the same range (tab. 4.3). The weighting factors of w_2 scatter considerably from 0.2 to 0.7, while α_2 varies in the magnitude of ten even if we provided the same initial values for each experiment. The optimised parameters K_s and α_2 of the repetitions P1*, P2*, and P3* differed notably from the corresponding experiments P1, P2, and P3 even if we considered for each pair P/P* the same initial parameters. Consequently, and being aware that both K_s and α_2 are sensitive to their corresponding initial parameters (see section 4.3.1), the problem of non uniqueness has to be concluded for the DPD approach as well.

Table 4.3 Mean and median of the optimised parameters θ_s [-], n [-], K_s [cm s⁻¹], w_2 [-], α_2 [cm⁻¹] and n_2 [-] of the MvG and DPD model approach as well as standard deviation, variation coefficient, minimum, maximum, and 95 % confidence intervals (CI). The repetitions P1*, P2* and P3* are not included.

approach	θ_s [-]		n [-]		K_s [cm s ⁻¹]		w_2 [-]	α_2 [cm ⁻¹]	n_2 [-]
	MvG	DPD	MvG	DPD	MvG	DPD		DPD	
mean	0.536	0.544	1.118	1.229	0.117	0.122	0.457	0.003	1.135
median	0.548	0.555	1.114	1.178	0.114	0.121	0.414	0.003	1.001
stand. dev.	0.025	0.023	0.020	0.127	0.023	0.044	0.151	0.001	0.374
variat. coef.	0.046	0.042	0.018	0.104	0.194	0.360	0.331	0.491	0.329
minimum	0.487	0.501	1.093	1.147	0.089	0.033	0.273	0.000	1.001
maximum	0.555	0.568	1.150	1.571	0.149	0.199	0.724	0.004	2.195
95 % CI	10E-4	10E-4	10E-3	10E-3	10E-3	10E-3	10E-2	10E-2	10E-4

Also, we observed that the parameter n_2 of the DPD approach is close to its lower limit except for two experiments (tab. 4.3). As shown in figure 4.6b, the form of most DPD water retention curves approximates those of the MvG approach (fig. 4.6a). Thus, a second pore fraction contributing to the water flow in the organic layer seems to be improbable.

Regarding MvG approach, the individual water retention curves are quite similar only differing in a shift along the θ axis, while the individual curves are well represented by the retention function basing on the averaged parameter set (fig. 4.6a).

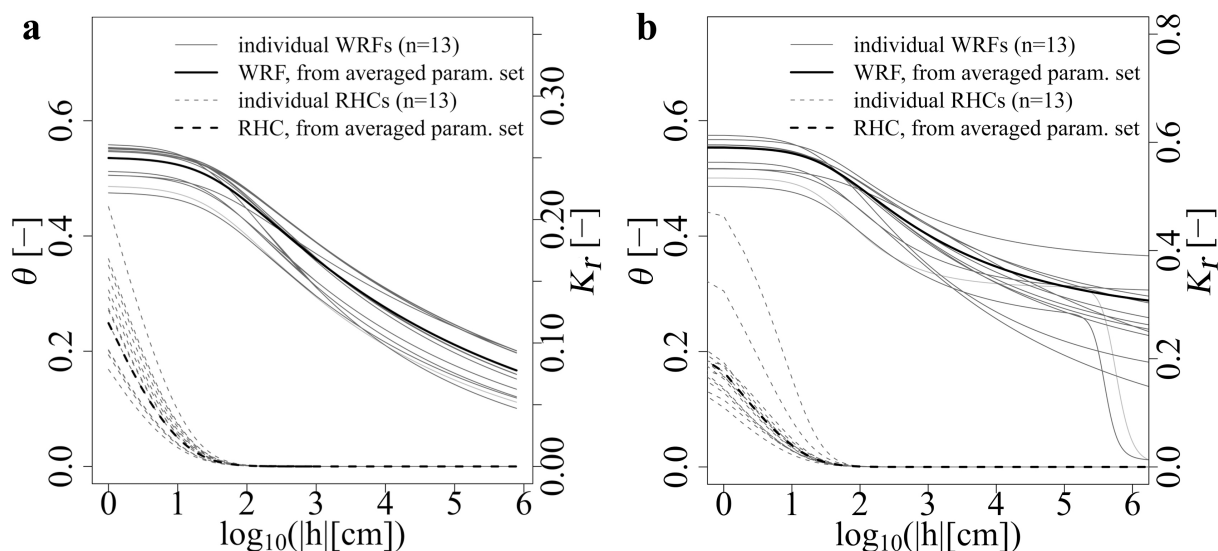


Figure 4.6 Water retention functions (WRF, θ) and relative hydraulic conductivity functions (RHC, K_r) derived from the optimised and averaged parameter sets of the MvG (a) and DPD (b) approach.

4.3.3 Direct modelling

The validation of the optimised parameter sets against the measured drainage hydrographs of the validation experiments Pv (tab. 4.1) is exemplarily shown for experiment P8 in figure 4.7a and for the averaged parameter set (tab. 4.3) of the MvG and DPD approach in figure 4.7b. The optimised parameter set of each model approach predicts the system response quite exactly, while the predictions based on averaged parameter sets fit marginally worse. As we found in all validation experiments Pv, the high predictive power of both the MvG and DPD approach is reflected by very high R^2 between measured and predicted discharge. However, there are some considerable deviations from the measured discharge at the beginning of the experiments. We found that R^2 between measured and predicted discharge is mainly determined through accuracy within the first 15 min. Model runs that reproduced the measured hydrograph well range between $R^2 = 0.96$ and 0.99. Model runs that under- or overpredict within the first 15 min have R^2 between 0.7 and 0.9. If we omit the first 15 min, i.e. the time span when models obviously react sensitively to initial irrigation rates, then for both model approaches MvG and DPD R^2 is about 0.99.

The extreme response within the first 15 min (fig. 4.7b) is due to the degree of saturation of the modelled sample column, which we defined as initial condition at the beginning of the model run. For each validation experiment Pv, we estimated the initial water content in the modelled column from the dry matter weight, sample volume, and equilibrium weight at the highest irrigation rate (92.6 mm h^{-1}) from the corresponding experiment P (tab. 4.1). Model runs with a small difference between initial water content and optimised saturated water content value θ_{sOPT} had to adjust an intense discharge at the moment as the calculation started with the highest irrigation rate (see modelled discharge DPD in fig. 4.7b). For model runs with a higher difference the modelled sample column had to be saturated first. In combination with a lower unsaturated hydraulic conductivity a lower discharge is produced (see modelled discharge MvG in fig. 4.7b) compared to the rather saturated samples where discharge is rather controlled by the saturated hydraulic conductivity.

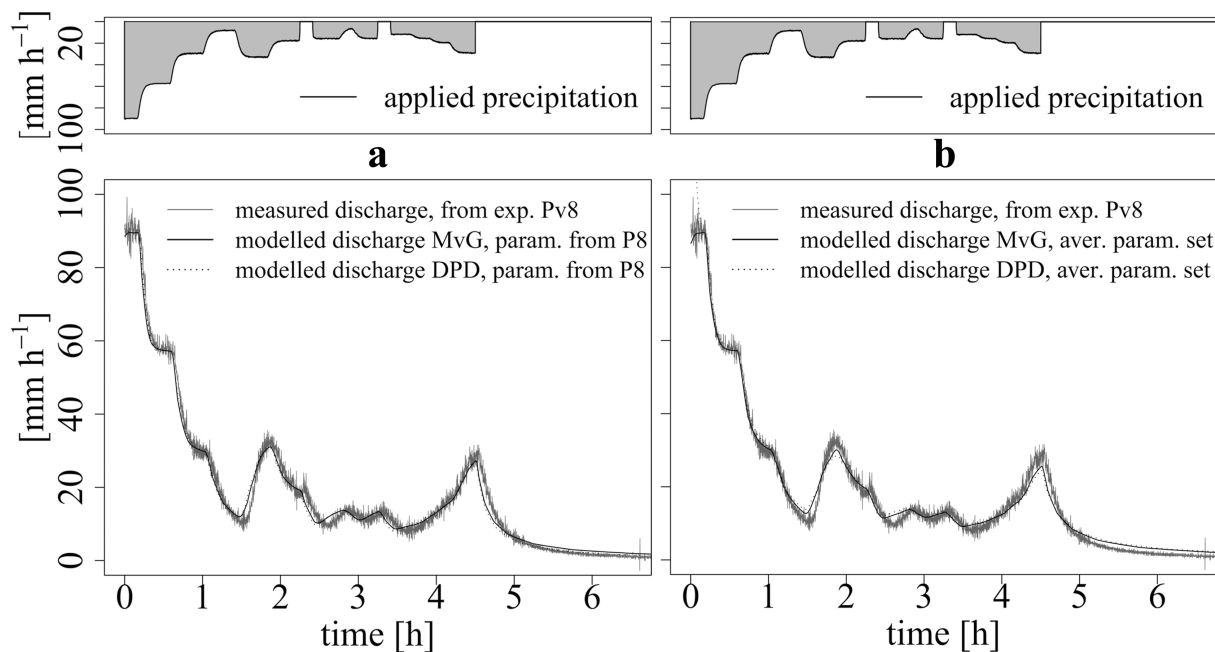


Figure 4.7 Exemplary observed drainage hydrograph and irrigation levels of the validation from experiment P8 (a). Curves show model prediction of the MvG- and DPD approach, each with the final (a) and the averaged (b, parameters from P1, ... , P10) parameter set. Note that units are given in [mm] and [h] instead of [cm] and [s].

Additionally, we observed that the simulated discharge predicts a more immediate reaction to positive changes in irrigation rates but with a smaller amplitude than measured (fig. 4.7a, b).

The observable systematic shifts between measured and predicted discharge hydrographs (fig. 4.7a, b) at increasing irrigation levels may be explained by hysteresis effects in the water retention curve. Here, in the dewatering phase the water content drops faster than it adds up at watering. Since we obtained the final parameters only by dewatering experiments, for

increasing irrigation levels, i.e. watering, the model overestimates water content and thereby also hydraulic conductivity. This results in a higher discharge than observed as documented in figure 4.7a and -b at hour 1.5 and hour 2.5. Models that include hysteresis effects are available, but require additional parameterisation of the watering- and dewatering water retention curve.

4.4 Conclusions

Soil hydraulic parameters for the organic layer were derived from multi rate irrigation experiments by means of inverse modelling. As could be shown, the model approaches applied in this study are principally capable to describe water flow in the ecologically vital organic layer of the RBSF investigation area. Consequently, we can confirm the hypothesis that the conventional soil hydraulic parameters provided in the MvG and DPD approach can be applied to the organic layer as typically present in the RBSF study area.

Since the DPD approach needs to be higher parameterised and a second discharge contributing pore fraction seems to be improbable, we recommend the MvG model as the best suited one. Due to the low scattering of the optimised parameter sets of the MvG model, usage of a mean parameter set is feasible resulting in salient model predictions in order to simulate flow and discharge dynamics.

Nevertheless, we could not overcome the problem of non uniqueness even if we had replaced α and α_l , and l and θ_r by values taken from literature (e.g. Fleischbein, 2004; Greiffenhagen et al., 2006; Kosugi et al., 2001; Schaap et al., 1997; Wösten and van Genuchten, 1988).

Consequently, according to Šimůnek and van Genuchten (1996) a definitive conclusion about the uniqueness of the inverse problem presented in this study and thus a physical interpretation of the obtained hydrological parameters is not possible.

In order to increase the chance for a well posed inverse problem, alternative measurements could be included into the objective function, and the number of parameters to be optimised should be reduced by measuring them independently (Šimůnek and van Genuchten, 1996). A completely different approach to the inverse parameter optimisation is suggested by Beven and Binley (1992). They propose that there is no “true” parameter set, because model and measurement are principally error prone and soil hydraulic properties can depend on time. Their “generalized likelihood uncertainty estimation” (GLUE) approach estimates the uncertainty of a certain parameter set, which allows an acceptable simulation of

an examined system. The result of a series of model runs on random parameter sets is a probability distribution of best fitting parameter sets limited by uncertainty intervals. This means also that the search for physically meaningful parameters is given up in advance of better model predictions.

Since the effect of hydrophobicity on water flow in the organic layer is ambitious to assess by column experiments as we used in this study, we “turned it off” by irrigating the samples over several hours. However, favoured by dry spells hydrophobicity may produce different hydraulic parameters than achieved in this study. Consequently, the transferability of the hydraulic parameters we estimated in this study to climates with a more pronounced drier season can be problematic. Regarding this limitation, the suitability of column experiments for the organic layer as we encountered in the RBSF study area is not given to fully assess its hydrological behaviour.

4.5 Acknowledgements

We would like to thank Jirka Šimůnek for his support with the modified version of Hydrus 1D, and Dyana León Taizha for decomposing numerous organic layer samples. This study was afforded and financed by the German Research Foundation (DFG) grant nr. DFG FOR 816 - HU 636/14-1.

4.6 References

- Bahr E. 2007. Verteilung und Charakteristika der Böden der tropischen Bergregenwaldregion Südecuadors in Abhängigkeit der Landnutzung. Diploma thesis, Technical University of Dresden, Dresden.
- Beck E, Makeschin F, Haubrich F, Richter M, Bendix J, Valarezo C. 2008. The Ecosystem (Reserva Biológica San Francisco). In *Gradients in a Tropical Mountain Ecosystem of Ecuador*, Ecological Studies, Beck E, Bendix J, Kottke I, Makeschin F, Mosandl R (eds). Springer-Verlag: Berlin, Heidelberg; 1-14.
- Bendix J, Rollenbeck R, Richter M, Fabian P, Emck P. 2008. Climate. In *Gradients in a Tropical Mountain Ecosystem of Ecuador*, Ecological Studies, Beck E, Bendix J, Kottke I, Makeschin F, Mosandl R (eds). Springer-Verlag: Berlin, Heidelberg; 63-73.
- Beven K, Binley A. 1992. The Future Of Distributed Models - Model Calibration And Uncertainty Prediction. *Hydrological Processes* **6** (3) : 279-298.

- Blow FE. 1955. Quantity and hydrologic characteristics of litter under upland oak forests in eastern Tennessee. *Journal of Forestry* **53** : 190-195.
- Bouma J. 1990. Using Morphometric Expressions For Macropores To Improve Soil Physical Analysis Of Field Soils. *Geoderma* **46** (1-3) : 3-11.
- Brechtel KM. 1970. Wald und Retention - Einfache Methoden zur Bestimmung der lokalen Bedeutung des Waldes für die Hochwasserdämpfung. *Deutsche Gewässerkundliche Mitteilungen* **14** (4) : 91-103.
- Brechtel HM, Krecmer V. 1971. Die Bedeutung des Waldes als Hochwasserschutz. *Österreichische Wasserwirtschaft* **23** (7-8) : 166-177.
- Bruijnzeel LA. 2001. Hydrology of Tropical Montane Cloud Forests: A Reassessment. *Land Use and Water Resources Research* **1** : 1.1-1.18.
- Durner W, Priessack E, Vogel HJ, Zurmühl T. 1999. Determination of Parameters for Flexible Hydraulic Functions by Inverse Modelling. In *Proceedings of the International Workshop on Characterization and Measurement of the Hydraulic Properties of Unsaturated Porous Media*, van Genuchten MT, Leij FJ, Wu L (eds). University of California, Riverside, USA; 817-829.
- Fleischbein K. 2004. Wasserhaushalt eines Bergregenwaldes in Ecuador: experimenteller und modellhafter Ansatz auf Einzugsgebietsebene. PhD thesis, Justus Liebig University of Giessen, Giessen.
- Fries A, Rollenbeck R, Göttlicher D, Nauss T, Homeier J, Peters T, Bendix J. 2009. Thermal structure of a megadiverse Andean mountain ecosystem in southern Ecuador, and its regionalization. *Erdkunde* **63**, 321–335.
- Goller R, Wilcke W, Leng MJ, Tobschall HJ, Wagner K, Valarezo C, Zech W. 2005. Tracing water paths through small catchments under a tropical montane rain forest in South Ecuador by an oxygen isotope approach. *Journal of Hydrology* **308** : 67-80.
- Greiffenhagen A, Wessolek G, Facklam M, Renger M, Stoffregen H. 2006. Hydraulic functions and water repellency of forest floor horizons on sandy soils. *Geoderma* **132** (1-2) : 182-195.
- Grieve IC, Proctor J, Cousins SA. 1990. Soil variation with altitude on Volcán Barva, Costa Rica. *Catena* **17** : 525–534.
- Hafkenschied R. 2000. Hydrology and biogeochemistry of tropical montane rain forests of contrasting stature in the Blue Mountains, Jamaica. PhD thesis, Free University of Amsterdam, Amsterdam.

- Hertel D, Leuschner C, Holscher D. 2003. Size and structure of fine root systems in old-growth and secondary tropical montane forests (Costa Rica). *Biotropica* **35** : 143–153.
- Homeier J, Dalitz H, Breckle SW. 2002. Waldstruktur und Baumartendiversität im montanen Regenwald der Estación Científica San Francisco in Südecuador. *Berichte der Reinhold Tüxen Gesellschaft* **14** (1) : 109-118.
- Hopmans JW, Šimůnek J. 1999. Review of Inverse Estimation of Soil Hydraulic Properties. In *Proceedings of the International Workshop on Characterization and Measurement of the Hydraulic Properties of Unsaturated Porous Media*, van Genuchten MT, Leij FJ, Wu L (eds). University of California, Riverside, USA; 643-659.
- Hopmans JW, Šimůnek J, Romano N, Durner W. 2002. Inverse Methods. In *Methods of Soil Analysis, Part 4 - Physical Methods*, Dane JH, Topp, GC (eds). Soil Science Society of America, Madison; 879-898.
- Hungerbühler D. 1997. Neogene basins in the Andes of southern Ecuador: evolution, deformation and regional tectonic implications. PhD thesis, ETH Zürich, Zürich.
- Huwe B, Zimmermann B, Zeilinger J, Quizhpe M, Elsenbeer H. 2008. Gradients and Patterns of Soil Physical Parameters at Local, Field and Catchment Scales. In *Gradients in a Tropical Mountain Ecosystem of Ecuador, Ecological Studies*, Beck E, Bendix J, Kottke I, Makeschin F, Mosandl R (eds). Springer-Verlag: Berlin, Heidelberg; 391-402.
- IUSS Working Group WRB. 2007. World Reference Base for Soil Resources 2006, first update 2007. *World Soil Resources Reports No. 103*. FAO, Rome.
- Kool JB, Parker JC, van Genuchten MT. 1985. Determining Soil Hydraulic Properties from One-step Outflow Experiments by Parameter Estimation: I. Theory and Numerical Studies. *Soil Science Society Of America Journal* **49** (6) : 1348-1354.
- Kosugi K, Mori K, Yasuda H. 2001. An inverse modeling approach for the characterization of unsaturated water flow in an organic forest floor. *Journal Of Hydrology* **246** (1-4) : 96-108.
- Kreutzer D, Martini J. 2002. Bestimmung und Regionalisierung der gesättigten hydraulischen Leitfähigkeiten in Böden unter tropischem Bergregenwald in Ecuador mit verschiedenen Methoden. Diploma thesis, Justus-Liebig-Universität Giessen, Giessen.
- Liess M, Glaser B, Huwe B. 2009. Digital soil mapping in southern Ecuador. *Erdkunde* **63** (4) : 309-319.
- Maraun M, Illig JD, Sandman D, Krashevskaya V, Norton RA, Scheu S. 2008. Soil Fauna. In *Gradients in a Tropical Mountain Ecosystem of Ecuador, Ecological Studies*, Beck E, Bendix J, Kottke I, Makeschin F, Mosandl R (eds). Springer-Verlag: Berlin, Heidelberg; 181-192.

Chapter 4 – References

- Marquardt, DW. 1963. An algorithm for Least-Squares Estimation of Nonlinear Parameters. *SIAM Journal of Applied Mathematics* **11** : 431-441.
- Mualem Y. 1976. New Model For Predicting Hydraulic Conductivity Of Unsaturated Porous-Media. *Water Resources Research* **12** (3) : 513-522.
- Pitman JJ. 1989. Rainfall interception by bracken litter - Relationship between biomass, storage and drainage rate. *Journal of Hydrology* **111** : 281-291.
- Putuhena WM, Cordery I. 1996. Estimation of interception capacity of the forest floor. *Journal of Hydrology* **180** : 283-299.
- Richards LA. 1931. Capillary Conduction of Liquids through Porous Mediums. *Physics* **1** (5) : 318-333.
- Rollenbeck R. 2006. Variability of precipitation in the Reserva Biológica San Francisco / Southern Ecuador. *Lyonia, A Journal of Ecology and Application* **9** (1) : 43-51.
- Russo D, Bresler E, Shani U, Parker JC. 1991. Analysis of Infiltration Events in Relation to Determining Soil Hydraulic-Properties by Inverse Problem Methodology. *Water Resources Research* **27** (6) : 1361-1373.
- Schaap MG, Delange L, Heimovaara TJ. 1996. TDR calibration of organic forest floor media. *Soil Technology* **11** (2) : 205-217.
- Schaap MG, Bouten W, Verstraten JM. 1997. Forest floor water content dynamics in a Douglas fir stand. *Journal Of Hydrology* **201** (1-4) : 367-383.
- Schrumpf M, Guggenberger G, Valarezo C, Zech W. 2001. Tropical Montane Rainforest Soils - Development and Nutrient Status Along an Altitudinal Gradient in the South Ecuadorian Andes. *Die Erde* **132** : 43-59.
- Schuh WM, Cline RL. 1990. Effect Of Soil Properties On Unsaturated Hydraulic Conductivity Pore-Interaction Factors. *Soil Science Society Of America Journal* **54** (6) : 1509-1519.
- Sharratt BS. 1997. Thermal conductivity and water retention of a black spruce forest floor. *Soil Science* **162** (8) : 576-582.
- Šimůnek J, van Genuchten MT. 1996. Estimating unsaturated soil hydraulic properties from tension disc infiltrometer data by numerical inversion. *Water Resources Research* **32** (9) : 2683-2696.
- Šimůnek J, Hopmans JW. 2002. Parameter Optimisation and Nonlinear Fitting. In *Methods of Soil Analysis, Part 4 - Physical Methods*, Dane JH, Topp GC (eds). Soil Science Society of America, Madison; 139-157.

Chapter 4 – References

- Šimůnek J, Šejna M, Saito H, Sakai M, van Genuchten, MT. 2008. The HYDRUS 1D Software Package for Simulating the One-Dimensional Movement of Water, Heat, and Multiple Solutes in Variably-Saturated Media Version 4.0. Department of Environmental Sciences, University of California Riverside, Riverside, California.
- Soethe N, Lehmann J, Engels C. 2006. The vertical pattern of rooting and nutrient uptake at different altitudes of a south Ecuadorian montane forest. *Plant and Soil* **286** (1-2) : 287–299.
- Tanner EVJ, Vitousek PM, Cuevas E. 1998. Experimental investigation of nutrient limitations of forest growth on wet tropical mountains. *Ecology* **79** : 10–22.
- Tiktak A, Bouten W. 1992. Modelling soil water dynamics in a forested ecosystem. III: Model description and evaluation of discretization. *Hydrological Processes* **6** (4) : 455-465.
- van Dam JC, Stricker JNM, Droogers P. 1994. Inverse Method to Determine Soil Hydraulic Functions from Multi step Outflow Experiments. *Soil Science Society Of America Journal* **58** (3) : 647-652.
- van Genuchten MT. 1980. A Closed-Form Equation For Predicting The Hydraulic Conductivity Of Unsaturated Soils. *Soil Science Society Of America Journal* **44** (5) : 892-898.
- Walsh RPD, Voigt PJ. 1977. Vegetation Litter - Underestimated Variable in Hydrology and Geomorphology. *Journal of Biogeography* **4** (3) : 253-274.
- Wilcke W, Yasin S, Valarezo C, Zech W. 2001. Nutrient budget of three microcatchments under tropical montane forest in Ecuador. *Die Erde* **132** : 61-74.
- Wilcke W, Yasin S, Abramoski U, Valarezo C, Zech W. 2002. Nutrient storage and turnover in organic layers under tropical montane rainforest in Ecuador. *European Journal Of Soil Science* **53** (1) : 15-27.
- Wilcke W, Yasin S, Fleischbein K, Goller R, Boy J, Knuth J, Valarezo C, Zech W. 2008. Water Relations. In *Gradients in a Tropical Mountain Ecosystem of Ecuador*, Ecological Studies, Beck E, Bendix J, Kottke I, Makeschin F, Mosandl R (eds). Springer-Verlag: Berlin, Heidelberg; 193-201.
- Wösten JHM, van Genuchten MT. 1988. Division S-6-Soil And Water Management And Conservation - Using Texture And Other Soil Properties To Predict The Unsaturated Soil Hydraulic Functions. *Soil Science Society Of America Journal* **52** (6) : 1762-1770.

**Chapter 5 A virtual experiment approach for assessing the
spatiotemporal occurrence of lateral shallow
subsurface flow in a steep forested hillslope
transect in the Andes of South Ecuador**

Folkert Bauer^{1,*}, Stefan Engelhardt¹, Jörg Zeilinger¹, and Bernd Huwe¹

¹ Department of Soil Physics
University of Bayreuth
Universitätsstraße 30
95440 Bayreuth, Germany

* corresponding author

Email: folkert.bauer@googlemail.com

phone: +49 921 55 2193; fax: +49 921 55 2246

in review at *Journal of Ecological Modelling*

Abstract

At ~2000 m above sea level in the tropical montane Andes of South Ecuador dye tracer studies have recently identified prerequisites of shallow subsurface flow in soils with stagnic moisture characteristics, while previous studies did not provide clear-cut information in this regard for Cambisols of steep hillslopes. Here, albeit their relevance recently discussed in literature, key parameters controlling the occurrence of subsurface flow such as the subsoil and bedrock permeability, or canopy evaporation remain unclear in the considered environment or were investigated separately such as the spatial variability of the saturated hydraulic conductivity (= K_{sat}). In order to consider these key parameters simultaneously, we conducted a series of virtual experiment to provide evidence for the presumed shallow subsurface flow and to assess its potential spatiotemporal occurrence in Cambisols of a steep hillslope. Therefore, we applied a two dimensional finite element model representing a steep forested hillslope transect of ~54 m length. We parameterised the model with data obtained by collective field intelligence from the considered environment. We included a ~16 months time series of throughfall and evapotranspiration, an organic layer abundant within the investigation area as well as the spatial variability of K_{sat} , the pressure head and their spatial trends obtained from field measurements. We defined different model set-ups to assess the spatiotemporal occurrence of the presumed subsurface flow on the subsoil hydraulic conductivity, on two widely differing evaporation rates, and on the stepwise reduction of the model by the trend and spatial variability of K_{sat} . We tested the plausibility of the model by comparing the calculated tensiometric responses with measured values. It turned out that particularly during wetter periods the modelled soil pressure heads reproduced satisfactorily the measured values. Spatially extended subsurface flow within the mineral topsoil occurred due to saturation excess exclusively. Therefore, laterally routed soil water was required, which necessitated an impervious bedrock. Contrary to the model set-up with one K_{sat} value per soil horizon, frequency of extended shallow subsurface flow was largely controlled by the spatial pattern of K_{sat} . Also, the frequency of the shallow subsurface flow was notably lowered if the trend of K_{sat} was omitted, and particularly if the proportion of canopy interception and evaporation was doubled. The results of this study show that a sound evidence of key parameters such as spatial patterns of K_{sat} , permeability of the subsoil, bedrock, and climate conditions is obligate if process conceptualisation regarding storm runoff generation, landslide initiation, solute and matter transport is in the spotlight.

Keywords: virtual experiment, montane rain forest, South Ecuador, steep hillslope, fast subsurface flow, spatial variability, hydraulic conductivity, model reduction

5.1 Introduction

As often reported, fast subsurface flow are a frequent phenomenon on steep forested hillslopes (Bonell et al., 1998; Mulholland et al., 1990) due to shallow soil horizons which are prone to develop fast subsurface flows by perched water tables (Chappell et al., 1990; Jenkins et al., 1994). The occurrence of saturated shallow subsurface flow is often linked to the decline of the hydraulic conductivity with increasing soil depth. If amount and intensity of rainfall are sufficiently high to rise the perched water table up to the soil surface, a shallow subsurface flow develops (DeWalle and Pionke, 1994), which may be even possible under relatively dry antecedent conditions (Bishop et al., 1990; Scherrer, 2007; Weiler and Naef, 2003). However, even without saturation of the mineral soil horizon, fast subsurface flow can occur within the organic layer, perched on the mineral soil surface due to highly contrasting saturated hydraulic conductivities at the organic layer/mineral soil interface (McDonnell et al., 1991).

In the Andes of South Ecuador, several authors who worked in the Reserva Biológica San Francisco (= RBSF, fig. 5.1) postulate a fast subsurface flow along the interface between mineral topsoil and overlying organic layer being highly abundant in the forested parts of the RBSF investigation area. This assumption bases on increased element concentrations (Wilcke et al., 2001) and precipitation isotope signatures (Goller et al., 2005) in the stream water during rainstorm events. Fleischbein et al. (2006) considers the largely contrasting saturated hydraulic conductivities between organic layer and mineral topsoil to facilitate this subsurface flow. However, these studies did not assign the presumed subsurface flow to a certain slope inclination or altitude. Via pedon scale dye tracer experiments in a gentler hillslope area above 2100 m above sea level (= ASL) within microcatchment 3 (= MC 3), Bauer et al. (in review, a; in review, b) found clear prerequisites for lateral subsurface flow in soils with stagnic moisture along the interface between mineral soil and organic layer. In this area, and slopes of less than 30 ° above 2100 m ASL Liess et al. (2009) found Stagnosols and Histosols (IUSS, 2007) prevailing. Similar soils have been found in the head regions of MC 1 and MC 2 (Fig. 5.1), while below 2100 m ASL Cambisols (IUSS, 2007) prevail (e.g. Kreutzer and Martini, 2002; Markwardt, 2005) for which saturated hydraulic conductivities seems to be higher than in the microcatchments head region according to Huwe et al. (2008). Here, at 2000 m ASL at the western ridge of MC 2 Zimmermann and Elsenbeer (2008) conducted *in*

situ measurements of the saturated hydraulic conductivity in a 0.4 ha plot covered by mature forest. They compared the measured hydraulic conductivities with 30 min rainfall intensity clusters to evaluate the formation of water perching upon the mineral topsoil layer. Since the study of Zimmermann and Elsenbeer (2009) involved the spatial variability of the hydraulic conductivity at local scale, they could show that between 20 cm and 50 cm below the mineral soil surface perched water tables may develop for a number of more intense rainstorms, potentially resulting in a shift to lateral flow paths and in positive pore-water pressures. However, as stated by Chappell and Sherlock (2005), K_{sat} can be crudely compared with rainfall intensities to assess the likelihood of infiltration excess overland flow or perched saturation. Moreover, the actual soil water content before rain storm events, potential laterally routed subsurface flow due to the predominant steep hillslope topography, the smoothing and interception effect of both the canopy (e.g. Keim et al., 2006; Keim and Skaugset, 2004) and the forest floor or organic layer (e.g. Blow, 1955; Kosugi et al., 2001; Schaap et al., 1997; Walsh and Voigt, 1977) were not considered by Zimmermann and Elsenbeer (2009). Regarding this, Huwe et al. (2008) suggest an advanced testing of the hypothesis that rapid subsurface flow occurs including the correlation structures at local scale of the saturated hydraulic conductivity estimated by Zimmermann and Elsenbeer (2009). This means also integration of ecoclimate- and ecophysiological parameters, which are suggested to be fundamental in ecological model calculations (e.g. Keim et al., 2006).

To our knowledge, only few field studies were accomplished in tropical montane rain forests in order to assess these parameters (e.g. Bruijnzeel, 2001; Küppers et al., 2008; Letts, 2003). In the RBSF study area, Motzer (2003) carried out an elaborate field study at plot scale in the mature forest of the western and eastern ridge of MC 2 at 1950 m and 1975 m ASL, respectively. Based on the measurements, Motzer (2003) calculated the energy balance and evapotranspirational water loss for the investigated sites via the Penman-Monteith approach (Monteith, 1965). Here, the amount of water intercepted and evaporated from canopy is considerably small with less than 100 mm/a. This result is highly contradicting to the study of Fleischbein et al. (2006), who evaluated the water budget of MC 2 using TOPMODEL (Beven et al., 1995). Their results bases on the assumption of an impervious bedrock and show a min. evaporation rate of 463 mm/a (max. 1033 mm/a), and a min. transpiration rate of 281 mm/a (max. 783 mm/a) for a 4 year period. The large discrepancy between the evaluated evaporation rates of Motzer (2003) and Fleischbein et al. (2006) is obvious, while the transpiration rate of Motzer (2003) equals the mean value estimated by Fleischbein et al. (2006) as shown in table 5.1. A further investigation conducted by Ösker (2008) on a plot at

2000 m ASL on the western ridge of MC 2 revealed ~16 % of the incident precipitation being intercepted and evaporated from the canopy (tab. 5.1).

Table 5.1 Summary of the proportions of transpiration and evaporation from incident precipitation as found by Motzer (2003), Fleischbein et al. (2006), and Ösker (2008).

	Motzer	Ösker	Fleischbein
Transpiration	~23% from precip.	n.d.	~23% from precip.
Evaporation	~3% from precip.	~16% from precip.	~32% from precip.
MC	Q2	Q2	Q2

Since the studies denoted in table 5.1 neglect evaporation processes at the forest floor, the evaporation rates account for canopy interception exclusively. Thus, amount and intensity of water passing the canopy and reaching the soil will differ considerably. Following Keim et al. (2006), this will have a certain impact on subsurface flow and runoff generation and would complicate calibration of models as additive tool to elucidate the occurrence and dynamic of flow paths. Summarising the facts, virtual experiments seem to be a more appropriate tool here, since these are considered as numerical experiments driven by collective field intelligence and thus do not primarily focus on calibrating a model to field data and observations as commonly done in hillslope hydrology studies (Weiler and McDonnell, 2004). As stated by Weiler and McDonnell (2004), the idea of virtual experiments originates from the dilemma in hillslope hydrology that the plenitude of experimental field studies on hillslope processes in the past decade have produced sparse generalisable results or definition of suitable state variables in different environments. This resulted in a lack of common conceptualisation of hillslope hydrology, which is, for example, the minimal transfer value among neighbouring hillslopes, since soil properties, slope and bedrock topography, and type of forest cover may considerably change. Therefore, virtual experiments aim to clarify or at least to locate weak points within an existing perceptual- or numerical model by exploring the effect of individual parameters such as duration and frequencies of rainfall, canopy interception, soil properties, bedrock permeability and -topography, slope angle, and hillslope geometry (Hopp and McDonnell, 2009; Keim et al., 2006; Weiler and McDonnell, 2004, Weiler and McDonnell, 2006). Also, generalisations for the purpose of model simplification can be proven promptly (Weiler and McDonnell, 2004).

With this paper, we aimed to elucidate three principal goals in order to improve the process conceptualisation regarding the occurrence of shallow subsurface flow (= sSF), namely lateral flow within and upon the mineral topsoil as proposed in several studies (e.g. Fleischbein et al.,

2006; Goller et al., 2005; Wilcke et al., 2001; Wilcke et al., 2008) in the RBSF investigation area.

Firstly, we apply a series of virtual experiments to check for the sensitivity of the presumed sSF on the hydraulic conductivity of the subsoil.

Secondly, we want to assess the effect of two different evaporation rates as proposed by Ösker (2008) and Fleischbein et al. (2006) on the formation of sSF. Concerning the first and second goal, the virtual experiments include the spatial variability of the saturated hydraulic conductivity and their trends estimated by Zimmermann and Elsenbeer (2008).

Thirdly, with respect to model simplification, which effect has the stepwise reduction of model complexity on the presumed sSF, i.e. if trend, and subsequently spatial variability of the saturated hydraulic conductivity is omitted.

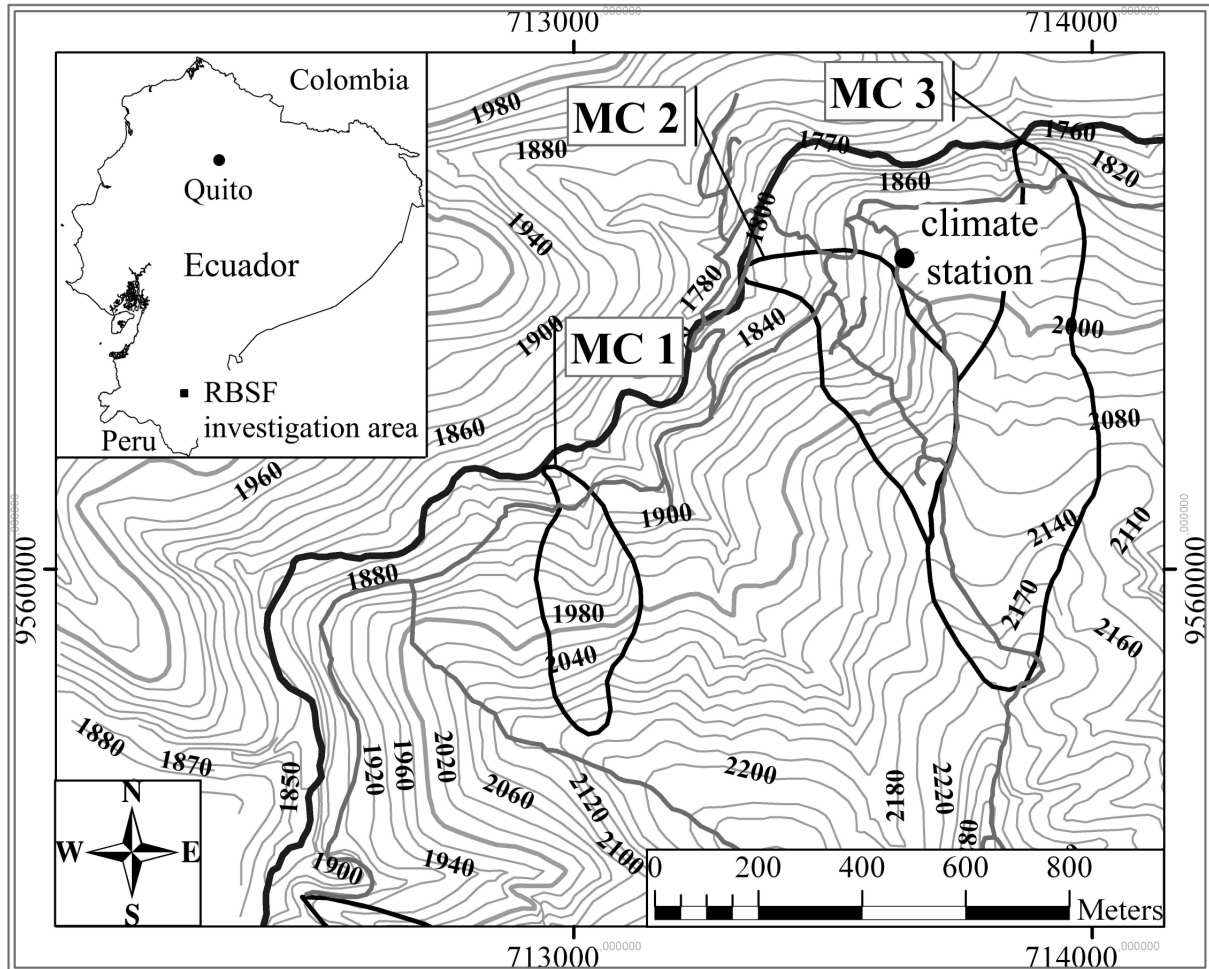
5.2 Materials and methods

5.2.1 Study area

The area we considered for the virtual experiment study approach is situated within the Reserva Biológica San Francisco (= RBSF) between the province capitals Loja and Zamora in South Ecuador (fig. 5.1). The investigation area, located at the northern rim of the Podocarpus National Park, encompasses 11.2 km² and an altitudinal gradient from 1750 m to 3200 m ASL. The area is part of the eastern slope of the Cordillera Real, which forms the weather divide between the humid Amazonian lowlands and the drier inter-Andean highlands. At the RBSF investigation area, the wetter months are between April and August while rainfall is high throughout the year (Bendix et al., 2008). Average annual precipitation amounts 2050 mm at 1960 m ASL and 4400 mm at 3160 m ASL (Rollenbeck, 2006), while the mean annual air temperature ranges between 19.4 °C at the valley bottom and 9.4 °C at the highest elevations (Fries et al., 2009). Balslev and Øllgaard (2002) classify the natural vegetation cover as evergreen montane forest, Bruijnzeel and Hamilton (2000) as lower montane forest. In the RBSF study area, most important tree families are Clusiaceae, Chloranthaceae, Melastomataceae, Lauraceae and Arecaceae (Homeier et al., 2002) often bearing vascular epiphytes (Werner et al., 2005). The ground vegetation layer is dominated by ferns and large herbs (Homeier et al., 2002; Homeier, 2004; Paulsch, 2002).

The bedrock of the RBSF study area belongs to the Chiguinda unit (within the Zamora series) consisting of interbedded paleozoic phyllites, metasandstones and quartzites (Hungerbühler, 1997). Below 2000 m ASL and within steeper slopes, soils are predominantly

loamy-skeletal (Yasin, 2001) as they developed mostly from landslide deposits and probably periglacial sediments (Fleischbein et al., 2006). Above 2100 m ASL, particularly in slopes of less than 30° Stagnosols and Histosols prevail (Liess et al., 2009).



Legend

- San Francisco River
- trails
- microcatchment boundary

Figure 5.1 Overview of the core area of the RBSF investigation site in South Ecuador. The black point north of MC 2 denotes the climate station. Altitudes are above sea level. Coordinate system is UTM WGS84 17S.

5.2.2 Study site and acquisition of field data

The study site we consider in our series of virtual experiments is located between 2000 m and 2050 m ASL on the western ridge of MC 2 (fig. 5.2) and covered by mature forest.

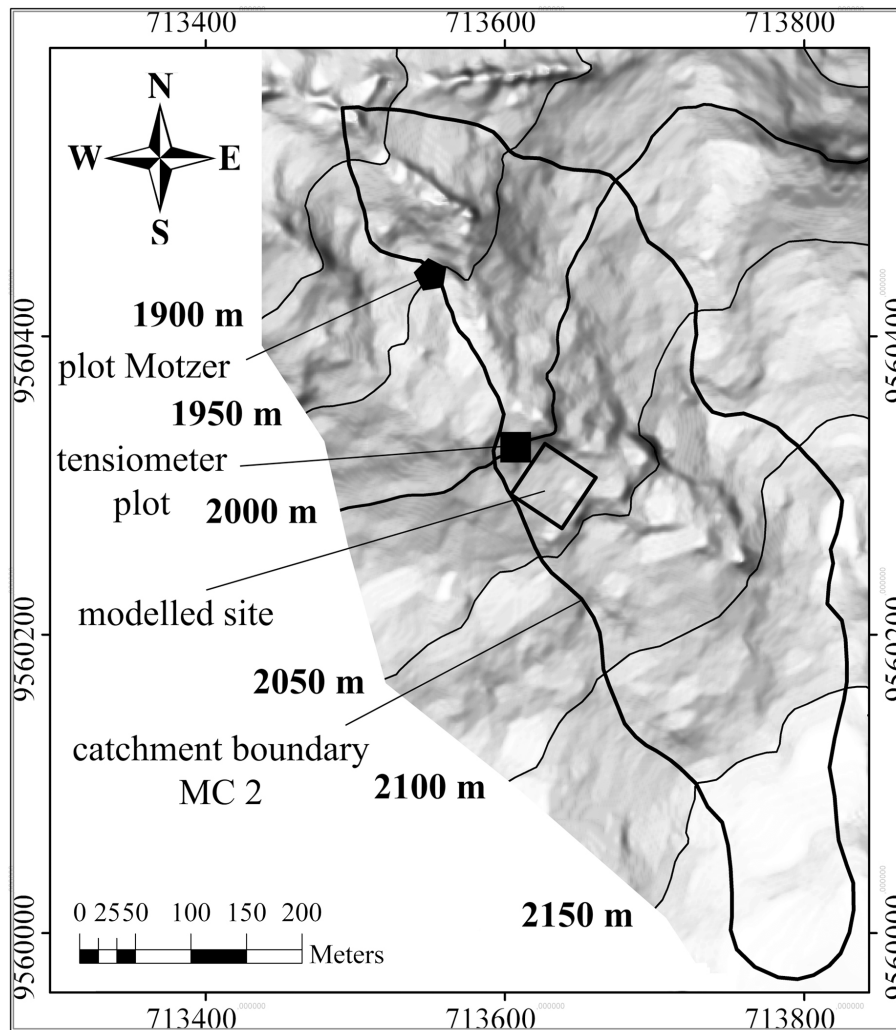


Figure 5.2 Digital elevation map of microcatchment 2 with delineated positions of the plots as mentioned in the text. Altitudes are above sea level. Coordinate system is UTM WGS84 17S.

5.2.2.1 Soil parameter and pressure heads

At ~2000 m at the western ridge of MC 2, Zimmermann and Elsenbeer (2008, 2009) conducted *in situ* measurements of K_{sat} using an Amoozometer (Amoozegar, 1989) on a 0.4 ha plot covered by a mature forest. At the same ridge between ~1970 m ASL and ~2060 m ASL, disturbed and 100 cm³ core samples from the A (n = 7), B (n = 5) and C (n = 6) horizons of 7 pits were taken. In the C horizons, K_{sat} was measured using a Guelph permeameter (Elrick and Reynolds, 1992). According to Huwe et al. (2008), direct comparisons between the K_{sat} values measured with the Amoozometer and the Guelph permeameter revealed comparable results. The soil samples were analysed to obtain the grain size fractions and bulk densities. The latter were determined from the undisturbed samples after 48 h of drying at 105 °C. We obtained the grain size distribution by wet sieving of the

sand fraction and by the sedimentation/aliquot-weighting method after Köhn (1928) for the silt- and clay fraction. We classified the fine soil fractions between 2 mm and 0.063 mm for Sand, between 0.063 mm and 0.002 mm for silt, and smaller than 0.002 mm for clay. The soils within the investigated ridge have been mainly classified as Cambisols and described in detail by Kreutzer and Martini (2002) and Markwardt (2005). At 2000 m ASL at the western ridge of MC 2 soil pressure heads were measured daily by tensiometers at 15 cm below the mineral soil surface within a 0.04 ha plot denoted as “tensiometer plot” in figure 5.2.

5.2.2.2 Climate data

Hourly values of incident precipitation ($= N_{field}$, in [mm/h]) (fig. 5.5), temperature ($= T$, in [°C]), relative humidity ($= rH$, in [%]), wind velocity ($= V_w$, in [$m\ s^{-1}$]) and global radiation ($= grad$, in [$W\ m^{-2}$]) were logged by a climate station north of MC 2 at ~1950 m ASL (fig. 5.1). The quality of N_{field} was improved by crosschecking with data from other climate stations installed within the RBSF study area (R. Rollenbeck, pers. comm.). This part of the summit was clear cut so that the measurements were not disturbed by the vegetation cover.

5.2.3 Virtual experiment model design

We performed the virtual experiments using the software package Hydrus 2D/3D ver. 1.08 (= Hydrus) (Šimůnek et al., 2006), which allows to create two dimensional (= 2D), respectively three dimensional (= 3D) finite element (= FE) models for simulating water movement in variably saturated porous media solved numerically by the Richards Equation (Richards, 1931). In order to calculate the considered model set ups within a manageable time, we derived a 2D FE model (fig. 5.3b) from a 3D FE model (fig. 5.3a) built in Hydrus. To create the surface layer of the latter, we used the corresponding Cartesian coordinates from a digital elevation model (= DEM) of MC 2 with contour lines of 1 m (fig. 5.2). To obtain the 2D FE model, we extracted the mesh nodes by their corresponding y (length), x (width), and z (height) Cartesian coordinates from a transect along the y axis as delineated in figure 5.3a. The resulting 2D FE slope has a horizontal length of 43 m, an average inclination of 30 °, and follows the fall line of the 3D FE model delineated as “2D transect” in figure 5.3a. The vertical thickness of the slope measures throughout 1.5 m. For the 3D and 2D FE model, respectively, we provided fixed soil horizons resembling the mean soil horizon thickness as observed in the field. Due to the presumed subsurface flow, spatial discretisation was 0.5 cm along the organic layer/mineral soil interface, and ≤ 10 cm within the A horizon. From the organic layer/mineral soil interface towards the surface of the organic layer, and from the A

horizon towards the model bottom the spatial discretisation increased gradually (fig. 5.3c) in order to save calculation time. The boundary conditions of the 2D FE slope are given in figure 5.3b. To our knowledge, there is no reliable information about bedrock permeability within the RBSF investigation area. Therefore, in the framework of the virtual experiments presented here we assume an impervious bedrock as suggested by Fleischbein et al. (2006). We started all model runs with an initial pressure head of -150 hPa over the whole model domain.

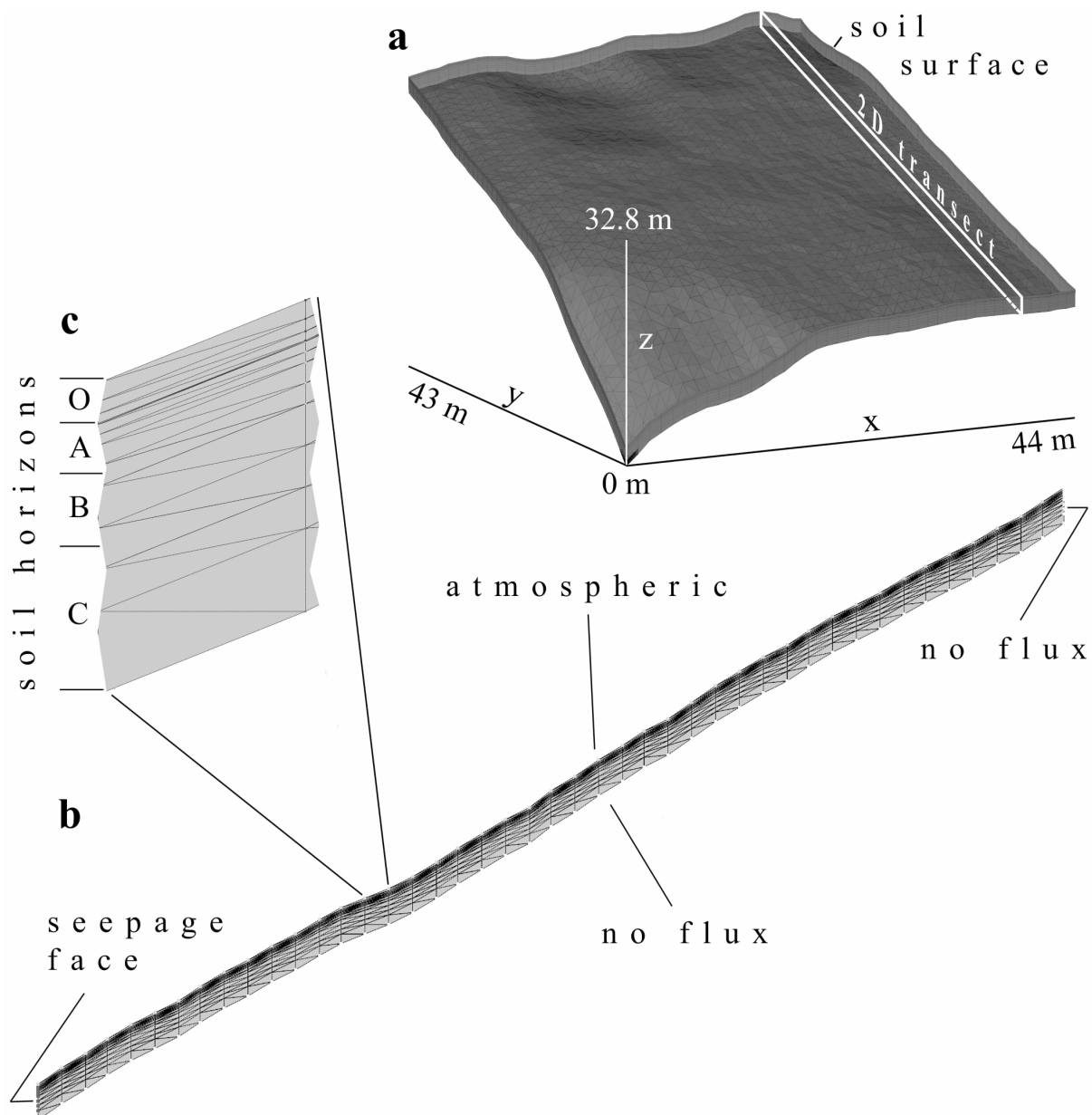


Figure 5.3 (a) 3D FE model of the slope at the western ridge of MC 2 between 2000 m and 2050 m ASL with viewing direction to SE; (b) 2D FE model derived from the 3D FE model as indicated in (a); (c) detail in the top left-hand corner shows positions of the soil horizons and the mesh structure.

5.2.4 Model input parameters: climate

Since Motzer (2003) calculated the energy balance and evapotranspirational water loss based on measurements within MC 2 (fig. 5.2), we adopted the Penman-Monteith approach (1) (Monteith, 1965) as applied by Motzer (2003):

$$ET_{pot} = \frac{1}{\lambda} \frac{s(Q_{net.rad} - Q_{soil}) + \rho_a c_p D g_a}{\Delta + \gamma \left(1 + \frac{g_a}{g_c}\right)}, \quad (1)$$

where ET_{pot} is the potential evapotranspiration in [mm/h], Δ the slope of the vapor pressure deficit in [hPa K⁻¹], $Q_{rad.net}$ is the radiation balance in [W m⁻²], Q_{soil} the soil heat flux in [W m⁻²] (3), ρ_a the density of dry air in [kg m⁻³], c_p the specific heat capacity at constant pressure in [J kg⁻¹ K⁻¹], D the vapor pressure deficit in [hPa], g_c the canopy conductance in [m s⁻¹] (fig. 5.4), g_a the aerodynamic conductance in [m s⁻¹] (2), γ the psychrometer constant in [hPa K⁻¹] and λ the latent heat of vaporisation in [J kg⁻¹]. We computed g_a by equation 2 usually used (Foken, 2008):

$$g_a = \frac{\kappa^2 V_w}{\ln\left(\frac{Z_w - d_0}{Z_r}\right) \cdot \ln\left(\frac{Z_{rH} - d_0}{0.1 \cdot Z_r}\right)}, \quad (2)$$

where κ is the Kármán constant [-], V_w the wind velocity in [m s⁻¹], Z_w [m] and Z_{rH} [m] the measuring heights [m] of V_w and rH , respectively, with both 20.9 m. Z_r [m] is the roughness parameter with 1.89 m, and d_0 [m] the zero plane displacement height with 12.6 m. The latter three parameters were adopted from Motzer (2003). However, some corrections were made to adapt equation 1 to local conditions. (i) Since the soil heat flux (= Q_{soil}) (3) was not measured within the modelled time span, we followed Motzer (2003) who illustrated Q_{soil} being ~5 % of the net radiation basing on daily values in accordance with other authors (e.g. Lippert, 2002; Monteith and Unsworth, 1990; Schellekens, 2000). Since positive soil heat fluxes are restricted to the second day time (Motzer, 2003), we estimated a latency of 4 hours relative to the diurnal variability of $Q_{rad.net}$. Thus, for each time step $Q_{soil}(t)$ is calculated as:

$$Q_{soil}(t) = Q_{net.rad}(t - 4h) \cdot 0.05. \quad (3)$$

(ii) We implemented the diurnal variation of the canopy conductance ($= g_c$) by a linear regression model (fig. 5.4) according to measurements of Motzer et al. (2005) on *Trichilia guianensis* (Meliaceae), *Ruagea cf. pubescens* (Meliaceae), *Naucleopsis sp.* (Moraceae), and *Hedyosmum anisodorum* (Chloranthaceae) being typical abundant at 1950 m ASL. Motzer et al. (2005) found the vapor pressure deficit ($= D$) and the photosynthetic active radiation ($= PAR$) mainly regulating the closing and opening of the stomata if there is no soil water deficit. Here, D is normalised by PAR and plotted against g_c (fig. 5.4). As proposed by Hupfer and Kuttler (1998), we estimated PAR by multiplying the global radiation ($= gRad$) with 0.3.

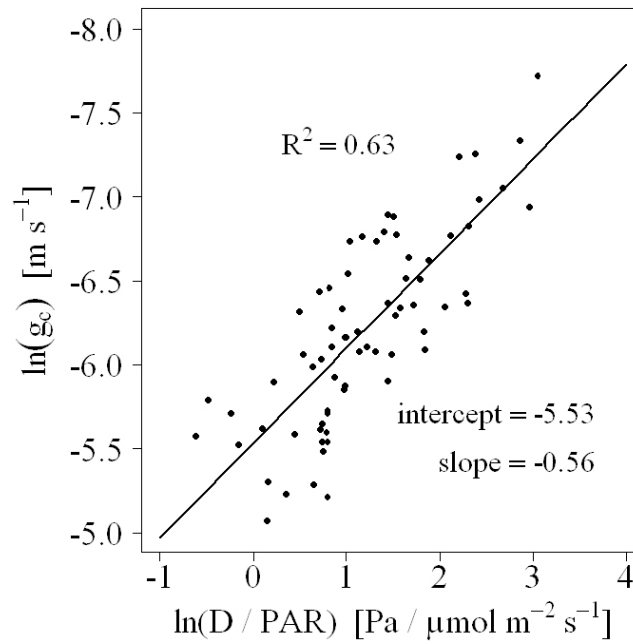


Figure 5.4 Diurnal variation of the canopy conductance (g_c) depending on the vapor pressure deficit (D) and the photosynthetic active radiation (PAR). Data with permission from Motzer (pers. comm.).

(iii) Since the direct effect of the evaporation on the forest floor can be neglected (Fleischbein et al., 2006; Motzer, 2003), we assume E_{pot} only affecting the canopy interception storage ($= C_{Int}$). The proportion of T_{pot} and E_{pot} was obtained from ET_{pot} (1) by applying Beer's law (4), (5) as proposed by Ritchie (1972). Here, the constant k was adjusted to approximate the annual actual proportions of $ET_a = 26.4\%$ and $T_a = 23.1\%$ to N_{field} as calculated by Motzer (2003).

$$T_{pot}(t) = ET_{pot}(t) \cdot (1 - e^{-k \cdot LAI}), \text{ with} \quad (4)$$

$$E_{pot}(t) = ET_{pot}(t) \cdot e^{-k \cdot LAI}, \quad (5)$$

where LAI is the leaf area index, and t the time in [h]. By adjusting the constant to $k = 0.3$ and providing a mean $LAI = 5.52$ [-] determined by Ösker (2008) in MC 2, we obtained a share of $E_{pot} = 5.9$ % and $T_{pot} = 24.8$ % to N_{field} over the modelled time span between 09.01.2005 and 12.26.2006. In Hydrus, we used the hourly values of T_{pot} as actual transpiration rates ($= T_{act}$), since the majority of the tree species within MC 2 still transpire at highest level even if the actual soil water content is below field capacity (R. Zimmermann, pers. comm.). Furthermore, we used $E_{pot}(t)$ (5) in order to empty $C_{Int}(t)$, for which we provided a maximum canopy storage capacity $C_{Int(max)} = 2.46$ mm as found by Fleischbein et al. (2005) in MC 2. Thus, we calculated the hourly throughfall N_{net} as

if $C_{Int}(t) - E_{pot}(t) < 0$

then

$$N_{net}(t) = N_{field}(t) - C_{Int(max)} \quad (6)$$

else

$$N_{net}(t) = N_{field}(t) - [C_{Int(max)} - (C_{Int}(t) - E_{pot}(t))], \text{ with} \quad (7)$$

$$0 \leq C_{Int}(t) \leq C_{Int(max)},$$

where $C_{Int}(t)$ is the canopy interception storage content at time t . We defined the difference between $N_{net}(t)$ and $N_{field}(t)$ as the actual evaporation $E_{act}(t)$, since the water stored in the canopy successively evaporates. For the modelled time span between 09.01.2005 and 12.26.2006, we computed a percentage of $E_{act} = 4.9$ %, $T_{act} = 24.8$ %, and thus $ET_{act} = 29.7$ % to N_{field} (tab. 5.2) compared to the annual $ET_{act} = 26.4$ % to N_{field} determined by Motzer (2003). As documented in table 5.1, the annual values of E_{act} determined by Fleischbein et al. (2006) and Ösker (2008) are notably higher than calculated by Motzer (2003). However, even within the min/max ranges of LAI and C_{Int} measured by Ösker (2008) and Fleischbein et al. (2006), respectively, we could not reproduce their high proportions of E_{act} to N_{field} basing on equations 1-7. Also, no other studies in the RBSF investigation were conducted considering the Penman-Monteith approach (Monteith, 1965).

For the purpose to assess the effect of the evaporation from the canopy on the presumed subsurface within the framework of virtual experiments, we simply amplified the $E_{pot}(t)$ values in equation 7 by constant factors to meet the annual proportions of E_{act} to N_{field} (tab. 5.2) as determined by Fleischbein et al. (2006) and Ösker (2008). Preliminary virtual experiments using E_{act} calculated according to Motzer (2003) could not handle the high

amount of throughfall. That is, the organic layer in the lower part of the model slope became throughout saturated while calculation errors considerably increased. Therefore, in the framework of virtual experiments presented in this paper we resort to E_{act} which we calculated regarding the findings of Ösker (2008) and Fleischbein et al. (2006).

Table 5.2 Summary of the reproduced percentages to N_{field} and absolute amounts of ET_{act} , E_{act} , and T_{act} of the corresponding researchers. The values refer to the time span between 09.01.2005 and 12.26.2006 provided in the virtual experiments.

	Motzer (2003)		Ösker (2008)		Fleischbein et al. (2006)	
N_{field}	2048.5 mm		2048.5 mm		2048.5 mm	
ET_{act}	29.7 %	608.8 mm	40.8 %	835.1 mm	56.7 %	1161.8 mm
E_{act}	4.9 %	100.8 mm	16.0 %	327.1 mm	31.9 %	653.8 mm
T_{act}	24.8 %	508.0 mm	24.8 %	508.0 mm	24.8 %	508.0 mm

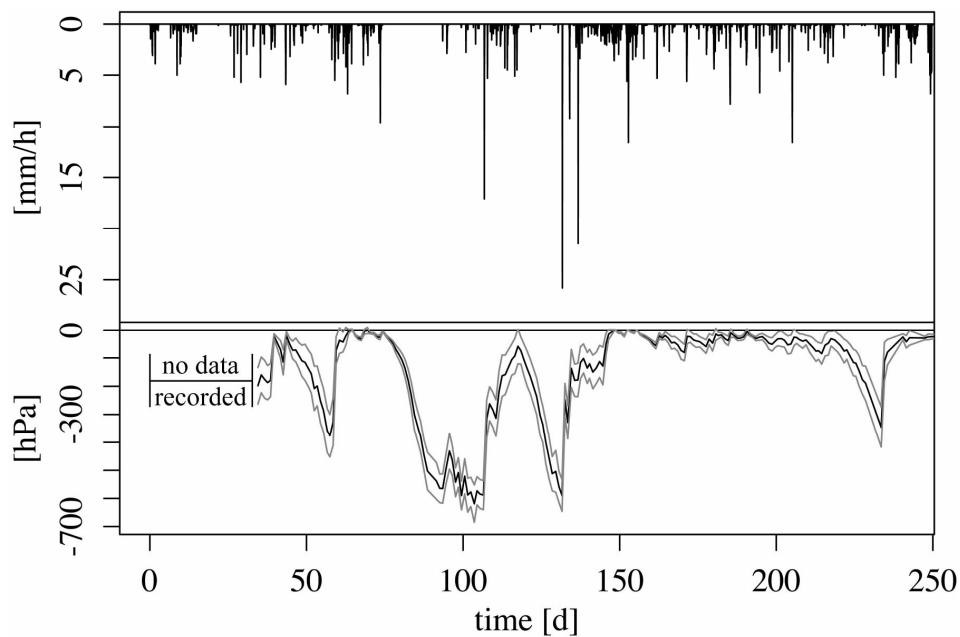


Figure 5.5 Hourly values of N_{field} recorded by the climate station delineated in figure 5.1. The grey lines below the precipitations denote the 95 % confidence intervals around the mean pressure head (black line). The pressure heads were measured in the “tensiometer plot” (fig. 5.2) ~15 cm below the mineral soil surface.

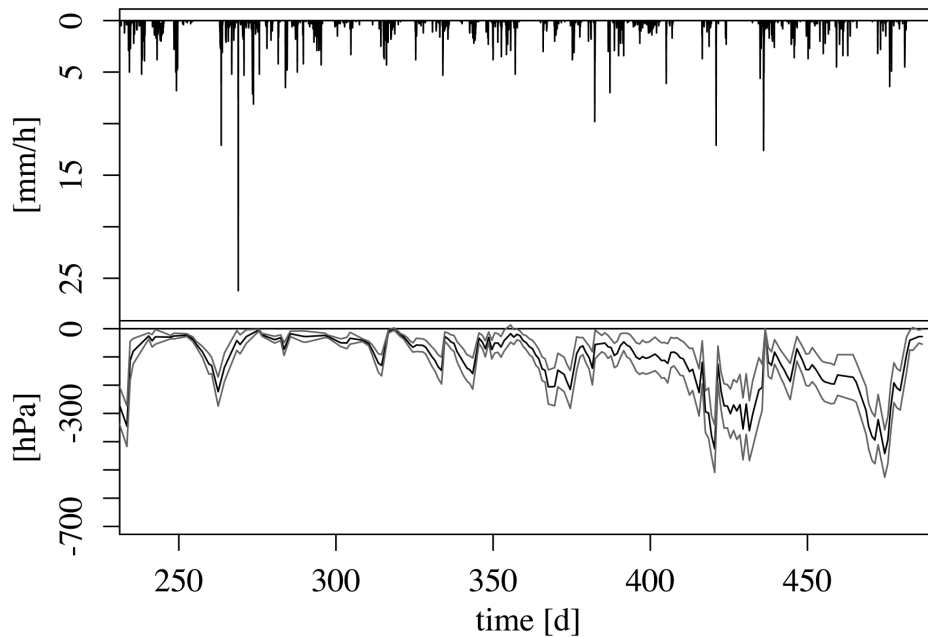


Figure 5.5 (continued from previous page)

5.2.5 Model input parameters: soil and organic layer

To parameterise the mineral soil horizons A, B, and C, we computed the van Genuchten-Mualem parameters using the software Rosetta lite ver 1.1 (Schaap et al., 2001). The input parameters for Rosetta were the mean percentage of the grain size fractions sand, silt, and clay, and the bulk density from the analysed soil samples (see subsection 5.2.2.1). The outputs of Rosetta are given in table 5.3. The estimated saturated hydraulic conductivities were substituted by medians of measured values, which we denote as reference values $K^*(h^*)$ in table 5.3. We refer to median values due to the largely lognormal distributed saturated hydraulic conductivity values of the A, B, and C horizon. Only for the organic layer (= O horizon, tab. 5.3), the mean was used because there was no evidence for lognormal distributed Ksat values, which were predicted by inverse modelling (Leutner et al., in review). As stated by Leutner et al. (in review), the predicted Ksat values resemble the Ksat values measured by Kreutzer and Martini (2002) in the organic layer within MC 2.

Since Zimmermann and Elsenbeer (2008) measured Ksat in three depths until 50 cm, we could assign their median Ksat values only to the A- and B horizon of the modelled slope (tab. 5.3). Due to the pronounced skewness, Zimmermann and Elsenbeer (2008) applied a \log_{10} -transformation on the Ksat data, which also allowed them to remove spatial trends by polynomial regression of first order. From the remaining residuals, they determined nugget, partial sill and range for each of the three measuring depths. Here, they used a spherical correlation function for the measuring depths 12.5 cm and 50 cm, and an exponential

correlation function for the 20 cm measuring depth. Since the values of the Ksat median, trend coefficients, nugget, partial sill, and range of the depths 12.5 cm and 20 cm are within the modelled A horizon, we expressed them as weighted harmonic mean with the measuring depth being the weight (tab. 5.4). Moreover, since Zimmermann and Elsenbeer (2008) used a spherical correlation function for the 12.5 cm and 50 cm measuring depth, we decided to use a spherical covariance function (tab. 5.4) for the merged data of the A horizon to produce isotropic Gaussian random fields.

For the B horizon, the median Ksat value (tab. 5.3) and variogram parameters (tab. 5.4) were taken as determined by Zimmermann and Elsenbeer (2008) at 50 cm measuring depth. For the depths 50 cm below the mineral soil surface, which resembles the C horizon in the 2D FE model (fig. 5.3c), we resort to own Ksat measurements (fig. 5.5) conducted within and close to the modelled plot denoted in figure 5.2. However, due to the relative small number of repetitions ($n = 6$), we omitted a geostatistical analysis in order to find a trend within the C horizon. The median Ksat value ($= 0.75$ cm/h) we estimated for the C horizon is higher than in the B horizon (tab. 5.3). In this regard, Zimmermann and Elsenbeer (2008) did not find the trend of Ksat to decrease significantly with depth at the sites they investigated within the RBSF study area.

Table 5.3 van Genuchten-Mualem Parameters computed by Rosetta. θ_r [-] is the residual water content, θ_s [-] the water content at saturation, α [1/cm] and n [-] are form parameter, $K^*(h^*)$ [cm/h] denotes the reference values, and l [-] the tortuosity, which we consider to be 0.5 according to Mualem (1976). The root length densities [cm cm⁻³] (= RLD) obtained from Soethe et al. (2006) are expressed as relative root length densities (= rRLD) [-]. The depth values equal the depths of the mesh nodes, to which a rRLD value was assigned. To all mesh nodes of the O horizon, we assigned rRLD = 1, and to the mesh nodes between 0 cm and -10 cm rRLD = 0.36.

horizon	depth [cm]	θ_r ¹ [-]	θ_s ¹ [-]	α ¹ [1/cm]	n ¹ [-]	$K^*(h^*)$ ^{2a} [cm/h]	l ¹ [-]	depth [cm]	rRLD [-]
O	+20	0.05	0.55	0.03	1.11	421.2 ^{2b}	0.5	+20	1
A	-25	0.068	0.465	0.0047	1.688	2.39 ^{2b}	0.5	-10	0.36
								-20	0.33
B_a ³	-40	0.053	0.404	0.0064	1.620	0.7 ^{2b}	0.5	-30	0.33
B_b ³	-60	0.053	0.404	0.0064	1.620	0.3 ^{2b}	0.5	-50	0.18
								-70	0.1
C	-130	0.054	0.397	0.0049	1.694	0.75 ^{2b}	0.5	-90	0.05
								-130	0.03

¹ calculated by Rosetta lite (Schaap et al., 2001) // ^{2a} reference hydraulic conductivity // ^{2b} values at saturation // ³ due to the strong decline of $K^*(h^*)$ between the A- and B horizon, we intercalated a further horizon (B_a) in the model to mitigate this steep gradient in order to avoid numerical problems. Note that except for $K^*(h^*)$ the remaining van Genuchten-Mualem parameters between B_a and B_b are identical.

We used this finding for our virtual experiments and provided model set-ups with a lower (0.2 cm/h) and higher (1.3 cm/h) Ksat value than the median (tab. 5.5) to observe their influence on the spatiotemporal occurrence of the presumed lateral flow within or upon the mineral topsoil. These values are within the min. (0.1 cm/h)/max. (9.4 cm/h) range of the Ksat values measured in the C horizon. The scenarios of increased and decreased Ksat of the C horizon resembles the observations of Bauer et al. (in review), who found mineral soil layers over permeable and impervious weathered bedrock via dye tracer experiments in the RBSF study area.

To simulate the organic layer adequately, we resort to Leutner et al. (in review), who determined the van Genuchten-Mualem parameters including Ksat of the organic layer by inverse modelling (tab. 5.3). In Hydrus, we implemented the actual transpiration T_{act} via the S-shape function suggested by van Genuchten (1987). Here, we did not consider water stress, since the majority of the tree species within MC 2 still transpire at highest level even if the actual soil water content is far below field capacity (R. Zimmermann, pers. comm.). The root water uptake modul of Hydrus requires input of the spatial root distribution, which we implemented according to the findings of Soethe et al. (2006).

5.2.6 Spatial variability of the saturated hydraulic conductivity $K(h)$ and pressure head h

In 5 from 6 of the 2D virtual experiments model set-ups we implemented the horizon wise spatial variability of the hydraulic conductivity $K(h)$ by means of 2D isotropic Gaussian random fields (= RFs). The RFs were computed using RandomFields (Schlather, 2001), a package provided for the statistical software program R ver. 2.9.1 (R Development Core Team, 2009), which requires input of a (partial) sill, range, nugget, and the choice of a covariance function (tab. 5.4).

The RFs contain scaling factors for Ksat (= α_K), which are normal distributed. Due to the lognormal distributed Ksat values, we transformed the α_K for the A and B horizon via $10^{(\alpha_K)}$ = α_K^{TR} (note that Zimmermann and Elsenbeer (2008) applied a \log_{10} transformation to obtain normal distributed Ksat values), and for the C horizon via $\exp(\alpha_K) = \alpha_K^{TR}$ to lognormal distributed scaling factors, which were then multiplied by the corresponding hydraulic conductivity reference value $K^*(h^*)$ (tab. 5.3) in Hydrus.

Table 5.4 Overview of parameters used in RandomFields to produce isotropic Gaussian random fields of scaling factors for Ksat (= α_K).

horizon	parameters used in RandomFields						trend coefficients used in equation 10		
	mean [cm/h]	partial sill	sill	nugget	range [cm]	covariance function	β_0	β_1	β_2
O ^a	421.2	--	6856 ^e	--	1	nugget	--	--	--
A ^b	0	0.32	--	0.57	614	spherical	1.183 ^b	-0.0074 ^b	0.013 ^b
B ^c	0	0.3	--	0.41	494	spherical	0.262 ^c	0.0067 ^c	0.01 ^c
C ^d	0	--	2.48 ^e	--	774 ^f	spherical	--	--	--

^a data from Leutner et al. (in review) // ^b weighted harmonic mean (see subsection 5.2.3) of data from Zimmermann and Elsenbeer (2008) // ^c data from Zimmermann and Elsenbeer (2008) // ^d own measurements // ^e variance of the normal distributed data supposed as sill // ^f range estimated from ranges found by Zimmermann and Elsenbeer (2008) in subsoils at different sites within the RBSF study area

We did not apply this to the O horizon, for which lognormal distributed Ksat values were not evident due to the Ksat values obtained by inverse modelling (Leutner et al., in review) instead of field measurements. Therefore, in the following α_K^{TR} may be synonymously used for α_K of the O horizon.

At each node of the 2D FE mesh in Hydrus a scaling factor α_K^{TR} was multiplied with the corresponding reference value $K^*(h^*)$ as follows (8):

$$K(h)_{ij} = \alpha_{K_{ij}}^{TR} \cdot K^*(h^*)_j, \quad (8)$$

where $K(h)_{ij}$ is the hydraulic conductivity of node i within the j^{th} horizon, and $\alpha_{K_{ij}}^{TR}$ the lognormal distributed scaling factor for Ksat at node i within the j^{th} horizon, where $j = O, A, B, C$. $K^*(h^*)_j$ is the reference value of the hydraulic conductivity of the j^{th} horizon.

We implemented the spatial variability of the pressure head as well, which necessitated a conversion of the $\alpha_{K_{ij}}^{TR}$ scaling factors according to Miller and Miller (1956) (9):

$$\alpha_{K_{ij}}^{TR} = \alpha_{h_{ij}}^{-2} \Leftrightarrow \alpha_{h_{ij}} = \frac{1}{\sqrt{\alpha_{K_{ij}}^{TR}}}, \quad (9)$$

where $\alpha_{h_{ij}}$ denotes the individual scaling factor of the pressure head at node i within the j^{th} horizon to be multiplied by the pressure head reference value h_j^* of the j^{th} horizon (10):

$$h_{ij} = \alpha_{h_{ij}} \cdot h_j^*, \quad (10)$$

where h_{ij} is the pressure head value of a node i within horizon j . As aforementioned, in subsection 5.2.5 a trend has to be included for the horizons A and B. Thus, to the normal distributed scaling factors $\alpha_{K_{ij}}$ the trends were added (11) as the inverse operation to the trend removal performed by Zimmermann and Elsenbeer (2008):

$$\alpha_{K_{ij} \text{ TREND}} = \alpha_{K_{ij}} + (\beta_{0_j} + \beta_{1_j} \cdot x_{ij} + \beta_{2_j} \cdot y_{ij}) \quad (11)$$

where x_{ij} and y_{ij} are the Cartesian coordinates [m] of node i of the j^{th} horizon ($j = A, B$), and β_{0_j} , β_{1_j} , and β_{2_j} are trend coefficients according to Zimmermann and Elsenbeer (2008) of the j^{th} horizon ($j = A, B$). However, by adding a trend the transformation of the normal distributed $\alpha_{K_{ij} \text{ TREND}}$ to a lognormal distributed $\alpha_{K_{ij} \text{ TREND}}^{\text{TR}}$ via $10^{(\alpha_{K_{ij} \text{ TREND}})}$ necessitated to divide $\alpha_{K_{ij} \text{ TREND}}^{\text{TR}}$ by its corresponding reference value $K^*(h^*)$ (tab. 5.3) to obtain scaling factors again. In Hydrus, these scaling factors were multiplied with the reference values $K^*(h^*)_j$ according to equation 8. Moreover, from $\alpha_{K_{ij} \text{ TREND}}^{\text{TR}}$ we computed the pressure head scaling factors $\alpha_{h_{ij} \text{ TREND}}$ according to equation 9.

With respect to the three goals we defined in section 5.1, we provided 6 virtual experimental model set-ups given in table 5.5. For each model set-up featuring RFs we performed a series of 15 virtual experiments to avoid misleading results, which we would obtain from single virtual experiment having a particular set of RFs.

Table 5.5 Summary of the virtual experiment model set-ups.

model set-up	evaporation		RFs	no RFs	trend	soil	
	Ösker (2008)	Fleischbein et al. (2006)				no trend	$K^*(h^*)$ of the C horizon [cm/h]
I_a	●		●		●		0.75 ¹
I_b	●		●		●		0.2
I_c	●		●		●		1.3
II		●	●		●		0.75 ¹
III_a	●		●			●	0.75 ¹
III_b	●			●		●	0.75 ¹

¹ median value

For each horizon O, A, B, and C defined in the 2D FE model we applied the following principal operations. Here, we repeated operation (i) several 10 times to obtain a population of RFs. Since we want to assess the effect of the spatial variability of Ksat within the mineral soil on the potential occurrence of shallow subsurface flow, we computed only one RF for the O horizon, which we used in all model set-ups.

(i) Generating 3D isotropic Gaussian random fields via the R package RandomFields using the turning bands method as recommended by Schlather (pers. comm.). Therefore, we transferred the x , y , and z coordinates of each mesh point from the considered soil horizon provided in the Hydrus 3D FE model (fig. 5.3a) to RandomFields. Figure 5.6 exemplarily documents the spatial distribution of $\alpha_{K_{ij}}^{TR}$ for the O- and C horizon, and $\alpha_{K_{ij}TREND}^{TR}$ for the A- and B horizon visualised along the soil horizon layers and the exterior walls of the 3D FE model.

(ii) Regarding equation 12, linear spatial trends are added to the 3D RFs generated in (i) for the A and B horizon. According to table 5.5, we did not perform this operation for the model set-ups III_a and III_b in order to evaluate possible effect of the trends on the water flow by comparing with the other model set-ups.

(iii) Reducing the 3D RFs to 2D RFs. Therefore, we extracted the scaling factors $\alpha_{K_{ij}}$ and their corresponding y (length), x (width), and z (height) Cartesian coordinates from a transect along the y axis as delineated in figure 5.3a.

(iv) From the population of 2D RFs of each horizon A, B, and C, 15 are randomly selected and randomly combined with the other mineral soil horizons to mitigate the effect of individual RF or combinations. Consequently, the model set-ups considering RFs (tab. 5.5) featured the same 15 combinations of the same RFs, whereas the RFs of horizons A and B of model set-up III_a did not feature the linear trends added by equation 12.

In Hydrus, the scaling factors were properly assigned to the corresponding mesh nodes via matching of the Cartesian coordinates. Since the scaling factors of Ksat and the pressure head are related to each other via the Miller-Miller Similitude (Miller and Miller, 1956), in the following we only refer to Ksat when we mention the trends of the A- and B horizon or spatial variabilities in order avoid confusion.

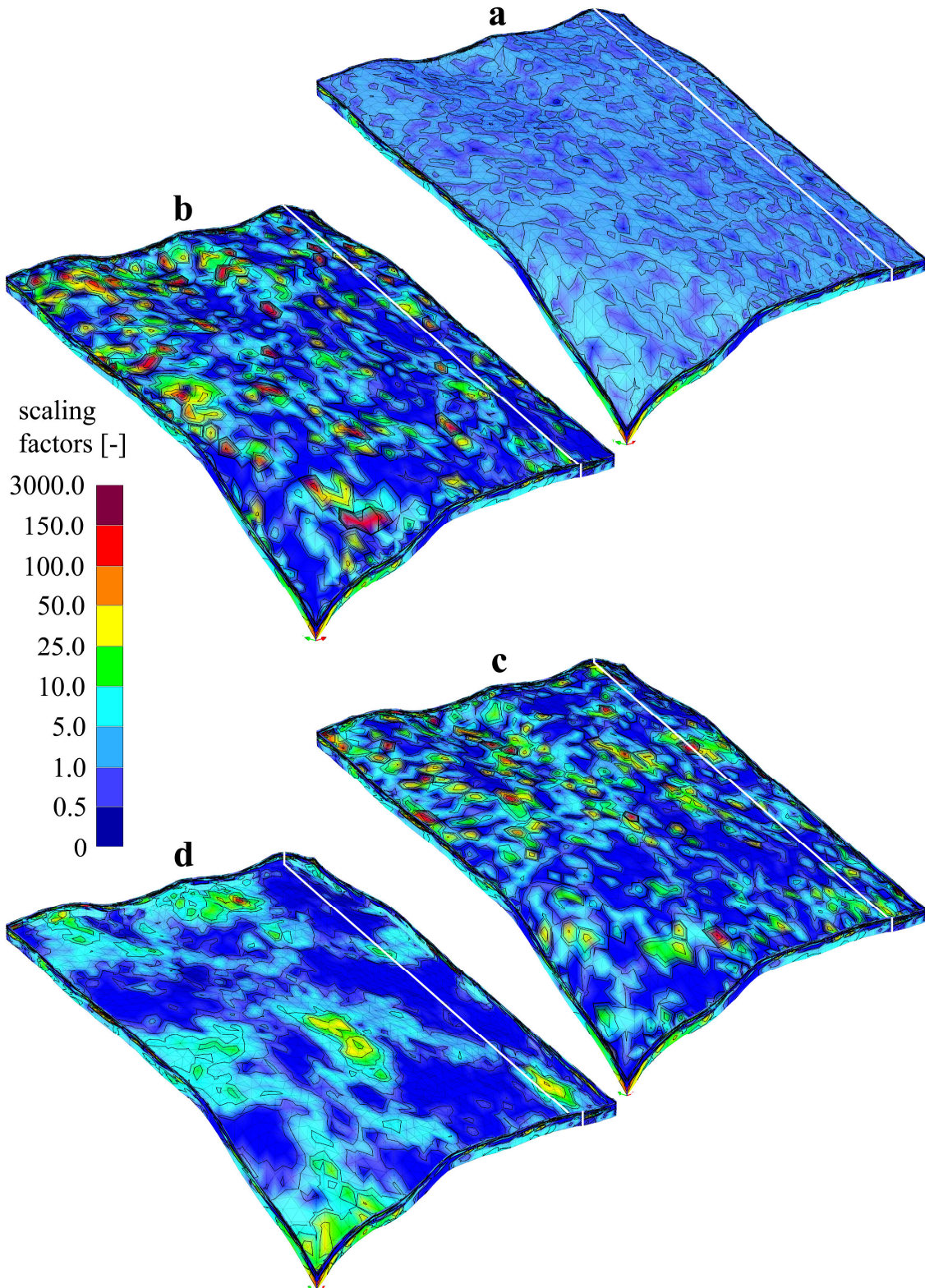


Figure 5.6 Scaling factors [-] for $K^*(h^*)$ generated by RandomFields (Schlather, 2001) and transferred to the 3D FE mesh. The distribution is shown for the top layer of the organic layer (a), for the basal layers of the A horizon (b), B horizon (c), and C horizon (d). The white line in each image denotes the course of the 2D FE slope. The exterior walls of the 3D FE mesh indicate the soil depth. Dimension of the 3D FE mesh are the same as shown in figure 5.3a. In (b) and (c) the linear trend decreasing calculated by equation 12 from the left-upper to the right-lower edge can be noticed.

5.2.7 Acquisition of modelled data

For the purpose to evaluate the spatiotemporal occurrence of sSF within the mineral topsoil and along the mineral topsoil/organic layer interface we implemented observation nodes in the 2D FE slope to simulate tensiometers measuring pressure heads at 20 cm depth below the mineral topsoil surface. As shown in figure 5.7, we implemented the observation nodes in the lower and upper part along the 2D FE slope in order to assess clearly a potential subsurface flow.

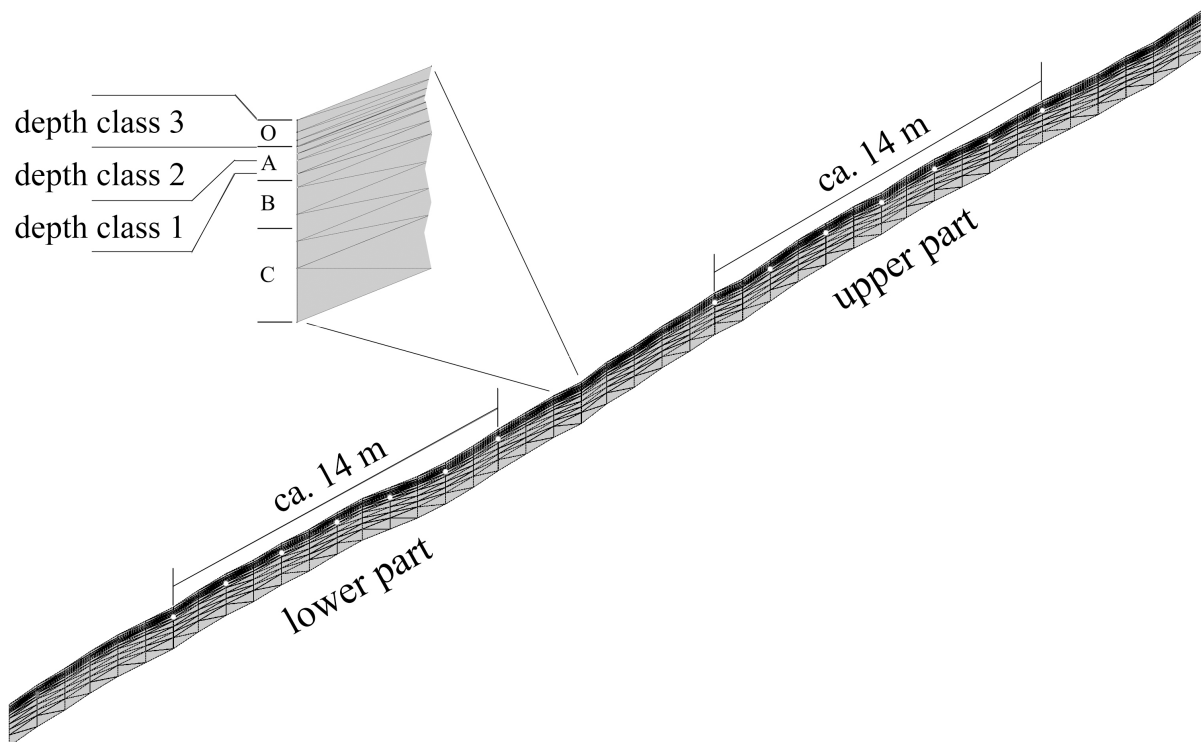


Figure 5.7 2D FE slope showing 14 observation nodes (white points). The observation nodes are situated 20 cm below the mineral soil surface. The detail in the top left-hand corner shows the soil horizons O, A, B, and C and positions of the depth ranges of the classes 1-3.

In order to detect water saturation within and upon the mineral topsoil, we defined three depth classes: class 1 ranging from -20 cm to -10 cm depth, class 2 from -10 cm to 0 cm at mineral soil surface, and class 3 from 0 cm to 20 cm being congruent with the organic layer denoted as O horizon in the model. Thus, depth classes 1 and 2 are within the mineral topsoil, i.e. the A horizon, while class 3 enables to assess water perching upon the mineral topsoil, i.e. within the organic layer (see detail in fig. 5.7). The observation nodes 20 cm below the mineral soil surface served as reference points for the three depth classes. Thus, positive pressure heads between 0 hPa and 10 hPa (note that in the model calculation 1 cm water column is approximately 1 hPa) indicate saturation in depth class 1, between 10 hPa and 20 hPa in depth class 2, and values higher than 20 hPa upon the mineral soil surface, i.e. within the organic

layer. The number of observation nodes recording positive pressure heads are used as a measure of the spatial extent of water saturation. Here, if more than half of the 7 observation nodes in the upper or lower part have recorded saturation, we speak of an extended spatial saturation within the lower or upper part of the modelled slope.

5.3 Results

Comparison between measured and modelled pressure heads reveals that drier periods are principally poorly reproduced by the model. This is clearly shown at day 100 (fig. 5.8a), where the measured pressure heads range between -500 and -700 hPa, while the modelled values do not fall below -300 hPa. Since evaporation at the forest floor can be neglected (Motzer, 2003; Fleischbein et al., 2006) and the measured values are notably below field capacity, we attribute the increase of the pressure heads' absolute value to transpirational water loss. This obviously do not apply in the model for which we considered the transpiration as the only sink term. Thus, we assume the calculated transpiration rates being too small to suitably reproduce transpirational water losses during drier periods.

Within the first 100 days, the discrepancy between modelled and measured pressure heads is largest (fig. 5.8a). On the one hand, we may attribute this to underestimated transpiration rates, on the other hand to the soil moisture characteristics, which we estimated by Rosetta. The “real” retention characteristics may allow smaller changes of the water content to change the pressure heads over a larger range than the estimated retention characteristic. This becomes clear looking at the period between day 30 and day 75, when the measured pressure heads rapidly tend to saturation, while the modelled would need more water input (fig. 5.8a). On the other hand, if we would assume the calculated transpiration rate to hamper saturation, we would expect a stronger drying of the soil layer than shown in figure 5.8a, particularly around day 100.

At day 130, the precipitation increases in intensity and amount which is even sufficient to saturate the modelled soil at 15 cm depth. During the wetter periods, e.g. between day 150 and day 200, and day 270 and day 400 the modelled pressure heads are close to the measured values (fig. 5.8a).

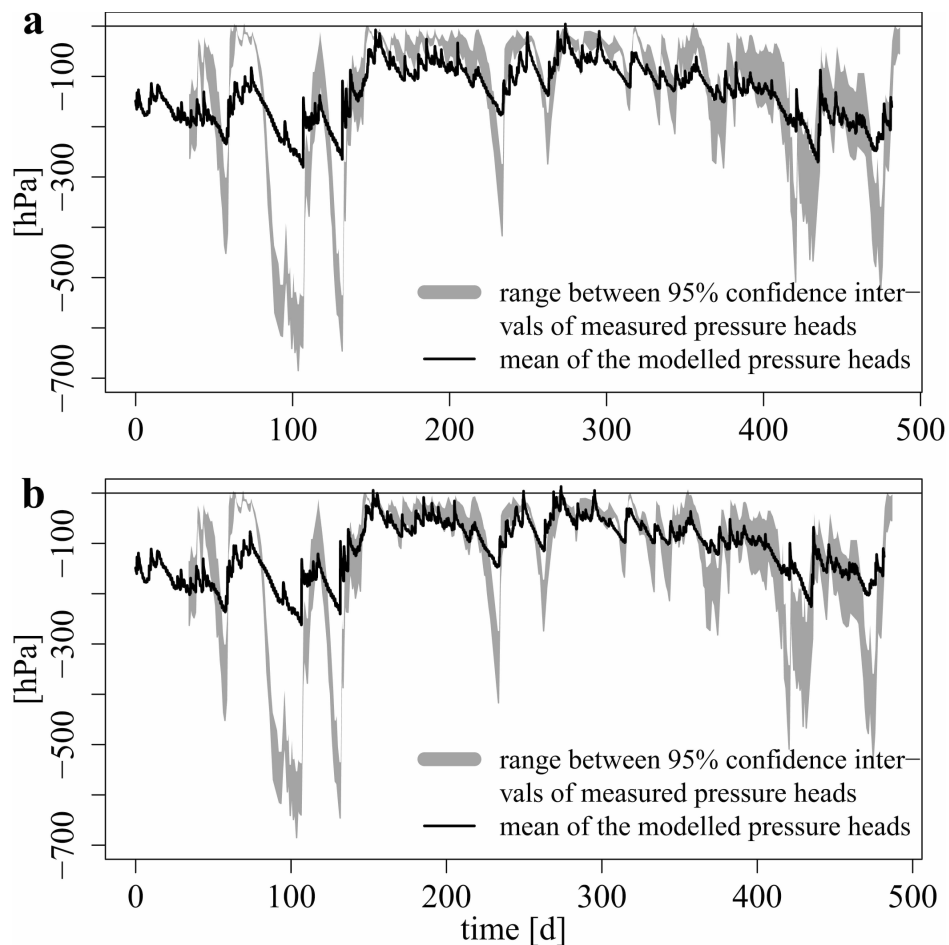


Figure 5.8 Hourly mean values of the modelled pressure heads (black line) 15 cm below the mineral soil surface taken from the lower part of the modelled slope. The grey line delineates the alternating width of the 95 % confidence intervals of the daily pressure heads measured at the tensiometer plot (fig. 5.2). (a) modelled pressure heads from experiment I_a; (b) modelled pressure heads from experiment I_b.

We obtained a better coincidence with the 95 % confidence intervals by lowering the K_{sat} of the C horizon from 0.75 cm/h (fig. 5.8a) to 0.2 cm/h (fig. 5.8b) according to table 5.5. However, the relative effect on the modelled pressure heads within the first 100 days is negligible, while the close to saturation of the measured pressure heads suggests prerequisites of a subsurface interflow even under relative dry conditions.

Figure 5.9 summarises the recorded saturation events within the mineral topsoil and the organic layer of the virtual experimental set-ups given in table 5.5. Here, for each model set-up the mean total time of water saturation within each depth class and the percental partition of the mean total time in dependence of the number of observation nodes having recorded saturation is shown. This is provided for both the lower and the upper part of the modelled slope (see figure 5.7 for details). Except for model set-up III_b which has only 1 model run since RFs were not considered, the mean total time of each model set-up was calculated as the

sum of total times of the 15 model runs divided by 15. As can be clearly seen in figure 5.9, for each model set-up the difference between the lower and upper part of the modelled slope concerning duration and lateral extent of water saturation is notably.

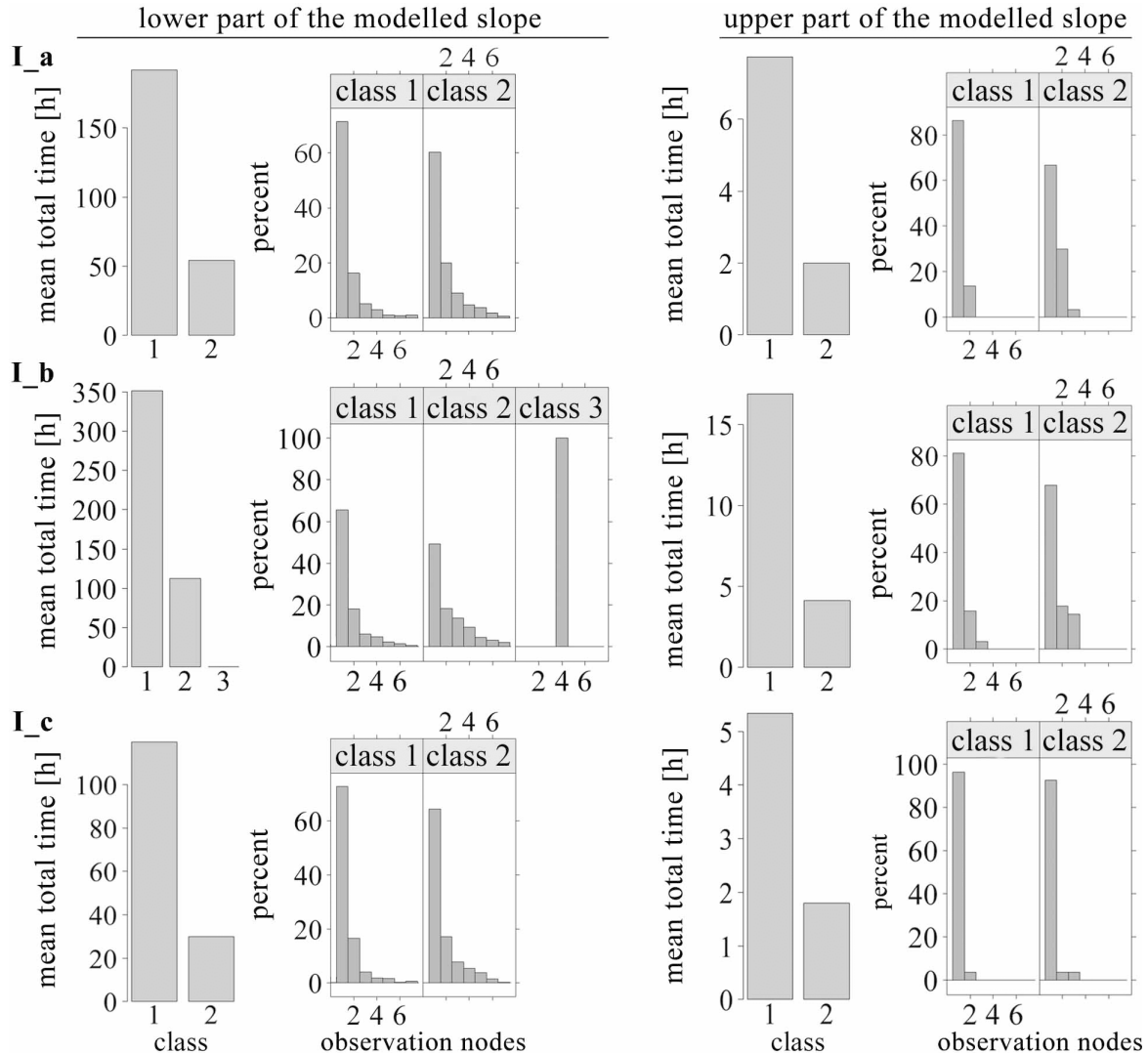


Figure 5.9 Summary of the saturation events in the 3 depth classes (defined in section 5.2.7) recorded over the ~16 month time series for the lower and the upper part of the modelled slope given for each model set-up (see table 5.5). For example, for model set-up I_b, in the lower part of the modelled slope a bar chart for each depth class is given, since in all three depth classes saturation was recorded. A bar chart shows the mean total sum of hours over the 15 model runs when saturation was recorded by one or more observation nodes (This does not account for model set-up III_b for which we did not provide RFs). To each bar chart belongs a histogram that shows the percental partition of the mean total time in dependence of the number of observation nodes having recorded saturation. For example, in model set-up I_b in class 3 saturation was recorded only by 4 observation nodes, which is denoted by 100 % in the histogram. With respect to the bar charts, note that at any time point along the modelled time series that class was considered which revealed the dominating number of observation nodes indicating saturation. For example, at any time class 1 showed 2 observation nodes, class 3 four observation nodes and class 3 one observation node with saturation, class 2 would be considered. If two depth classes reveal the same number of observation nodes indicating water saturation, we considered the next higher class number.

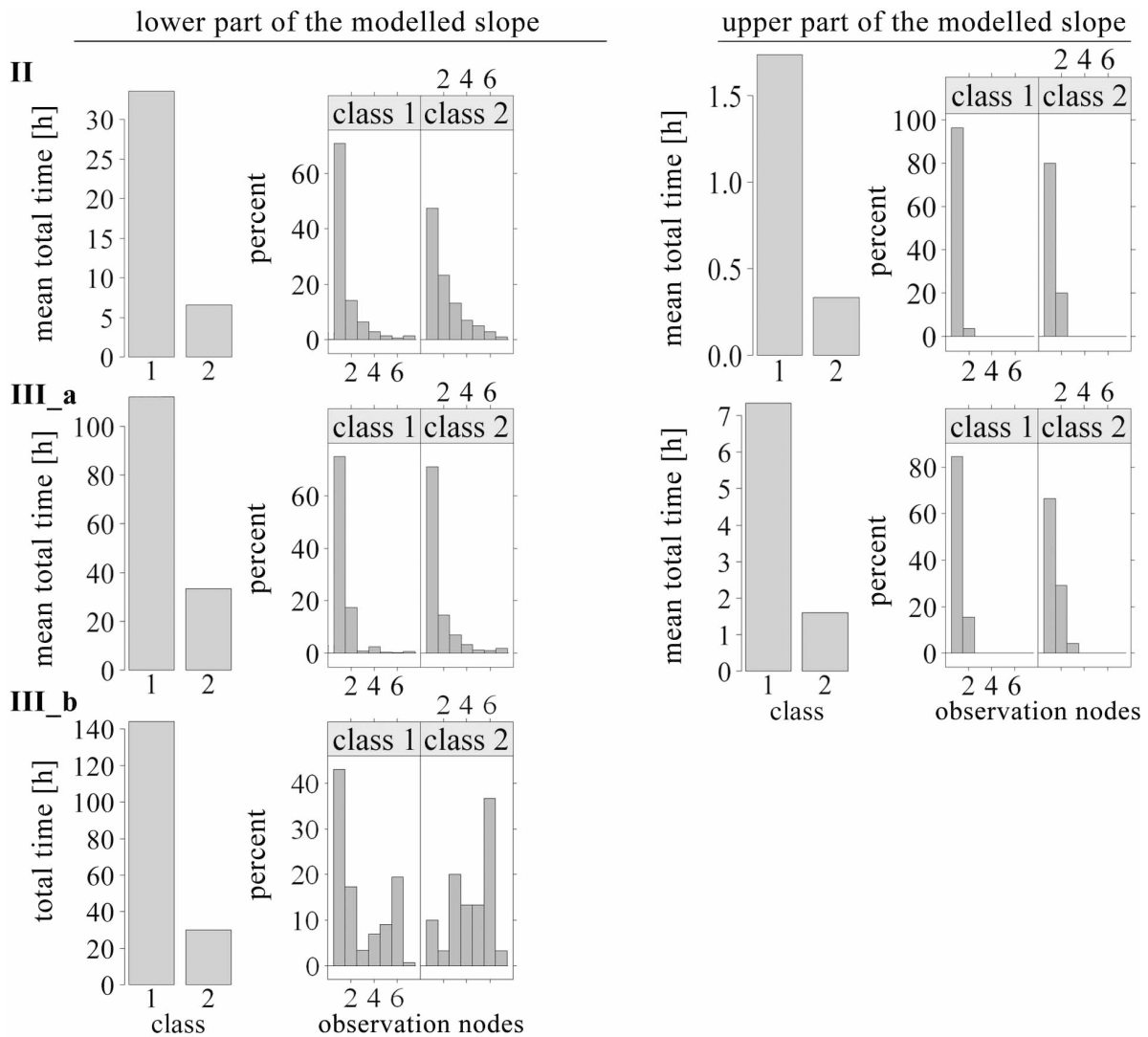


Figure 5.9 (continued from previous page)

Note that for all model set-ups most saturation events were recorded in depth class 1, while only in model set-up I_b saturation was recorded in depth class 3, i.e. within the organic layer. For model set-up III_b no saturation was recorded in the 3 depth classes within the upper part of the slope, while all other model set-ups reveal at least a few hours of saturation events recorded by a smaller number of observation nodes than in the lower part of the slope.

Obviously, laterally routed soil water from the upper part facilitated the saturation in the lower part of the model slope as illustrated in figure 5.11. Thus, the upper part of the model slope serves as contributing area, where water saturation within the mineral topsoil occurs infrequently and locally as indicated by the low number of observation nodes having recorded saturation. Undocumented virtual experiments simulating a permeable bedrock revealed constrained subsurface flow, which mitigated notably the effect of saturation in and upon the mineral topsoil in the lower part of the slope.

Effect of varying C horizon Ksat

Clear differences occurred between model set-ups I_a, I_b, and I_c in figure 5.9, for which we decreased and increased, respectively, the Ksat of the C horizon. As shown by the results of model set-up I_c, increasing the Ksat of the C horizon reduced the number of hours featuring water saturation in depth classes 1 and 2 compared to model set-up I_a and I_b. For the latter, the decreased Ksat of the C horizon increased the mean total number of hours of saturation in depth classes 1 and 2 considerably. Moreover, saturation was additionally recorded in depth class 3 (fig. 5.9).

Effect of different evaporations

As clearly documented by the results of model set-ups I_a and II in figure 5.9, in the lower part of the slope the temporal occurrence of saturation within depth classes 1 and 2 is reduced many times over if the amount of water intercepted and evaporated from the canopy is doubled according to table 5.2.

Effect of model reduction

In model set-up I_a, I_b, I_c, and II we included the trends of Ksat in the A- and B horizon, which decrease from the upper left corner to the lower right corner as shown in figure 5.6b and 5.6c. Here, the white line delineates the course of the 2D FE model; thus, the trends of Ksat decrease from the upper to the lower part of the 2D slope. In the model set-ups III_a we did not consider the trends of Ksat in the A- and B horizon, and in III_b we omitted the spatial variabilities of Ksat in all soil horizons.

By omitting the trends, the mean total time of hours featuring water saturation in depth classes 1 and 2 decreased notably in the lower part of the slope compared to model set-up I_a (fig. 5.9), which only differs from III_a by the trends (tab. 5.5). Also a shift to smaller numbers of observation nodes having recorded saturation can be noticed for model set-up III_a (fig. 5.9) indicating a tendency to a more local occurrence of saturation events in the lower part of the modelled slope.

Contrary, the results of model set-up III_b without spatial variabilities for Ksat reveal an increased number of observation nodes having recorded saturation in depth class 1 and particularly in depth 2 (fig. 5.9). This indicates a larger lateral extent of saturation along the hillslope, which furthermore persisted longer compared to the model set-ups featuring RFs. In case of depth class 2, for more than 35 % of the total time 6 observation nodes have recorded saturation (fig. 5.9). The reason therefore is illustrated in figure 5.11 for model set-up III_b,

which shows a continuous saturated zone expanding with proceeding rainfall (fig. 5.5) from day 273.25 to day 273.75 from the lowermost part of the slope in upslope direction. However, compared to the model set-ups featuring RFs most of the hours of larger lateral extent in depth class 2 is concentrated within this time span as documented by figure 5.10 for set-up III_b. Thus, most of the shallow subsurface run off along the hillslope occurred over several hours at a distinct event. Consequently, the resulting temporal dynamic and intensity of subsurface solute- and matter fluxes at the hillslope scale would be completely different to models that include the spatial variability of Ksat.

Effect of spatial variability of Ksat

For each model run of each model set-up, figure 5.10 shows the temporal occurrence of saturation events within and upon the mineral topsoil in the lower part of the modelled slope, when at least 4 observation nodes have recorded saturation. Also, for each model run the lateral extent of saturation in all 3 depth classes is indicated by grey vertical lines (4 – 5 observation nodes having recorded saturation) and black vertical lines (6 – 7 observation nodes having recorded saturation). The depth classes are indicated by the length of the vertical lines (see figure 5.10 for details).

Generally, for all model set-ups at least two mayor shallow saturation events between day 260 and day 300 can be seen. Except for model set-up II, further events were recorded shortly after day 150. Note that all these events occurred during the wetter period as indicated in figure 5.5.

In accordance with figure 5.9, in figure 5.10 saturation occurred mostly in depth class 1 followed by depth class 2. In depth class 3, i.e. in the organic layer, saturation occurred only in model runs 2, 3, 5, 12, and 14 of model set-up I_b between day 270 and day 275. Moreover, model set-up II reveals the lowest, whereas model set-up I_b the highest frequency of saturation events, and more saturation events of larger lateral extent due to the less permeable C horizon (see table 5.5 for details). Also, some events persisted longer or appeared in a higher depth class compared to the other model set-ups.

Nevertheless, even if model set-up I_b feature the highest frequency of saturation events, it has also model runs with low frequency of saturation events such as runs 8, 9, 11, and 15 (fig. 5.10). As for the other model set-ups featuring RFs, this can be only attributed to the RFs, since all other parameters within a model set-up were kept constant.

This issue is exemplarily visualised in figure 5.11. Here, the C horizon of all model runs with number 2 features patches of Ksat scaling factors between 0 and 0.5 within both the

lower and upper part of the slope, while model runs with number 7 only in the lower part. At these patches, the water flow is retarded leading to soil patches moister than the surrounding soil. With proceeding rainfall from day 273.25 until day 273.75 (fig. 5.11), the patches of moisture soil extend laterally and towards the mineral soil surface forming a nearly saturated continuous zone which is larger and develops faster in model run 2 than in model run 7.

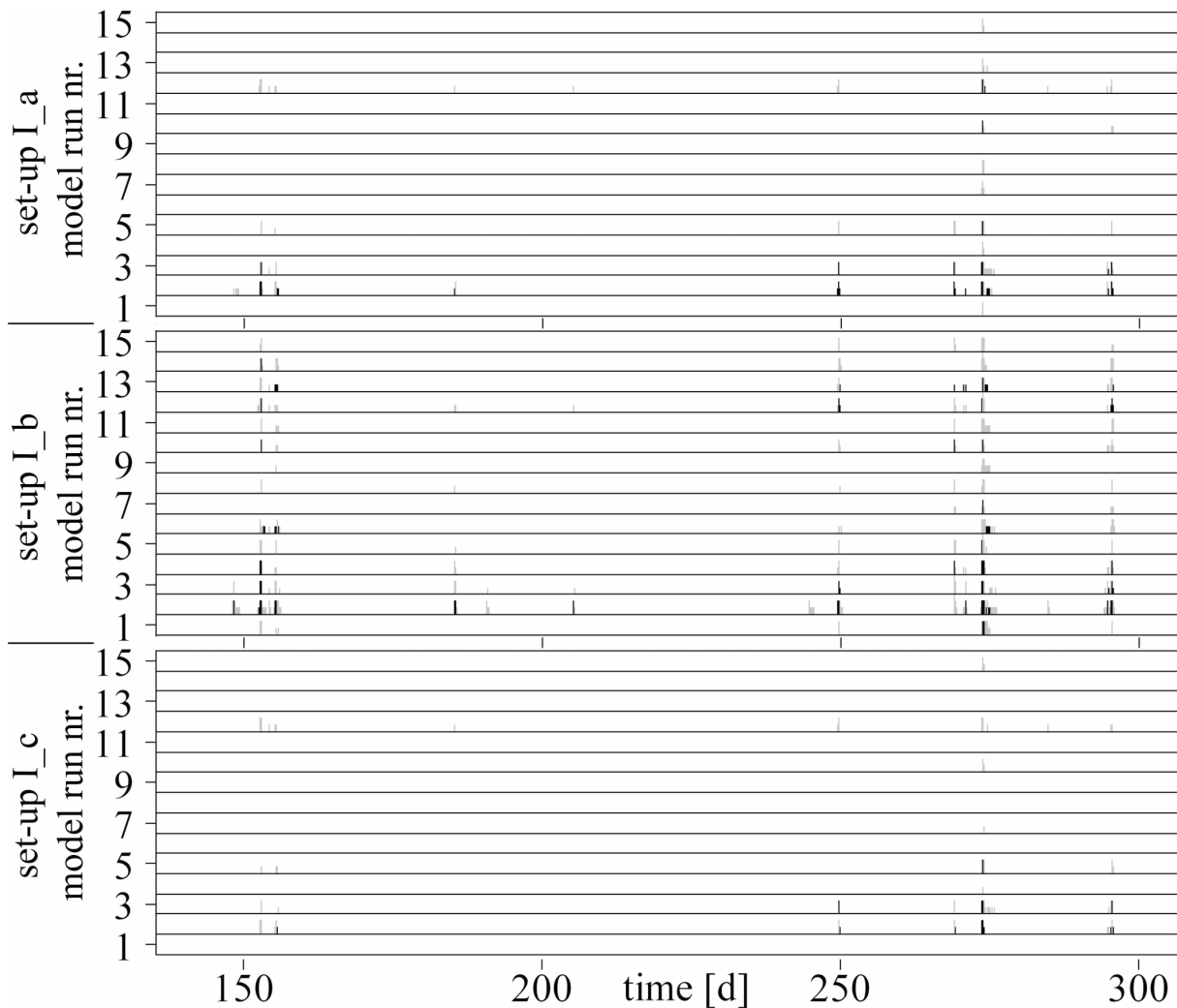


Figure 5.10 Summary of the spatiotemporal occurrence of saturation events given for the lower part of the modelled slope of the 6 model set-ups. For each model set-up featuring RFs model runs from 1 to 15 are given. Remember that all model runs having the same number have the same combination of RFs. Note that we did consider RFs for model set-up III_b. Saturation within a certain depth class of each model run is indicated by the vertical extent of the grey or black line, i.e. 1/3 of the maximum extent corresponds to depth class 1, 2/3 to depth class 2, and 3/3 to depth class 3. The minimum width of a vertical line equals 1 hour. A grey line indicates 4 to 5 from 7 observation nodes having detected saturation, and a black line 6 to 7 from 7 observation nodes having recorded saturation. For example, at day 250 in model run 8 of model set-up I_b 4 to 5 observation nodes have recorded saturation within depth class 1.

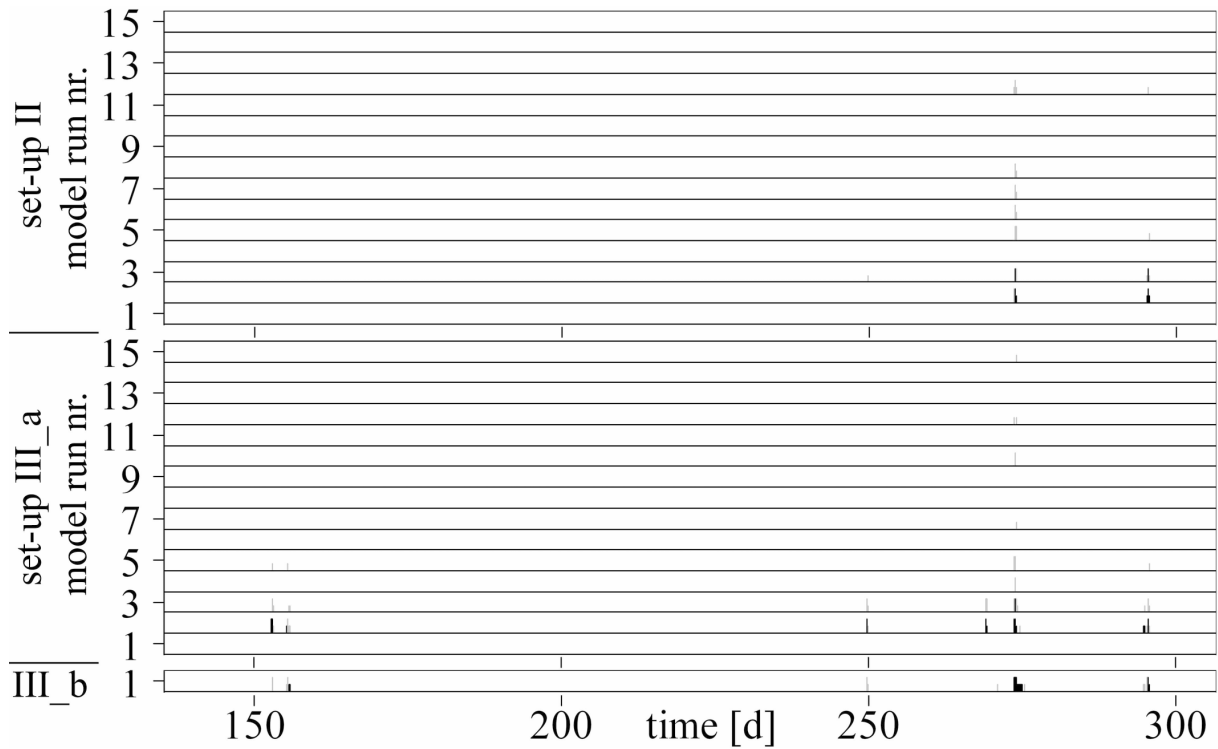


Figure 5.10 (continued from previous page)

This process is amplified if the permeability of the C horizon is reduced by comparing the model runs with number 2 or number 7 of the model set-ups I_b and I_c (see table 5.5 for model set-up details) in figure 5.11.

Consequently, formation rate and lateral extent of such a continuous saturated zone, and therefore the occurrence of sSF is not only controlled by the permeability of the C horizon, but also substantially by the spatial pattern of K_{sat} within the soil layer.

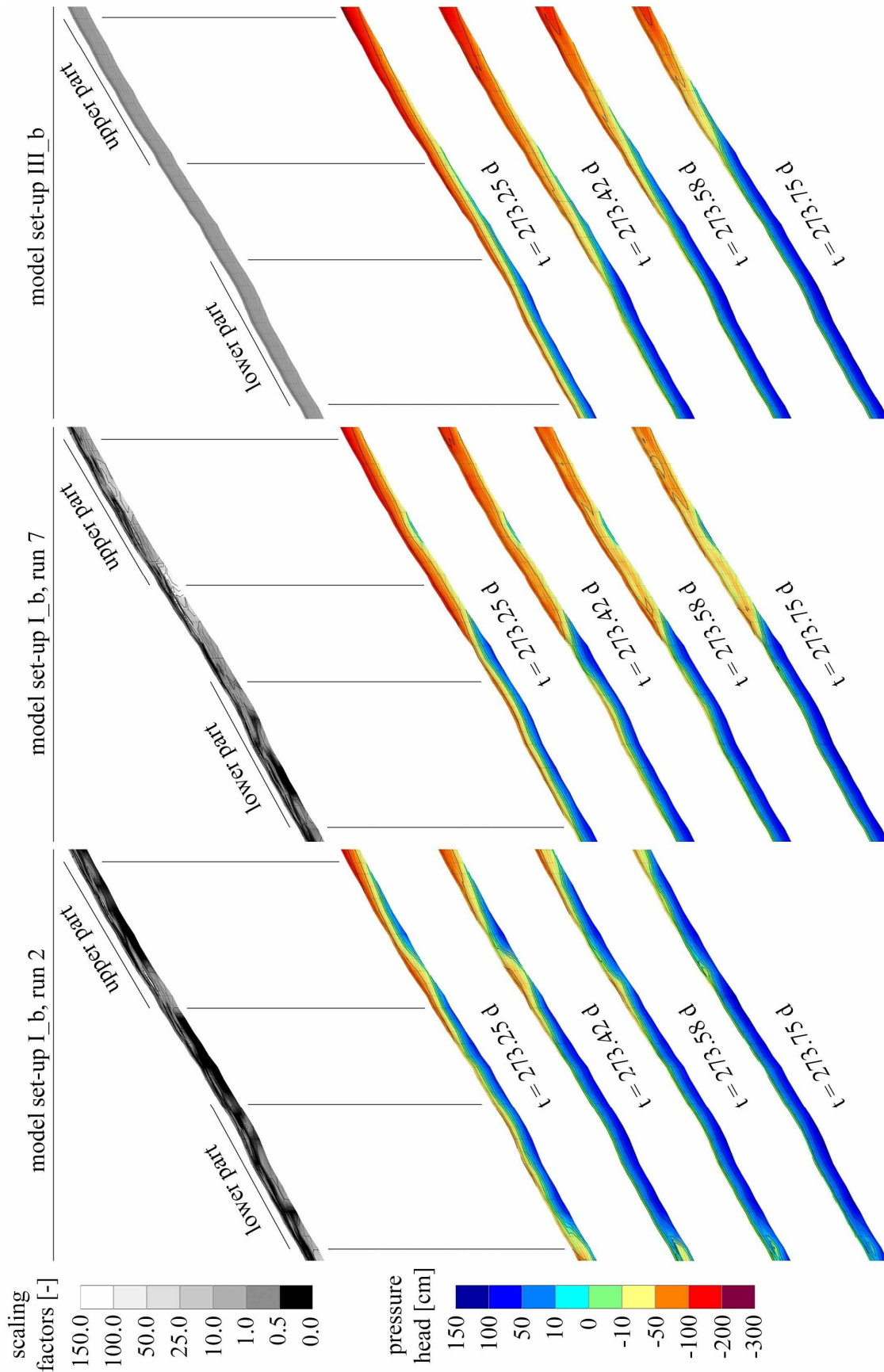


Figure 5.11 Exemplary model runs of model set-ups I_b, I_c, II, and III_b. In the uppermost modelled slope of each column, scaling factors for the reference Ksat value are given. Below, a time series over half a day is shown for the pressure heads. Note that time data correspond to the time axis given in figure 5.5.

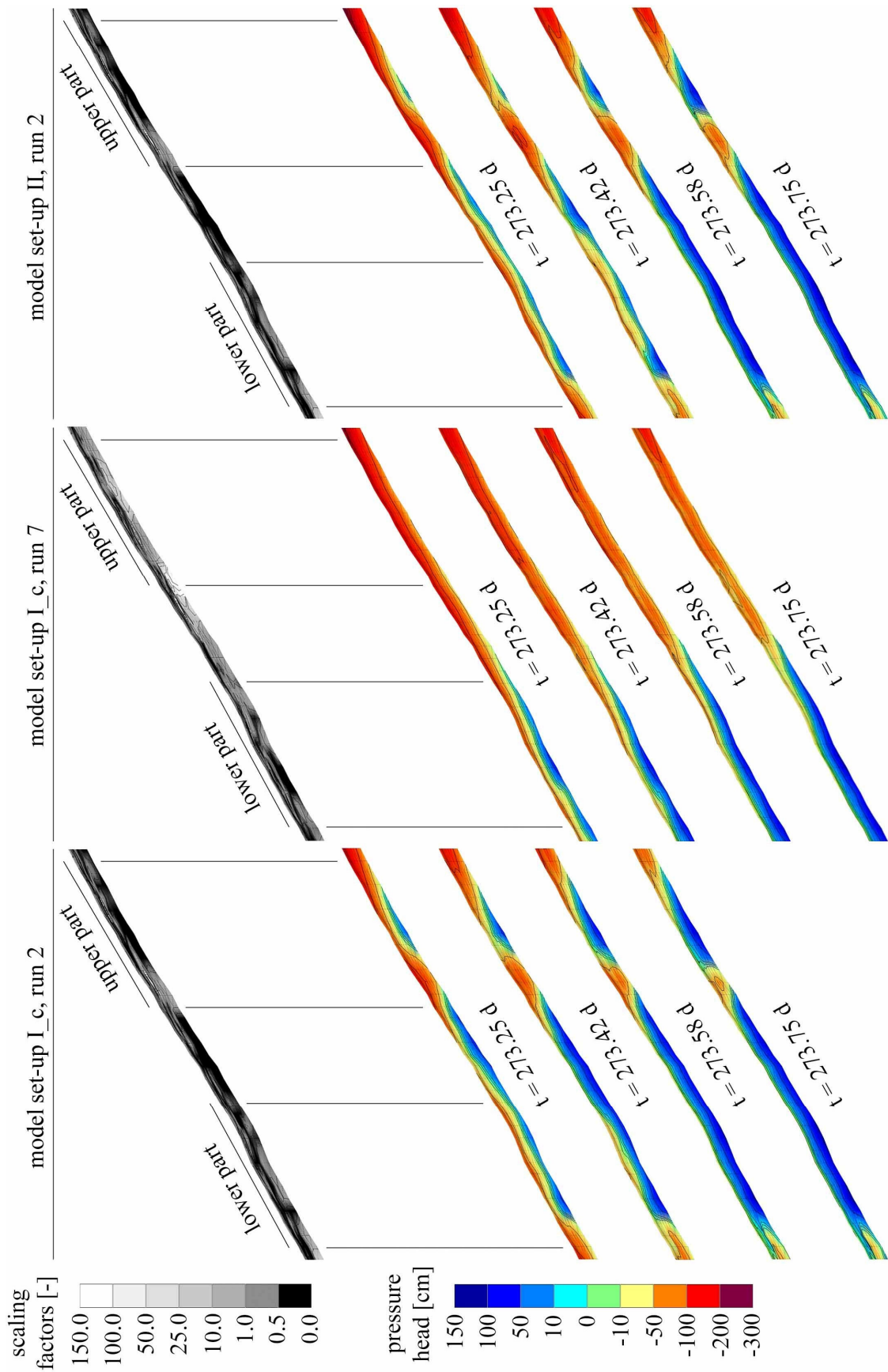


Figure 5.11 (continued from previous page)

5.4 Discussion

Role of bedrock permeability

With respect to the assumption of Fleischbein et al. (2006), we provided an impervious bedrock in our virtual experiment series, which favoured lateral subsurface flow from the upper to the lower part of the slope. Therefore, as shown in figure 5.11, the upper part of the modelled slopes remained drier while the lower part can be nearly throughout saturated. The development and rise of a transient water table led to the saturation of the higher permeable mineral topsoil, which provided the prerequisites of sSF. Weiler and McDonnell (2004) attributed this process, known as transmissivity feedback (Rodhe, 1987), particularly to glaciated till-mantled terrain, and more temperate as well subtropical areas with saprolite underlying the mineral soil cover. This may also apply to the RBSF study area, where recent soils are assumed to have also developed from periglacial cover beds (Fleischbein et al., 2006).

However, a permeable bedrock empties the soil water storage between rainstorm events and thus lowers the frequency of subsurface flow (Tromp-van Meerveld and Weiler, 2008). Notwithstanding its constitutive role, a limited number of studies (e.g. Ebel et al., 2007; Hopp and McDonnell, 2009; Montgomery et al., 1997; Onda et al., 2001; Tromp-van Meerveld and Weiler, 2008) have recognised the importance of bedrock permeability to control the pressure head of the soil, runoff generation, and landslide initiation. Moreover, simulations of Tromp-van Meerveld and Weiler (2008) emphasise the knowledge of the bedrock permeability to be important, if hillslope models are to be calibrated and validated for long time series.

Consequently, further investigations are required to elucidate the issue of bedrock permeability in the RBSF study area, if physically based models used in future studies concerning solute- and matter transport or landslide initiation should provide meaningful results.

Role of infiltration excess

The shallow subsurface flow caused by saturation excess depends primarily on the precipitation volume compared to sSF caused by infiltration excess (Scherrer et al., 2007). This becomes clear by comparing the temporal dynamics of the precipitation in figure 5.5 with that of the saturation events shown in figure 5.10. Figure 5.5 shows two distinct extreme rainfall events, both higher than 25 mm/h. In all model set-ups, the first event at the end of a short drier period did not produce saturation in the 3 depth classes. The second extreme

rainfall event within a wetter period produced no or a rather weak saturation events compared to the subsequent rainfall events at day 275 with intensities lower than 10 mm/h.

Therefore, in our virtual experiment series throughfall rates below 10 mm/h are able to produce extended lateral flows within the uppermost part of the topsoil, i.e. in depth class 2 as documented in figure 5.10. In contrast, Zimmermann and Elsenbeer (2009), who considered only sSF due to infiltration excess, showed that for precipitation intensities between 7.4 mm/h and 35.8 mm/h formation of impermeable layers is mainly restricted to the subsoil, i.e. below 20 cm soil depth.

Nevertheless, there remains the issue if in our series of virtual experiments surface near lateral flow caused by infiltration excess may be possible. Since we provided hourly values of incident precipitation, high intensities lasting for several minutes are smoothed, which may otherwise produce water perching upon the mineral topsoil due to exceeding of its infiltrability. However, the infiltration capacity of the organic layer we provided in our virtual experiment series would buffer the high throughfall rates, while perching upon the organic layer is impossible due to its high permeability (tab. 5.3). On the other hand, as illustrated by Leutner et al. (in review) a ~20 cm thick saturated organic layer transmits throughfall signals of intensities higher than 20 mm/h within few seconds to the mineral topsoil. The resulting dampening of the throughfall signal may be too low to prevent exceeding of the mineral topsoil infiltrability. Thus, rapid interflow along the organic layer/mineral soil interface via infiltration excess may be conceivable for extreme rainfall events. However, unlike the virtual experiments for which we provided a homogeneous distributed throughfall, in forested environments spatial patterns of vegetation may trigger runoff thresholds according to Cammeraat (2004). Analogously, the spatial patterns of Ksat we implemented via RFs in our virtual experiments provided sections with higher Ksat values, which exacerbate the formation of extended water perching upon the mineral topsoil due to infiltration excess. In this regard, figure 5.9 reveals no perching upon the mineral topsoil, i.e. in depth class 3 of the upper part of the modelled slope, which did not receive laterally routed water due to the *no flux* boundary at the right side of the modelled slope (see figure 5.3b for details). Also in depth classes 1 and 2, the small number of observation nodes indicates a local occurrence of saturation, which we attribute to sections with Ksat values lower than the reference values (tab. 5.3).

Consequently, our virtual experiment series reveal that sSF due to saturation excess may be the prevailing form of rapid subsurface interflow in Cambisols of steep hillslopes within the RBSF study are under the precondition of an impervious bedrock.

Role of water evaporated from the canopy

Analogous to storm size and the smoothening effect of the canopy (Keim et al., 2006), we found the amount of water intercepted by and evaporated from the canopy being crucial concerning the occurrence of sSF. As illustrated in figure 5.11 for model set-up II, the spatial extent of moister soil patches and therefore the formation of sSF is substantially controlled by the amount of the water evaporated from the canopy. Since studies of evapotranspiration in tropical montane environments are scarce (e.g. Bruijnzeel, 2001; Küppers et al., 2008; Letts, 2003), we cannot verify the widely differing estimates (tab. 5.1) of Motzer (2003), Ösker (2008), and Fleischbein et al. (2006) for plausibility. Nevertheless, the inclusion of this issue in the virtual experiments documents a clear effect on the frequency of surface near lateral flow and stresses the need for further investigations concerning canopy interception and evaporation in the RBSF study area.

5.5 Outlook and conclusions

By conducting a number of virtual experiment series we evaluated the spatiotemporal occurrence of a fast lateral subsurface within the mineral topsoil and along the mineral soil/organic layer interface. We provided 2D FE model representing a steep forested hillslope transect of ~54 m length. We parameterised the model with data mostly sampled within the considered site or nearby, included time series of throughfall and evapotranspiration, an organic layer abundant within the investigation area as well as the horizon wise spatial variabilities of the saturated hydraulic conductivity, the pressure heads and their spatial trends.

In the framework of virtual experiments we could show that particularly during wetter periods the modelled soil pressure heads reproduced satisfactorily the measured pressure heads. Within these periods, spatially extended sSF in the mineral topsoil occurred due to saturation excess. Therefore, subsurface flow from the upper part of the modelled slope water was required, which, in turn, necessitated an impervious bedrock. Spatially extended subsurface flow along the base of the organic layer due to infiltration excess of the mineral topsoil was not evident.

The results of this study highlighted the crucial importance of the subsoil permeability and rainfall evaporated from the canopy if process conceptualisation regarding location, frequency and lateral extent of shallow subsurface flow at the hillslope scale is in the spotlight. Moreover, simulations of Tromp-van Meerveld and Weiler (2008) emphasise the knowledge

of the bedrock permeability to be important if, for example, hillslope models are to be calibrated and validated for long time series. Consequently, further investigations are required to elucidate the issue of bedrock permeability in the RBSF study area. This accounts also for the amount of water intercepted by and evaporated from the canopy, which remains unclear up to now in the RBSF investigation area.

In particular, we identified the spatial variability of K_{sat} and the pressure head as a key parameter controlling substantially the frequency and lateral extent of sSF. By omitting the spatial variability formation of a continuous saturated zone along the hillslope is favoured. In terms of assessing the risk of landslide initiation by physically based models this may lead to biased risk estimations, since a saturated zone dissected by highly permeable zones may lower the risk of landslide initiation.

Further parameters that we did not consider in this study are the degree of slope inclination, bedrock topography, varying soil thickness, and hillslope geometry. Their importance on hydrological processes at the hillslope scale have been emphasised by the virtual experiment studies of Hopp and McDonnell (2009) and Weiler and McDonnell (2006). With respect to the occurrence of sSF, we suggest these parameters to be simultaneously considered with the spatial variability of K_{sat} and the pressure head in further virtual experiment studies.

5.6 Acknowledgements

We would like to thank Dr. Reiner Zimmermann, Institute of Botany, University of Hohenheim for his useful comments on tree transpiration, Dr. Thorsten Peters, Institute of Geography, University of Erlangen-Nuremberg for providing climate data, Dr. Thomas Motzer for his greatly permission to use his data of diurnal canopy conductance variation (fig. 3), and Prof. Dr. Martin Schlather, Centre for Statistics, University of Göttingen for his helpful support in RandomFields. This study was supported and funded by the German Research Foundation (DFG) grant nr. DFG FOR 402/1-1 Hu 636/9-3 and DFG FOR 816 - HU 636/14-1.

5.7 References

Amoozegar, A., 1989. A compact, constant-head permeameter for measuring saturated hydraulic conductivity of the vadose zone. *Soil Sci. Soc. Am. J.* 53, 1356-1361.

Chapter 5 – References

- Balslev, H., Øllgaard, B., 2002. Mapa de vegetación del sur de Ecuador, in: Aguirre, M.Z., Madsen, J.E., Cotton, E., Balslev, H. (Eds.), *Botanica Austroecuatorialiana. Estudios sobre los Recursos Vegetales en las Provincias de El Oro, Loja y Zamora-Chinchipec*, Quito, pp 51-64.
- Bendix, J., Rollenbeck, R., Richter, M., Fabian, P., Emck, P., 2008. Climate, in: Beck, E., Bendix, J., Kottke, I., Makeschin, F., Mosandl, R. (Eds.), *Gradients in a Tropical Mountain Ecosystem of Ecuador*, Springer Verlag, Berlin, Heidelberg, pp 63-73.
- Beven, K.J., Lamb, R., Quinn, P.F., Romanowicz, R., Freer, J., 1995. TOPMODEL, in: Singh, V.P. (Ed.), *Computer Models of Watershed Hydrology*. Water Resources Publications: Highlands Ranch, Colorado, USA, pp 627–668.
- Bishop, K.H., Grip, H., O'Neill, A., 1990. The origins of acid runoff in a hillslope during storm events. *J. Hydrol.*, 116, 35-61.
- Blow, F.E., 1955. Quantity and hydrologic characteristics of litter under upland oak forests in eastern Tennessee. *J. Forest.* 53, 190-195.
- Bonell, M., Barnes, C.J., Grant, C.R., Howard, A., Burns, J., 1998. High rainfall, response-dominated catchments: A comparative study of experiments in tropical northeast Queensland with temperate New Zealand, in: McDonnell J.J., Kendall C. (Eds.), *Isotope Tracers in Catchment Hydrology*. Elsevier Science Publishers, Amsterdam, pp 347-390.
- Bruijnzeel, L.A., Hamilton, L.S., 2000. Decision Time for Cloud Forest. IHP Humid tropics Programme Series 13(44).
- Bruijnzeel, L.A., 2001. Hydrology of tropical montane cloud forests: A reassessment. *LUWRR* 1, 1-18.
- Cammeraat, E.L.H., 2004. Scale dependent thresholds in hydrological and erosion response of a semi-arid catchment in southeast Spain. *Agric. Ecosyst. Environ.* 104, 317-332.
- Chappell, N.A., Ternan, J.L., Williams, A.G., Reynolds, B., 1990. Preliminary analysis of water and solute movement beneath a coniferous hillslope in mid-Wales, U.K. *J. Hydrol.* 116, 201-215.
- Chappell, N.A., Sherlock M.D., 2005. Contrasting flow pathways within tropical forest slopes of Ultisol soils. *Earth Surf. Process. Landforms* 30, 735-753.
- DeWalle, D.R., Pionke, H.B., 1994. Stream low generation on a small agricultural catchment during autumn recharge; II. Stormflow periods. *J. Hydrol.* 163, 23-42.
- Ebel, B.A., Loague, K., Vanderkwaak, J.E., Dietrich, W.E., Montgomery, D.R., Torres, R., Anderson, S.P., 2007. Near-surface hydrologic response for a steep, unchanneled catchment near Coos Bay, Oregon: 2. Physics-based simulations. *Am. J. Sci.* 307, 709-748.

- Elrick, D.E., Reynolds, W.D., 1992. Methods for analyzing constant head well permeameter data. *Soil. Sci. Soc. Am. J.* 56, 320-323.
- Fleischbein, K., Wilcke, W., Goller, R., Boy, J., Valarezo, C., Zech, W., Knoblich K., 2005. Rainfall interception in a lower montane forest in Ecuador: effects of canopy properties. *Hydrol. Process.* 19, 1355-1371.
- Fleischbein, K., Wilcke, W., Valarezo, C., Zech, W., Knoblich, K., 2006. Water budgets of three small catchments under montane Forest in Ecuador: experimental and modelling approach. *Hydrol. Process.* 20, 2491-2507.
- Foken, T., 2008. *Micrometeorology*. Springer, Berlin
- Fries, A., Rollenbeck, R., Göttlicher, D., Nauss, T., Homeier, J., Peters, T., Bendix, J., 2009. Thermal structure of a megadiverse Andean mountain ecosystem in southern Ecuador, and its regionalization. *Erdkunde* 63, 321-335.
- Goller, R., Wilcke, W., Leng, M.J., Tobschall, H.J., Wagner, K., Valarezo, C., Zech, W., 2005. Tracing water paths through small catchments under a tropical montane rain forest in South Ecuador by an oxygen isotope approach. *J. Hydrol.* 308, 67-80.
- Homeier, J., Dalitz, H., Breckle, S.W., 2002. Waldstruktur und Baumartendiversität im montanen Regenwald der Estación Científica San Francisco in Südecuador. *Berichte der Reinhold-Tüxen-Gesellschaft* 14, 109-118.
- Homeier, J., 2004. Baumdiversität, Waldstruktur und Wachstumsdynamik zweier tropischer Bergregenwälder in Ecuador und Costa Rica. *Dissertationes Botanicae*, Berlin.
- Hopp, L., McDonnell, J.J., 2009. Connectivity at the hillslope scale: Identifying interactions between storm size, bedrock permeability, slope angle and soil depth. *J. Hydrol.* 376, 378-391.
- Hungerbühler, D., 1997. Neogene basins in the Andes of southern Ecuador: evolution, deformation and regional tectonic implications. PhD thesis. URL <http://e-collection.ethbib.ethz.ch/view/eth:40985> (accessed on January 2010), ETH Zürich, Zürich.
- Hupfer, P., Kuttler, W., 1998. *Witterung und Klima*, 10th ed. Teubner Verlag, Stuttgart, Leipzig
- Huwe, B., Zimmermann, B., Zeilinger, J., Quizhpe, M., Elsenbeer, H., 2008. Gradients and patterns of soil physical parameters at local, field and catchment scales, in: Beck, E., Bendix, J., Kottke, I., Makeschin, F., Mosandl, R., (Eds.), *Gradients in a Tropical Mountain Ecosystem of Ecuador*. *Ecological Studies*, Springer, Berlin, Heidelberg, 198, 375-387.
- IUSS Working Group WRB, 2007. *World Reference Base for Soil Resources 2006*, first update 2007. *World Soil Resources Reports No. 103*. FAO, Rome.

- Jenkins, A., Ferrier, R.C., Harriman, R., Ogunkoya, Y.O., 1994. A case study in catchment hydrochemistry: Conflicting interpretations from hydrological and chemical observations. *Hydrol. Processes* 8, 335-349.
- Keim, R.F., Skaugset, A.E., Link, T.E., Iroumé, A., 2004. A stochastic model of throughfall for extreme events. *HESS* 8, 23-34.
- Keim, R.F., Meerveld, H., McDonnell, J.J., 2006. A virtual experiment on the effects of Evaporation and intensity smoothing by canopy interception on subsurface stormflow Generation. *J. Hydrol.* 327, 352-364.
- Kessler, M., 1999. Plant species richness and endemism during natural landslide succession in a perhumid montane forest in the Bolivian Andes. *Ecotropica* 5, 123-136.
- Köhn, M., 1928. 3. Bemerkungen zur mechanischen Bodenanalyse. III. Ein neuer Pipetteapparat. *Zeitschrift für Pflanzenernährung, Düngung und Bodenkunde A. Wissenschaftlicher Teil*, XI, 50-54.
- Kosugi, K., Mori, K., Yasuda, H., 2001. An inverse modelling approach for the characterization of unsaturated water flow in an organic forest floor. *J. Hydrol.* 246(1-4), 96-108.
- Kreutzer, D., Martini, J., 2002. Bestimmung und Regionalisierung der gesättigten hydraulischen Leitfähigkeiten in Böden unter tropischem Bergregenwald in Ecuador mit verschiedenen Methoden. Unpubl. diploma thesis, University of Giessen, Giessen.
- Küppers, M., Motzer, T., Schmitt, D., Ohlemacher, C., Zimmermann, R., Horna, V., Küppers, B.I.L., Mette, T., 2008. Stand Structure, Transpiration Responses in Trees and Vines and Stand Transpiration of Different Forest Types within the Mountain Rainforest, in: Beck, E., Bendix, J., Kottke, I., Makeschin, F., Mosandl, R. (Eds.), *Gradients in a Tropical Mountain Ecosystem of Ecuador*, Springer Verlag, Berlin, Heidelberg, pp 243-258.
- Letts, M.G., 2003. Carbon Assimilation and Productivity in a North-west Andean Tropical Montane Cloud Forest. PhD thesis. URL <http://people.uleth.ca/~matthew.letts/letts%20thesis%202003.pdf> (accessed on July 2010), Kings College London, London.
- Liess, M., Glaser, B., Huwe, B., 2009. Digital Soil Mapping In Southern Ecuador. *Erdkunde* 63(4), 309-319.
- Lippert, J., 2002. Bestandsklima und Evapotranspiration eines neotropischen Bergregenwaldes im Podocarpus Nationalpark, Ecuador. Unpubl. diploma thesis, University of Heidelberg, Heidelberg.

- Markwardt, S., 2005. Validity of two pedotransfer functions in two microcatchments of a tropical mountain rainforest in Southern Ecuador. Unpubl. diploma thesis, University of Bayreuth, Bayreuth.
- McDonnell, J.J., Owens, I.F., Stewart, M.K., 1991. A case study of shallow flow paths in a steep zero-order basin. *Water Resour. Bul.* 27, 679-685.
- Miller, E.E., Miller, R.D., 1956. Physical theory for capillary flow phenomena. *J. Appl. Phys.* 27, 324-332.
- Monteith, J.L., 1965. Evaporation and environment. *Symp. Soc. Exp. Biol.* 19, 206-234.
- Monteith, J.L., Unsworth, M.H., 1990. *Principles of Environmental Physics*, 2. ed. London.
- Montgomery, D.R., Dietrich, W.E., Torres, R., Anderson, S.P., Heffner, J.T., Loague, K., 1997. Hydrologic response of a steep, unchanneled valley to natural and applied rainfall. *Water Resour. Res.*, 33(1), 91-109.
- Motzer, T., 2003. Bestandesklima, Energiehaushalt und Evapotranspiration eines tropischen Bergregenwaldes (Süd-Ecuador). Unpubl. Phd thesis, University of Mannheim, Mannheim.
- Motzer, T., Munz, N., Küppers, M., Schmitt, D., Anhuf, D., 2005. Stomatal conductance, transpiration and sap flow of tropical montane rain forest trees in the southern Ecuadorian Andes. *Tree Physiol.* 25, 1283-1293.
- Mulholland, P.J., Wilson, G.V., Jardine, P.M., 1990. Hydrogeochemical response of a forested watershed to storms: effects of preferential flow along shallow and deep pathways. *Wat. Resour. Res.* 26, 3021-3036.
- Onda, Y., Komatsu, Y., Tsujimura, M., Fujihara, J., 2001. The role of subsurface runoff through bedrock on storm flow generation. *Hydrol. Process.* 15, 1693-1706.
- Ösker, M., 2008. Untersuchungen zur räumlichen Heterogenität von Kronenstruktur und Bestandesniederschlag in einem tropischen Bergregenwald. Phd thesis. URL <http://opus.ub.uni-hohenheim.de/volltexte/2009/342/pdf/OESKER2008Dissertation.pdf> (accessed on July 2010), University of Hohenheim, Hohenheim.
- Paulsch, A., 2002. Development and application of a classification system for undisturbed and disturbed tropical montane forests based on vegetation structure. PhD thesis. URL <http://opus.ub.uni-bayreuth.de/volltexte/2002/1/> (accessed on January 2010), University of Bayreuth, Bayreuth.
- R Development Core Team, 2009. R: A language and environment for statistical computing. R Foundation for Statistical Computing. URL <http://www.R-project.org> (accessed on July 2010), Vienna, Austria.

- Richards L.A., 1931. Capillary Conduction of Liquids through Porous Mediums. *Physics* 1 (5), 318-333.
- Ritchie, J.T., 1972. A model for predicting evaporation from a row crop with incomplete cover, *Water Resour. Res.*, 8(5), 1204-1213.
- Rodhe, A., 1987. The origin of stream water traced by Oxygen-18. PhD thesis. Uppsala University, Uppsala, 260 pp.
- Rollenbeck, R., 2006. Variability of precipitation in the Reserva Biológica San Francisco / Southern Ecuador. *Lyonia* 9 (1), 43-51.
- Schaap, M.G., Bouten, W., Verstraten, J.M., 1997. Forest floor water content dynamics in a Douglas fir stand. *J. Hydrol.* 201(1-4), 367-383.
- Schaap, M.G., Leij, F.J., van Genuchten, M.T., 2001. Rosetta: a computer program for estimating soil hydraulic parameters with hierarchical pedotransfer functions. *J. Hydrol.* 251, 163-176.
- Schellekens, J., 2000. Hydrological processes in a humid tropical rain forest: a combined experimental and modelling approach. Phd thesis. URL <http://dare.uvu.nl/bitstream/1871/10314/1/5319.pdf> (accessed on July 2010), Free University of Amsterdam, Amsterdam.
- Scherrer, S., Naef, F., Faeh, A.O., Cordery, I., 2007. Formation of runoff at the hillslope scale during intense precipitation. *Hydrol. Earth Syst. Sci.*, 11, 907-922.
- Schlather, M., 2001. Simulation of stationary and isotropic random fields. *R-News* 1(2), 18-20. URL http://www.stochastik.math.uni-goettingen.de/~schlather/R/Random_Fields/ (accessed July 2010).
- Šimůnek, J., vanGenuchten, M.T., Sejna, M., 2006. The HYDRUS Software Package for Simulating Two- and Three-dimensional Movement of Water, Heat, and Multiple Solutes in Variably-Saturated Media: Technical Manual. Version 1.0. PC-Progress, Prague, Czech Republic.
- Soethe, M., Lehmann, J., Engels, C., 2006. The vertical pattern of rooting and nutrient uptake at different altitudes of a south Ecuadorian montane forest. *Plant Soil* 286 (1-2), 287-299.
- van Genuchten, M. Th., 1987. A numerical model for water and solute movement in and below the root zone. Unpubl. Res. Rep. (121), USDA ARS, U.S. Salinity Laboratory, Riverside, California.
- Tromp-van Meerveld, H.J., Weiler, M., 2008. Hillslope dynamics modeled with increasing complexity, *J. Hydrol.* 361, 24-40.
- Walsh, R.P.D., Voigt, P.J., 1977. Vegetation Litter - Underestimated Variable in Hydrology and Geomorphology. *J. Biogeogr.* 4(3), 253-274.

Chapter 5 – References

- Weiler, M., Naef, F., 2003. An experimental tracer study of the role of macropores in infiltration in grassland soils. *Hydrol. Process.* 17(2), 477-493.
- Weiler, M., McDonnell, J.J., 2004. Virtual experiments: a new approach for improving process conceptualization in hillslope hydrology. *J. Hydrol.* 285, 3-18.
- Weiler, M., McDonnell, J.J., 2006. Testing nutrient flushing hypotheses at the hillslope scale: A virtual experiment approach. *J. Hydrol.* 319, 339-356.
- Werner F.A., Homeier, J., Gradstein, S.R., 2005. Diversity of vascular epiphytes on isolated remnant trees in the montane forest belt of southern Ecuador. *Ecotropica* 11, 21-40.
- Wilcke, W., Yasin, S., Valarezo, C., Zech, W., 2001. Change in water quality during the passage through a tropical montane forest in Ecuador. *Biogeochemistry* 55, 45-72.
- Wilcke, W., Yasin, S., Fleischbein, K., Goller, R., Boy, J., Knuth, J., Valarezo, C., Zech, W., 2008. Water Relation, in: Beck, E., Bendix, J., Kottke, I., Makeschin, F., Mosandl, R. (Eds.), *Gradients in a Tropical Mountain Ecosystem of Ecuador*. Ecological Studies, Springer, Berlin, pp 193-201.
- Yasin, S., 2001. Water and nutrient dynamics in microcatchments under montane rain forest in the South Ecuadorian Andes. Bayreuth. *Bodenkd. Ber.*, Bayreuth.
- Zimmermann, B., Elsenbeer, H., 2008. Spatial and temporal variability of soil saturated hydraulic conductivity in gradients of disturbance. *J. Hydrol.* 361, 78-95.
- Zimmermann, B., Elsenbeer, H., 2009. The near-surface hydrological consequences of disturbance and recovery: A simulation study. *J. Hydrol.* 364, 115-127.

Appendices

Appendix A List of other publications

Bauer, F., Huwe, B. 2007. Preferential Flow and Discharge Behaviour Dependent on Anthropogenic and Natural Disturbances in the Highlands of Southern Ecuador, *Mitteilungen der Deutschen Bodenkundlichen Gesellschaft* 110(1): 171-172

Viñan Esparza, P., Bauer, F., Huwe, B., Valarezo, C. 2007. Observation and Simulation of Water Fluxes in the Vadose Zone of Undisturbed and Disturbed Sites in the Highlands of Southern Ecuador, *Mitteilungen der Deutschen Bodenkundlichen Gesellschaft* 110(1): 143-144

Appendix B Content of data DVD

The structure of the data DVD follows the chapters in this thesis. The structure of the data DVD follows the chapters in the thesis mentioned above. Names of the folders on the data DVD are given in []. Within each folder, a detailed descriptions (text file) is given about the folder content and scripts. Names of folders or scripts that starts with “1_”, “2_”, and so on denote the order you have to open or execute, respectively. It is urgently recommended to read the READ ME files! The meanings of the abbreviations assigned to the file names or used as column labels within the text files are written in the pdf – file “list of abbreviations”. All *R*- and Matlab scripts deposited in the folders can be used. If your computer has a D:\ partition, then make a new folder named *data DVD* on partition or drive D:\. Copy [Chapter 2], ..., [Chapter 5] from the DVD to this folder. Now you may use all scripts without changing the file paths written within each script. Otherwise, you have to adjust the paths. The scripts on this DVD work without problems with following version of *R* (R Development Core Team 2009) and Matlab (The Math Works, 2008a):

Matlab, version 7.7. URL <http://www.mathworks.com> (accessed on July 2010)

R, version 2.9.1 URL <http://www.r-project.org/> (accessed on July 2010)

Problems may occur with older or newer versions. Note that you may have to install additional libraries to *R*. These libraries are given within the first lines of each script. If a

Appendices

library is not installed on the *R* you are using, you have to follow the instructions given by the *R* console. For Matlab, you will also need to have the Image Processing Toolbox (The Math Works, 2008b) installed. For our computations we used the version 6.2.

To work smoothly with the text files, *R*-scripts, and produced postscript files following software is recommended:

text files: Textpad; URL <http://www.textpad.com/> (accessed on July 2010)

R-scripts: Tinn-R; URL <http://www.sciviews.org/Tinn-R/> (accessed on July 2010)

Postscript graphics: ghostview; URL <http://pages.cs.wisc.edu/~ghost/> (accessed on July 2010)

The content of the DVD is as follows:

In [chapter 2], you will find the data of the bulk density [bulk density], saturated hydraulic conductivity [Ksat], fine soil texture [soil texture], and soil moisture characteristics [soil moisture characteristics] as text files. In the latter, you find also the R-Scripts to represent the data graphically. In [fotos, binary images, 1-H, dye stain widths] for each experimental plot investigated in chapter 2 and chapter 3, you will find the original fotos and processes fotos, binary images, computed probability density functions, dye coverages, and corresponding fitted generalised Pareto distribution and parameters of the pedon scale dye tracer experiments.

[chapter 3] contains data of the fine soil texture [soil texture], bulk density [bulk density], and multivariate regression analysis [multivariate statistics]. In [fotos, binary images, 1-H, dye stain widths] for each experimental plot investigated in chapter 3, you will find the original fotos and processes fotos, binary images, computed probability density functions, dye coverages, and corresponding fitted generalised Pareto distribution and parameters of the pedon scale dye tracer experiments.

[chapter 4] contains in [graphs] the discharge graphs of the measured and fitted discharge curves of the inverse modelling Hydrus 1D as well as the measured and calculated discharge curves of the validation experiments, in [Hydrus Projects] all Hydrus 1D projects regarding the inverse modelling experiments and validation experiments, in [material functions] the material function estimated by the inverse modelling procedure, in [parameter optimisation] the observed discharge curves and fitted discharge curves of the inverse modelling Hydrus 1D projects, in [response-surface analysis] the parameter sections of the response surface

Appendices

analysis, in [sensitivity analysis] the variation of optimised parameters due to their initial value, and in [validation] the modelled discharge curves of the validation experiments. In this folder, [classes and correlations] contains the coefficient of determination R^2 as goodness of fit between the measured and modelled discharge curves of the validation experiments. In chapter 4, we used the Hydrus 1D version 4.05 (Šimůnek et al., 2008).

[chapter 5] contains in [Hydrus Projects] all Hydrus 2D/3D projects according to the model set-ups I_a, I_b, I_c, II, III_a, and III_b. [3D block] contains a 3D FE model, from which we derived the 2D FE models in the folders below. [input data climate] and [input data soil] contain the input data for the used model set-ups. In [RandomFields and R-scripts] all necessary files and R-scripts are given to produce Gaussian random fields [1_PRODUCING RFs], to include them in the 2D- and 3D FE slope models [2_ASSEMBLING_the_RF_s_for_2D_and_3D_model], and to process and visualise the results [3_PROCESSING of model results] produced by Hydrus 2D/3D. In chapter 5, we used the Hydrus 2D/3D version 1.08 (Šimůnek et al., 2006).

References

R Development Core Team, 2009. R: A language and environment for statistical computing. R Foundation for Statistical Computing. URL <http://www.R-project.org> (accessed on July 2010), Vienna, Austria.

Šimůnek, J., vanGenuchten, M.T., Sejna, M., 2006. The HYDRUS Software Package for Simulating Two- and Three-dimensional Movement of Water, Heat, and Multiple Solutes in Variably-Saturated Media: Technical Manual. Version 1.0. PC-Progress, Prague, Czech Republic.

Šimůnek J, Šejna M, Saito H, Sakai M, van Genuchten, MT. 2008. The HYDRUS 1D Software Package for Simulating the One-Dimensional Movement of Water, Heat, and Multiple Solutes in Variably-Saturated Media Version 4.0. Department of Environmental Sciences, University of California Riverside, Riverside, California.

The MathWorks, Inc., 2008b. Image Processing Toolbox, ver 6.2. URL <http://www.mathworks.com/products/image/> (accessed on July 2010).

The MathWorks, Inc., 2008a. Matlab, ver 7.7. URL <http://www.mathworks.com> (accessed on January 2010).

Declaration of authenticity

To the best of my knowledge and belief, this thesis contains no material previously published or written by another person, except where due reference has been made.

This thesis contains no material which has been accepted or definitely rejected for the award of any other doctoral degree in any university

Erklärung

Hiermit erkläre ich, dass ich vorliegende Arbeit selbständig verfasst und keine anderen als die von mir angegebenen Quellen und Hilfsmittel benutzt habe.

Ferner erkläre ich, dass ich anderweitig mit oder ohne Erfolg nicht versucht habe, diese Dissertation einzureichen. Ich habe keine gleichartige Doktorprüfung an einer anderen Hochschule endgültig nicht bestanden.

Bayreuth,